Supersymmetric Models in Low Dimensions on the Lattice

Inauguraldissertation
der Philosophisch-naturwissenschaftlichen Fakultät
der Universität Bern

vorgelegt von

David Baumgartner

von Bangerten/BE

Leiter der Arbeit:

Prof. Dr. Urs Wenger

Albert Einstein Zentrum für fundamentale Physik
Institut für theoretische Physik, Universität Bern

Supersymmetric Models in Low Dimensions on the Lattice

vorgelegt von

David Baumgartner

von Bangerten/BE

Von der Philosophisch-naturwissenschaftlichen Fakultät angenommen.

Bern, 1. November 2012   Der Dekan:

Prof. Dr. S. Decurtins

Abstract

Simulations of supersymmetric models on the lattice with (spontaneously) broken supersymmetry suffer from a fermion sign problem related to the vanishing of the Witten index. We propose a novel approach which solves this problem in low dimensions by formulating the path integral on the lattice in terms of fermion loops. The formulation is based on the exact hopping expansion of the fermionic action and allows the explicit decomposition of the partition function into bosonic and fermionic contributions. We then devise a simulation algorithm which separately samples the fermionic and bosonic sectors, as well as the relative weight between them. These techniques are exercised to study $\mathcal{N} = 2$ supersymmetric quantum mechanics. Employing the transfer matrix approach which is based on the hopping expansion, we obtain exact results at finite lattice spacing. Thereby covering all aspects of interest for this model, we are able to study the continuum limit for both broken and unbroken supersymmetry. In particular, we reveal how supersymmetry is restored in this limit and we observe the emergence of the Goldstino mode in the context of broken supersymmetry. Furthermore, we are able to show that these exact results coincide with - and thus validate - the results from Monte Carlo simulations when engaging the algorithm designed for the studying of supersymmetric systems in low dimensions. Finally, we consider the two-dimensional $\mathcal{N} = 1$ Wess-Zumino model for which we demonstrate the loop representation and present numerical confirmation for the decomposition of the partition function into bosonic and fermionic contributions.

In memory of
Hermann Bürki

Contents

Contents

Contents

Introduction

In contemporary theoretical physics, the concept of *symmetry* plays a crucial role. In this context the term symmetry refers to a physical or mathematical feature of a physical system which remains unchanged after the system has undergone a particular transformation. A physical system exhibiting this characteristic is called invariant under the symmetry in question. Symmetries may be discrete, such as for example the reflection symmetry, or continuous such as the rotation symmetry.

The standard model (SM) for particle physics describes the interaction of subatomic particles. Its construction is based on symmetry considerations and it unifies the dynamics of three of the four elementary forces of nature. Included in the standard model are the weak and the electromagnetic interaction [1–3] as well as the strong interaction [4]. Although the standard model is an enormously powerful theory, efforts are being made to find a unified description of nature by constructing more general theories. However, the extension of the standard model's symmetries by further ones on this account is severely restricted by the famous Coleman-Mandula no-go theorem [5]. Yet, there is one possible way to circumvent the theorem, which is by extending the Poincaré algebra with anticommuting *supersymmetry* generators [6]. These generators relate particles with semi-integer spins, the fermions, to those with integer spins, the bosons.

The first renormalisable supersymmetric model was the Wess-Zumino model [7] in four dimensions (1974), containing two real scalar fields and one Majorana fermion. Since then, many more supersymmetric models have been constructed, including supersymmetric gauge theories or supersymmetric sigma models. For an introduction, we refer to [8–10].

One main feature of supersymmetric theories is the prediction of mass degenerate multiplets of fermionic and bosonic particles if the ground state of the theory is invariant under the supersymmetry transformation. In nature, these degeneracies have not been observed, such that, if supersymmetry is indeed a

true symmetry of nature, it must be spontaneously broken at some scale [11]. However, the question of spontaneous supersymmetry breaking cannot be addressed easily in perturbation theory and therefore, non-perturbative methods are desirable.

In the past, Euclidean lattice theory and Monte Carlo importance sampling have proven to be very successful tools for the studying of problems in a non-perturbative context. Consequently, a lot of effort has been put into the lattice formulation of supersymmetric theories, e.g. [12–17]. This task, however, turned out to be far from trivial because of the explicit breaking of symmetries in connection with the discretisation. For lattice regularised theories which are composed of local lattice operators, the remnant subgroups of the Poincaré group, the discrete rotations and the finite translations by multiples of the lattice spacing, guarantee that the Poincaré symmetry is fully restored in the continuum. Inasmuch as supersymmetry is an extension of the Poincaré algebra, a complete realisation of the continuum algebra on the lattice is not possible. Yet, in contrast to the Poincaré symmetry, in general no subgroup of the supersymmetry is left on the lattice which could play the role of the discrete subgroups above. It is therefore a priori not at all clear how to find a lattice formulation of a supersymmetric theory for which supersymmetry is restored in the continuum [18]; a problem which can eventually be traced back to the failure of the Leibniz rule on the lattice [19–21].

In addition to the explicit breaking of supersymmetry by the finite lattice spacing, other supersymmetry breaking effects cause further complications for the investigation of supersymmetric theories on the lattice, such as for example supersymmetry breaking at finite temperature[1] or tunnelling between originally separate ground states due to a finite spatial volume.

Even $\mathcal{N} = 2$ supersymmetric quantum mechanics represented as a $(0 + 1)$-dimensional quantum field theory subsumes all the complications of the lattice formulation of a supersymmetric theory discussed above [22, 23]. Therefore, besides being worth studying in their own right [24], supersymmetric quantum mechanics provides an ideal testing ground for techniques designed for the application to higher dimensional supersymmetric models as well as for dimensionally reduced models e.g. [25–27]. Consequently, supersymmetric quantum

---

[1]This problem can be dealt with by assigning periodic boundary conditions to the fermionic variables in (imaginary-)time direction.

mechanics on the lattice have been the subject of intensive studies to date. Over time, different discretisation schemes have been developed in order to meet the requirement of the correct continuum limit of the theory [28–30]. In the context of unbroken supersymmetry, these schemes have well established numerical support [31–34]. For broken supersymmetry, however, the model reveals a severe fermionic sign problem for simulations with standard Monte Carlo methods [35, 36]. Because of this additional obstruction, first results in the context of broken supersymmetry were published only recently [37].

In this thesis, we introduce a novel approach with which it is possible to solve supersymmetric quantum mechanics thoroughly for both unbroken and broken supersymmetry. In particular, instead of proceeding the standard way by integrating out the fermions, we propose to reformulate the system and its degrees of freedom in terms of bond variables [38]. On the one hand, this representation circumvents the fermionic sign problem for broken supersymmetry, and on the other hand, the bond formulation is the basis for the highly efficient Prokof'ev-Svistunov worm algorithm [39] which we employ for our Monte Carlo simulations. Moreover, the bond formulation as well as the worm algorithm are applicable to two-dimensional models as well, which is what we aim at ultimately.

For the observation of dynamical supersymmetry breaking, we focus on the two-dimensional Wess-Zumino model which can be defined both with complex or real fields, exhibiting a $\mathcal{N} = 2$ or $\mathcal{N} = 1$ supersymmetry, respectively. The $\mathcal{N} = 2$ model [40] has the merit that it possesses one exact lattice supersymmetry which guarantees that the full symmetry is restored in the continuum [41–44]. Our interest, however, lies in the $\mathcal{N} = 1$ model for which Golterman and Petcher (1989) have constructed via perturbation theory a lattice formulation with Wilson-type discretisation which ensures that for vanishing lattice spacing the continuum Ward identities are exactly satisfied [45][2]. Numerical investigations have demonstrated that the lattice action by Golterman-Petcher indeed yields the expected continuum results [62]. In view of a complete numerical treatment, we propose to employ the bond formulation for the two-dimensional $\mathcal{N} = 1$ Wess-Zumino model as well and to benefit thereby from the efficiency of the worm algorithm for Monte Carlo simulations.

---

[2]Note, that this model has been studied using various other approaches, such as the Hamilton formalism [46–54] and renormalisation group methods [55, 56]. Moreover, extensive lattice investigations have been conducted by employing the SLAC derivative [32, 57–61].

Contents

The thesis is organised as follows: We start with a prefatory chapter where we introduce the tools and techniques on which we rely later by means of the Ising model. In particular, we exemplify for this model the hopping expansion along with the reformulation of the degrees of freedom in terms of bond variables. We then use the bond formulation of this particularly simple model for the development of the constrained path representation of the partition function and we review in detail the Prokof'ev-Svistunov worm algorithm. In chapter 2 we proceed by recapitulating the construction of supersymmetric quantum mechanics in the Schroedinger formalism and we establish the main characteristics thereof. In this context, particular attention is paid to the difference between quantum mechanical systems with unbroken and broken supersymmetry. In chapter 3 we change over to quantum field theory. Starting from the formulation of supersymmetric quantum mechanics as a $(0 + 1)$-dimensional quantum field theory, we discuss its lattice formulation. We emphasise the complications arising for the discretised theory, such as the issue of the correct continuum limit related to the explicit breaking of supersymmetry or the sign problem of the fermion determinant for broken supersymmetry. We then demonstrate that these dilemmas can be managed with modified lattice actions and the bond formulation. The subsequent two chapters serve us for the presentation of our numerical studies of supersymmetric quantum mechanics formulated as a lattice field theory. We commence chapter 4 with the introduction of the transfer matrix technique, which allows for the calculation of exact results at finite lattice spacing for both unbroken and broken supersymmetry. We then present and discuss the results we obtained employing this technique. In chapter 5 we adapt the worm algorithm for supersymmetric quantum mechanics and demonstrate its feasibility for unbroken and broken supersymmetry by comparing the Monte Carlo simulation results with the exact results from chapter 4. Finally, in chapter 6, we extend our considerations to the two-dimensional $\mathcal{N} = 1$ Wess-Zumino model. We begin the chapter with the revision of the lattice formulation for this model as proposed by Golterman and Petcher. This is our jumping-off point for the derivation of the representation of the model's degrees of freedom in terms of bond variables. To validate our approach in two dimensions as well, we close the chapter by presenting first results for Monte Carlo simulations of this model.

Chapter 1

The Worm Algorithm and the Ising Model

We base all our numerical lattice calculations on the concept of the hopping expansion. By applying this expansion to a model on the lattice, its degrees of freedom are expressed in terms of bonds connecting neighbouring lattice sites. The resulting bond configurations may obey certain constraints, such that for example fermionic degrees of freedom are represented as self-avoiding loops. For the Monte Carlo update of these bond configurations, we then adapt the worm algorithm first introduced by Prokof'ev and Svistunov in [39, 63] to low-dimensional quantum field theories with bosonic as well as fermionic degrees of freedom. We propose to use the worm algorithm not only because it is highly efficient, but also because it will serve to circumvent the fermionic sign problem occurring in the context of broken supersymmetry.

As we have pointed out, the hopping expansion technique is crucial for all our lattice calculations. Therefore, we consider it to be useful to review it in detail by the example of the Ising model in the first section of this chapter. In the second section, we will follow the work of [39, 64] and derive the worm algorithm for this particularly simple model. Once the concept is understood well, the application to the lattice formulations of supersymmetric quantum mechanics in chapter 3 and to the $\mathcal{N} = 1$ Wess-Zumino model in chapter 6 will be fairly straightforward.

We conclude this chapter by briefly discussing other formulations of the Ising model and addressing the problem of how to calculate expectation values of observables in the bond formulation.

1.1 The Hopping Expansion of the Ising Model

To demonstrate the hopping expansion, we consider the Ising model in two dimensions. In standard notation, the Hamiltonian for this model is given by

$$H = -J \sum_{\langle xy \rangle} s_x s_y, \tag{1.1}$$

where the coupling parameter J determines the interaction strength between the spin variables $s_x = \pm 1$ and the sum runs over nearest neighbour sites $\langle xy \rangle$. The minus sign is merely conventional and dictates the sign of the coupling parameter J, which in this case is positive for a ferromagnetic model as opposed to an antiferromagnetic model for which a negative sign is assigned to J. The partition function for a grid of the extension $V = L_1 \times L_2$, totalling N lattice sites, and a reservoir at a temperature T then reads

$$Z = \sum_{s_1 = \pm 1} \sum_{s_2 = \pm 1} \cdots \sum_{s_N = \pm 1} \exp\left(\beta \sum_{\langle xy \rangle} s_x s_y \right), \tag{1.2}$$

which we will abbreviate with

$$Z = \sum_{\{s_x\}} \exp\left(\beta \sum_{\langle xy \rangle} s_x s_y \right). \tag{1.3}$$

The label $\{s_x\}$ stands for the sum over all possible states the spin variables can take. Also, we have introduced the dimensionless coupling parameter $\beta = J/T$. With the help of the lattice unit vectors $\hat{\mu}$ in the directions $\mu = 1, 2$, we can choose an explicit representation of the nearest neighbour interaction $\langle xy \rangle$ and rewrite the partition function Z as

$$Z = \sum_{\{s_x\}} \exp\left(\beta \sum_{x} \sum_{\mu=1}^{2} s_x s_{x+\hat{\mu}} \right). \tag{1.4}$$

We now Taylor expand each summand in the exponential in β to get

$$Z = \sum_{\{s_x\}} \left[\prod_{x} \prod_{\mu} \left(\sum_{n(x,\mu)=0}^{\infty} \frac{\beta^{n(x,\mu)} (s_x s_{x+\hat{\mu}})^{n(x,\mu)}}{n(x,\mu)!} \right) \right]. \tag{1.5}$$

Because all terms in the expansion are included, this reformulation is still exact. At this point, we assign a geometrical implication to the number $n(x, \mu)$.

If we introduce the undirected lattice *bond* $b(x, \mu)$, the *bond occupation number* $n(x, \mu)$ counts the number of such bonds connecting two neighbouring spins at sites x and $x + \hat{\mu}$ for each summand in the expansion.

1.2 The Constrained Path Formulation

1.2.1 The Partition Function

As we have derived eq.(1.5) by expanding the partition function of the Ising model, we now proceed by discussing the concept of *constrained paths* (CP). First, we select one specific bond configuration $\{n(x, \mu)\}$, which is done by choosing one fixed $n(x, \mu)$ in each sum of the expansion eq.(1.5), and call the summand of the partition function thus obtained $W(\{n(x, \mu)\})$. Then, we can rewrite the partition function as the sum over all possible choices of $W(\{n(x, \mu)\})$,

$$Z = \sum_{\{n(x,\mu)\}} W(\{n(x, \mu)\}), \tag{1.6}$$

where (omitting from now on the argument $\{n(x, \mu)\}$)

$$W = \sum_{\{s_x\}} \left[\prod_x \prod_\mu \left(\frac{\beta^{n(x,\mu)} (s_x s_{x+\hat{\mu}})^{n(x,\mu)}}{n(x, \mu)!} \right) \right]. \tag{1.7}$$

For W to be non-zero, the chosen $n(x, \mu)$ have to fulfil certain constraints, as we will see below. The non-zero terms, represented graphically, lead to a picture where we have bond configurations on the lattice which obey these constraints[1] yet to be specified, hence the name constrained path. The weight of such a path in the total ensemble is then given by W of eq.(1.7). We can, however, manipulate eq.(1.7) to transform it into a much more convenient form. Imposing periodic boundary conditions for the spin variables in both directions $\mu = 1, 2$,

$$s_{x+L_\mu \cdot \hat{\mu}} = s_x, \tag{1.8}$$

---

[1]This is the case for the Ising model. For other models which we will encounter, there will be no constraints on the bond configurations.

we derive

$$
\begin{aligned}
W &= \sum_{\{s_x\}} \left[\prod_x \prod_\mu \left(\frac{\beta^{n(x,\mu)} (s_x s_{x+\hat{\mu}})^{n(x,\mu)}}{n(x,\mu)!} \right) \right] \\
&= \left(\prod_x \prod_\mu \frac{\beta^{n(x,\mu)}}{n(x,\mu)!} \right) \sum_{\{s_x\}} \left[\prod_x \prod_\mu (s_x s_{x+\hat{\mu}})^{n(x,\mu)} \right] \\
&= \left(\prod_x \prod_\mu \frac{\beta^{n(x,\mu)}}{n(x,\mu)!} \right) \sum_{\{s_x\}} \left[\prod_x \prod_\mu s_x^{n(x,\mu)+n(x-\hat{\mu},\mu)} \right] \\
&= \left(\prod_x \prod_\mu \frac{\beta^{n(x,\mu)}}{n(x,\mu)!} \right) \left[\prod_x \left(\sum_{s_x=\pm 1} s_x^{\sum_\mu n(x,\mu)+n(x-\hat{\mu},\mu)} \right) \right] \quad (1.9) \\
&= \left(\prod_x \prod_\mu \frac{\beta^{n(x,\mu)}}{n(x,\mu)!} \right) \left[\prod_x Q(k(x)) \right], \quad (1.10)
\end{aligned}
$$

where we introduced the *site occupation number*

$$
k(x) = \sum_\mu n(x,\mu) + n(x - \hat{\mu}, \mu), \quad (1.11)
$$

which counts the total number of bonds that are connected to the site x, and the *site weight*

$$
Q(k) = \sum_{s_x \pm 1} s_x^k. \quad (1.12)
$$

For the Ising model we can perform the summation over the two spin states explicitly, yielding the site weight

$$
Q(k) = \begin{cases} 2 & \text{if} \quad k = 0 \bmod 2, \\ 0 & \text{if} \quad k = 1 \bmod 2. \end{cases} \quad (1.13)
$$

In order to get a non-zero weight W, we are thus left with the constraint of $k(x)$ being an even number at each site x. For the Ising model, we finally end up with a particularly simple form for the weight of a constrained path,

$$
W \equiv W_{\mathcal{Z}} = 2^N \left(\prod_x \prod_\mu \frac{\beta^{n(x,\mu)}}{n(x,\mu)!} \right), \quad (1.14)
$$

where the constraint is given by

$$
k(x) \bmod 2 = 0 \quad \forall x. \quad (1.15)
$$
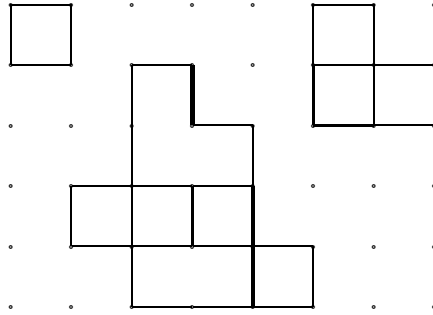
Figure 1.1: Graphical representation of a typical constrained path configuration $\{n(x,\mu)\} \in \mathcal{Z}$ on a lattice with the extent of $L_1 \times L_2 = 8 \times 6$. Lattice points are depicted with circles. The thickness of the solid lines is proportional to the bond occupation number $n(x,\mu)$. Note that the total number of bonds running into one site is even for all sites.

All bond configurations $\{n(x,\mu)\}$ which satisfy condition eq.(1.15) belong to the configuration space of constrained path configurations CP. So far, we have only encountered configurations which contribute to the partition function Z, such that they satisfy eq.(1.11) in addition. We abbreviate the configuration space of these configurations with $\mathcal{Z}$, supplying the weights eq.(1.14) with the same letter as subscript, $W_{\mathcal{Z}} \equiv W$. The partition function is then given by the sum over all these weights,

$$Z = \sum_{\{n(x,\mu)\} \in \mathcal{Z}} W_{\mathcal{Z}}(\{n(x,\mu)\}). \tag{1.16}$$

In figure 1.1 an example of a constrained path configuration in the configuration space $\mathcal{Z}$ is displayed.

This is the reformulation of the partition function of the Ising model where the degrees of freedom, e.g. the spin variables $s_x \in \{-1, 1\}$, have been replaced by bond numbers $n(x,\mu) \in \mathbb{N}_0$.

1.2.2 The Spin-Spin Correlation Function

Now, let us consider the spin-spin correlation function. By definition, it is given by

$$\langle s_{x_1} s_{x_2} \rangle = G(x_1, x_2) = \frac{g(x_1 - x_2)}{Z}, \tag{1.17}$$

where

$$g(x_1 - x_2) = \sum_{\{s_x\}} s_{x_1} s_{x_2} \exp\left(\beta \sum_{\langle xy \rangle} s_x s_y\right).$$

(1.18)

In analogy to the configurations contributing to the partition function, we will abbreviate the configuration space of configurations contributing to g with $\mathcal{G}$. Configurations in $\mathcal{G}$ differ from configurations in $\mathcal{Z}$ in one respect: They carry an additional spin variable s at the sites x_1 and x_2. How this affects the weight of a configuration is most easily seen in eq.(1.9). If we insert the additional spin variables at sites x_1 and x_2, we find for the weight of a configuration in $\mathcal{G}$,

$$W_{\mathcal{G}} = \left(\prod_x \prod_\mu \frac{\beta^{n(x,\mu)}}{n(x,\mu)!}\right) \left[\prod_x \left(\sum_{\{s_x\}} s_x^{k(x)+\delta_{x_1,x}+\delta_{x_2,x}}\right)\right].$$

(1.19)

We now adapt the definition for the site occupation number eq.(1.11) and include the additional spin variables as

$$k(x) = \sum_\mu n(x,\mu) + n(x - \hat{\mu}, \mu) + \delta_{x_1,x} + \delta_{x_2,x}.$$

(1.20)

Using this definition, the weight $W_{\mathcal{G}}$ of a configuration in the configuration space $\mathcal{G}$ looks the same as the weight $W_{\mathcal{Z}}$ of a configuration in $\mathcal{Z}$,

$$W_{\mathcal{G}} = \left(\prod_x \prod_\mu \frac{\beta^{n(x,\mu)}}{n(x,\mu)!}\right) \left[\prod_x Q(k(x))\right].$$

(1.21)

In general, the additional spin variables change the weight of a configuration via the site weight $Q(k(x))$ at the sites x_1 and x_2. Yet, for the Ising model, the additional spin variables have no influence on the weight of a configuration since the site weight Q is independent of the site occupation number k. The constrained path condition eq.(1.15) also holds in the configuration space $\mathcal{G}$. Configurations with a non-zero weight in $\mathcal{G}$ therefore possess an odd number of bonds running into the sites x_1 and x_2 for $x_1 \neq x_2$. The additional variables s_{x_1} and s_{x_2} compensate for the odd bond occupation number. For $x_1 = x_2$, each bond configuration in $\mathcal{G}$ corresponds to a bond configuration in $\mathcal{Z}$, having an even number of bonds running into each site x. In figure 1.2 a typical configuration in the configuration space $\mathcal{G}$ is displayed.
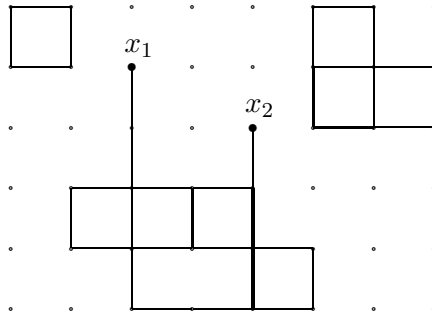
Figure 1.2: Graphical representation of an open worm configuration similar to the constrained path configuration figure 1.1. The configuration is in the configuration space $\mathcal{G}$ and contributes to the spin-spin expectation value $\langle s_{x_1} s_{x_2} \rangle$. An even total number of bonds is running into each site, except for the sites x_1 and x_2, where the additional spin variables s_{x_1} and s_{x_2} are represented by solid circles.

1.3 The Worm Algorithm

After the hopping expansion of the partition function and its decomposition into constrained paths, we are prepared to use this set-up for a Monte Carlo simulation. First, we present the worm algorithm as proposed in the original work by Prokof'ev and Svistunov [39]. In their set-up, the configuration space $\mathcal{G}$ is never left and the Monte Carlo estimator for Z, which is not accessible in the configuration space $\mathcal{G}$, is calculated via reweighing. Only then in a second step, we will discuss modifications of the worm algorithm which allow us to leave the configuration space $\mathcal{G}$ and to enter the configuration space $\mathcal{Z}$. This adaption of the originally proposed algorithm will be necessary when we deal with models which require the update of both a bosonic and a fermionic bond configuration.

In the following, we will derive the acceptance ratios $P_X(\varphi \to \varphi')$ for the transition from a given state φ to a new state φ' for all Monte Carlo update steps X. These acceptance ratios combine to the total acceptance probability $P_{A,X}(\varphi \to \varphi')$ for the update step in question as given in eq.(A.13),

$$P_{A,X}(\varphi \to \varphi') = \min\{1, P_X(\varphi \to \varphi')\}. \tag{1.22}$$

1.3.1 The Prokof'ev-Svistunov Worm Algorithm

In this section, we will follow the work of Prokof'ev and Svistunov to get an understanding of the worm algorithm. By doing so, we will adapt their terminology and conventions. First, we note that bond configurations in $\mathcal{Z}$ and those bond configurations in $\mathcal{G}$ contributing to $g(0)$ have identical bond elements. For the Ising model they even have identical weights since the site weight $Q(k) = 2$ is independent of the occupation number k. Thus, the Monte Carlo estimators for $g(x)$ and Z for an ergodic Metropolis algorithm sampling configurations in the configuration space $\mathcal{G}$ are updated according to their weights as

$$
\begin{aligned}
g(x|\mathcal{G}) &= g(x) + \delta_{x_1 - x_2, x}, & (1.23) \\
Z(\mathcal{G}) &= Z + \delta_{x_1 - x_2, 0}. & (1.24)
\end{aligned}
$$

The worm algorithm itself is based on the motion of the worm endpoints x_1 and x_2 on the lattice grid and is extremely simple. It consists of two elementary update steps which are proposed according to a given configuration. If $x_1 = x_2$, it is suggested with probability p_0 to *move* both endpoints to a randomly chosen site x_0 on the lattice. With probability $p_1 = 1 - p_0$, the proposition is to *shift* the endpoint x_1 to one of the neighbouring sites. In the following, we will call the endpoint x_1 *head*, as opposed to the endpoint x_2 which we will call *tail*. For a configuration where $x_1 \neq x_2$, the proposition is always to shift the head[2]. Thus, every Metropolis update step in the configuration space $\mathcal{G}$ automatically samples the two-point function and gives a contribution to $g(x)$. Detailed balance provides us with the acceptance ratios for each update step, which we will discuss in detail next. For pedagogical reasons, we consider it useful to derive the acceptance ratios including the site weights Q. For each acceptance ratio we then give the value for the Ising model which is independent of Q.

The Move Update Step

The move update involves removal of the additional spin variables at the site $x_1 = x_2 = x$ and their replacement at the site $x_1 = x_2 = y$. Thus, the site occupation number $k(x) \to k(x) - 2$ is decreased by 2 at the site x, whereas it is increased by 2 at the site y, such that $k(y) \to k(y) + 2$. In general, this

---

[2]As the additional spin variables are interchangeable, one could just as well move the tail instead of the head in the shift update step.

changes the site weights Q at both sites x and y, which is reflected in the move acceptance ratio $P_{\mathrm{mv}}(x \to y)$ via

$$P_{\mathrm{mv}}(x \to y) = \frac{Q(k(y) + 2)}{Q(k(y))} \frac{Q(k(x) - 2)}{Q(k(x))}. \tag{1.25}$$

Because for the Ising model the site weights Q are independent of the occupation number (see eq.(1.13)), the move uptate is automatically self-balanced,

$$P_{\mathrm{mv}}(x \to y) = 1. \tag{1.26}$$

The Shift Update Step

The shift update changes the bond configuration. Shifting the head to a next neighbour site is always associated with either an increase or a decrease of the bond occupation number between the sites x and y by one. In the following, we will use the shorthand notation

$$n_{xy} = \begin{cases} n(x, \mu) & \text{if } y = x + \hat{\mu}, \\ n(y, \mu) & \text{if } y = x - \hat{\mu}, \end{cases} \tag{1.27}$$

for the number of bonds between the sites x and y. In the graphical representation, the shift update corresponds to drawing or erasing one bond line between the sites x and y, respectively. The proposition whether to add or to subtract one bond is suggested with equal probability $1/2$. Furthermore, the next neighbour site to which the head shifts is chosen at random with probability $1/4$ for each site. The shifts $x \to y$ with $n_{xy} \to n_{xy} + 1$ are balanced with shifts $y \to x$ and $n_{xy} \to n_{xy} - 1$. This leads to the acceptance ratios

$$P_{\mathrm{sh}}(x \to y) = \begin{cases} r \dfrac{\beta}{n_{xy} + 1} \dfrac{Q(k(y) + 2)}{Q(k(y))} & \text{if } n_{xy} \to n_{xy} + 1, \\ r \dfrac{n_{xy}}{\beta} \dfrac{Q(k(x) - 2)}{Q(k(x))} & \text{if } n_{xy} \to n_{xy} - 1, \end{cases} \tag{1.28}$$

where we need to balance the move update via the factor

$$r = \begin{cases} \frac{1}{p_1} & \text{if } x_1 = x_2 = x, \\ p_1 & \text{if } x_1 = x; \ x_2 = y, \\ 1 & \text{otherwise}. \end{cases} \tag{1.29}$$

We thus see that the weight of one bond is β. Furthermore, each additional bond is suppressed with the factor $1/(n_{xy} + 1)$. For the Ising model, the acceptance ratios simplify to

$$P_{\text{sh}}(x \to y) = \begin{cases} r\dfrac{\beta}{n_{xy} + 1} & \text{if } n_{xy} \to n_{xy} + 1, \\ r\dfrac{n_{xy}}{\beta} & \text{if } n_{xy} \to n_{xy} - 1. \end{cases} \tag{1.30}$$

This is the worm algorithm as proposed by Prokof'ev and Svistunov. Using these update steps, one has a very efficient algorithm for the simulation of the Ising model at hand. However, for later purposes, we need an algorithm which is able to switch between the configuration spaces $\mathcal{Z}$ and $\mathcal{G}$. The necessary modifications are discussed next.

1.3.2 The Modified Algorithm

As mentioned above, it is also possible to leave the configuration space $\mathcal{G}$ by removing the additional spin variables s_{x_1} and s_{x_2} from the lattice. Considering eq.(1.13) it becomes clear that this is only possible if $x_1 = x_2$. Otherwise, the removal of the spin variables would lead to a bond configuration with an odd site occupation number at sites x_1 and x_2 and thus with zero weight. In the modified algorithm, similarly to the original version of the algorithm, we probe the configuration space $\mathcal{G}$ to sample the Monte Carlo estimator for $g(x)$ which we update via

$$g(x|\mathcal{G}) = g(x) + \delta_{x_1 - x_2, x}. \tag{1.31}$$

However, we do not sample the estimator for Z via reweighing as before. Instead, we modify the move update step in such a way, that it actually corresponds to a *remove* step. For $x_1 = x_2$, we suggest with probability p_{rm} to remove both additional spin variables, and with probability $p_1 = 1 - p_{\text{rm}}$ to shift the head. By removing the additional spin variables, we leave the configuration space $\mathcal{G}$ and enter the configuration space $\mathcal{Z}$. Once the additional spin variables are removed, we suggest to put them back at a randomly chosen site on the lattice with probability 1. For each update step where the system ends up in the configuration space $\mathcal{Z}$, the estimator for Z is updated as

$$Z(\mathcal{Z}) = Z + 1. \tag{1.32}$$

For $x_1 \neq x_2$, the algorithm proceeds by the usual worm update steps and shifts the head around the lattice. How the removal of the spin variables affects the acceptance ratios is discussed next.

The Remove Update Step

The remove step $x \to \varnothing$ is suggested with probability p_{rm} if $x_1 = x_2 = x$ and it is balanced with the step $\varnothing \to x$ where the additional spin variables are put back on the lattice at the same site. Therefore, for the remove step only the Q-ratio at site x is involved in the acceptance ratio via

$$P_{\mathrm{rm}}(x \to \varnothing) = \frac{1}{p_{\mathrm{rm}}V} \frac{Q(k(x) - 2)}{Q(k(x))}, \tag{1.33}$$

which for the Ising model simplifies to

$$P_{\mathrm{rm}}(x \to \varnothing) = \frac{1}{p_{\mathrm{rm}}V}. \tag{1.34}$$

Note that we need to balance the proposition of continuing the worm if $x_1 = x_2$ via the factor p_{rm}. The additional factor V balances the proposition to put the variables s_{x_1} and s_{x_2} on the same site x when re-entering the configuration space $\mathcal{G}$. This update step which allows to switch from the configuration space $\mathcal{Z}$ to the configuration space $\mathcal{G}$ is called the *put* update step and its acceptance ratio is given by

$$P_{\mathrm{put}}(\varnothing \to x) = p_{\mathrm{rm}}V \frac{Q(k(x) + 2)}{Q(k(x))}, \tag{1.35}$$

which yields for the Ising model

$$P_{\mathrm{put}}(\varnothing \to x) = p_{\mathrm{rm}}V. \tag{1.36}$$

The Shift Update Step

The shift update is the same as for the originally proposed algorithm. Thus, the acceptance ratios are given in eq.(1.28) involving arbitrary Q-ratios and in eq.(1.30) for the Ising model. Remember that the probability p_1 in eq.(1.29) for the modified algorithm is given by $p_1 = 1 - p_{\mathrm{rm}}$. This algorithm, of course, yields the same results as the one proposed by Prokof'ev and Svistunov.

The worm algorithm for the Ising model in this representation has all the features we will encounter for the worm algorithm for bosonic fields in quantum field theory. Yet, we can also reformulate the Ising model such that the resulting worm algorithm has similar features to the worm algorithm for fermionic fields.

1.4 Other Formulations of the Ising Model

We have now discussed in great detail the hopping expansion and the worm algorithm for the Ising model. Still, we consider it instructive to elaborate a little further on this model. For example, it is possible to reformulate the model such that after the hopping expansion, one ends up with a reduced configuration space where the bond occupation number is restricted to 0 and 1. On the one hand, this improves the efficiency of the worm algorithm further. On the other hand, the reduction of the configuration space leads to a representation of the bond configurations which is very similar to the 8-vertex representation for fermions [65]. For an extensive study of the Ising model, the interested reader is referred to [66].

1.4.1 The Dimer Formulation

Since the Ising model is particularly simple, we can use a geometric relation to reduce the configuration space in the constrained path representation, keeping the exactness of the expansion. The spin variables only take the values $s_x = \pm 1$, such that the identity

$$e^{\beta s_x s_y} = \cosh(\beta)(1 + \tanh(\beta)s_x s_y) = \cosh(\beta) \sum_{n=0}^{1} \tanh^n(\beta)(s_x s_y)^n \quad (1.37)$$

holds. Using this identity, we rewrite the partition function eq.(1.4) as

$$Z = \cosh^{2N}(\beta) \sum_{\{s_x\}} \left[\prod_x \prod_\mu \left(\sum_{n(x,\mu)=0}^{1} \tanh^{n(x,\mu)}(\beta)(s_x s_{x+\hat\mu})^{n(x,\mu)} \right) \right], \quad (1.38)$$

where we have reduced the bond configuration space from configurations with $n(x,\mu) \in \mathbb{N}_0$ to configurations with $n(x,\mu) \in \{0,1\}$. We will call this formulation the dimer formulation. Analogously to the fully expanded representation, we reformulate the partition function in terms of constrained paths where we derive the weight of a constrained path configuration with fixed $n(x,\mu) \in \{0,1\}$ as

$$
\begin{aligned}
W_{\mathcal{Z}} &= \cosh^{2N}(\beta) \sum_{\{s_x\}} \left[\prod_x \prod_\mu \left(\tanh^{n(x,\mu)}(\beta)(s_x s_{x+\hat\mu})^{n(x,\mu)} \right) \right] \\
&= 2^N \cosh^{2N}(\beta) \prod_x \prod_\mu \tanh^{n(x,\mu)}(\beta). \quad (1.39)
\end{aligned}
$$
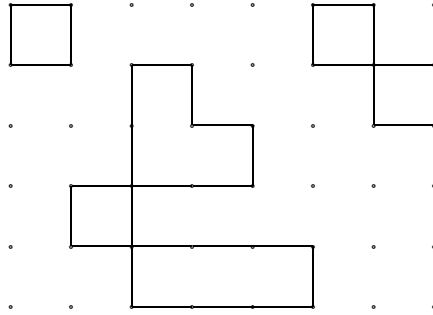
Figure 1.3: Constrained path configuration in the dimer representation similar to the constrained path configuration depicted in figure 1.1. In the dimer formulation, the number of bonds $n(x, \mu) \in \{0, 1\}$. Note, that an even number of bonds is running into each site, forming undirected closed loops.

This is in analogy to eq.(1.14) in the formulation with the complete expansion. The constrained path condition eq.(1.15) holds in this formulation as well. In the dimer formulation, the constrained paths are therefore self-crossing non-backtracking loops. In figure 1.3 an example of a bond configuration in the dimer formulation is displayed.

The reduction of the configuration space allows the introduction of the 8-vertex model. In the 8-vertex model, the lattice is divided into plaquettes, one for each lattice site. For the Ising model, there are eight such plaquettes, hence the name, out of which every possible bond configuration can be composed. Each plaquette is associated with a specific weight, such that the total weight of the configuration is given by the product of all weights of the used plaquettes.

The worm algorithm in the dimer formulation is slightly modified with respect to the original algorithm. We can still decide whether the algorithm samples the configuration space $\mathcal{G}$ and updates the estimator for Z via reweighing or switches between the configuration spaces $\mathcal{G}$ and $\mathcal{Z}$ by removing and replacing the additional spin variables. Therefore, the move/remove update step remains the same as before. What changes is the shift update step. Since $n_{xy} \in \{0, 1\}$, we do not let the algorithm propose randomly whether the bond occupation number n_{xy} should be increased or decreased. Rather, the algorithm decides randomly in which direction the head is shifted. If in this

$w = 2\cosh^2(\beta)\tanh(\beta)$

$w = 2\cosh^2(\beta)\tanh(\beta)$

$w = 2\cosh^2(\beta)\tanh(\beta)$

$w = 2\cosh^2(\beta)\tanh(\beta)$

$w = 2\cosh^2(\beta)\tanh(\beta)$

$w = 2\cosh^2(\beta)\tanh(\beta)$

$w = 2\cosh^2(\beta)$

$w = 2\cosh^2(\beta)\tanh^2(\beta)$
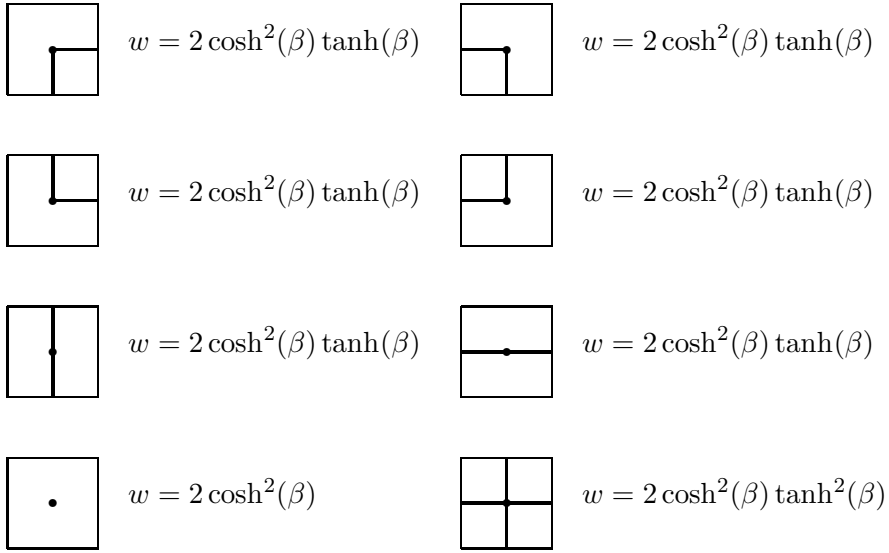
Figure 1.4: The eight different plaquettes for the 8-vertex model and their respective weights w. Note that straight lines are equally favourable as corners, which follows from comparing the weights of the plaquettes in question. The weight of an empty site is $2\cosh^2(\beta)$ and the weight of a bond is $\tanh(\beta)$, which combine to the total weight w of a plaquette according to the number of bonds running into a site.

direction a bond already exists, the algorithm automatically proposes to re-move the bond, whereas if there is no bond, the suggestion is always to add a bond.

As discussed, we can read off the acceptance ratios for the move update from eqs.(1.25,1.26) and the ones for the remove/put update from eqs.(1.33,1.34) and eqs.(1.35,1.36), respectively.

The shift update step is modified such that for a shift $x \to y$ and $n_{xy} = 1$ the proposition is always to remove the bond, $n_{xy} \to 0$, while for $n_{xy} = 0$ the proposition is always to add a bond, $n_{xy} \to 1$. Detailed balance gives us the acceptance ratios as

$$
P_{\text{sh}}(x \to y) = \begin{cases} r \tanh(\beta) & \text{if } n_{xy} = 0, \\ r\dfrac{1}{\tanh(\beta)} & \text{if } n_{xy} = 1, \end{cases} \tag{1.40}
$$

where the factor r balances the move/remove update step and can be read off from eq.(1.29). The weight for a bond is given by $\tanh(\beta)$, which is also reflected in the weights w of the plaquettes of figure 1.4.

After the reformulation of the Ising model in terms of bonds, the question of a physical interpretation of a constrained path arises. As it turns out, the dimer formulation is equivalent to yet another representation with a very obvious physical meaning. For completeness, we quickly discuss this formulation as well.

1.4.2 The Dual Lattice Formulation

For this other formulation we need to introduce not only a lattice Λ on which the spin variables are sitting, but also its dual Λ^D. In figure 1.5, we show an example for Λ and Λ^D.

We now consider an arbitrary spin configuration on the lattice Λ. We separate next neighbouring spins pointing in the opposite direction by placing a bond on the dual lattice Λ^D, thus forming domains with spins pointing in the same direction as shown in figure 1.6. From eq.(1.3), we see that the contribution to the partition function for two next neighbouring spins s_{x_1} and s_{x_2} with opposite sign is $e^{-\beta}$, while it is e^{β} for two next neighbouring spins with the
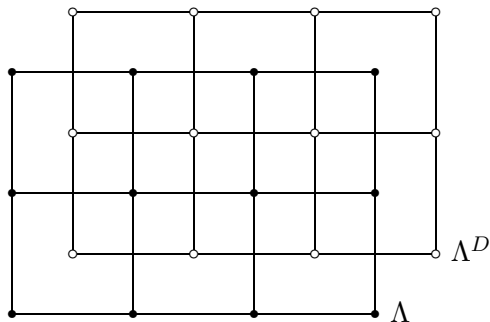
Figure 1.5: The physical lattice Λ with a spin variable sitting on each lattice site, represented by solid dots, and its dual lattice Λ^D, whose lattice sites are represented by circles.

same sign. As we set a bond on the dual lattice between two spins with opposite sign, the weight of the configuration changes by a factor $\mathrm{e}^{-2\beta}$. Thus, this factor of $\mathrm{e}^{-2\beta}$ corresponds to the weight of one bond in the dual formulation.

In this representation, we see what the algorithm does. A closed loop separates domains of spins oriented in the same direction. Opening a loop thus generates a non-interpretable state which becomes again physically manifest when the loop closes, generating a new distribution of domains with spins pointing in the same direction.

We now find a translation to get from the dual lattice formulation to the dimer formulation and vice versa. In order to do so, we write down the weights for a constrained path for each representation. We recall eq.(1.39) and identify the weight for a constrained path configuration in the dual representation $W_{\mathcal{Z}}^D$ on a lattice with N sites as

$$W_{\mathcal{Z}}^D = 2\mathrm{e}^{2\beta^D(N-N_b)}, \tag{1.41}$$

where we introduced $N_b = \sum_x \sum_\mu n(x,\mu)$, the total bond number of a configuration. A configuration in the dimer formulation is a priori not distinguishable from a configuration in the dual formulation because the systems are *self-dual*. Therefore, we identify the weights of the bonds to be the same ones in both formulations,

$$\mathrm{e}^{-2\beta^D} = \tanh(\beta). \tag{1.42}$$
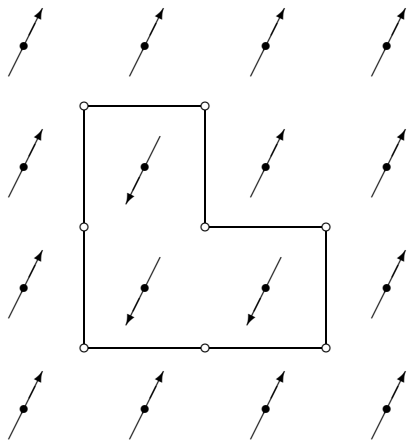
Figure 1.6: Arbitrary spin configuration on a $L_1 \times L_2 = 4 \times 4$ lattice Λ. Spins with an opposite sign are separated by a bond on the dual lattice Λ^D. Thus, similarly to figure 1.3, closed loops are formed. In contrast to the dimer formulation, these configurations live on the dual lattice.

The transition from one formulation to the other is then achieved by transforming the coupling parameter as

$$\beta^D = -\frac{1}{2}\ln(\tanh(\beta)), \tag{1.43}$$

and scaling the weights by an overall factor of $2^{N-1}\cosh^N(\beta)\sinh^N(\beta)$. Up to this transformation, both formulations are identical. The self-duality of the systems further allows us to locate the critical coupling parameter β_c by demanding $\beta^D = \beta = \beta_c$ in eq.(1.43). One finds

$$\beta_c = \frac{1}{2}\ln\left(1 + \sqrt{2}\right) = 0.440686\dots. \tag{1.44}$$

1.5 The Measurement of Observables

The formulations above have in common that we have replaced the original degrees of freedom, the spin variables $s_x = \pm 1$, by the bond occupation number $n(x, \mu)$ between sites x and $x + \hat{\mu}$. In the original formulation with the spin variables, observables are normally measured via exactly these spin variables.

Therefore, we need to address the question of how we can measure observables in the bond formulation. We illustrate how to do this with the help of three examples, the internal energy, the specific heat and the mass gap.

The Internal Energy U

We start with two examples which concern observables expressed in terms of expectation values of bond occupation numbers. The simplest example is the internal energy U. It is defined as the expectation value of the energy, $U = \langle E \rangle$, such that it can be calculated as

$$\langle E \rangle = \frac{1}{Z} \sum_\varphi E_\varphi e^{-\beta E_\varphi} = -\frac{1}{Z} \frac{\partial Z}{\partial \beta} = -\frac{\partial}{\partial \beta} \ln(Z). \tag{1.45}$$

Hence, the internal energy is given by minus the derivative of the logarithm of the partition function with respect to β. In order to find an expression for the internal energy in terms of bonds, we can make use of this formula. Deriving

$$-\frac{\partial}{\partial \beta} \ln(Z) = -\frac{1}{Z} \frac{\partial}{\partial \beta} \sum W_{\mathcal{Z}}, \tag{1.46}$$

where $W_{\mathcal{Z}}$ is given by eq.(1.14), we find that the internal energy is proportional to the expectation value for the total bond number,

$$\langle E \rangle = -\frac{1}{\beta} \langle N_b \rangle. \tag{1.47}$$

In the dimer formulation, $W_{\mathcal{Z}}$ is given by eq.(1.39), and we find analogously

$$\langle E \rangle^{\text{dim}} = -\tanh(\beta) \left(2N + \frac{1}{\sinh^2(\beta)} \langle N_b \rangle \right). \tag{1.48}$$

As the dimer formulation and the dual lattice formulation are equivalent, the expectation value $\langle \mathcal{O} \rangle^{\text{dim}}$ of any observable $\mathcal{O}$ holds for both formulations.

The Specific Heat C

Similarly to the expectation value of the energy, one can calculate the expectation value of the square of the energy $\langle E^2 \rangle$ via derivatives of Z as

$$\langle E^2 \rangle = \frac{1}{Z} \sum_\varphi E_\varphi^2 e^{-\beta E_\varphi} = \frac{1}{Z} \frac{\partial^2 Z}{\partial \beta^2}. \tag{1.49}$$

The quantities $\langle E \rangle$ and $\langle E^2 \rangle$ combine to the specific heat C as

$$C = \beta^2 \left(\langle E^2 \rangle - \langle E \rangle^2 \right) = \beta^2 \frac{\partial^2 \ln(Z)}{\partial \beta^2}. \tag{1.50}$$

We then find for the specific heat expressed in expectation values of the total bond numbers

$$C = \langle N_b^2 \rangle - \langle N_b \rangle - \langle N_b \rangle^2, \tag{1.51}$$

and in the dimer formulation

$$C^{\mathrm{dim}} = \frac{\beta^2}{\cosh^2(\beta)} \left[2N + \frac{1}{\sinh^2(\beta)} \left(\langle N_b^2 \rangle - \langle N_b \rangle^2 \right) - \left(1 + \frac{1}{\tanh^2(\beta)} \right) \langle N_b \rangle \right]. \tag{1.52}$$

The Mass Gap

Finally, we calculate the mass gap for the Ising model via the spin-spin correlation function at fixed spatial momentum. We label the site vectors x being now on a torus with Euclidean time and one space dimension $T \times L$ as $x \equiv (t, x^1)$[3]. The correlation function $G_{p_1}(t)$ at fixed momentum $p_1 \in \{0, \frac{2\pi}{L}k\}$, $k = 0, \ldots, L-1$, is then calculated via the Fourier transformation of the spatial correlation function as

$$G_{p_1}(t) = \sum_{x^1} G(t, x^1) \mathrm{e}^{-i p_1 x^1}. \tag{1.53}$$

The notation for the spatial correlation function here is a compact form of the one introduced in section 1.2.2 and stands for $G(x_1, x_2) = G(x_1 - x_2, 0) = G((\Delta t, \Delta x), (0,0)) \equiv G(t, x^1)$. For the mass gap, one needs the correlation function for zero momentum, such that

$$G_0(t) = \sum_{x^1} G(t, x^1)^4. \tag{1.54}$$

The effective mass m_{eff} is defined as the rate with which the time-dependent correlation function decays,

$$G_0(t) \sim \exp\left(-m_{\mathrm{eff}} t \right). \tag{1.55}$$

---

[3]It should be clear from the context, that x^1 here denotes the spatial component of the two-component vector x. This is in contrast to x_1 which is itself a two-component vector and denotes the lattice point where the additional spin variable s_{x_1} is inserted.

[4]Note, that we can alternatively define directly the Monte Carlo estimator $g_0(t|\mathcal{G}) = g_0(t) + \delta_{t_1 - t_2, t}$, where $x_i \equiv (t_i, x_i^1)$, such that $G_0(t) = g_0(t)/Z$.
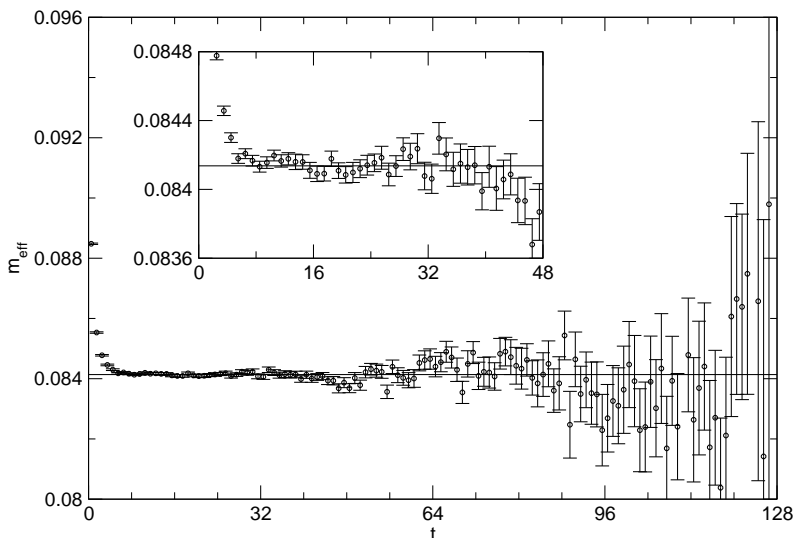
Figure 1.7: The Ising model in the dimer formulation. Effective mass plateau for a lattice of the extent $T \times L = 256 \times 64$ at $\beta = 0.42$ for $Z = 5 \cdot 10^9$. The horizontal line represents the exact result.

The spin variables for the spin-spin correlation function are interchangeable, such that the correlation function for a finite lattice of the extent T is symmetric around $T/2$. The correlation function is therefore composed of two exponentials which combine to a cosh function

$$G_0(t) = A \cosh\left(m_{\text{eff}}(T/2 - t)\right). \tag{1.56}$$

It is now possible to extract the time-dependent effective mass at a time $t+1/2$ by solving the ratio

$$\frac{G_0(t+1)}{G_0(t)} = \frac{\cosh\left(m_{\text{eff}}(T/2 - (t+1))\right)}{\cosh\left(m_{\text{eff}}(T/2 - t)\right)}. \tag{1.57}$$

numerically for m_{eff}. For $t \gg 1$, the contributions from higher excited states vanish and the ratio approaches the true mass gap, forming a plateau. In figure 1.7, we show an example for the effective mass plateau on a lattice of the extent $T \times L = 256 \times 64$. The simulation for the Ising model in the dimer formulation has been performed near the critical point $\beta = 0.42$ for an extensive run of $Z = 5 \cdot 10^9$.

The figure shows a mass plateau which reproduces the exact result from [67] for this set-up, $m_{\mathrm{eff}} = 0.084137\ldots$, to a very high precision. Those contributions to the effective mass which are due to higher excited states vanish for $t > 6$. For $t > 6$, the exact result is confirmed within statistical errors.

Note, that the bond formulation for the Ising model excludes cancellations for *any* observable. This lack of negative contributions can be traced back to the summation over the degrees of freedom for the spin variables in eq.(1.12). As a consequence, cancellations in the update process are completely eliminated and all estimators are improved.

Chapter 2

Supersymmetric Quantum Mechanics

In this chapter, we review the basics of supersymmetric quantum mechanics. As the lattice field approach of supersymmetric quantum mechanics in the chapters 3, 4, and 5 is the centrepiece of this thesis, we consider it to be useful to put some effort into gaining familiarity with supersymmetric quantum mechanics in the Schroedinger formulation first. The introductory theoretical part is guided by the textbook by Cooper, Khare, and Sukhatme [68] and [69].

To start with, we will review the construction of supersymmetric quantum systems via factorisation of the Hamiltonian operator. The question of a deeper understanding of the main feature of supersymmetric systems, namely the degeneracy of the energy levels, will lead to a discussion of the underlying algebra. The gained insight will allow us to relate the degeneracy of the energy levels in supersymmetric quantum mechanics to the degeneracy of bosonic and fermionic masses in supersymmetric quantum field theories. After these considerations in the context of unbroken supersymmetry, we will review the concept of broken supersymmetry and conclude the theoretical part with the introduction of the Witten index.

After having established the theoretical framework of supersymmetric quantum mechanics in the first part of the chapter, we will employ numerical methods to solve the Schroedinger equation for different supersymmetric quantum systems in the second part. The reason for these investigations are twofold. On the one hand, we will calculate physical situations which are analogous to the situations in our field theoretical approach. The results for both unbroken and broken supersymmetry will serve us in chapters 4 and 5 to confirm our lattice results directly. On the other hand, we will reveal the mechanisms of the non-trivial transition of supersymmetric quantum systems from broken supersymmetry to unbroken supersymmetry and vice versa.

2.1 Supersymmetry and the Schroedinger Equation

2.1.1 The Factorisation of the Hamilton Operator

We start with the one-dimensional Schroedinger equation for a single particle of mass m in a potential V_1, for which the Hamilton operator is given by

$$H_1 = -\frac{\hbar^2}{2m}\frac{d^2}{dx^2} + V_1(x). \tag{2.1}$$

We will now construct a supersymmetric quantum system by factorising the Hamilton operator H_1. In one dimension and for a bounded non-negative Hamilton operator, this is always possible. For such a Hamilton operator, any potential can be shifted by a constant such that its ground state energy equals zero. Without loss of generality, we are thus allowed to assume that the ground state energy of H_1 is zero, $E_0^{(1)} = 0$. The Schroedinger equation for the ground state then reads

$$-\frac{\hbar^2}{2m}\frac{d^2}{dx^2}\psi_0(x) + V_1(x)\psi_0(x) = 0. \tag{2.2}$$

Once we introduce the operators

$$A = \frac{\hbar}{\sqrt{2m}}\frac{d}{dx} + \frac{1}{\sqrt{2}}W(x), \qquad A^\dagger = -\frac{\hbar}{\sqrt{2m}}\frac{d}{dx} + \frac{1}{\sqrt{2}}W(x), \tag{2.3}$$

and write the Hamilton operator as a product of these operators,

$$H_1 = A^\dagger A, \tag{2.4}$$

we identify the potential V_1 as

$$V_1(x) = \frac{1}{2}\left(W^2(x) - \frac{\hbar}{\sqrt{m}}W'(x)\right). \tag{2.5}$$

The quantity W is called *prepotential*[1]. We define the operator A to act on ψ_0 as

$$A\psi_0(x) = 0. \tag{2.6}$$

---

[1]In the literature, there is a lot of ambiguity about the naming of the quantity W. In the context of supersymmetric quantum mechanics, W is usually referred to as superpotential. This is somewhat misleading, as W carries dimension of $E^{1/2}$. Furthermore, this is in contradiction to superfield formalism in field theory. There, another quantity P arises, which is called superpotential as well. To be consistent throughout this work, we choose the term *prepotential* for W and the term *superpotential* for P.

The Schroedinger equation for the ground state is then automatically satisfied since

$$H_1\psi_0(x) = A^\dagger A\psi_0(x) = 0. \tag{2.7}$$

We now define a second Hamilton operator H_2 where the order of the operators A and $A^\dagger$ is reversed,

$$H_2 = AA^\dagger. \tag{2.8}$$

Using the representation eq.(2.3) of the operators A and $A^\dagger$, we find that H_2 corresponds to the Hamilton operator

$$H_2 = -\frac{\hbar^2}{2m}\frac{d^2}{dx^2} + V_2(x) \tag{2.9}$$

with the potential

$$V_2(x) = \frac{1}{2}\left(W^2(x) + \frac{\hbar}{\sqrt{m}}W'(x)\right). \tag{2.10}$$

The potentials V_1 and V_2 are called supersymmetric partner potentials. We shall see in the following that the eigenvalues and eigenstates of H_1, containing the potential V_1, and H_2, containing the partner potential V_2, are related. To reveal the connection between the Hamilton operators H_1 and H_2, we first note that the eigenvalues of H_1 and H_2 by construction are positive semi-definite, $E_n^{(1,2)} \geq 0$. Now, we consider the Schroedinger equation for H_1 and $n > 0$,

$$H_1\psi_n^{(1)}(x) = A^\dagger A\psi_n^{(1)} = E_n^{(1)}\psi_n^{(1)}. \tag{2.11}$$

This implies for the eigenstates of H_2 that

$$H_2(A\psi_n^{(1)}) = AA^\dagger A\psi_n^{(1)} = AH_1\psi_n^{(1)} = E_n^{(1)}(A\psi_n^{(1)}). \tag{2.12}$$

Thus, we find that the operator A, acting on an eigenstate $\psi_n^{(1)}$ of H_1 with $n > 0$, transforms this state into an eigenstate of H_2. Yet, the energy of the state is not affected by the transformation under A. Analogously, we proceed for the Schroedinger equation for H_2.

$$H_2\psi_n^{(2)} = AA^\dagger\psi_n^{(2)} = E_n^{(2)}\psi_n^{(2)}, \tag{2.13}$$

implies that

$$H_1(A^\dagger\psi_n^{(2)}) = A^\dagger AA^\dagger\psi_n^{(2)} = A^\dagger H_2\psi_n^{(2)} = E_n^{(2)}(A^\dagger\psi_n^{(2)}). \tag{2.14}$$

In this case, an eigenstate $\psi_n^{(2)}$ of H_2 is converted into an eigenstate of H_1 when the operator $A^\dagger$ acts on it. As previously the operator A, the operator $A^\dagger$ leaves invariant the energy of the state it acts upon. We are now able to establish the following relations between the eigenvalues and the eigenstates of the two Hamilton operators H_1 and H_2:

$$E_0^{(1)} = 0, \tag{2.15}$$

$$E_n^{(2)} = E_{n+1}^{(1)}, \tag{2.16}$$

$$\psi_n^{(2)} = \frac{1}{\sqrt{E_{n+1}^{(1)}}} A\psi_{n+1}^{(1)}, \tag{2.17}$$

$$\psi_{n+1}^{(1)} = \frac{1}{\sqrt{E_n^{(2)}}} A^\dagger \psi_n^{(2)}. \tag{2.18}$$

For energies larger than zero, the spectra of the Hamilton operators H_1 and H_2 are therefore degenerate. However, there is an additional zero energy ground state for the Hamilton operator H_1. In figure 2.1, the energy levels for both H_1 and H_2 are represented schematically. Furthermore, applying the operator $A^\dagger$ to a given eigenstate of H_1 converts this eigenstate into an eigenstate of H_2 with the same energy, whereas the operator A acts in the opposite way.

The concept of supersymmetry and the factorisation of the Hamilton operator has a wide variety of applications. They range from the construction of isospectral potentials and finding solutions thereof to the calculation of scattering amplitudes. Supersymmetry applies also in the context of periodic potentials and it can even be used to solve the Dirac equation for massive particles in external fields. For a thorough discussion of these applications, the interested reader is referred to [68].

2.1.2 The Supersymmetry Algebra

The reason for the degeneracy of the energy spectra of H_1 and H_2 lies within the properties of the underlying supersymmetry algebra. In this paragraph, we will work out the algebra and discuss its implications. We start by combining the Hamilton operators H_1 and H_2 in a matrix Hamilton operator of the form

$$H = \begin{pmatrix} H_1 & 0 \\ 0 & H_2 \end{pmatrix}. \tag{2.19}$$
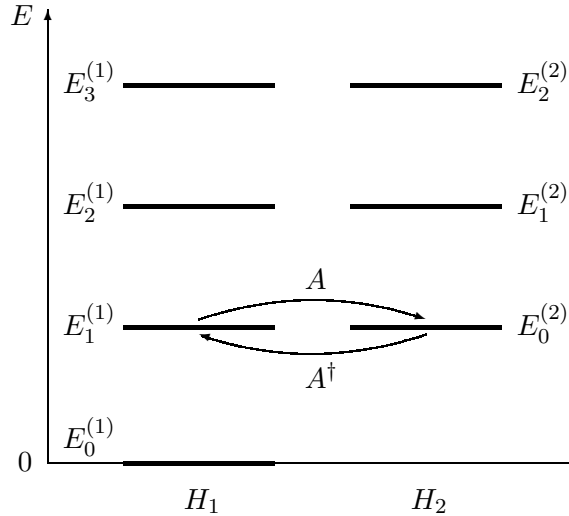
Figure 2.1: The energy spectra of the Hamilton operators H_1 and H_2. All energy levels are exactly degenerate, except for the additional zero energy level for H_1. The operators A and $A^\dagger$ convert eigenstates of H_1 into eigenstates of H_2 and vice versa, respectively. The energy of the states is not affected by the operators A and $A^\dagger$.

H acts on the combined Hilbert space $\mathcal{H} = \mathcal{H}_1 \otimes \mathcal{H}_2$. Using block notation, the vectors in this space have the components

$$\psi = \begin{pmatrix} \psi^{(1)} \\ \psi^{(2)} \end{pmatrix}. \tag{2.20}$$

We now adapt the matrix representation for the creation and annihilation operators $A^\dagger$ and A by incorporating them in the definition of the *supercharge operators* $\mathcal{Q}$ and $\mathcal{Q}^\dagger$ as

$$\mathcal{Q} = \begin{pmatrix} 0 & 0 \\ A & 0 \end{pmatrix}, \qquad \mathcal{Q}^\dagger = \begin{pmatrix} 0 & A^\dagger \\ 0 & 0 \end{pmatrix}. \tag{2.21}$$

The supercharge operators form together with the Hamilton operator H the closed superalgebra $sl(1/1)$ with the commutation relations,

$$[H, \mathcal{Q}] = [H, \mathcal{Q}^\dagger] = 0, \tag{2.22}$$

and the anticommutation relations

$$\{\mathcal{Q}, \mathcal{Q}^\dagger\} = H, \qquad \{\mathcal{Q}, \mathcal{Q}\} = \{\mathcal{Q}^\dagger, \mathcal{Q}^\dagger\} = 0. \tag{2.23}$$

31

Now, eq.(2.22) implies that the source of the degeneracy of the spectra of H_1 and H_2 is inherent in the supersymmetry algebra. Moreover, we observe that the algebra contains commutation relations, which are a characteristic of bosonic variables, as well as anticommutation relations, which are a characteristic of fermionic variables. It is thus tempting to interpret the operators $\mathcal{Q}$ and $\mathcal{Q}^\dagger$ as fermionic operators which change bosonic degrees of freedom into fermionic degrees of freedom and vice versa. This interpretation would also imply that the Hamilton operator H is a bosonic operator. We will verify this assumption in the next paragraph using the example of a supersymmetric harmonic oscillator.

2.1.3 The Supersymmetric Harmonic Oscillator

In the following, we give reasons why the supercharge operators indeed change bosonic degrees of fermions into fermionic ones and vice versa. Starting from the construction of a supersymmetric quantum mechanical harmonic oscillator, we generalise the concept to an arbitrary supersymmetric quantum mechanical theory.

The Harmonic Oscillator

Before we start with the construction of a supersymmetric harmonic oscillator, we briefly review the characteristics of the regular quantum mechanical harmonic oscillator in terms of ladder operators. The Hamilton operator for the harmonic oscillator is given by

$$H = \frac{p^2}{2m} + \frac{1}{2}m\omega^2 x^2. \tag{2.24}$$

As we are only interested in the conceptual idea, we will set $m = \hbar = \omega = 1$ for convenience. Energies will then be expressed in units of $\hbar\omega$. The Hamilton operator thus simplifies to

$$H = \frac{1}{2}p^2 + \frac{1}{2}x^2. \tag{2.25}$$

The coordinate operator x and the momentum operator p obey the commutation relation

$$[x, p] = i. \tag{2.26}$$

Dirac proposed to use the ladder operators a (the lowering operator) and its adjoint $a^\dagger$ (the rising operator) to find the energy spectrum without having

to solve differential equations. The ladder operators are composed of the coordinate operator x and the momentum operator p and their explicit representation is given by

$$a = \frac{1}{\sqrt{2}}(x + ip), \qquad a^\dagger = \frac{1}{\sqrt{2}}(x - ip). \tag{2.27}$$

It is easy to see that they fulfil the commutation relation

$$[a, a^\dagger] = 1^2. \tag{2.28}$$

The states of the harmonic oscillator are now built upon the ground state $|0\rangle$ which is defined via

$$a|0\rangle = 0. \tag{2.29}$$

The ladder operators act on any state $|n\rangle$ as

$$a|n\rangle = \sqrt{n}|n - 1\rangle, \qquad a^\dagger|n\rangle = \sqrt{n+1}|n + 1\rangle. \tag{2.30}$$

Apparently, the lowering operator has the property of decreasing the state by one, whereas the rising operator increases the state by one, hence their names. The n-th excited state can thus be calculated from the ground state via

$$|n\rangle = \frac{(a^\dagger)^n}{\sqrt{n!}}|0\rangle. \tag{2.31}$$

The ladder operators can be combined to the number operator $N = a^\dagger a$ whose eigenvalues are the numbers of the states it acts on,

$$N|n\rangle = n|n\rangle. \tag{2.32}$$

Expressing the operators x and p through the ladder operators a and $a^\dagger$, the Hamilton operator eq.(2.25) can be written in terms of the number operator,

$$H = N + \frac{1}{2}. \tag{2.33}$$

This form of H is very convenient because one can simply read off the energy spectrum of the harmonic oscillator to be

$$E_n = n + \frac{1}{2}. \tag{2.34}$$

---

[2]This commutation relation corresponds to the commutation relation for a bosonic field variable. In the following, the ladder operators a and $a^\dagger$ are therfore referred to as *bosonic* operators.

The Supersymmetric Harmonic Oscillator

We now extend the quantum mechanical harmonic oscillator to a supersymmetric harmonic oscillator. To do so, we write the supercharge operators $\mathcal{Q}$ and $\mathcal{Q}^\dagger$ as a product of the bosonic creation and annihilation operators $a^\dagger$ and a and the newly introduced fermionic creation and annihilation operators $\psi^\dagger$ and ψ as

$$\mathcal{Q} = a\psi^\dagger, \qquad \mathcal{Q}^\dagger = a^\dagger\psi. \tag{2.35}$$

The fermionic operators obey the usual algebra for fermionic creation and annihilation operators, i.e. they satisfy the anticommutation rules

$$\{\psi^\dagger, \psi\} = 1, \qquad \{\psi, \psi\} = \{\psi^\dagger, \psi^\dagger\} = 0. \tag{2.36}$$

In matrix representation, they are defined as

$$\psi = \begin{pmatrix} 0 & 1 \\ 0 & 0 \end{pmatrix}, \qquad \psi^\dagger = \begin{pmatrix} 0 & 0 \\ 1 & 0 \end{pmatrix}. \tag{2.37}$$

From the definition eq.(2.37) follows the commutation relation

$$[\psi, \psi^\dagger] = \sigma_3 = \begin{pmatrix} 1 & 0 \\ 0 & -1 \end{pmatrix}, \tag{2.38}$$

such that the Hamilton operator for the supersymmetric harmonic oscillator can be written as

$$H = \{\mathcal{Q}, \mathcal{Q}^\dagger\} = \begin{pmatrix} H_1 & 0 \\ 0 & H_2 \end{pmatrix} = \left(-\frac{1}{2}\frac{d^2}{dx^2} + \frac{1}{2}x^2 \right) \mathbb{1} - \frac{1}{2}[\psi, \psi^\dagger]. \tag{2.39}$$

Note the term which is proportional to the commutator of the the fermionic annihilation and creation operators. On the one hand, this term removes the zero point energy $E_0^{(1)} = 1/2$ for the Hamilton operator H_1. On the other hand, it increases the energies of the Hamilton operator H_2 by the same value, such that the zero point energy $E_0^{(2)} = 1/2$ is lifted up to $E_0^{(2)} = 1$. The spectra of the two harmonic oscillators are thus indeed degenerate up to the zero energy level for H_1. The supersymmetric harmonic oscillator is illustrated in figure 2.2.

Let us now consider the Fock space for the supersymmetric harmonic oscillator. The state vectors in this Fock space $|n_b, n_f\rangle = |n_b\rangle \otimes |n_f\rangle$ contain the bosonic
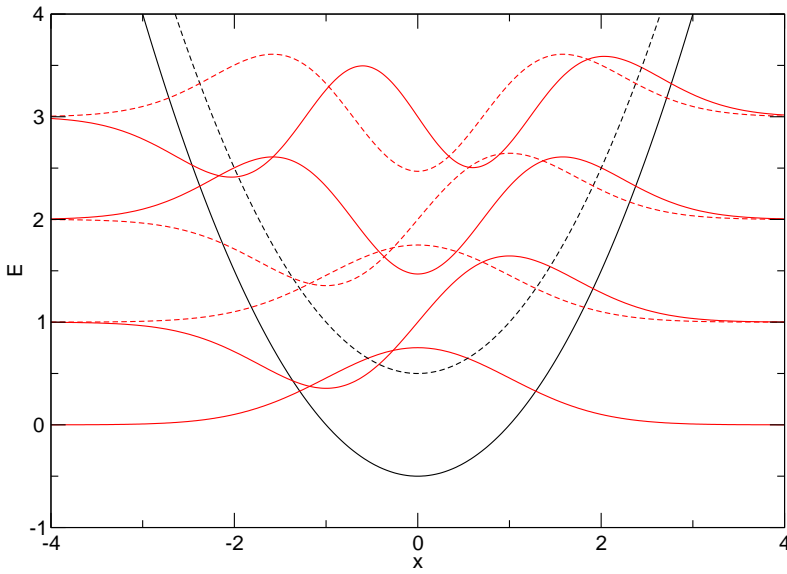
Figure 2.2: The supersymmetric harmonic oscillator. The partner potentials V_1 (solid black line) and V_2 (dashed black line). Wave functions represented with a solid line (dashed line) are eigenfunctions to the Hamilton operator H_1 (H_2).

quantum numbers n_b and the fermionic ones n_f. We have chosen the ground state of H_1 to have zero fermion number $n_f \equiv F = 0$, such that we can introduce the fermion number operator

$$N_f = \frac{1}{2} \left(1 - [\psi, \psi^\dagger] \right).$$

(2.40)

Remember that because of the anticommutation relations eq.(2.36), the fermion number F is restricted to 0 and 1. With the above definition of the Fock space states, the bosonic operators and the fermionic operators act on these states as

$$
\begin{aligned}
a|n_b, n_f\rangle &= \sqrt{n_b}|n_b - 1, n_f\rangle & (2.41) \\
a^\dagger|n_b, n_f\rangle &= \sqrt{n_b + 1}|n_b + 1, n_f\rangle & (2.42) \\
\psi|n_b, n_f\rangle &= |n_b, n_f - 1\rangle & (2.43) \\
\psi^\dagger|n_b, n_f\rangle &= |n_b, n_f + 1\rangle. & (2.44)
\end{aligned}
$$

Obviously, the operator $\mathcal{Q} = a\psi^\dagger$ changes a bosonic state into a fermionic one, while the operator $\mathcal{Q}^\dagger = a^\dagger\psi$ acts in the opposite way, converting a fermionic state into a bosonic one. However, the operators $\mathcal{Q}$ and $\mathcal{Q}^\dagger$ do not change the energy of the state they are acting on. Thus, the degeneracy of the energy levels which is inherent to all supersymmetric theories becomes manifest. To construct the general form of a supersymmetric theory, one replaces in the definition of $\mathcal{Q}$ and $\mathcal{Q}^\dagger$ the creation and annihilation operators for the harmonic oscillator $a^\dagger$ and a with the bosonic operators $A^\dagger$ and A of eq.(2.3), e.g. $\mathcal{Q} = A\psi^\dagger$ and $\mathcal{Q}^\dagger = A^\dagger\psi$. Modifying eq.(2.39) in this way, we get the Hamilton operator for a general supersymmetric quantum mechanical theory,

$$H = \left(-\frac{\hbar^2}{2m} \frac{d^2}{dx^2} + \frac{1}{2} W^2(x) \right) \mathbb{1} - \frac{1}{2} \frac{\hbar}{\sqrt{m}} W'(x) [\psi, \psi^\dagger].$$

(2.45)

Restoring all units, we find that the prepotential for the supersymmetric harmonic oscillator is given by

$$W(x) = \sqrt{m}\omega x.$$

(2.46)

2.1.4 Broken Supersymmetry

The above considerations explain the degeneracy of the spectra of H_1 and H_2. They hold because we imposed condition eq.(2.6) from the beginning.

Let us now proceed the other way around. Starting from a given prepotential $W(x)$, we derive the constraints on $W(x)$ under which the differential equation eq.(2.6) leads to a normalisable ground state wave function with zero energy. By construction, we only allow the ground state wave function $\psi_0^{(1)}(x)$ to be a candidate for the zero-energy mode. Through this choice, we associate the Hamilton operator H_1 with the bosonic states and fermion number $F = 0$, and the Hamilton operator H_2 with the fermionic states where $F = 1$. We observe that the solution of eq.(2.6) is given by

$$\psi_0^{(1)}(x) \propto \exp\left(-\frac{\sqrt{m}}{\hbar} \int^x dx' W(x') \right). \tag{2.47}$$

Thus, we realise that the wave function is only normalisable if we impose that

$$\lim_{x\to\pm\infty} W(x) = \pm\infty. \tag{2.48}$$

Otherwise, there is no normalisable ground state wave function $\psi_0^{(1)}$ for $E_0 = 0$. To see the implication of a normalisable zero-energy ground state, we need to recall the concept of spontaneous symmetry breaking. Consider a symmetry transformation under which the Hamilton operator of a theory is invariant. Now, if the ground state of the theory is not invariant under the same symmetry transformation, the symmetry is said to be broken spontaneously. Thus, for a symmetry to be unbroken, the generator of the symmetry transformation needs to annihilate the ground state. For supersymmetric quantum mechanics, this amounts to

$$\mathcal{Q}|0\rangle = \mathcal{Q}^\dagger|0\rangle = 0. \tag{2.49}$$

Since the Hamilton operator commutes with both supercharges, eq.(2.22), eqs.(2.49) immediately imply that unbroken supersymmetry is always associated with a ground state of zero energy. For the case where there is no normalisable zero-energy ground state, e.g. for a polynomial prepotential where the highest power N is even,

$$W(x) = \sum_{i=0}^{N} g_i x^i, \tag{2.50}$$

the ground state $|0\rangle$ is not annihilated by the supercharges $\mathcal{Q}$ and $\mathcal{Q}^\dagger$. Thus, supersymmetry is broken spontaneously, yielding degenerate, positive ground state energies $E_0^{(1)} = E_0^{(2)} > 0$ for both Hamilton operators H_1 and H_2.
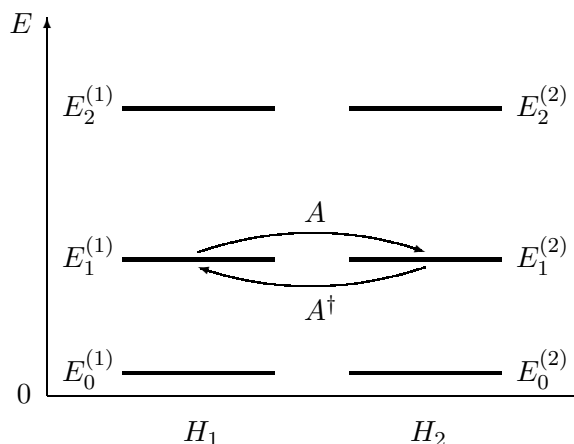
Figure 2.3: Broken supersymmetry. Schematic representation of the energy spectra of the Hamilton operators H_1 and H_2. All energy levels are exactly degenerate. Note that the lowest energy levels are lifted, such that $E_0^{(1)} = E_0^{(2)} > 0$. The operators A and $A^\dagger$ take the system from the bosonic to the fermionic sector and vice versa without affecting the energy of the state they are acting on.

Analogously to eq.(2.15) for unbroken supersymmetry, we can now establish a set of relations between the partner Hamilton operators H_1 and H_2 for broken supersymmetry:

$$E_n^{(i)} > 0, \qquad \forall n, \qquad i = 1, 2 \tag{2.51}$$

$$E_n^{(1)} = E_n^{(2)}, \tag{2.52}$$

$$\psi_n^{(2)} = \frac{1}{\sqrt{E_n^{(1)}}} A \psi_n^{(1)}, \tag{2.53}$$

$$\psi_n^{(1)} = \frac{1}{\sqrt{E_n^{(2)}}} A^\dagger \psi_n^{(2)}. \tag{2.54}$$

In figure 2.3, the energy levels with these characteristics are represented graphically for both Hamilton operators H_1 and H_2.

2.1.5 The Witten Index

In his seminal work on supersymmetry breaking [70], Witten introduced the quantity

$$\Delta = n_b^0 - n_f^0, \tag{2.55}$$

to count the difference of the number of bosonic zero energy states n_b^0 and the number of fermionic zero energy states n_f^0. Formally it is defined as

$$\Delta = \mathrm{Tr}\left[(-1)^F\right],\tag{2.56}$$

where F is the fermion number operator. For supersymmetric quantum mechanics the object $(-1)^F$ can be represented by the Pauli matrix σ_3. The eigenvalues of $(-1)^F$ are then ± 1 and in our conventions, the eigenvalue $+1$ corresponds to the Hamilton operator H_1 and thus to the bosonic system, whereas the eigenvalue -1 corresponds to the Hamilton operator H_2, which is associated with the fermionic system. In the case of unbroken supersymmetry, there is one single bosonic state with $E = 0$ and we thus expect $\Delta = 1$. For broken supersymmetry, there are no zero energy states such that $\Delta = 0$.

In field theories, the Witten index needs to be regulated via the inverse temperature β,

$$\Delta(\beta) = \mathrm{Tr}\left[(-1)^F \mathrm{e}^{-\beta H}\right].\tag{2.57}$$

For the case of supersymmetric quantum mechanics, the regulated Witten index reads

$$\Delta(\beta) = \mathrm{Tr}\left[\mathrm{e}^{-\beta H_1}\right] - \mathrm{Tr}\left[\mathrm{e}^{-\beta H_2}\right].\tag{2.58}$$

Thus, the Witten index needs to be calculated in dependence of β and only then one can take the limit $\lim_{\beta \to 0} \Delta(\beta)$.

2.2 Numerical Analysis of Supersymmetric Quantum Mechanics

To get a picture of supersymmetric quantum mechanics, we first solve the one-dimensional Schroedinger equation numerically by approximating both the lowest energy levels and the corresponding wave functions for the partner Hamilton operators H_1 and H_2. To perform these calculations, we employ the shooting method which is based on the Numerov algorithm. These techniques are explained thoroughly in appendix E.

In the following analysis, we will investigate supersymmetric quantum systems with both unbroken and broken supersymmetry. In particular, we will treat exactly the same situations as we will consider in the language of $(1 + 0)$-dimensional field theory in the chapters 4 and 5. The degeneracy of the mass

spectrum for bosons and fermions is the key feature of supersymmetric field theories. In the case of supersymmetric quantum mechanics, the mass gaps translate to energy gaps in the Schroedinger formalism. Solving the Schroedinger equation for the energy levels will therefore yield results which are directly comparable to the mass gaps obtained in the field theoretical framework. Furthermore, in the course of a thorough numerical study of the Schroedinger equation, we will reveal the underlying mechanisms of the non-trivial transition from unbroken to broken supersymmetry and vice versa.

In the following calculations, we will set the mass of the particle governing the kinetic part of the Schroedinger equation $m = 1$. Furthermore, we will work in natural units, such that we also set $\hbar = 1$. For each case we consider in this section, we will introduce the quantity μ in the prepotential which corresponds to the bare mass in lattice field theory. All energies are expressed in units of this parameter μ.

2.2.1 Unbroken Supersymmetry

The Energy Spectrum for Fixed Coupling

Our first step is the numerical treatment of unbroken supersymmetric quantum mechanics. To allow for a normalisable zero energy ground state, our choice for the prepotential is the simplest polynomial of odd degree for which the potential V is non-zero,

$$W(x) = \mu x + g x^3. \tag{2.59}$$

This prepotential describes exactly the same physics as we will consider in our formulation in the language of field theory. Therefore, the results obtained in this section will be directly comparable with the results obtained from our calculations in field theory. The partner potentials V_1 and V_2 we derive from this prepotential are

$$V_1(x) = \frac{1}{2} \left(\mu^2 x^2 + 2\mu g x^4 + g^2 x^6 - \mu - 3gx^2 \right), \tag{2.60}$$

$$V_2(x) = \frac{1}{2} \left(\mu^2 x^2 + 2\mu g x^4 + g^2 x^6 + \mu + 3gx^2 \right). \tag{2.61}$$

We now introduce the dimensionless coupling $f = g/\mu^2$ which governs the physics of the system. For our numerical investigations we choose a coupling strength of $f = 1$, which lies well outside of the perturbative regime. The

n	$E_n^{(1)}/\mu$	$E_n^{(2)}/\mu$
0	0.0000000	1.6865005
1	1.6865005	4.3718166
2	4.3718166	7.6309535
3	7.6309535	11.3748469
4	11.3748469	15.5397848
5	15.5397848	20.0819162

Table 2.1: Unbroken supersymmetric quantum mechanics. The lowest energy levels for a coupling strength $f = 1$.

lowest energies for this coupling strength are shown in table 2.1[3]. They are degenerate except for the additional zero energy ground state for the Hamilton operator H_1. The degeneracy of the energy levels is visualised in figure 2.4 where the partner potentials V_1 and V_2 and the wave functions of the lowest energy modes are displayed.

Transition from Unbroken Supersymmetry to the Free Case

We next investigate the dependence of the energy levels on the coupling f. In the limit $f \to 0$, the partner potentials eqs.(2.60) go over into these of the supersymmetric harmonic oscillator smoothly. In figure 2.5, the transition of V_1 and V_2 is visualised by choosing different couplings f and plotting the partner potentials accordingly. Note that for couplings stronger than the critical coupling $f_c = 1/3$, the potential V_1 develops the shape of a double well potential. The reason for the rather trivial transition from unbroken supersymmetry to the free case lies in the fact that taking the limit $f \to 0$ maintains unbroken supersymmetry even for a coupling exactly at $f = 0$. For any coupling f, the spectrum is thus degenerate up to the characteristic additional zero energy ground state $E_0^{(1)} = 0$ for H_1. In figure 2.6, the lowest energy levels for both Hamilton operators H_1 and H_2 are drawn in dependence of the coupling f.

---

[3]Note, how accurately the algorithm resolves the energy levels for each partner potential.

Figure 2.4: Unbroken supersymmetric quantum mechanics. The partner potentials V_1 (solid line) and V_2 (dashed line) at $f = 1$. Wave functions represented with a solid line (dashed line) are eigenfunctions of the Hamilton operator H_1 (H_2).

2.2.2 Broken Supersymmetry

The Energy Spectrum for Fixed Coupling

Now we turn to quantum mechanics with broken supersymmetry. The condition on a polynomial prepotential for broken supersymmetry is that is must be of even degree. Our choice in this case is the even function

$$W(x) = -\frac{\mu^2}{4\lambda} + \lambda x^2. \tag{2.62}$$

Also this prepotential describes the same physics as we will consider in our formulation in field theory and thus yield directly comparable results. The partner potentials for broken supersymmetry we work with are then

$$V_1(x) = \frac{\mu^4}{32\lambda^2} - \lambda x - \frac{\mu^2}{4}x^2 + \frac{\lambda^2}{2}x^4, \tag{2.63}$$

$$V_2(x) = \frac{\mu^4}{32\lambda^2} + \lambda x - \frac{\mu^2}{4}x^2 + \frac{\lambda^2}{2}x^4. \tag{2.64}$$

Figure 2.5: Unbroken supersymmetric quantum mechanics. The partner potentials V_1 (black) and V_2 (red) for different coupling strengths $f = 0.0$ (solid line), $f = f_c = 0.33$ (dashed line), and $f = 5.0$ (dotted line).

The above partner potentials can be transformed into each other by the variable transformation $x \to -x$,

$$V_1(x) = V_2(-x). \tag{2.65}$$

Thus, the partner potentials V_1 and V_2 are related by a mirror symmetry and the energy levels for the prepotential in eq.(2.62) are trivially degenerate. The dimensionless coupling constant to govern the physics for this choice of a prepotential is $f = \lambda/\mu^{3/2}$. As before for unbroken supersymmetry, we choose a coupling strength of $f = 1$ for the numerical investigation of broken supersymmetry. Thus, we are in this case beyond the perturbative regime as well. The lowest energy levels are shown in table 2.2. All energy levels are degenerate and the ground state energy for both H_1 and H_2 is lifted above zero. Thus, all features expected for the energy levels of broken supersymmetry are numerically confirmed. The degeneracy of all energy levels is visualised in figure 2.7 where the partner potentials V_1 and V_2 and the wave functions of the lowest energy modes are displayed.
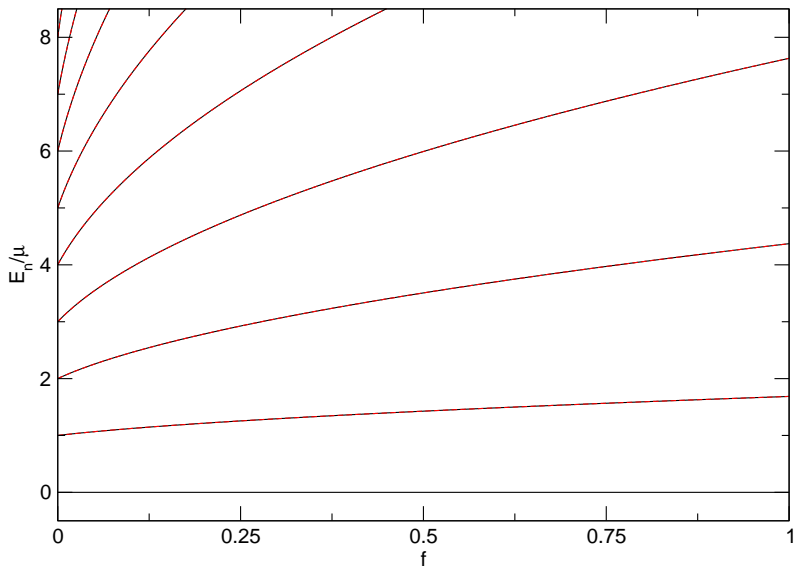
Figure 2.6: Unbroken supersymmetric quantum mechanics. Shown are the lowest energy levels versus f for H_1 (solid black line) and H_2 (dashed red line). In the limit $f \to 0$ the spectrum of the supersymmetric harmonic oscillator is recovered.

n	$E_n^{(1)}/\mu$	$E_n^{(2)}/\mu$
0	0.1685113	0.1685113
1	1.6731608	1.6731608
2	3.4040974	3.4040974
3	5.4276534	5.4276534
4	7.6694244	7.6694244
5	10.0948941	10.0948941

Table 2.2: Broken supersymmetric quantum mechanics. The lowest energy levels for a coupling strength of $f = 1$.
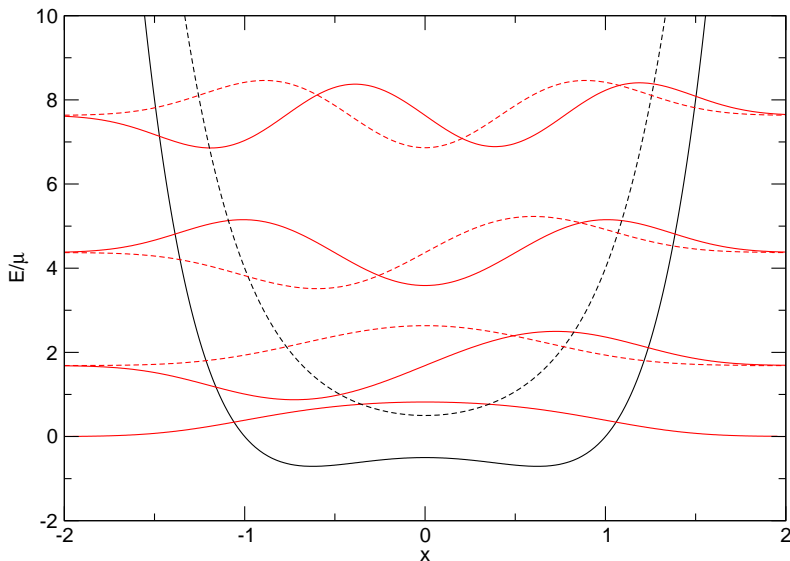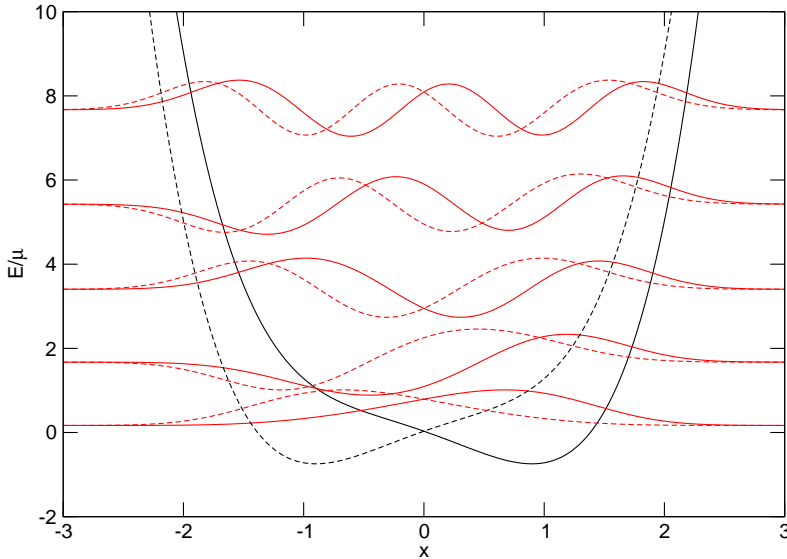
Figure 2.7: Broken supersymmetric quantum mechanics. The partner potentials V_1 (solid line) and V_2 (dashed line) at $f = 1$. Wave functions represented with a solid line (dashed line) are eigenfunctions of the Hamilton operator H_1 (H_2).

Transition from Broken Supersymmetry to the Free Case

Next, we investigate the dependence of the energy levels on the coupling strength f for broken supersymmetry. The transition from broken supersymmetry to the free case is much less trivial than the transition from unbroken supersymmetry to the free case. The system with broken supersymmetry has degenerate energy levels for any state $n \geq 0$ and strictly positive ground state energies $E_0^{(1)} = E_0^{(2)} > 0$ as long as $f \neq 0$. However, the free case at exactly $f = 0$ has unbroken supersymmetry and thus a single zero energy ground state for H_1. Thus, instead of a smooth transition, one of the ground states must disappear all of a sudden when $f = 0$. We will reveal in the following the mechanism behind this transition.

We find it instructive to consider first the partner potentials for different couplings f. Because we express all energies in units of μ, we have a certain freedom of choice for the parameters μ and λ to describe the same physical situation. Thus, by adjusting all parameters correctly, we can fix the minima of the potentials V_1 and V_2 at $x = 1$ and $x = -1$ for any coupling f, respec-
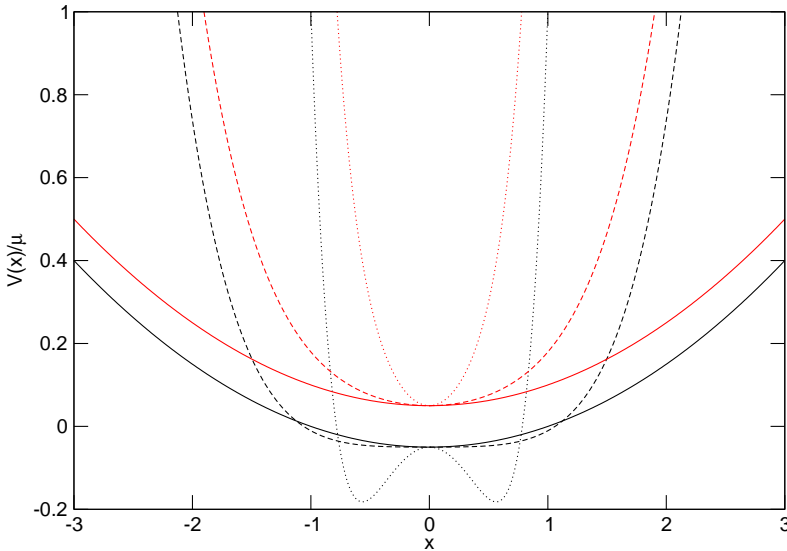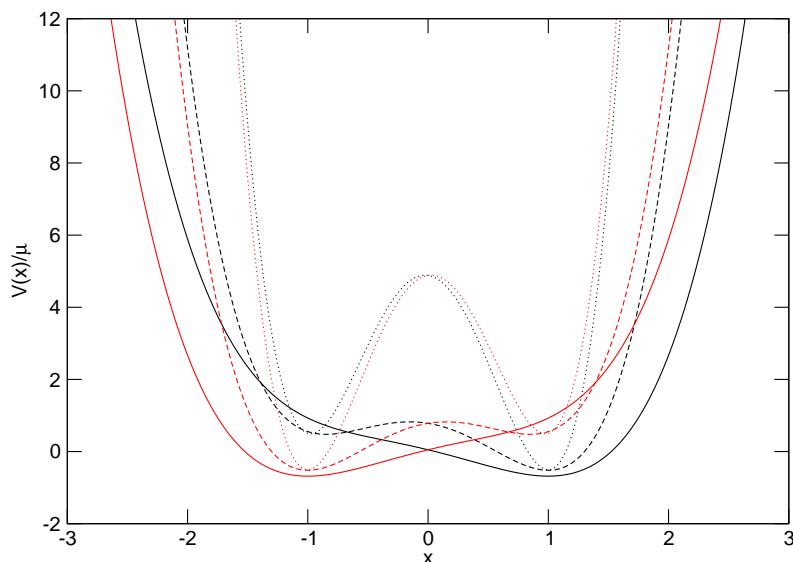
Figure 2.8: Broken supersymmetry. Partner potentials V_1 (black) and V_2 (red) for different coupling strengths $f = 0.8$ (solid line), $f = 0.2$ (dashed line), and $f = 0.08$ (dotted line). The minima are fixed at $x = \pm 1$.

tively[4]. We observe that the potentials develop a second well for couplings weaker than the critical value $f_c = 0.3102\ldots$ In the process where $f \to 0$, the potential barrier between the wells grows and the characteristic of a double well potential becomes more and more dominant. When $f \to 0$, the barrier becomes infinitely high and at the coupling $f = 0$, the partner potentials decouple completely into two independent supersymmetric harmonic oscillators around $x = \pm 1$. In figure 2.8 the transition of the partner potentials from a single well potential to a double well potential is visualised by plotting the partner potentials V_1 and V_2 for different couplings f.

It is now clear that the energy levels in each potential well must reach degeneracy in the limit where $f \to 0$. The well with the lower lying minimum, e.g. the ground state energy of the potential in question, must in addition have an unpaired energy that goes to zero. In figure 2.9, we plot the potential V_1 and the wave functions of the lowest energy levels for different coupling strengths

---

[4]This is achieved by solving the equation $\partial_x V_i(x) = \pm 1$ for μ. The resulting condition together with the definition of the f fixes the parameters μ and λ for any given coupling strength.

(a) $f = 2$

(b) $f = 0.31$

(c) $f = 0.12$

(d) $f = 0.08$
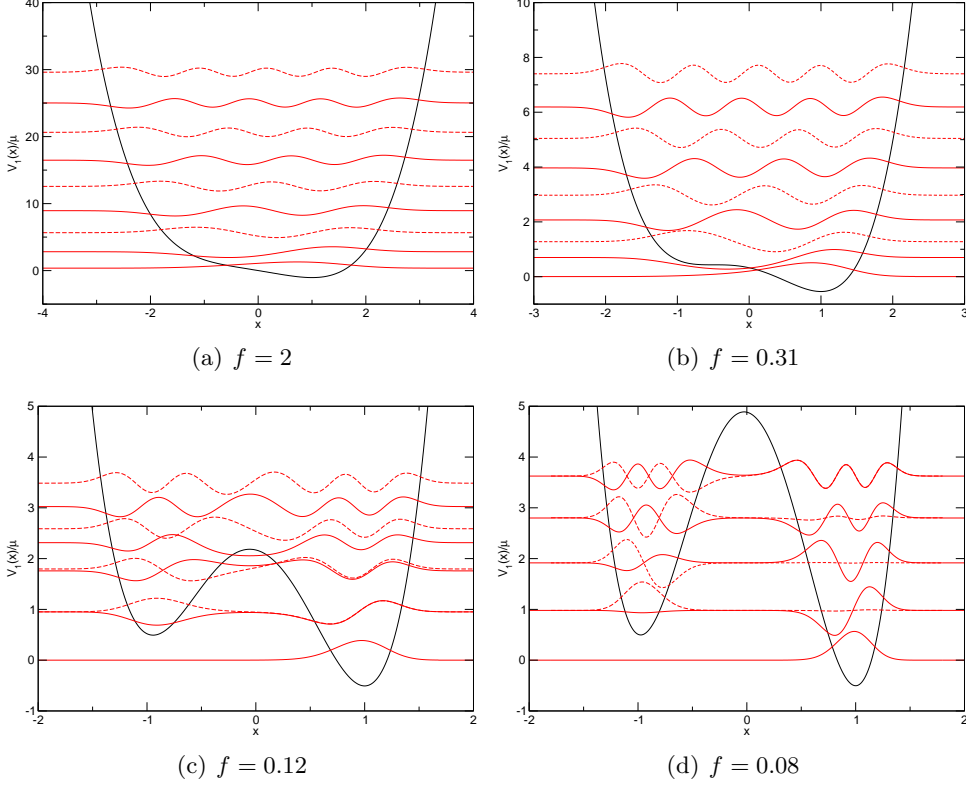
Figure 2.9: Broken supersymmetry. The potential V_1 for different couplings f. Wave functions represented by a solid line (dashed line) will in the limit $f = 0$ be associated with the oscillator on the right (on the left).

f. We observe that the degeneracy of the energy levels in both wells becomes apparent as the coupling becomes weaker. Since the lower energy levels are much more affected by the potential barrier, the degeneracy of these levels is reached first. Note that the amplitude of each wave function indicates with which well the respective energy is associated.

After this pre-analysis of the mechanism, we are now able to understand the transition from broken supersymmetry to the free and unbroken case. Each energy level must in fact become doubly degenerate for weaker couplings since on the one hand, the broken system is degenerate in H_1 and H_2. On the other hand, each partner potential itself yields degenerate energy levels for
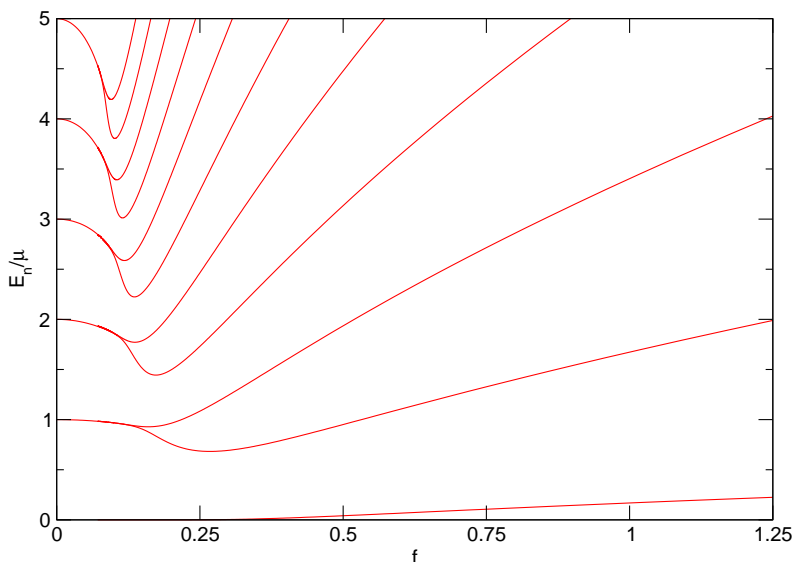
Figure 2.10: Broken supersymmetric quantum mechanics. Shown are the lowest energy levels of H_1 versus the coupling strength f.

both wells. From this double degeneracy, the ground state for both H_1 and H_2 is excluded. For each one of the Hamilton operators H_1 and H_2 the ground state sitting in the lower potential minimum remains unpaired when $f \to 0$. Thus, the ground state maintains only single degeneracy between H_1 and H_2 up to the point where $f = 0$, where one of the ground states decouples with the associated well. For a further illustration, we plot in figure 2.10 the lowest energies in dependence of the coupling f. The results are calculated for the Hamilton operator H_1. Due to the mirror symmetry of the partner potentials, calculating the energy levels for H_2 would, of course, yield the same diagram.

Perturbation Theory

It is interesting to compare the numerical results with perturbation theory in the weak coupling regime. As we need to do the perturbative expansion in the coupling parameter f, the form of the prepotential given in eq.(2.62) is not convenient. We observe, however, that performing a shift in the variable $x \to \tilde{x} = x + \frac{\mu}{2\lambda}$ of the partner potentials eq.(2.63) yields another pair of

partner potentials $\tilde{V}_1(\tilde{x})$ and $\tilde{V}_2(\tilde{x})$,

$$\tilde{V}_1(x) = \frac{\mu^2}{2}x^2 - \frac{\mu}{2} - \lambda(x - \mu x^3) + \frac{\lambda^2}{2}x^4, \qquad (2.66)$$

$$\tilde{V}_2(x) = \frac{\mu^2}{2}x^2 + \frac{\mu}{2} + \lambda(x + \mu x^3) + \frac{\lambda^2}{2}x^4, \qquad (2.67)$$

where the tilde for the variable x has been omitted for convenience. As a side remark, we note that these are the partner potentials one obtains by starting from the prepotential

$$\tilde{W}(x) = \mu x + \lambda x^2. \qquad (2.68)$$

If we express the parameter λ in terms of the coupling parameter f, we see that the potentials given in eqs.(2.66),

$$\tilde{V}_1(x) = \frac{\mu^2}{2}x^2 - \frac{\mu}{2} - f\mu^{3/2}(x - \mu x^3) + f^2\frac{\mu^3}{2}x^4, \qquad (2.69)$$

$$\tilde{V}_2(x) = \frac{\mu^2}{2}x^2 + \frac{\mu}{2} + f\mu^{3/2}(x + \mu x^3) + f^2\frac{\mu^3}{2}x^4, \qquad (2.70)$$

are perfectly suitable for a perturbative expansion. We now split the Hamilton operator into the free part H^0 and the perturbed part V^{I} and V^{II}, where the Roman superscript refers to the order in f at which the perturbation of the potential occurs,

$$\tilde{H}_i(x) = H_i^0 + fV_i^{\mathrm{I}} + f^2V_i^{\mathrm{II}}, \qquad i = 1, 2. \qquad (2.71)$$

Explicitly, the perturbation potentials read

$$V_1^{\mathrm{I}} = \mu^{3/2}(\mu x^3 - x), \quad V_2^{\mathrm{I}} = \mu^{3/2}(\mu x^3 + x), \quad V_{1,2}^{\mathrm{II}} = \frac{\mu^3}{2}x^4, \qquad (2.72)$$

and the free part $\tilde{H}_i^0$ corresponds to the supersymmetric harmonic oscillator. The first order corrections to the energies are then given by the matrix elements

$$E_n^{(i),\mathrm{I}} = \langle n^0|V_i^{\mathrm{I}}|n^0\rangle, \qquad (2.73)$$

where $|n^0\rangle$ denotes the nth eigenstate of an unperturbed harmonic oscillator. All these terms vanish identically. The corrections to second order are calculated as

$$E_n^{(i),\mathrm{II}} = \sum_{k \neq n} \frac{\langle k^0|V_i^{\mathrm{I}}|n^0\rangle}{E_n^{(i),0} - E_k^{(i),0}} + \langle n^0|V_i^{\mathrm{II}}|n^0\rangle. \qquad (2.74)$$

n	$E_n^{(1),\text{II}}/\mu$	$E_n^{(2),\text{II}}/\mu$
0	0	-3
1	-3	-12
2	-12	-27
3	-27	-48
4	-48	-75
5	-75	-108

Table 2.3: Broken supersymmetric quantum mechanics. The correction factors to the energies for perturbation theory to $\mathcal{O}(f^2)$.
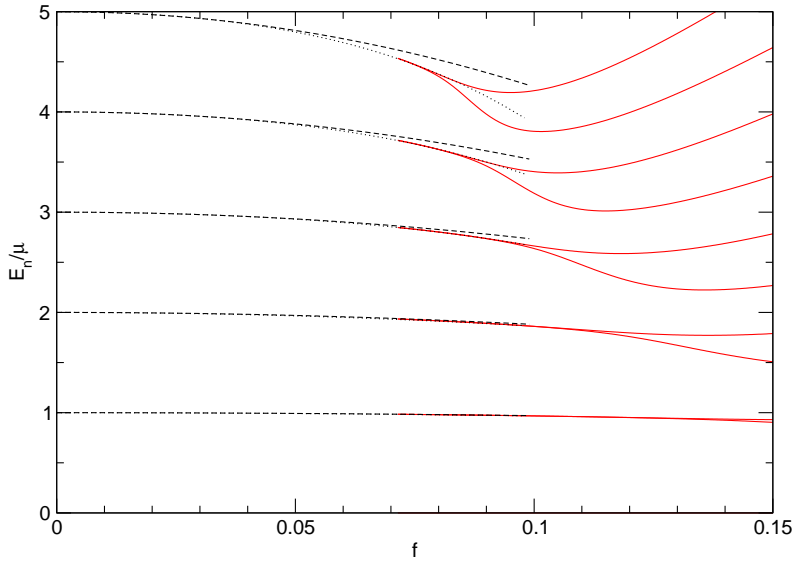
Figure 2.11: Broken supersymmetric quantum mechanics. Comparison of the perturbative result up to $\mathcal{O}(f^2)$ (dashed black line) to a quartic fit (dotted black line). The solid red lines are the numerical results.
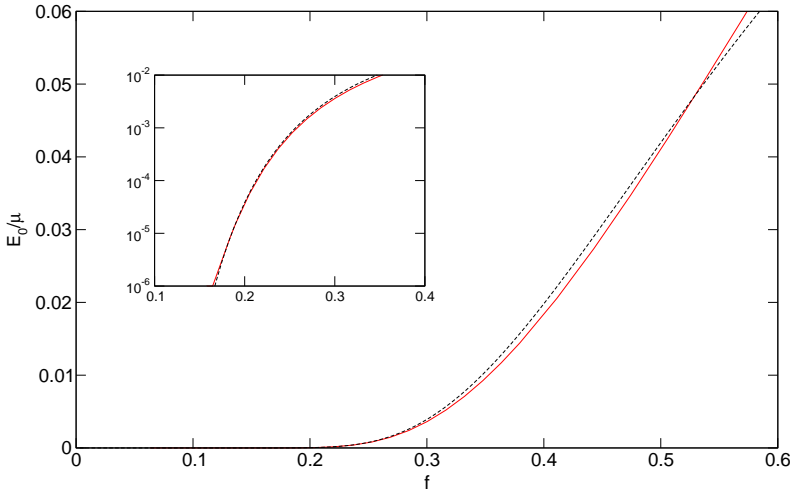
Figure 2.12: Broken supersymmetric quantum mechanics. Comparison of the WKB approximation (black line) with the numerical results for the ground state energy (red line).

The corrections to $\mathcal{O}(f^2)$ are shown in table 2.3 and in figure 2.11, the energies including second order corrections are compared to a quartic extrapolation fitted to the numerical values. The correction factor for the degenerate energy levels is equal for both Hamilton operators H_1 and H_2. Furthermore, we note that the second order correction to the zero energy groundstate of H_1 is zero, $E_0^{(1),\text{II}} = 0$. This is no coincidence, but rather one of the features of supersymmetric quantum mechanics. It is not possible to calculate corrections to the zero-energy ground state by means of standard perturbation theory. This phenomenon is called non-renormalisation theorem [71, 72] and it essentially states that spontaneous symmetry breaking cannot be seen via perturbation theory. Rather, it is necessary to employ semi-classical methods to find corrections for the ground state. Using for instance the WKB approximation, the correction to the ground state energy reads

$$E_0(f)/\mu \approx \frac{1}{2\pi} \exp\left(-\frac{1}{3f^2}\right). \tag{2.75}$$

The comparison of the WKB approximation of the ground state to the numerical results in figure 2.12 reveals that the WKB approximation scheme yields very adequate results for a coupling strength below $f = 0.60$ indeed.

2.2.3 Transition from Unbroken to Broken Supersymmetry

The only scenario that has not been addressed yet is the transition from unbroken supersymmetry to broken supersymmetry. This somehow resembles the inverse problem of the section above. For this set-up, however, the unbroken system maintains a zero energy mode which disappears when the system undergoes the transition to broken supersymmetry. To observe this transition, we choose a prepotential of the form

$$W(x) = -\frac{\mu^2}{4\lambda} + \lambda x^2 + gx^3. \tag{2.76}$$

The term proportional to g has an odd exponent and thus ensures that supersymmetry is unbroken. In the limit where $g \to 0$, this prepotential goes over into the prepotential eq.(2.62). Therefore, we should be able to recover the energy spectrum we have encountered for broken supersymmetry in this limit. The partner potentials we derive from this prepotential read

$$V_1(x) = \frac{\mu^4}{32\lambda^2} - \lambda x - \frac{\mu^2 + 6g}{4}x^2 - \frac{g\mu^2}{4\lambda}x^3 + \frac{\lambda^2}{2}x^4 + g\lambda x^5 + \frac{g^2}{2}x^6, \tag{2.77}$$

$$V_2(x) = \frac{\mu^4}{32\lambda^2} + \lambda x - \frac{\mu^2 - 6g}{4}x^2 - \frac{g\mu^2}{4\lambda}x^3 + \frac{\lambda^2}{2}x^4 + g\lambda x^5 + \frac{g^2}{2}x^6. \tag{2.78}$$

We define the physical situation by the two couplings we used in the previous considerations, $f_\lambda = \lambda/\mu^{3/2}$ and $f_g = g/\mu^2$. To observe the transition from unbroken to broken supersymmetry, we keep f_λ fixed, $f_\lambda = 1$, and take the limit where $f_g \to 0$.

First, we consider again the partner potentials for different couplings f_g. We observe that for strong couplings f_g and $x > 1$ the term $\backsim g^2/2$ is dominant and the potentials are centred around $x \approx 0$. In the process of the coupling f_g becoming smaller and smaller, the partner potentials develop a second well which is seperated from the well around $x \approx 0$ by a potential barrier. When f_g goes to zero, the potential barrier between the wells grows towards infinity. Simultaneously, the minimum of the left potential well shifts more and more to large negative values for x. When $f_g = 0$, the left potential well is located at minus infinity and therefore decouples completely from the system, leaving the potential well for broken supersymmetry for $f_\lambda = 1$. In figure 2.13 the transition from the single well partner potentials to the double well potentials is illustrated by plotting the partner potentials for different values of the coupling f_g.
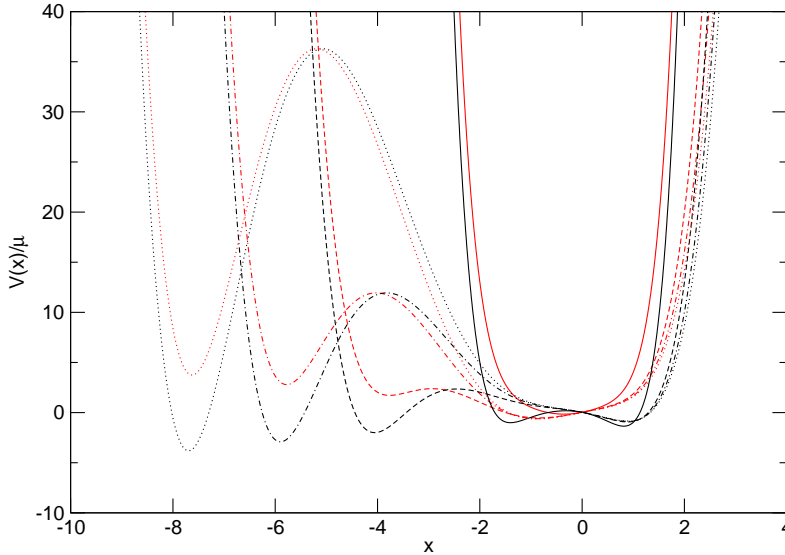
Figure 2.13: Transition unbroken to broken supersymmetry. Partner potentials V_1 (black) and V_2 (red) for different coupling strengths $f_g = 1$ (solid line), $f_g = 0.25$ (dashed line), $f_g = 0.17$ (dashed-dotted line), and $f_g = 0.13$ (dotted line).

Similarly to the transition from broken supersymmetry to the free case, for small couplings, each wave function is associated with one of both potential wells. This is again indicated by the amplitude of a wave function. As the zero energy mode needs to disappear for $f_g = 0$, this mode belongs to the potential well which is located at minus infinity in the limit $f_g = 0$. Furthermore, for finite coupling f_g, there are energy modes which do not appear in the spectrum of broken supersymmetric quantum mechanics. They also disappear together with the left well. What remains after the decoupling is the completely degenerate spectrum of broken supersymmetric quantum mechanics. The transition is illustrated in figure 2.14 where the partner potentials V_1 and V_2 and the wave functions for the lowest energies are plotted for different couplings f_g.

In figure 2.15, the complete energy spectrum is shown in dependence of the coupling f_g. There is one single zero energy mode for H_1 for all couplings $f_g \neq 0$. However, this mode vanishes with the associated potential well at $f_g = 0$. So do the energy levels which do not belong to the spectrum of broken supersymmetric quantum mechanics. In addition, these levels have the characteristic that they are pushed towards infinity when $f_g \to 0$. In the plot,
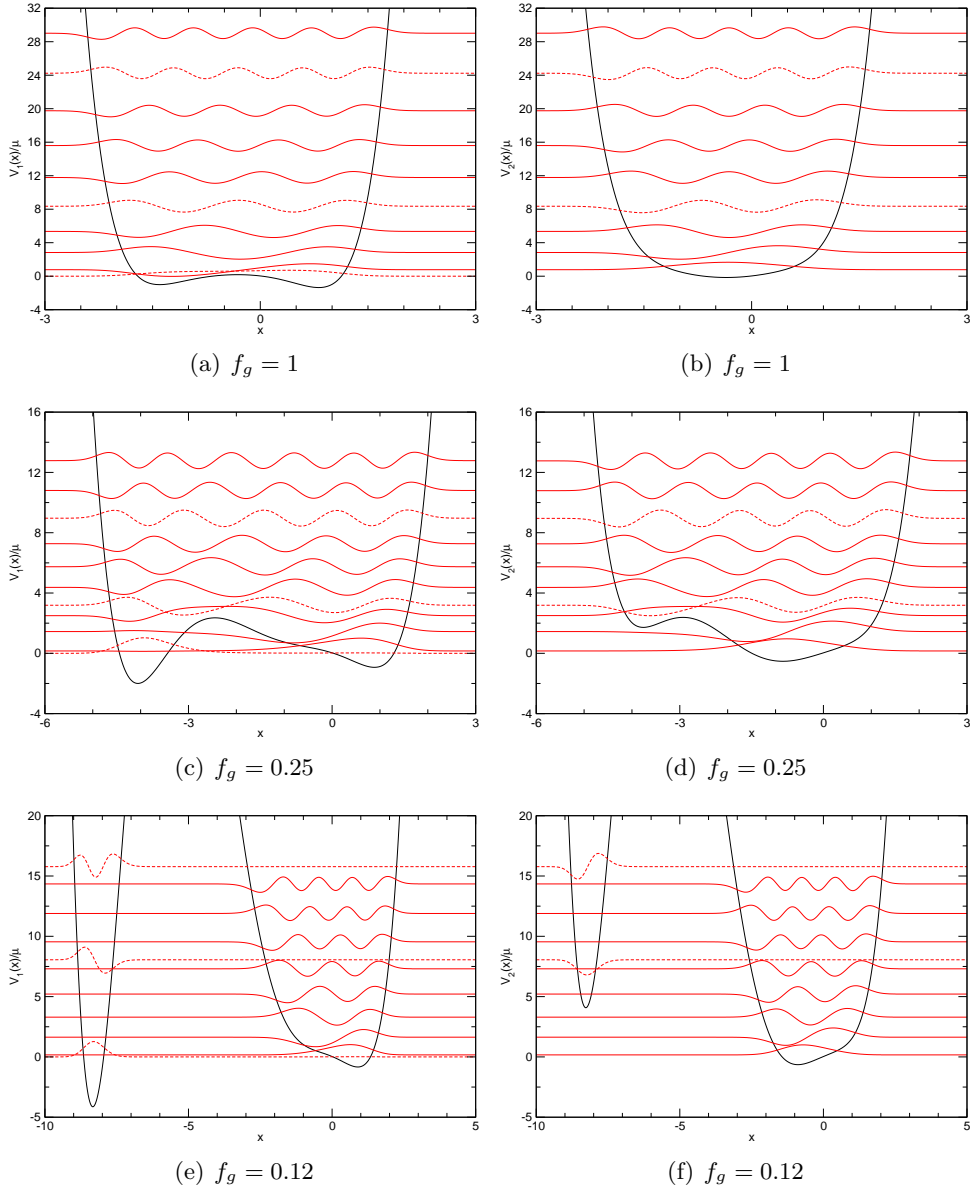
Figure 2.14: Transition from unbroken to broken supersymmetry. Shown are the partner potentials V_1 and V_2 for different couplings f_g. Wave functions represented by a dashed line will decouple in the limit $f_g \to 0$.
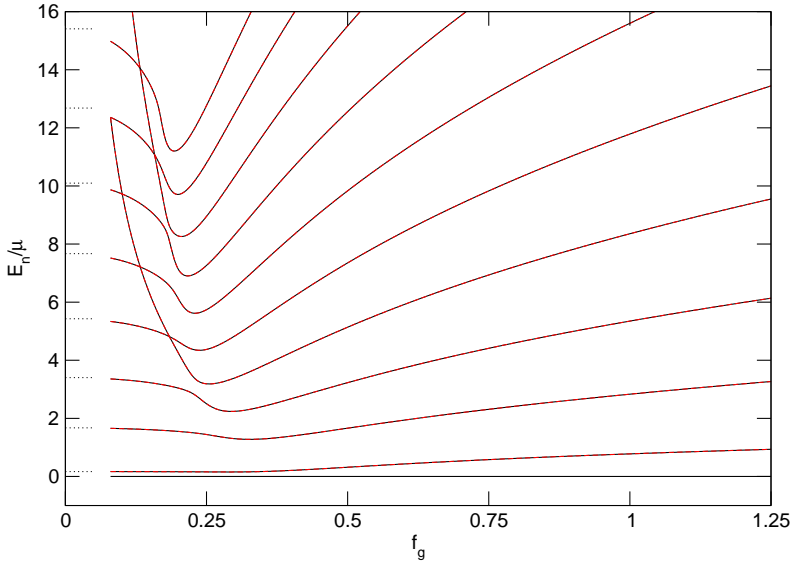
Figure 2.15: Transition from unbroken to broken supersymmetry. Energy levels for the potential $V_1(x)$ (solid black line) and $V_2(x)$ (dashed red line) in dependence of f_g. The unbroken spectrum for $f_g = 0$ is indicated with a black dotted line.

these are the energy levels which diverge for small couplings. The other energy levels approach the spectrum of broken supersymmetric quantum mechanics for a coupling $f_\lambda = 1$ asymptotically as we expected from the beginning.

Chapter 3

Supersymmetric Quantum Mechanics on the Lattice

This chapter is dedicated to the theoretical aspects of supersymmetric quantum mechanics formulated as a lattice quantum field theory. In the first two sections, we will derive the Euclidean continuum action for supersymmetric quantum mechanics and discretise this action with a Wilson type derivative for the fermion in order to get a lattice field theory formulation. We will then discuss in detail the fermion determinant which appears in standard Metropolis algorithms. In particular, we will disclose the relation between the fermion determinant and the Witten index and the thus resulting severe sign problem in the context of broken supersymmetry. This will motivate why we propose to circumvent this problem by means of the hopping expansion and to employ the Prokof'ev and Svistunov worm algorithm for Monte Carlo simulations. The standard discretised action established in the second section will serve us to derive in detail the hopping expansion for the bosonic degrees of freedom as well as for the fermionic ones. This will allow us to reformulate the system in terms of bosonic and fermionic bonds. In this context, we will reveal the decomposition of the configuration space into the bosonic and fermionic subspaces and address the problem of how to calculate expectation values of observables for different boundary conditions. Finally, the last two sections will serve us to elaborate further on the discretisation of the action. The standard discretised action derived in the first section does not reproduce the correct continuum limit of the model. We will find the reason for the spoiled continuum limit for the standard discretised action and be able to cure it by means of a counterterm. In the last section of this chapter, we will discuss the Q-exact actions which are based on twisted supersymmetry. These actions preserve one of the supersymmetries for finite lattice spacing exactly which is sufficient to ensure that the correct continuum limit of the theory is reached.

3.1 The Euclidean Action

3.1.1 The Action and the Supersymmetry Transformations

We have derived the Hamilton operator for supersymmetric quantum mechanics in section 2.1.3. Via standard procedure, the Hamiltonian can be reformulated in the path integral formalism. The Euclidean action for finite imaginary time t[1] reads

$$S = \int_0^\beta dt \; \frac{1}{2}\left(\frac{d\phi(t)}{dt}\right)^2 + \frac{1}{2}P'(\phi(t))^2 + \overline{\psi}(t)\left(\partial_t + P''(\phi(t))\right)\psi(t). \qquad (3.1)$$

$\phi(t)$ is the commuting bosonic coordinate and the two anticommuting fermionic coordinates in Dirac representation are denoted by $\overline{\psi}(t)$ and $\psi(t)$. The arbitrary polynomial $P(\phi(t))$ is called *superpotential* and the derivative is taken with respect to ϕ, $P' = \frac{\partial P}{\partial \phi}$. The superpotential for the field theory thus translates to the prepotential in the Schroedinger formalism via $P' = W$. For infinite temporal extent and for fields vanishing at infinity, the action is invariant under $\mathcal{N} = 2$ supersymmetry transformations $\delta_{1,2}$,

$$
\begin{array}{rclcrcl}
\delta_1\phi & = & \overline{\epsilon}\psi, & \qquad & \delta_2\phi & = & \overline{\psi}\epsilon, \\
\delta_1\psi & = & 0, & & \delta_2\psi & = & \left(\dot{\phi} - P'\right)\epsilon, \\
\delta_1\overline{\psi} & = & -\overline{\epsilon}\left(\dot{\phi} + P'\right), & & \delta_2\overline{\psi} & = & 0,
\end{array}
\qquad (3.2)
$$

where $\overline{\epsilon}$ and ϵ are Grassmann parameters. (See appendix C for a detailed review of the Grassmann algebra.) To keep the notation short, we have abbreviated the total time derivative by $\frac{d\phi}{dt} = \dot{\phi}$. For a finite temporal extent, however, the variation of the action under both supersymmetry transformations $\delta_{1,2}$ yields a non-vanishing term,

$$\delta_1 S = \int_0^\beta dt \left(-\overline{\epsilon}\left(\psi P''\dot{\phi} + \dot{\psi}P'\right)\right) = \overline{\epsilon}\psi P'\Big|_0^\beta, \qquad (3.3)$$

$$\delta_2 S = \int_0^\beta dt \left(\dot{\overline{\psi}}\dot{\phi} + \overline{\psi}\ddot{\phi}\right)\epsilon = \overline{\psi}\dot{\phi}\epsilon\Big|_0^\beta. \qquad (3.4)$$

The last term can only be brought to zero by imposing periodic boundary conditions for the fermionic degrees of freedom, i.e.

$$\psi(\beta) = \psi(0), \qquad \overline{\psi}(\beta) = \overline{\psi}(0). \qquad (3.5)$$

---

[1]Note, that for antiperiodic boundary conditions for the fermionic variable, β can be interpreted as the inverse temperature.

Thus, choosing thermal (and therefore antiperiodic) boundary conditions which is the natural choice for fermionic degrees of freedom explicitly breaks supersymmetry.

Note at this point, that since for both periodic and antiperiodic boundary conditions $\int dt \; \overline{\psi}\dot{\psi} = \int dt \; \psi\dot{\overline{\psi}}$, such that we can write eq.(3.1) equivalently as

$$\tilde{S} = \int dt \; \frac{1}{2}\left(\frac{d\phi(t)}{dt}\right)^2 + \frac{1}{2}P'(\phi(t))^2 + \psi(t)\left(\partial_t - P''(\phi(t))\right)\overline{\psi}(t). \qquad (3.6)$$

We will use this representation in section 3.8 for the construction of a lattice action which preserves the supersymmetry δ_2 on the lattice.

3.1.2 Accidental Symmetries of the Actions Using P_u or P_b

It is worth discussing quickly additional accidental symmetries of the action which arise for our specific choices of the superpotentials for unbroken and broken supersymmetry.

First, we consider the action with the superpotential $P_u = \frac{1}{2}\mu\phi^2 + \frac{1}{4}g\phi^4$. The resulting action is the one we use for unbroken supersymmetry. It is invariant under a parity transformation $\phi \to \tilde{\phi} = -\phi$, since

$$\left(P'(\tilde{\phi})\right)^2 = \left(P'(\phi)\right)^2, \qquad P''(\tilde{\phi}) = P''(\phi), \qquad (3.7)$$

and has thus an accidental $\mathbb{Z}_2$-symmetry.

For broken supersymmetry, we choose the superpotential $P_b = -\frac{\mu^2}{4\lambda}\phi + \frac{1}{3}\lambda\phi^3$. In this case, there is no such simple accidental symmetry transformation under which the action is invariant. Yet, writing out the action for this superpotential explicitly,

$$S = \int dt \; \frac{1}{2}\left(\frac{d\phi(t)}{dt}\right)^2 - \frac{1}{4}\mu^2\phi^2(t) + \frac{1}{2}\lambda^2\phi^4(t) + \overline{\psi}(t)\frac{d\psi(t)}{dt} + 2\lambda\phi(t)\overline{\psi}(t)\psi(t), \tag{3.8}$$

we see that it is invariant under a combined CP symmetry,

$$\phi(t) \quad \to \quad -\phi(t), \qquad (3.9)$$
$$\psi(t) \quad \to \quad \overline{\psi}(t), \qquad (3.10)$$
$$\overline{\psi}(t) \quad \to \quad \psi(t). \qquad (3.11)$$

To interpret this symmetry, we have to rely on the considerations for broken supersymmetry in chapter 2. In the Schroedinger formalism, we have seen that the partner potentials for the bosonic and the fermionic system are connected through a mirror symmetry for the superpotential P_b. The combined symmetry eq.(3.9) is nothing but a manifestation of this mirror symmetry in the field theory language.

3.2 The Lattice Action: Standard Discretisation

We now formulate the theory on a discrete lattice [73]. The time direction is discretised, such that the continuous variable $t \in [0, \beta]$ is replaced by a finite set of L_t sites $t_n = \frac{\beta}{L_t} n$ on a lattice Λ. Thus, the sites are separated by a lattice spacing of $a = \frac{\beta}{L_t}$. A formal definition of the lattice Λ is given by

$$\Lambda = \{x \equiv x_0 = t \in a\mathbb{Z} \mid 0 \leq x \leq a(\beta - 1)\}. \tag{3.12}$$

This discretisation results in a replacement of the temporal integration in the action by a discrete sum over all lattice sites,

$$\int_0^\beta dt \to a \sum_{x=0}^{L_t-1}, \tag{3.13}$$

where the lattice spacing a in front of the sum accounts for the infinitesimal measure dt. Furthermore, the continuous derivatives need to be replaced by a suitable lattice derivative. Let us now consider the simplest lattice discretisation S_L for this model which we will call the standard discretisation. In this case, we replace the continuum derivative with the Wilson operator

$$\Delta^W(r) = \Delta^S - \frac{ra}{2}\Delta^2,$$

where the Wilson parameter $r \in [-1, 1]\backslash\{0\}$. The operators Δ^2 and Δ^S are composed of the lattice forward derivative operator Δ^+ and the lattice backward derivative operator Δ^-. The lattice operators in question are defined

as

$$\Delta^- f_x = \frac{1}{a}(f_x - f_{x-a}), \tag{3.14}$$

$$\Delta^+ f_x = \frac{1}{a}(f_{x+a} - f_x), \tag{3.15}$$

$$\Delta^S = \frac{1}{2}(\Delta^+ + \Delta^-), \tag{3.16}$$

$$\Delta^2 = \Delta^+ \Delta^-. \tag{3.17}$$

Using the Wilson operator removes all fermion doublers from the system. We note that the naive choices for the replacement of the continuum derivative, Δ^+ and Δ^-, are contained in the one-dimensional Wilson operator, since for $r = \pm 1$ we have $\Delta^W(\pm 1) = \Delta^\mp$. We we will use the backward derivative Δ^- for the replacement of the continuum derivative. The discretised action then reads

$$S_L = a \sum_x \frac{1}{2}(\Delta^- \phi_x)^2 + \frac{1}{2}P'(\phi_x)^2 + \overline{\psi}_x(\Delta^- + P''(\phi_x))\psi_x. \tag{3.18}$$

In the following, we will work in lattice units by setting the lattice spacing $a = 1$. The action eq.(3.18) written out in lattice units reads explicitly

$$S_L = \sum_x \frac{1}{2}(P'(\phi_x)^2 + 2\phi_x^2) - \phi_x \phi_{x-1} + (1 + P''(\phi_x))\overline{\psi}_x \psi_x - \overline{\psi}_x \psi_{x-1}. \tag{3.19}$$

This is the standard discretisation for the action of supersymmetric quantum mechanics. Replacing the time derivative with the backward derivative for the supersymmetry transformations eq.(3.2) as well, we find their representation on the lattice,

$$
\begin{array}{llll}
\delta_1 \phi & = & \overline{\epsilon}\psi, & \delta_2 \phi & = & \overline{\psi}\epsilon, \\
\delta_1 \psi & = & 0, & \delta_2 \psi & = & (\Delta^- \phi - P')\,\epsilon, \\
\delta_1 \overline{\psi} & = & -\overline{\epsilon}(\Delta^- \phi + P'), & \delta_2 \overline{\psi} & = & 0.
\end{array} \tag{3.20}
$$

At this point, it needs to be stressed that the action eq.(3.18) *does not* reproduce the continuum limit of the theory correctly. In figure 3.1, we illustrate this failure by extrapolating the lowest mass gaps of the fermion and the boson for unbroken supersymmetry to the continuum[2]. Note, that the extrapolation

---

[2]The calculation is based on the extraction of the mass gaps via the eigenvalues of the transfer matrix and will be discussed thoroughly in chapter 4.
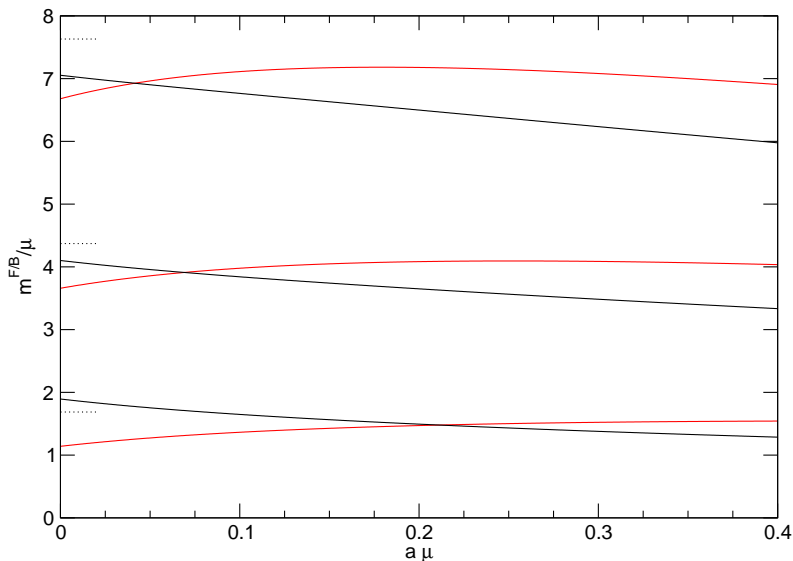
Figure 3.1: Standard discretisation. Continuum extrapolation for $a\mu \to 0$ of the bosonic (red lines) and fermionic (black lines) mass gaps for unbroken supersymmetry and a coupling $f = 1$. The expected continuum values are indicated by dotted lines.

of the masses does not reproduce the values which are expected for continuum physics. The mass gaps for the boson and the fermion are not even degenerate in the continuum and supersymmetry is not restored for this discretisation. In sections 3.7 and 3.8, we will elaborate further on this problem and establish modified actions which describe the continuum physics correctly. However, even though the standard discretised action does not reproduce the correct continuum physics, we still consider it to be instructive to use this action for the discussion of the hopping expansion for supersymmetric quantum mechanics.

For the path integral formulation of supersymmetric quantum mechanics as a one-dimensional lattice field theory, we define the measure as

$$\int \mathcal{D}\phi \mathcal{D}\overline{\psi}\mathcal{D}\psi \equiv \prod_{x=0}^{L_t-1} \int_{-\infty}^{\infty} d\phi_x \int d\overline{\psi}_x \int d\psi_x, \tag{3.21}$$

such that the partition function for the standard discretised action is given by

$$Z = \int \mathcal{D}\phi \mathcal{D}\overline{\psi}\mathcal{D}\psi \; \mathrm{e}^{-S_L(\phi,\overline{\psi},\psi)}.$$

In principle, it is now straightforward to simulate this partition function with any Metropolis algorithm. However, employing standard Metropolis algorithms for a system with broken supersymmetry, one encounters a severe fermionic sign problem. To address this problem, we propose the application of the hopping expansion to this model and simulating the system with the worm algorithm. But before working out the details of the hopping expansion, we devote the next section to the investigation of the origin of the sign problem.

3.3 The Fermion Determinant and the Sign Problem

In standard Metropolis algorithms, for a system with bosonic and fermionic degrees of freedom, the fermions in the path integral are usually integrated out. One is then left with the expectation value of the fermion determinant $\det(D(\phi))$ and a purely bosonic action $S^B(\phi)$. Proceeding this way and integrating out the fermions in the partition function for the action eq.(3.18), we get

$$Z = \int \mathcal{D}\phi \ \det(D(\phi)) \ e^{-S_L^B(\phi)}, \tag{3.22}$$

where the purely bosonic part $S_L^B(\phi)$ of the action expressed in lattice units reads

$$S_L^B(\phi) = \sum_x \frac{1}{2}(\Delta^-\phi_x)^2 + \frac{1}{2}P'(\phi_x)^2. \tag{3.23}$$

It is worth elaborating a little further on the fermion determinant, since it is exactly this determinant which causes the standard Metropolis approach in the case of broken supersymmetry to fail. The fermion determinant $\det(D(\phi))$ can be calculated analytically both in the continuum [32, 68, 74] and in the lattice formulation.

The Fermion Determinant in the Continuum

For the evaluation of the fermion determinant in the continuum, regularisation is necessary. A suitable choice is given by dividing the determinant by the fermion determinant of the free theory, $\det(\partial_t + \mu)$. Moreover, the computation of the fermion determinant depends essentially on the choice of the boundary conditions for the fermionic degrees of freedom. The action eq.(3.1) is only invariant under supersymmetry transformations for periodic boundary conditions. Hence, these are the boundary conditions of main interest. Nonetheless,

we will take into account both periodic boundary conditions (PBC) and antiperiodic boundary conditions (aPBC). A detailed step by step derivation of the following results can be found in appendix F. For antiperiodic boundary conditions $\psi(\beta) = -\psi(0)$, the regularised determinant yields

$$\det\left(D(\phi)\right) \doteq \det\left(\frac{\partial_t + P''(\phi)}{\partial_t + \mu}\right) = \frac{\cosh\left(\frac{1}{2}\int_0^\beta dt\ P''(\phi)\right)}{\cosh\left(\frac{1}{2}\beta\mu\right)}. \tag{3.24}$$

We observe that for these boundary conditions the determinant is always positive. Furthermore, separating the cosh function in terms of exponentials, we find that

$$\det\left(D(\phi)\right) \propto \exp\left(\frac{1}{2}\int_0^\beta dt\ P''(\phi)\right) + \exp\left(-\frac{1}{2}\int_0^\beta dt\ P''(\phi)\right). \tag{3.25}$$

Inserting the determinant thus expressed as the sum of exponentials into eq.(3.22), the partition function decomposes into two parts. These two parts are nothing else but the partition function in the bosonic sector and the fermionic sector, respectively, such that we find

$$\int \mathcal{D}\phi\ \det\left(D(\phi)\right)\ e^{-S_L^B(\phi)} = \mathrm{Tr}[e^{-\beta H_1}] + \mathrm{Tr}[e^{-\beta H_2}] \equiv Z_0 + Z_1. \tag{3.26}$$

Thus, since we have calculated the determinant for antiperiodic boundary conditions,

$$\int \mathcal{D}\phi\ \det\left(D(\phi)\right)\ e^{-S_L^B(\phi)} = Z_0 + Z_1 = Z_{aPBC}. \tag{3.27}$$

For periodic boundary conditions, $\psi(\beta) = \psi(0)$, the calculation for the regularised fermion determinant yields

$$\det\left(D(\phi)\right) = \frac{\sinh\left(\frac{1}{2}\int_0^\beta dt\ P''(\phi)\right)}{\sinh\left(\frac{1}{2}\beta\mu\right)}. \tag{3.28}$$

For this choice of boundary conditions the fermion determinant is not necessarily positive. Writing out the sinh function as a sum of exponentials, we find that

$$\int \mathcal{D}\phi\ \det\left(D(\phi)\right)\ e^{-S_L^B(\phi)} = \mathrm{Tr}[e^{-\beta H_1}] - \mathrm{Tr}[e^{-\beta H_2}] = Z_0 - Z_1 = Z_{PBC}. \tag{3.29}$$

Recalling the definition of the regulated Witten index $\Delta(\beta)$ from eq.(2.58), we realise that the Witten index is in fact proportional to the expectation value of the fermion determinant, such that

$$\Delta(\beta) \propto Z_{PBC}. \tag{3.30}$$

We will now see in particular what the implications of the above calculated analytical results are. To do so, we consider two different superpotentials, namely the one we will use in our numerical calculations for unbroken supersymmetry and the one we will use for broken supersymmetry.

First, we consider the superpotential

$$P_u(\phi) = \frac{1}{2}\mu\phi^2 + \frac{1}{4}g\phi^4. \tag{3.31}$$

This superpotential is invariant under a parity transformation $\phi \to \tilde{\phi} = -\phi$. Furthermore, for $\mu > 0$ and $g \geq 0$, $P_u''(\phi) > 0$. Eqs.(3.28,3.29) then imply that $Z_{PBC} \neq 0$ such that also the Witten index is non-zero, $\Delta \neq 0$. Thus, for this superpotential supersymmetry is unbroken, hence the subscript u. We observe that this is in agreement with what we expect from our previous considerations about supersymmetric quantum mechanics in chapter 2. The prepotential W translates to the first derivative of the superpotential P' and therefore, a superpotential of even degree is associated with a prepotential of odd degree and thus with unbroken supersymmetry.

Next, we consider the superpotential

$$P_b(\phi) = -\frac{\mu^2}{4\lambda}\phi + \frac{1}{3}\lambda\phi^3. \tag{3.32}$$

On the one hand, this superpotential is odd under a parity transformation, and so is its second derivative, $P_b''(\tilde{\phi}) = -P_b''(\phi)$. On the other hand, writing the bosonic action $S_b^B(\phi)$ for this superpotential explicitly,

$$S_b^B(\phi) = \int dt \, \frac{1}{2}\left(\frac{d\phi}{dt}\right)^2 - \frac{1}{2}\left(\frac{\mu^2}{2}\phi^2 - \lambda^2\phi^4\right) {}^3, \tag{3.33}$$

we see immediately that this part of the action is invariant under a parity transformation, $S_b^B(\phi) = S_b^B(\tilde{\phi})$. Therefore, eq.(3.28) implies that for PBC

---

[3]Note, that we have omitted the constant term.

for each configuration contributing to the partition function, there is another one with the same weight but the opposite sign, namely the parity transformed one. Consequently, eq.(3.30) suggests that the Witten index vanishes because $\Delta \propto Z_{PBC} = 0$. For this superpotential, supersymmetry is broken, hence the subscript b. Also this is in agreement with what we expect from the discussion in chapter 2, since the superpotential P_b translates exactly to the prepotential we encountered when we treated the case of broken supersymmetry in section 2.2.2.

The Fermion Determinant on the Lattice

Next, we calculate the fermion determinant on the lattice. The lattice provides regularisation, such that we can calculate the determinant directly without the necessity of dividing it by the determinant of the free theory. Using the lattice discretisation introduced in the previous section 3.2, the determinant of the fermion matrix can easily be seen to be

$$\det\left(\Delta^- + P''(\phi_x)\right) = \prod_x (1 + P''(\phi_x)) \mp 1, \tag{3.34}$$

where the -1 $(+1)$ in the last term is associated with PBC (aPBC). The fermion determinant decomposes in this form into a bosonic part (e.g. the product over all lattice sites x) and a fermionic part (the summand ∓ 1). At this point, we observe that taking the continuum limit of the theory causes difficulties. Namely, we would expect that we should be able to recover the regulated continuum determinant if we take the lattice determinant, divide it by the determinant of the free lattice theory, and then take the lattice spacing to zero, $a \to 0$. However, working out carefully this naive continuum limit, we find

$$\lim_{a \to 0} \det\left(\frac{\Delta^- + P''(\phi_x)}{\Delta^- + \mu \mathbb{1}}\right) = \frac{\exp\left(\frac{1}{2}\int_0^\beta dt\ P''(\phi)\right)}{\exp\left(\frac{1}{2}\beta\mu\right)} \det\left(\frac{\partial_t + P''(\phi)}{\partial_t + \mu}\right) \tag{3.35}$$

for both periodic and antiperiodic boundary conditions. Taking the lattice spacing to zero apparently yields an additional factor in front of the continuum determinant. This factor can be understood as coming from radiative corrections we have not yet accounted for and it is a different manifestation of the problem that we did not recover the correct continuum limit when we extrapolated the masses into the continuum in figure 3.1.

Let us now proceed by discussing the determinant of the fermion matrix on the lattice for both superpotentials P_u and P_b explicitly.

Using the superpotential for unbroken supersymmetry P_u, the determinant yields

$$\det(\Delta^- + P_u''(\phi_x)) = \prod_x (1 + \mu + 3g\phi_x^2) \mp 1. \qquad (3.36)$$

For parameters $\mu > 0$ and $g \geq 0$ the determinant is strictly positive for both, PBC and aPBC. Interpreting the determinant as the weight of a configuration, this superpotential is therefore suitable for standard Monte Carlo algorithms.

Using the superpotential for broken supersymmetry P_b, the determinant yields

$$\det(\Delta^- + P_b''(\phi_x)) = \prod_x (1 + 2\lambda\phi_x) \mp 1. \qquad (3.37)$$

Thus, the determinant for broken supersymmetry is indefinite even for $\lambda > 0$. On the one hand, this is what we expect since the vanishing of the Witten index associated with broken supersymmetry requires an indefinite fermion determinant. On the other hand, this causes serious problems for standard Monte Carlo simulations, where strictly positive weights for any configuration are required. This sign problem remains severe, even in the limit where the lattice spacing goes to zero. This very fluctuation of the determinant is the heart of the fermionic sign problem for standard Metropolis algorithms in the case of broken supersymmetric quantum mechanics.

To circumvent the fermionic sign problem for a superpotential of odd degree and thus for broken supersymmetry, we therefore propose to apply the hopping expansion to supersymmetric quantum mechanics. In the next section, we will discuss this expansion and reformulate the degrees of freedom in terms of bosonic and fermionic bonds with the help of the discretised action eq.(3.19).

3.4 The Hopping Expansion

3.4.1 The Partition Function

We illustrate the hopping expansion by means of the standard discretised lattice action eq.(3.19). Later in this work, when we actually perform numerical calculations, we will use discretisation schemes which are different from the standard discretisation. However, up to rather straightforward modifications,

the following derivation of the reformulation of the path integral in terms of fermionic and bosonic bonds applies to any chosen action. Analogously to the hopping expansion for the Ising model, we need to express the partition function in terms of constrained paths

$$Z = \sum_{CP} W_{CP}. \tag{3.38}$$

For the reformulation, we start by splitting the action into a purely bosonic part and a part containing the fermionic variables in combination with the bosonic variables

$$S_L = S_L^B(\phi) + S_L^F(\phi, \overline{\psi}, \psi), \tag{3.39}$$

where the individual parts read

$$S_L^B(\phi) = \sum_x \frac{1}{2}(\Delta^- \phi_x)^2 + \frac{1}{2}P'(\phi_x)^2, \tag{3.40}$$

$$S_L^F(\phi, \overline{\psi}, \psi) = \sum_x \overline{\psi}_x(\Delta^- + P''(\phi_x))\psi_x. \tag{3.41}$$

The partition function in terms of the thus separated contributions to the action is then given by

$$Z = \int \mathcal{D}\phi \; \mathrm{e}^{-S_L^B(\phi)} \int \mathcal{D}\overline{\psi}\mathcal{D}\psi \; \mathrm{e}^{-S_L^F(\phi, \overline{\psi}, \psi)}, \tag{3.42}$$

where we make use of the fact that Grassmann numbers and real numbers commute.

Expanding the Fermionic Part

First, we apply the hopping expansion to the fermionic Boltzmann factor. Due to the nilpotency of the Grassmann variables, all terms of second or higher order vanish in the expansion of the exponential. The identity

$$\mathrm{e}^{-S_L^F} = \prod_x \left(1 - (1 + P''(\phi_x))\overline{\psi}_x\psi_x\right) \prod_x \left(1 + \overline{\psi}_x\psi_{x-1}\right) \tag{3.43}$$

therfore holds. The term in the first parentheses is called the monomer term and the one in the second parentheses the hopping term. Introducing the fermionic monomer weight $M(\phi) = 1 + P''(\phi)$ and the occupation number for

the fermionic monomers $m(x) \in \{0,1\}$ as well as the fermionic bond number $n^F(x) \in \{0,1\}$, we write

$$
e^{-S_L^F} = \prod_x \left(\sum_{m(x)=0}^{1} \left(-M(\phi_x)\overline{\psi}_x\psi_x \right)^{m(x)} \right) \prod_x \left(\sum_{n^F(x)=0}^{1} \left(\overline{\psi}_x\psi_{x-1} \right)^{n^F(x)} \right).
$$
(3.44)

In $(1+0)$ dimensions, as it is the case for supersymmetric quantum mechanics, there is only one lattice unit vector, $\hat{\mu} = \hat{0}$. We therefore omit to write explicitly the direction of the fermionic bond $b^F(x,\mu) = b^F(x,0) \equiv b^F(x)$. This suppression of the direction will apply to any other kind of bond in this chapter. Unlike the bonds resulting from the expansion in the Ising model, the fermionic bonds b^F are directed since the order of the variables ψ_x and $\overline{\psi}_x$ is relevant. The weight of a fermionic bond w^F can be read off directly from the hopping term e.g. in eq.(3.19) and is identified to be $w^F = 1$. Integrating out the fermionic variables leaves us with constraints on the variables $m(x)$ and $n^F(x)$. To give a non-zero contribution to the path integral, each site x must be occupied by exactly one variable ψ_x and one variable $\overline{\psi}_x$. The condition on the monomer number and the fermionic bond number is then

$$
m(x) + \frac{1}{2}\left(n^F(x) + n^F(x-1) \right) = 1, \qquad \forall x.
$$
(3.45)

Characterising a configuration by both variables $m(x)$ and $n^F(x)$ is thus redundant. We will choose to express the configuration in terms of the monomer number $m(x)$ only. Furthermore, condition eq.(3.45) implies that there are only two possible fermion configurations with non-zero weight. On the one hand, eq.(3.45) is satisfied if $m(x) = 1$ and $n^F(x) = 0$ $\forall x$. Each site is then saturated with the monomer term, and applying the Grassmann integration rules, we identify the fermionic contribution to the weight of a configuration to be the monomer weight $M(\phi)$ at each site x. In this case, there are no fermionic bonds and such a configuration contributes to the bosonic sector. On the other hand, eq.(3.45) is also satisfied if $n^F(x) = 1$ and $m(x) = 0$ $\forall x$. For such a configuration, all sites x are connected with a fermionic bond, thus forming a fermionic loop winding around the lattice. The fermionic contribution to the site weight for such a configuration is then a factor 1. Applying the Grassmann integration rules yields the additional characteristic factor (-1) for a closed fermion loop. Finally, the overall sign for such a configuration is fixed by the boundary conditions for the fermions. This is in accordance with the

sign of the fermionic contribution to the fermion determinant on the lattice in eq.(3.34). The boundary conditions are discussed in section 3.5.

Expanding the Bosonic Part

We now turn to the bosonic part of the path integral. Expanding the bosonic Boltzmann factor yields

$$
\mathrm{e}^{-S_L^B} = \prod_x \left(\sum_{n^B(x)=0}^{\infty} \frac{(\phi_{x-1}\phi_x)^{n^B(x)}}{n^B(x)!} \right) \prod_x \mathrm{e}^{-V(\phi_x)}, \tag{3.46}
$$

where the bosonic self interaction is abbreviated, $\frac{1}{2}(P'(\phi_x)^2 + 2\phi_x^2) = V(\phi_x)$. The sum over the bosonic hoppings in eq.(3.46) implies that the weight of a bosonic bond is $w^B = 1$. After this expansion and using the result from the expansion in the fermionic variables, we write the partition function as

$$
Z = \int \mathcal{D}\phi \prod_x \left(\sum_{n^B(x)=0}^{\infty} \frac{(\phi_{x-1}\phi_x)^{n^B(x)}}{n^B(x)!} \right) \prod_x \mathrm{e}^{-V(\phi_x)} \prod_x \left(\sum_{m(x)=0}^{1} M(\phi_x)^{m(x)} \right). \tag{3.47}
$$

To select one particular configuration, we now choose one arbitrary entry in each sum. This is done by fixing both the bosonic bond number $n^B(x) = $ fix and the monomer number $m(x) = $ fix for each site. After a rearrangement in the bosonic fields, analogously to the rearrangement of the spin variables in the Ising model, the weight of the chosen configuration factorises as

$$
W = \prod_x \frac{1}{n^B(x)!} \int_{-\infty}^{\infty} d\phi_x \ \phi_x^{N^B(x)} \mathrm{e}^{-V(\phi_x)} M(\phi_x)^{m(x)}, \tag{3.48}
$$

where $N^B(x) = n^B(x) + n^B(x-1)$ counts the total number of bosonic bonds running into one site x. We now introduce the site weight Q, defined as the integral over the bosonic degrees of freedom,

$$
Q(N, m) = \int_{-\infty}^{\infty} d\phi \ \phi^N \mathrm{e}^{-V(\phi)} M(\phi)^m. \tag{3.49}
$$

Each configuration is either associated with the fermionic sector, such that $m(x) = 0$ for each site, or with the bosonic sector, such that $m(x) = 1$ for each site. It is therefore appropriate to use the fermion number $F \in \{0, 1\}$ to characterise the fermionic contribution to a configuration. Throughout this

chapter, we will use the notation where the subscript for the site weights Q_F refers to the sector, indicating whether the underlying fermionic structure is empty or contains a loop,

$$Q_F(N) = \int_{-\infty}^{\infty} d\phi \; \phi^N e^{-V(\phi)} M(\phi)^{1-F}. \tag{3.50}$$

Note that in general, these integrals are analytically not solvable. For the purpose of an actual simulation, one first needs to evaluate the site weights numerically and tabulate them before proceeding with the Monte Carlo updates. In the notation introduced above, the weight for a configuration is given by

$$W_F = \left(\prod_x \frac{1}{n^B(x)!} \right) \left[\prod_x Q_F(N(x)) \right]. \tag{3.51}$$

In the hopping expansion, the configuration space for Z decomposes naturally into two subspaces, one associated with the bosonic sector $F = 0$ and one associated with the fermionic sector $F = 1$. In allusion to the derivation of the hopping expansion for the Ising model, we will abbreviate the configuration space for Z_F with $\mathcal{Z}_F$, even though there are not necessarily constraints on the bosonic bonds to justify the term constraint paths. Renaming the weight of a configuration $W_F \equiv W_{\mathcal{Z}_F}$, the partition function for each sector can now be written as the sum over all configurations therein,

$$Z_F = \sum_{CP \subset \mathcal{Z}_F} W_{\mathcal{Z}_F}. \tag{3.52}$$

How the partition functions Z_0 for the bosonic and Z_1 for the fermionic sector have to be composed to an overall partition function Z depends on the boundary conditions for the fermionic degrees of freedom. This problem will be addressed in section 3.5.

3.4.2 Graphical Representation

For supersymmetric quantum mechanics too, there is a graphical representation for each bond configuration. Similarly to the Ising model, we introduce certain building blocks out of which we can construct a configuration. Formulating the model on the lattice by standard discretisation yields two types of bonds which are the undirected bosonic bonds b^B, where $n^B \in \mathbb{N}_0$, and the directed fermionic bonds b^F, where $n^F \in \{0, 1\}$. Later, we will employ other

$$\psi_{x-1} \quad\longrightarrow\quad \overline{\psi}_x \qquad\qquad \phi_{x-1} \quad\text{-------}\quad \phi_x$$

Figure 3.2: The graphical representation for the directed fermionic bond b^F (solid line with arrow) and the undirected bosonic bond b^B (dashed line).

discretisation schemes and encounter additional types of bosonic bonds. We will represent the fermionic bond by a solid line, drawing an arrow to indicate its direction, and a dashed line for the bosonic bond. Each bond carries a field variable at both endings. The fermionic bond carries the Grassmann variable ψ at the left ending and the Grassmann variable $\overline{\psi}$ at the right ending. These variables are needed to saturate the Grassmann integration at each site. The arrow of the fermionic bond is pointed from the variable ψ the the variable $\overline{\psi}$. Defining the direction of the arrow in this sense will indicate the direction of the propagation of the fermion in the graphical representation for the fermionic two-point function. The bosonic bond carries the variable ϕ at both endings. In figure 3.2 the bonds and the variables they carry are depicted.

Any configuration contributing to the configuration space of the partition function consists of a superposition of a fermionic configuration (e.g. a closed loop winding around the lattice or a totally empty lattice) and a bosonic configuration. In general, there are no constraints on the bosonic bond numbers. We illustrate two possible configurations on a $L_t = 8$ lattice in figure 3.3.

3.5 Boundary Conditions

3.5.1 The Partition Function

For our finite lattice we need to specify the boundary conditions. For the bosonic field, we will always choose periodic boundary conditions (PBC) such that

$$\phi_{x+L_t} = \phi_x. \tag{3.53}$$

For the fermionic field, we allow for two different choices to each of which we assign a fixed parameter ε. If we define this parameter to be $\varepsilon = 0$ for periodic boundary conditions and to be $\varepsilon = 1$ for antiperiodic boundary conditions

(a) $F = 1$

(b) $F = 0$
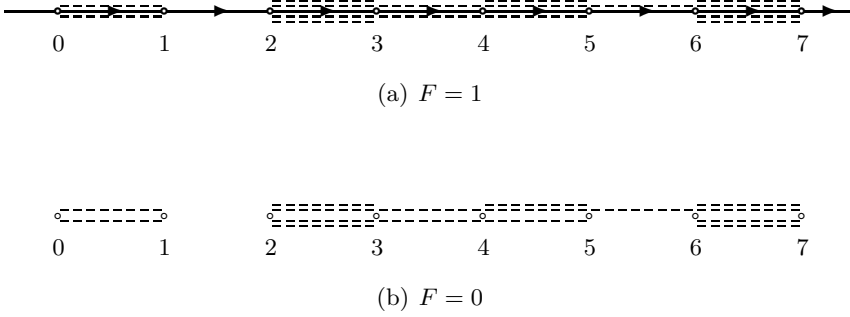
Figure 3.3: Illustration of a possible bosonic bond configuration in the fermionic sector $F = 1$ and the same configuration in the bosonic sector $F = 0$ on a $L_t = 8$ lattice.

(aPBC), the periodicity of the fermionic fields is described as

$$\overline{\psi}_{x+L_t} = (-1)^{\varepsilon}\overline{\psi}_x, \qquad \psi_{x+L_t} = (-1)^{\varepsilon}\psi_x. \tag{3.54}$$

We now associate each bond configuration with one of two different topological classes $\mathcal{L}_i$, which are distinguished by the number of windings of the fermionic loop around the lattice. It is the topological class together with the boundary conditions which determine the overall sign of a configuration. As the lattice is extended in only one direction, we have either a loop winding around the lattice and crossing the boundary once, in which case the configuration falls into the class $\mathcal{L}_1$, or there is no fermionic bond crossing the boundary, e.g. for such a configuration each site is saturated with a monomer term. The latter configurations belong to the topological class $\mathcal{L}_0$. Keeping track of all signs, the overall sign of a configuration is given by $(-1)^{(\varepsilon+1)l}$, where

$$l = \begin{cases} 0 & \text{if } CP \in \mathcal{L}_0, \\ 1 & \text{if } CP \in \mathcal{L}_1. \end{cases} \tag{3.55}$$

The partition functions for aPBC and PBC are then formed as

$$Z_{aPBC} = Z_{\mathcal{L}_0} + Z_{\mathcal{L}_1} \tag{3.56}$$

for $\varepsilon = 1$ and

$$Z_{PBC} = Z_{\mathcal{L}_0} - Z_{\mathcal{L}_1} \tag{3.57}$$

for $\varepsilon = 0$. We note that the topological sectors correspond exactly to the bosonic and the fermionic sector of the model, $Z_{\mathcal{L}_0} = Z_{F=0} \equiv Z_0$ and $Z_{\mathcal{L}_1} = Z_{F=1} \equiv Z_1$. In the following, we will always refer to the sector, rather than to the topological class.

3.5.2 Observables

We also need to take into account the boundary conditions when we calculate the expectation value of observables. In general, the expectation value for any observable $\langle \mathcal{O} \rangle$ is given by

$$\langle \mathcal{O} \rangle = \frac{1}{Z} \int \mathcal{D}\phi \mathcal{D}\overline{\psi} \mathcal{D}\psi \; \mathcal{O} \; e^{-S}. \tag{3.58}$$

In supersymmetric quantum mechanics, the explicit expression for the expectation value of any observable is composed as

$$\langle \mathcal{O} \rangle_{aPBC} = \frac{\langle\!\langle \mathcal{O} \rangle\!\rangle_0 + \langle\!\langle \mathcal{O} \rangle\!\rangle_1}{Z_0 + Z_1} \tag{3.59}$$

for antiperiodic boundary conditions and as

$$\langle \mathcal{O} \rangle_{PBC} = \frac{\langle\!\langle \mathcal{O} \rangle\!\rangle_0 - \langle\!\langle \mathcal{O} \rangle\!\rangle_1}{Z_0 - Z_1} \tag{3.60}$$

for periodic boundary conditions. Here, we have denoted the non-normalised expectation value of the observable in the sector F by $\langle\!\langle \mathcal{O} \rangle\!\rangle_F = \langle \mathcal{O} \rangle_F \cdot Z_F$.

At this point, we realise the main issue one encounters in the lattice formulation of supersymmetric quantum mechanics. As supersymmetry is only restored in the continuum for PBC, these are in fact the boundary conditions of interest. Yet, for broken supersymmetry, the Witten index is zero, $\Delta = 0$, and, consequently, $Z_{PBC} = 0$ as well. Considering eq.(3.60), it is obvious that, a priori, one has to divide by zero in each expectation value $\langle \mathcal{O} \rangle_{PBC}$. Now, the lattice provides regularisation for this problem. For finite lattice spacing, supersymmetry is explicitly broken, such that $Z_{PBC} \neq 0$. It is therefore easily possible to calculate expectation values for PBC at finite lattice spacing. We will then see that in the continuum limit for most observables both the nominator and the denominator go to zero in such a way that their ratio remains finite. For these observables, it is therefore possible to give continuum values for PBC even in the context of broken supersymmetry.

3.6 Correlation Functions

An important example for an observable is the two-point function. Typically it is used to measure the mass of a particle by extracting the difference between the first excited state and the vacuum energy of the field in question. In this subsection, we will derive the representation of configurations contributing to the bosonic or the fermionic correlation function in the hopping expansion scheme. This is very useful since the worm algorithm will update the configuration space of the partition function via the two-point functions of the bosonic and fermionic variables.

3.6.1 The Bosonic Two-Point Function

The bosonic two-point function is defined as

$$\langle \phi_{x_1} \phi_{x_2} \rangle = \frac{g^B(x_1 - x_2)}{Z}, \tag{3.61}$$

where

$$g^B(x_1 - x_2) = \int \mathcal{D}\phi \mathcal{D}\overline{\psi} \mathcal{D}\psi \ \phi_{x_1} \phi_{x_2} \ \mathrm{e}^{-S}. \tag{3.62}$$

To have a consistent notation, we will abbreviate the configuration space of the bosonic two-point function g^B with $\mathcal{G}^B$. Comparing eq.(3.62) with the definition of the partition function eq.(3.42), we see that configurations in $\mathcal{G}^B$ differ from configurations in $\mathcal{Z}$ by the additional bosonic field variables ϕ inserted in the path integral at the sites x_1 and x_2. In the following, we will refer to these extra bosonic variables as bosonic sources. The fermionic sector F is not affected by these sources. Thus, analogously to the the configuration space $\mathcal{Z}$, the configuration space $\mathcal{G}^B$ decomposes into the bosonic configuration space with $F = 0$ and the fermionic configuration space with $F = 1$. We denote the separated configuration spaces by adding the subscript F to the configuration space of the two-point function, $\mathcal{G}^B \equiv \mathcal{G}^B_F$. The weight of a configuration in $\mathcal{G}^B_F$ can be derived by modifying the weight of the same bond configuration in $\mathcal{Z}_F$. To do so, we define the *bosonic site occupation number*

$$k(x) = n^B(x) + n^B(x-1) + \delta_{x,x_1} + \delta_{x,x_2} = N^B(x) + \delta_{x,x_1} + \delta_{x,x_2}, \tag{3.63}$$

which counts the number of bosonic field variables at the site x. Note that these variables may stem from the ending of a bosonic bond (e.g. $n^B(x)$ and

(a) $F = 1$

(b) $F = 0$
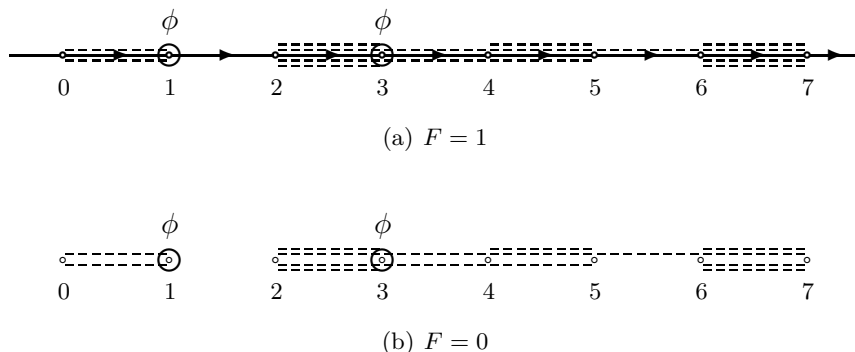
Figure 3.4: Graphical representation of possible configurations similar to the closed path configurations in figure 3.3, contributing to the bosonic two-point function (a) in the fermionic sector $F = 1$ and (b) the same configuration in the bosonic sector $F = 0$ on a $L_t = 8$ lattice. The additional bosonic variables are marked with a $\bigcirc$.

$n^B(x - 1))$ or from a bosonic source $(\delta_{x,x_i})^4$. Equipped with this compact notation, we proceed analogously to the calculation for the Ising model and identify the weight of a configuration where bosonic sources are inserted at the sites x_1 and x_2 as

$$W_{\mathcal{G}_F^B} = \left(\prod_x \frac{1}{n^B(x)!} \right) \left[\prod_x Q_F(k(x)) \right] . \tag{3.64}$$

This expression looks the same as the expression we have derived for the weight of a configuration contributing to the partition function. Yet, one must bear in mind that the site occupation number and thus the site weight is altered at the sites x_1 and x_2. The weight of a bond configuration with additional bosonic variables is therefore different from the same bond configuration without the additional variables.

A priori, if there are no constraints on the site occupation numbers, each bond configuration in $\mathcal{G}_F^B$ corresponds to a bond configuration in $\mathcal{Z}_F$. It is therefore possible to switch between the configuration spaces independently of the underlying bond configuration. One only has to take into account that

---

[4]In order to calculate an arbitrary n-point function, we would, of course, have to add n bosonic sources to a given configuration, which would contribute to the bosonic site occupation number with n additional δ_{x,x_n} summands.

a bond configuration in $\mathcal{G}_F^B$ has a weight which is different from the weight of the same bond configuration in $\mathcal{Z}_F$ due to the additional sources. The weights of a bond configuration in the different configuration spaces are related by ratios of the site weights at the sites where the bosonic sources are inserted. In figure 3.4, the graphical representation for a bosonic two-point is depicted.

For some actions, there are restrictions imposed on the bond configurations. In such a case, the bond configurations in the configuration spaces $\mathcal{Z}_F$ and $\mathcal{G}_F^B$ are then no longer necessarily the same. Rather, the bond configurations of $\mathcal{Z}_F$ form a subset of the bond configurations of $\mathcal{G}_F^B$. It is then only possible to switch from one configuration space into the other when the underlying bond configuration belongs to both configuration spaces $\mathcal{G}_F^B$ and $\mathcal{Z}_F$. We will elaborate on such cases in detail when we discuss the update algorithm for different discretisation schemes in chapter 5.

3.6.2 The Bosonic Correlation Function at Finite β

The bosonic two-point function we have derived above serves for the calculation of the bosonic correlation function at finite temperature,

$$C^B(x_1 - x_2) \equiv \langle \phi_{x_1} \phi_{x_2} \rangle - \langle \phi \rangle^2. \tag{3.65}$$

This correlation function consists thus of the bosonic two-point function and the square of the expectation value for the bosonic field variable ϕ. To be able to calculate the complete correlation function, we therefore need to be able to calculate the expectation value $\langle \phi \rangle$. The expectation value for the moments of the field variable ϕ are defined as

$$\langle \phi^n \rangle = \langle \phi_{x_i}^n \rangle = \frac{1}{Z} \int \mathcal{D}\phi \mathcal{D}\overline{\psi} \mathcal{D}\psi \; \phi_{x_i}^n \; e^{-S}. \tag{3.66}$$

A configuration contributing to the n-th moment of the expectation value therefore has n additional bosonic variables ϕ at the site x_i. It is easy to see that the weight for such a configuration is the same as in eq.(3.64). The only difference lies in the site occupation number, which is modified due to the additional field variables as

$$k(x) = N^B(x) + n\delta_{x,x_i}. \tag{3.67}$$

With these considerations, we are now able to calculate the bosonic correlation function at finite temperature. Next, we need to consider also the fermionic correlation function.

3.6.3 The Fermionic Correlation Function

The fermionic correlation function at finite temperature is defined as the fermionic two-point function,

$$C^F(x_1 - x_2) \equiv \langle \psi_{x_1} \overline{\psi}_{x_2} \rangle = \frac{g^F(x_1 - x_2)}{Z}, \tag{3.68}$$

where

$$g^F(x_1 - x_2) = \int \mathcal{D}\phi \mathcal{D}\overline{\psi} \mathcal{D}\psi \; \psi_{x_1} \overline{\psi}_{x_2} \; \mathrm{e}^{-S}. \tag{3.69}$$

Similarly to the bosonic correlation function, configurations contributing to the fermionic correlation function have additional fermionic variables $\overline{\psi}$ and ψ inserted in the path integral. We will refer to these variables as the source and the sink, respectively. To derive the weight of a configuration in the configuration space $\mathcal{G}^F$, we cannot simply adapt the procedure for the calculation of the weights for the configurations contributing to the bosonic two-point function. Rather, we need to start from scratch by expanding the fermionic Boltzmann factor in eq.(3.44). Including the additional fermionic variables in the expansion yields

$$\psi_{x_1} \overline{\psi}_{x_2} \mathrm{e}^{-S^F_L} =$$

$$\psi_{x_1} \overline{\psi}_{x_2} \prod_x \left(\sum_{m(x)=0}^{1} \left(-M(\phi_x) \overline{\psi}_x \psi_x \right)^{m(x)} \right) \prod_x \left(\sum_{n^F(x)=0}^{1} \left(\overline{\psi}_x \psi_{x-1} \right)^{n^F(x)} \right). \tag{3.70}$$

For this expression, the integral over the fermionic degrees of freedom still has to be carried out. To give a non zero contribution, Grassmann integration requires exactly one pair of variables $\overline{\psi}$ and ψ at each site x. For given sites x_1 and x_2 of the additional fermionic variables, we have to adjust the numbers $m(x)$ and $n^B(x)$ in order to achieve the necessary pairing of the variables for each site.

We first consider the case where $x_1 = x_2 \equiv y$. It is easy to see that the only possibility to saturate each site is given by the choice

$$n^F(x) \;=\; 0 \qquad \forall x, \tag{3.71}$$

$$m(x) \;=\; \begin{cases} 0 & \text{if } x = y \\ 1 & \text{else.} \end{cases} \tag{3.72}$$

For such a configuration, the site y is saturated through the source and the sink, contributing a factor 1 to the bosonic integration. All other sites are saturated via the monomer term, which has to be accounted for by including the factor $M(\phi)$ into the bosonic integration for each of these sites. Note, that eq.(3.71) implies that the fermionic correlation function exists *only* in the bosonic sector.

If the additional fermionic variables are not at the same site, e.g. $x_1 \neq x_2$, source and sink can only be paired with the ending of a fermionic bond. Keeping in mind that the fermionic bonds are directed, it is easy to see that one needs $(x_1 - x_2) \bmod L_t$ of these bonds to connect the source with the sink, thus forming an open fermionic string. Each site along the string is then automatically saturated by the variables of one ingoing and one outgoing bond. Those sites which are saturated with either the source or the sink and a fermionic bond attached to it yield a factor 1 to the bosonic integration, as well as all sites along the open string. The other sites again contribute with the monomer weight $M(\phi)$ to the bosonic integration. Because the fermionic bonds are directed, the order of the source and the sink matters and we need to distinguish between the cases $x_2 > x_1$ and $x_1 > x_2$ to characterise a configuration with the numbers $m(x)$ and $n^B(x)$. For $x_2 > x_1$, the open string connects source and sink without crossing the boundary and each configuration is characterised by the numbers

$$
n^F(x) \;=\; \begin{cases} 1 & \text{if } x_2 \leq x < x_1 \\ 0 & \text{else,} \end{cases} \tag{3.73}
$$

$$
m(x) \;=\; \begin{cases} 0 & \text{if } x_2 \leq x \leq x_1 \\ 1 & \text{else.} \end{cases} \tag{3.74}
$$

For $x_1 < x_2$, the fermionic string winds around the lattice and the numbers to characterise the configuration are given by

$$
n^F(x) \;=\; \begin{cases} 0 & \text{if } x_1 \leq x < x_2 \\ 1 & \text{else,} \end{cases} \tag{3.75}
$$

$$
m(x) \;=\; \begin{cases} 1 & \text{if } x_1 < x < x_2 \\ 0 & \text{else.} \end{cases} \tag{3.76}
$$

Whether the open fermionic string crosses the boundary of the lattice or not is relevant for the overall sign of the configuration. Namely, the crossing

of the boundary yields one extra factor of (-1) for antiperiodic boundary conditions. We are now able to give an explicit expression for the weight of a configuration contributing to $\mathcal{G}^F$. Each site x_i contributing a factor 1 to the bosonic integration amounts to a site weight $Q_1(k(x_i))$[5] while a site x_j contributing the monomer weight $M(\phi_{x_j})$ to the bosonic integration yields a site weight $Q_0(k(x_j))$. The bosonic bond configuration is not affected by these considerations, such that the bosonic contribution to the weight is the same one as we have found for the partition function. To be able to write the weight of a configuration in a compact form, we define a set of lattice sites $\mathcal{F}$, containing solely sites which are saturated via any combination of source, sink, and fermionic bonds, as

$$\mathcal{F} = \begin{cases} \{x \in \Lambda \mid x_2 \leq x \leq x_1\} & \text{if } x_2 \leq x_1 \\ \{x \in \Lambda \mid x \leq x_1 \cup x \geq x_2\} & \text{if } x_1 < x_2. \end{cases} \tag{3.77}$$

Using this notation, we end up with the weight of a configuration contributing to $\mathcal{G}^F$ in the compact form

$$W_{\mathcal{G}^F} = \left(\prod_x \frac{1}{n^B(x)!}\right) \left[\prod_{x \in \mathcal{F}} Q_1(k(x))\right] \left[\prod_{x \notin \mathcal{F}} Q_0(k(x))\right]. \tag{3.78}$$

Eq.(3.78) implies that the configuration space $\mathcal{G}^F$ does not decompose into the bosonic sector $F = 0$ and the fermionic sector $F = 1$. Thus, the subscript F in the naming of the configuration space is not necessary. Rather, all configurations in this configuration space are associated with the bosonic sector, such that this configuration space mediates between the bosonic and the fermionic sector. Note further, that eq.(3.78) implies that the fermionic correlation function is not invariant under the exchange of the source and the sink variables. In figure 3.5, the graphical representation of an example for the fermionic correlation function where $x_1 > x_2$ and an example for the correlation function where $x_2 > x_1$ are depicted.

Note, that we are free to interpret the fermionic correlation function $C^F(x-y)$ measured in the configuration space $\mathcal{G}^F \equiv \mathcal{G}_0^F$ as well as the antifermionic correlation function $-C^{\overline{F}}(y-x)$, measured in the configuration space $\mathcal{G}_1^{\overline{F}}$. We will, however, only refer to the fermionic correlation function in the following.

---

[5]Note, that the bosonic site occupation number counts only bosonic field variables at a site x. Therefore, in the configuration space $\mathcal{G}^F$, $k(x) = N^B(x)$.
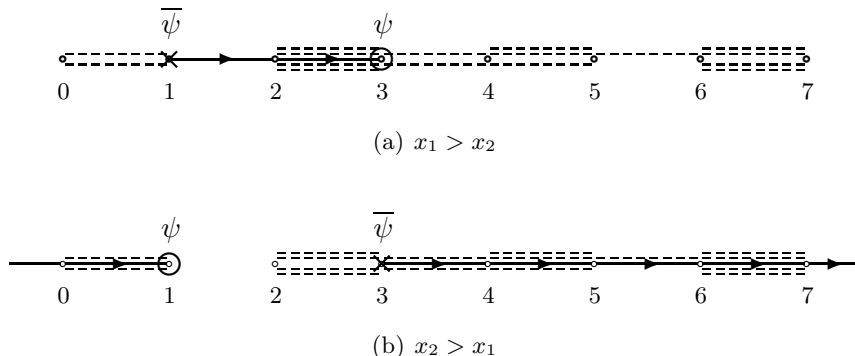
(a) $x_1 > x_2$

(b) $x_2 > x_1$

Figure 3.5: Graphical representation of possible configurations similar to the constrained path configurations in figure 3.3, contributing to the fermionic two-point function (a) for $x_1 > x_2$ and (b) the same configuration for $x_2 > x_1$ on a $L_t = 8$ lattice. The additional variables are marked with a $\bigcirc$ for ψ_{x_1} and a $\times$ for $\overline{\psi}_{x_2}$.

3.6.4 Configuration Spaces

We have seen that the hopping expansion decomposes the configuration spaces for the partition function $\mathcal{Z}$ and for the bosonic two point function $\mathcal{G}^B$ into subspaces, namely the bosonic sector $F = 0$, and the fermionic sector $F = 1$. Switching from one configuration space to another is induced by adding and removing additional field variables. The configuration space $\mathcal{G}^F$, even though it is associated with the bosonic sector, mediates between the bosonic and the fermionic sector. In figure 3.6, we depict schematically the different configuration spaces and how one can switch from one to another by adding or removing additional field variables.

As we have pointed out before, this derivation was based upon the standard discretised action eq.(3.19) for pedagogical reasons. Now that we know how to apply the hopping expansion to supersymmetric quantum mechanics, it must be our next concern to elaborate on the problem of the spoiled continuum limit of the theory. Essentially, there are two ways of dealing with this complication. The standard way, which is by finetuning, amounts in this case to adding a counterterm to the action. For $\mathcal{N} = 2$ supersymmetric quantum mechanics, there is also another way to account for dangerous divergencies: it is possible to find actions which preserve one of the supersymmetries exactly for finite lattice spacing. The remaining two sections of this chapter are dedicated to a
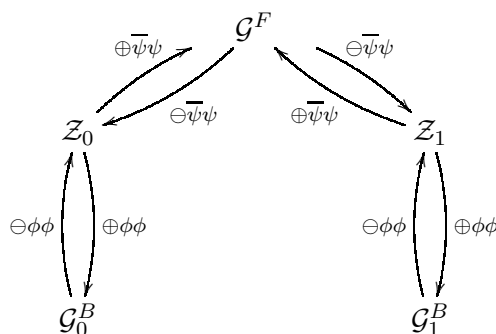
Figure 3.6: Schematic representation of the configuration spaces. Note the configuration space $\mathcal{G}^F \equiv \mathcal{G}_0^F = \mathcal{G}_1^{\overline{F}}$ which mediates between the bosonic and the fermionic sector. By the symbols $\oplus$ and $\ominus$, we label the addition and removal of the source and sink field variables, respectively.

detailed discussion of these actions.

3.7 The Lattice Action with Counterterm

First, we review the construction of the lattice action with a counterterm. The argument involves power counting in terms of the lattice spacing a which we therefore need to restore in this section. The analysis is based on [23] and it involves an investigation of the reason for the failure of the theory to reproduce the correct continuum limit as well as the construction of a counterterm which modifies the action in such a way that in the continuum supersymmetry is restored.

Lattice Perturbation Theory

Let us start with the review of the power counting for a lattice theory. The superficial lattice degree of divergence of a Feynman diagram is defined as the exponent D in a^{-D} at small lattice spacing. For a one-dimensional theory, a factor a^{-1} is assigned to the measure of every momentum loop integral. Recalling the bosonic and the fermionic lattice propagators in momentum

space,

$$\tilde{\Delta}^B(k) = \frac{1}{(2\frac{1}{a}\sin(\pi k/N))^2 + \mu^2}, \tag{3.79}$$

$$\tilde{\Delta}^F(k) = \frac{-i\frac{1}{a}\sin(2\pi k/N) + \mu + 2r\frac{1}{a}\sin^2(\pi k/N)}{\frac{1}{a^2}\sin^2(2\pi k/N) + (\mu + 2r\frac{1}{a}\sin^2(\pi k/N))^2}, \tag{3.80}$$

we can identify their behaviour for small lattice spacings as being of order a^2 and a, respectively.

As an illustration, we restrict the analysis in the following to the superpotential P_u and the case of unbroken supersymmetry. The interacting part of the lattice action for unbroken supersymmetry using the superpotential eq.(3.31) is given by

$$S_L^{\text{int}} = a \sum_x \left(\mu g \phi_x^4 + \frac{1}{2} g^2 \phi_x^6 + 3g\phi_x^2 \overline{\psi}_x \psi_x \right). \tag{3.81}$$

For any Feynman diagram of this action, we have to count the number of the vertices for the boson self-interaction ϕ_x^4 by V_4, the number of vertices for the boson self-interaction ϕ_x^6 by V_6, and the number of vertices for the boson-fermion interaction $\phi_x^2 \overline{\psi}_x \psi_x$ by $\tilde{V}_4$. For none of these vertices momentum is involved and thus each one of them has a UV degree of $D = 0$. To calculate the divergence of a diagram, the usual relations between the number of loops L, the number of internal boson and fermion lines I_B and I_F, the number of external boson and fermion lines E_B and E_F, and the vertices V_4, V_6, and $\tilde{V}_4$ lead to the set of equations

$$D = L - 2I_B - I_F, \tag{3.82}$$

$$L = 1 + I_B + I_F - V_4 - V_6 - \tilde{V}_4, \tag{3.83}$$

$$E_B + 2I_B = 4V_4 + 6V_6 + 2\tilde{V}_4, \tag{3.84}$$

$$E_F + 2I_F = 2\tilde{V}_4. \tag{3.85}$$

We need to address the divergent diagrams which requires that we find all solutions with $D \geq 0$ [75] and $L > 0$. The only solution is

$$D = E_F = I_B = V_4 = V_6 = 0, \qquad L = I_F = \tilde{V}_4 = 1, \qquad E_B = 2. \tag{3.86}$$

This one-loop correction to the boson two-point function and the corresponding Feynman diagram is shown in figure 3.7(a).
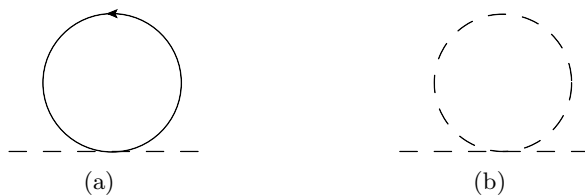
Figure 3.7: One-loop contributions to the bosonic propagator. The solid directed line represents the fermion and the dashed line represents the boson.

The Loop Integrals in the Continuum

We now consider the loop integral for this graph in the continuum. Introducing an UV cutoff of π/a, the integral yields

$$\Sigma^{(a)} = 6g \int_{-\pi/a}^{\pi/a} \frac{dp}{2\pi} \frac{-ip + \mu}{p^2 + \mu^2} = 6g \left(\frac{1}{2} + \mathcal{O}(a\mu) \right). \tag{3.87}$$

Thus, rather than being log-divergent as one could have expected from power counting alone, this diagram is finite. The reason lies in the fact that the potentially divergent part is odd with respect to $p \to -p$ and cancels after the integration.

To calculate the total amplitude at $\mathcal{O}(g)$ in perturbation theory, we also need to consider the bosonic one-loop diagram in figure 3.7(b). This is the other diagram which contributes to the bosonic two-point function. Calculating the loop for this integral yields the finite result

$$\Sigma^{(b)} = -12\mu g \int_{-\pi/a}^{\pi/a} \frac{dp}{2\pi} \frac{1}{p^2 + \mu^2} = -6g \left(1 + \mathcal{O}(a\mu) \right). \tag{3.88}$$

Adding up both one-loop corrections to the boson propagator, the final result gives

$$A = -3g(1 + \mathcal{O}(a\mu)). \tag{3.89}$$

After having established the results for the loop integrals in the continuum, we now repeat the same calculations on the lattice.

The Loop Integrals on the Lattice

We need to find the reason why, after discretising the theory via standard discretisation, supersymmetry is not restored in the continuum limit. As the

answer for this puzzle lies within the fermionic loop integral eq.(3.87), we now consider the discretised expression of the integral $\Sigma^{(a)}$,

$$\Sigma_L^{(a)} = \frac{6g}{Na} \sum_{k=0}^{N-1} \frac{-i\frac{1}{a}\sin(2\pi k/N) + \mu + 2r\frac{1}{a}\sin^2(\pi k/N)}{\frac{1}{a^2}\sin^2(2\pi k/N) + \left(\mu + 2r\frac{1}{a}\sin^2(\pi k/N)\right)^2}. \tag{3.90}$$

Let us look carefully at the continuum limit of this expression. The naive procedure of taking the limit involves the following three steps. Firstly, one replaces the discrete momenta with the continuum variable, $2\pi k/(aN) \to p$. Secondly, the sum needs to be substituted with an integral, $1/(aN)\sum_k \to \int \frac{dp}{2\pi}$, and thirdly, one sends the lattice spacing to zero, $a \to 0$. Following this procedure, one recovers the continuum result eq.(3.87). However, this is not the correct way to proceed. Instead, one first needs to compute the sum, and only after calculating the sum one is allowed to take the limit $a \to 0$. Doing the required steps in this order, one finds the fermionic one-loop contribution to the bosonic two-point function to be

$$\Sigma_L^{(a)} = 6g(1 + \mathcal{O}(r\mu a)). \tag{3.91}$$

The result for the lattice calculation apparently differs by a factor 2 from the continuum result eq.(3.87). This discrepancy of the continuum and the lattice result originates from the Wilson mass term $2r\frac{1}{a}\sin^2(\pi k/N)$ which is even and has a non-vanishing contribution to the total sum. Taking the limit naively as described above, this contribution is neglected. Therefore, in order to account for the difference and to match the continuum theory, one must add the same sum to the action. The counterterm which compensates for the additional contribution due to the Wilson mass term then reads

$$\delta_{\mu^2} = \frac{6g}{Na} \sum_{k=0}^{N-1} \frac{2r\frac{1}{a}\sin^2(\pi k/N)}{\frac{1}{a^2}\sin^2(2\pi k/N) + \left(\mu + 2r\frac{1}{a}\sin^2(\pi k/N)\right)^2}. \tag{3.92}$$

This sum has the desired continuum limit and it corresponds to a shift of the bosonic mass,

$$\delta_{\mu^2} = 3g. \tag{3.93}$$

Therefore, we need to add a term to the standard discretised action which contributes to the bosonic mass. This implies that the desired term needs to be proportional to ϕ_x^2,

$$S_L^c = S_L + \frac{a}{2}\sum_x 3g\phi_x^2. \tag{3.94}$$

As we are free to add a constant to the action, we can rewrite this equation in terms of the superpotential as

$$S_L^c = S_L + \frac{a}{2}\sum_x(3g\phi_x^2 + \mu) = S_L + \frac{a}{2}\sum_x P_u''(\phi_x). \qquad (3.95)$$

As stated at the beginning of this section, we derived the counterterm in the action eq.(3.95) specifically for the case of the superpotential P_u. However, it can be shown that the counterterm $\frac{a}{2}\sum_x P''$ holds for any superpotential P [23]. Thus, the expression eq.(3.95) is not only valid for P_u, but it is rather the general form for the action with counterterm for any superpotential P,

$$S_L^c = S_L + \frac{a}{2}\sum_x P''(\phi_x). \qquad (3.96)$$

Note, that we have already encountered this counterterm when discussing the fermion determinant. Going back to eq.(3.35), we identify the counterterm in its continuum form exactly as the argument of the exponential which appeared as an additional factor in front of the continuum determinant when we took the lattice spacing of the lattice determinant to zero. The explicit expressions for the action S_L^c can be found in appendix G for both superpotentials P_u and P_b.

The counterterm has no influence on the hopping expansion of the model such that the derivation is exactly the same as for the standard discretised action. Only the coefficients of the potential V for the bosonic self-interaction are modified, resulting in a different set of site weights Q. Before we turn to the results for the action with counterterm, we discuss in the next section yet another way to achieve the correct continuum result by making use of the properties of supersymmetry.

3.8 The Q_i-Exact Lattice Actions

In this section, we discuss another discretisation for supersymmetric quantum mechanics which leads to the correct continuum limit of the theory [28, 29]. For these considerations, we have to bear in mind that the model has an $\mathcal{N} = 2$ supersymmetry. Recalling the lattice supersymmetry transformations eq.(3.20), the lattice variation $\delta_1 S_L$ of the standard discretised action gives

$$\delta_1 S_L = -\bar{\epsilon}\sum_x \psi_x P''(\phi_x)(\Delta^-\phi_x) + P'(\phi_x)(\Delta^-\psi_x). \qquad (3.97)$$

Note, that this is the lattice version of the surface term in the continuum, eq.(3.3). As the Leibniz rule does not apply on the lattice, it is not possible to integrate this term by parts. Yet, this is necessary for the vanishing of the variation of the action. The lattice action S_L is therefore not invariant under the supersymmetry transformation δ_1. However, we identify the sum in eq.(3.97) as minus the variation of the lattice operator

$$O = \sum_x P'(\phi_x)(\Delta^- \phi_x) \tag{3.98}$$

under the same supersymmetry transformation δ_1, such that we have

$$\delta_1 S_L = -\delta_1 O. \tag{3.99}$$

It is now clear that we can restore the invariance of the action S_L under the supersymmetry transformation δ_1 simply by adding the term O to the discretised action. By introducing the supercharges Q_i via the definitions $\delta_1 = \bar{\epsilon} Q_1$ and $\delta_2 = Q_2 \epsilon$, we write out explicitly the thus constructed action,

$$S_L^{Q_1} = \sum_x \frac{1}{2}(\Delta^- \phi_x)^2 + \frac{1}{2}P'(\phi_x)^2 + \overline{\psi}_x(\Delta^- + P''(\phi_x))\psi_x + \sum_x P'(\phi_x)(\Delta^- \phi_x), \tag{3.100}$$

for which we find the compact form

$$S_L^{Q_1} = \sum_x \frac{1}{2}\left((\Delta^- \phi_x) + P'(\phi_x)\right)^2 + \overline{\psi}_x(\Delta^- + P''(\phi_x))\psi_x. \tag{3.101}$$

This is the Q_1-exact lattice action which preserves the supersymmetry δ_1 exactly for finite lattice spacing. Keeping this single supersymmetry on the lattice is sufficient to protect the theory from those contributions which otherwise spoil the continuum limit. Note, that this action corresponds to the *Ito prescription* in [32]. For explicit expressions of the Q_1-exact action for both superpotentials P_u and P_b, the interested reader is again referred to appendix G.

It is also possible to construct a Q_2-exact lattice action in a very similar way. Discretising the continuum action $\tilde{S}$ in eq.(3.6) with the backward derivative yields

$$\tilde{S}_L = \sum_x \frac{1}{2}(\Delta^- \phi_x)^2 + \frac{1}{2}P'(\phi_x)^2 + \psi_x(\Delta^- - P''(\phi_x))\overline{\psi}_x. \tag{3.102}$$

This action is indeed invariant under the supersymmetry transformation δ_2 if the lattice operator O we have introduced above is subtracted,

$$S_L^{Q_2} = \sum_x \frac{1}{2}(\Delta^- \phi_x)^2 + \frac{1}{2}P'(\phi_x)^2 + \psi_x(\Delta^- - P''(\phi_x))\overline{\psi}_x - \sum_x P'(\phi_x)(\Delta^- \phi_x).$$
(3.103)

This is the Q_2-exact lattice action which preserves the supersymmetry δ_2 exactly for finite lattice spacing. Even though, in principle, it is possible to employ both Q_i-exact actions for numerical calculations, we will use only the Q_1-exact action.

Unlike the actions with counterterm, the Q_i-exact actions do have an impact on the hopping expansion of the action. To be more specific, the Q_i-exact discretisations demand for a new kind of bosonic bond. This is most easily seen by calculating the term O explicitly for both superpotentials P_u and P_b.

We start by considering the additional term O for unbroken supersymmetry, using the superpotential P_u,

$$O = \sum_x P'_u(\phi_x)(\Delta^- \phi_x) = \sum_x \mu\phi_x^2 + g\phi_x^4 - \mu\phi_x\phi_{x-1} - g\phi_x^3\phi_{x-1}. \qquad (3.104)$$

For the Q_1-exact action, this term needs to be added to the standard discretised action. Keeping in mind the positive sign in front of the operator, we now look at the different terms it generates one by one. The first two terms $\mu\phi_x^2$ and $g\phi_x^4$ modify the potential $V(\phi)$ for the bosonic self-interaction. This is similar to the actions with counterterm and has no influence on the hopping expansion. Only the site weights Q have to be adapted. The term $-\mu\phi_x\phi_{x-1}$ contributes to the weight of the bond b^B such that this bond weight picks up an additional mass term, such that $w = 1 + \mu$. The term $-g\phi_x^3\phi_{x-1}$ is new for our considerations. Apparently, this term is some sort of hopping term and generates a new kind of bosonic bond. The weight of this bond can directly be read off to be g. This kind of bond is different from the bonds we have encountered so far in the sense that it carries one bosonic variable ϕ at the left ending and three bosonic variables ϕ^3 at the right ending, such that this bosonic bond is also directed. Thus, for the Q_1-exact action, we now have to distinguish two different types of bosonic bonds. We label the bonds by indicating the number of bosonic variables they carry at each ending. The bond we have used so far is therefore called $b_{1\to1}^B$ and the new bond $b_{1\to3}^B$. Moreover, the new bosonic bond also demands for a modification of the site

Figure 3.8: The graphical representation of the bosonic bonds $b_{1\rightarrow 3}^B$ and $b_{1\rightarrow 2}^B$ which appear in the context of the hopping expansion for the Q_1-exact action for the super-potentials P_u and P_b, respectively.

occupation number. Because the bonds may carry more than one bosonic variable at an ending, the site occupation number is no longer defined by the number of bosonic bonds running into one site. Rather, it must be modified according to the number of bosonic variables the bonds carry, such that

$$k(x) = n_{1\rightarrow 1}^B(x) + n_{1\rightarrow 1}^B(x-1) + n_{1\rightarrow 3}^B(x) + 3n_{1\rightarrow 3}^B(x-1)^6. \qquad (3.105)$$

To calculate the weight of a configuration contributing to $\mathcal{Z}_F$ (or, equivalently, to the configuration space $\mathcal{G}_F^B$) for the Q_1-exact action, it is straightforward to derive a modified form of eq.(3.51) via hopping expansion. One finds

$$W_{\mathcal{Z}_F} = W_{\mathcal{G}_F^B} = \left(\prod_x \frac{(1+\mu)^{n_{1\rightarrow 1}^B}}{n_{1\rightarrow 1}^B(x)!} \right) \left(\prod_x \frac{g^{n_{1\rightarrow 3}^B}}{n_{1\rightarrow 3}^B(x)!} \right) \left[\prod_x Q_F \left(k(x) \right) \right]. \quad (3.106)$$

In a similar way, one can modify eq.(3.78) to calculate the weight of a configuration contributing to the fermionic two-point function, yielding

$$W_{\mathcal{G}^F} = \left(\prod_x \frac{(1+\mu)^{n_{1\rightarrow 1}^B}}{n_{1\rightarrow 1}^B(x)!} \right) \left(\prod_x \frac{g^{n_{1\rightarrow 3}^B}}{n_{1\rightarrow 3}^B(x)!} \right) \left[\prod_{x\in\mathcal{F}} Q_1(k(x)) \right] \left[\prod_{x\notin\mathcal{F}} Q_0(k(x)) \right].$$
$$(3.107)$$

In figure 3.8 on the left, the graphical representation for the new bosonic bond $b_{1\rightarrow 3}^B$ is depicted. Since the characteristics of the new bond depend directly on the superpotential, we need to repeat the above considerations for the superpotential P_b.

---

[6]This is the site occupation number for a configuration in the configuration space $\mathcal{Z}_F$. For a configuration in the configuration space $\mathcal{G}_F^B$, one needs to account for the additional bosonic variables by adding δ_{x,x_1} and δ_{x,x_2} to the site occupation number as well.

For the superpotential P_b, the explicit expression for the surface term reads

$$O = \sum_x P_b'(\phi_x)(\Delta^- \phi_x) = \sum_x \lambda\phi_x^3 - \lambda\phi_x^2\phi_{x-1}. \tag{3.108}$$

Analogously to the case for the superpotential with unbroken supersymmetry, the term $\lambda\phi_x^3$ modifies the potential V of the bosonic self-interaction and therefore changes the site weight Q. The hopping term $-\lambda\phi_x^2\phi_{x-1}$ generates the bosonic bond $b_{1\to2}^B$ for which the weight λ can also be read off directly. This bond carries one bosonic variable ϕ at the left ending and two bosonic variables ϕ^2 at the right ending. For this action, the site occupation number therefore needs to be modified as

$$k(x) = n_{1\to1}^B(x) + n_{1\to1}^B(x-1) + n_{1\to2}^B(x) + 2n_{1\to2}^B(x-1), \tag{3.109}$$

where additional sources for configurations of the two-point function have to be accounted for as pointed out before. The weight for a configuration in the configuration space $\mathcal{Z}_F$ or $\mathcal{G}_F^B$ is therefore found to be

$$W_{\mathcal{Z}_F} = W_{\mathcal{G}_F^B} = \left(\prod_x \frac{1}{n_{1\to1}^B(x)!}\right)\left(\prod_x \frac{\lambda^{n_{1\to2}^B}}{n_{1\to2}^B(x)!}\right)\left[\prod_x Q_F(k(x))\right]. \tag{3.110}$$

Analogously, the adapted weight for a configuration contributing to the fermionic two-point function reads

$$W_{\mathcal{G}^F} = \left(\prod_x \frac{1}{n_{1\to1}^B(x)!}\right)\left(\prod_x \frac{\lambda^{n_{1\to2}^B}}{n_{1\to2}^B(x)!}\right)\left[\prod_{x\in\mathcal{F}} Q_1(k(x))\right]\left[\prod_{x\notin\mathcal{F}} Q_0(k(x))\right]. \tag{3.111}$$

With these modifications for the weights of a configuration, we have now covered all necessary adaptions for the analysis of supersymmetric quantum mechanics by employing the Q_1-exact action.

We conclude this section with a few remarks. There are other discretisations possible which preserve half of the supersymmetry on the lattice. For example, using a Wilson type discretisation also for the bosonic derivative instead of the backward derivative renders the results for all topological observables supersymmetric, even though the action itself is not [76]. This discretisation as well as other discretisations (e.g. the Stratanovich prescription [31, 32, 77]) are less convenient in the bond language since they generate even more additional types of bosonic bonds. Therefore, we restrict our numerical investigations

for actions which preserve one supersymmetry on the lattice to the Q_1-exact action.

In the next two chapters, we present our methods for the numerical calculations and the results we obtained for the lattice field theory formulation of supersymmetric quantum mechanics.

Chapter 4

Supersymmetric QM on the Lattice: Results Part I

The reformulation of the system in terms of bosonic and fermionic bonds as derived in chapter 3 provides a perfect set-up for Monte Carlo simulations. In chapter 5 we will derive an algorithm for the update of the bosonic as well as for the fermionic bond configuration and discuss the results we obtain by applying the algorithm to supersymmetric quantum mechanics. Yet, for a system in one dimension, the bond formulation allows for solving the system exactly[1], even for finite lattice spacing. In the present chapter, we will elaborate on this approach and discuss exact lattice results for supersymmetric quantum mechanics.

In the first section, we will explain how such exact lattice results are calculated and introduce the concept of *transfer matrices*. We will derive explicitly the construction of such transfer matrices for supersymmetric quantum mechanics. We will then work out the calculation of various observables such as correlation functions, Ward identities, and the mass gaps by using transfer matrices. After these technical considerations, we will show the exact numerical results we obtained employing the transfer matrix technique in the remaining two sections. The first and main section of the results will focus on supersymmetric quantum mechanics formulated with the action with counterterm. We will solve the system thoroughly for both, unbroken and broken supersymmetry and present results for various observables of interest. In the remaining section, we will discuss necessary modifications of the transfer matrices to describe the system in the formulation with the Q_1-exact action and present exact lattice results for observables of interest for unbroken supersymmetry.

---

[1]Exactly, that is up to a cutoff we need to introduce for the bosonic bond occupation number to render the system finite. The cutoff affects the numerical results only close to the continuum.

4.1 The Transfer Matrices

In this section, we will derive the formulation of supersymmetric quantum mechanics in terms of transfer matrices. As we have done previously for the hopping expansion, we will use the the lattice formulation with the action S_L for the following considerations. On the one hand, this formulation catches all conceptual features of the construction of the transfer matrices and on the other hand, we can thereby rely on the relevant formulas derived in chapter 3.

4.1.1 The Transfer Matrices and the Partition Function

We start by considering a configuration contributing to the configuration space of the partition function. After the hopping expansion, the degrees of freedom are expressed in terms of the number of fermionic bonds $n^F \in \{0, 1\}$ and bosonic bonds $n^B_{1\to1} \in \mathbb{N}_0$. These bonds connect next neighbouring lattice sites. We now define a matrix T which takes the system at a site from one bond state $|m^F, m^B_{1\to1}\rangle$ to another bond state $|n^F, n^B_{1\to1}\rangle$. Since there is no upper limit on the bosonic bonds, the matrix T is infinitely large. To be able to handle the matrix numerically, we therefore need to introduce an artificial cutoff on the bosonic states. This seems reasonable since in the hopping expansion, the bosonic bonds are suppressed by a factor $1/n^B_{1\to1}!$ and the contributions of these heavily suppressed states with high occupation numbers is negligible[2]. Setting the bosonic cutoff to N^{cut} possible states yields a $2N^{cut} \times 2N^{cut}$ transfer matrix, where the factor 2 stems from the two possible fermionic bond states.

For a configuration in the configuration space $\mathcal{Z}_F$, the fermion number is conserved at each site and the transfer matrix decomposes into block diagonal form for the bosonic and fermionic sector. Therefore, we define these sub-matrices as the transfer matrices $T^F_{m,n} \equiv T^F_{m^B_{1\to1}, n^B_{1\to1}}$[3], which take the system from the state $|F, m^B_{1\to1}\rangle$ to the state $|F, n^B_{1\to1}\rangle$. In figure 4.1 an example for the graphical representation of an entry of the transfer matrix for each sector $F = 0, 1$ is shown. Explicitly, the transfer matrices are given by

---

[2] Our calculations with transfer matrices where the bosonic cutoff is set to be of $\mathcal{O}(10^3)$ justify this assumption.

[3] Note, that a bosonic bond state n is in general characterised by the bond numbers of several types of bosonic bonds. However, for the action S_L, the numbering of the bosonic states n coincides with the bond number $n^B_{1\to1}$.
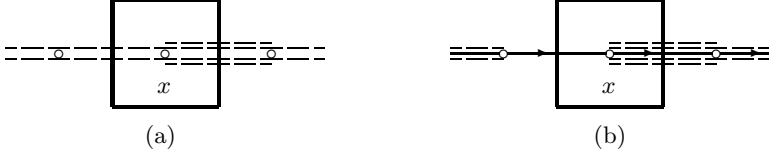
(a)   (b)

Figure 4.1: Graphical representation of the transfer matrix. Figure (a) represents the entry $T_{2,4}^0$ of the bosonic transfer matrix and figure (b) shows the entry $T_{0,4}^1$ of the fermionic transfer matrix.

$$T_{m,n}^F = \frac{1}{\sqrt{m_{1\to 1}^B!}} \frac{1}{\sqrt{n_{1\to 1}^B!}} \, Q_F\left(m_{1\to 1}^B + n_{1\to 1}^B\right). \tag{4.1}$$

For a lattice of length L_t the partition function for both the fermionic and the bosonic sector can then be calculated independently in terms of T^F as

$$Z_F = \mathrm{Tr}\left[\left(T^F\right)^{L_t}\right]. \tag{4.2}$$

Diagonalising the transfer matrices, we observe that the same partition function can be calculated equally via the eigenvalues λ_k^F of T^F,

$$Z_F = \sum_{k=0}^{N-1} \left(\lambda_k^F\right)^{L_t}. \tag{4.3}$$

The partition functions may then be combined as usual to the partition functions for periodic and antiperiodic boundary conditions as

$$Z_{PBC} = Z_0 - Z_1, \qquad Z_{aPBC} = Z_0 + Z_1. \tag{4.4}$$

4.1.2 Correlation Functions

Next, we extend the concept of transfer matrices to the calculation of correlation functions. Recalling how the two-point functions are calculated in the bond language, we realise that the transfer matrix approach also provides a perfect tool for the exact calculation of the bosonic as well as the fermionic two-point function.

The Bosonic Correlation Function

We first consider the bosonic two-point function. To get a contribution to the expectation value of $\langle \phi_{x_1} \phi_{x_2} \rangle$, we have to add an additional bosonic field

Figure 4.2: Graphical representation of the bosonic transfer matrix of a site with additional bosonic variables. Figure (a) represents the matrix element $T_{2,4}^0(1)$ and figure (b) the matrix element $T_{2,4}^0(2)$ of a site with one and two additional sources, respectively.

variable at the sites x_1 and x_2. The graphical representation for an entry of such a transfer matrix with additional bosonic variables is shown in figure 4.2. Note that we still use the symbol $\bigcirc$ for each additional source. The additional variables affect the weight of the configuration via the occupation number $k(x) = n_{1\to1}^B(x) + n_{1\to1}^B(x-1) + \delta_{x,x_1} + \delta_{x,x_2}$. Thus, we introduce modified transfer matrices which allow for additional bosonic sources,

$$T_{m,n}^F(i) \equiv T_{m,n}^F(\phi^i) = \frac{1}{\sqrt{m_{1\to1}^B!}} \frac{1}{\sqrt{n_{1\to1}^B!}} \, Q_F\left(m_{1\to1}^B + n_{1\to1}^B + i\right), \qquad (4.5)$$

such that we can calculate the non-normalised expectation value g_F^B by using the transfer matrices $T^F(\delta_{x,x_1} + \delta_{x,x_2})$ for each site x. The originally defined transfer matrices in eq.(4.1) correspond to transfer matrices with no additional sources, $T^F(0) \equiv T^F$. Using translational invariance and the commutativity properties of the bosonic field variables, we define $t = (x_1 - x_2) \bmod L_t$. The non-normalised bosonic two-point function then reads explicitly

$$g_F^B(t) = \begin{cases} \mathrm{Tr}\left[T^F(1)\left(T^F(0)\right)^{t-1} T^F(1)\left(T^F(0)\right)^{L_t-t-1}\right] & \text{if } t \neq 0, \\[2mm] \mathrm{Tr}\left[T^F(2)\left(T^F(0)\right)^{L_t-1}\right] & \text{if } t = 0. \end{cases} \qquad (4.6)$$

For the bosonic correlation function we also need the expectation value of ϕ. From the previous considerations it is easy to see that the non-normalised expectation value for any moment of ϕ can be calculated as

$$\langle\!\langle \phi^i \rangle\!\rangle_F = \mathrm{Tr}\left[T^F(i)\left(T^F(0)\right)^{L_t-1}\right]. \qquad (4.7)$$

(a) $\overline{T}(\overline{\psi})$ (b) $\overline{T}(\psi)$ (c) $\overline{T}(\overline{\psi}\psi)$ (d) $T^1(0)$
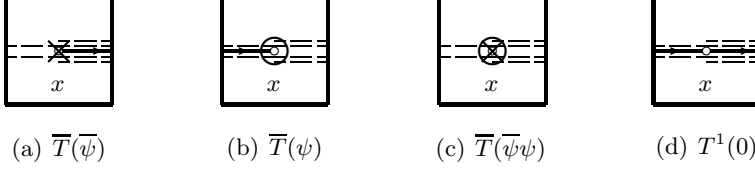
Figure 4.3: Graphical representation of the entry $\overline{T}_{2,4}$ of the transfer matrices with additional fermionic sources (figures 4.3(a) - 4.3(c)). All of these entries can be represented by the entry $T_{2,4}^1(0)$ (figure 4.3(d)).

The bosonic correlation function for periodic and antiperiodic boundary conditions is then calculated according to eqs.(3.59,3.60). Explicitly, they read

$$C^B(t)_{PBC} \;\; = \;\; \frac{g_0^B(t) - g_1^B(t)}{Z_0 - Z_1} - \left(\frac{\langle\!\langle \phi \rangle\!\rangle_0 - \langle\!\langle \phi \rangle\!\rangle_1}{Z_0 - Z_1} \right)^2, \tag{4.8}$$

$$C^B(t)_{aPBC} \;\; = \;\; \frac{g_0^B(t) + g_1^B(t)}{Z_0 + Z_1} - \left(\frac{\langle\!\langle \phi \rangle\!\rangle_0 + \langle\!\langle \phi \rangle\!\rangle_1}{Z_0 + Z_1} \right)^2. \tag{4.9}$$

The Fermionic Correlation Function

To calculate the fermionic correlation function in the transfer matrix approach, we need to recall the structure of a bond configuration contributing to the fermionic two-point function. The translation invariance holds true for the fermionic correlation function too, such that we define $t = (x_1 - x_2) \bmod L_t$. Similarly to the bosonic case, we need to introduce new transfer matrices. In particular, we need a transfer matrix representing a site with a fermionic source and sink $\overline{T}(\overline{\psi}\psi)$, one representing a site with a fermionic source, $\overline{T}(\overline{\psi})$, and one with the fermionic sink, $\overline{T}(\psi)$. As usual, single additional fermionic variables have to be paired with a fermionic bond, an outgoing one to the right for a site with a source variable $\overline{\psi}$ and an incoming one from the left for a site with a sink variable ψ. The graphical representation for an entry of these transfer matrices is shown in figure 4.3. The non-normalised fermionic correlation can then be composed of these matrices as

$$g^F(t) \;\; = \;\; \begin{cases} \mathrm{Tr}\left[\overline{T}(\overline{\psi}) \left(T^1(0)\right)^{t-1} \overline{T}(\psi) \left(T^0(0)\right)^{L_t - t - 1} \right] & \text{if } t \neq 0, \\[2ex] \mathrm{Tr}\left[\overline{T}(\overline{\psi}\psi) \left(T^0(0)\right)^{L_t - 1} \right] & \text{if } t = 0. \end{cases} \tag{4.10}$$

Since the weight of a site saturated with an additional fermionic source paired with a fermionic bond is the same as the weight of a site saturated with two fermionic bonds or a source and a sink variable, the newly introduced transfer matrices all have the same entries as the transfer matrix $T^1(0)$, such that $\overline{T}(\overline{\psi}) = \overline{T}(\psi) = \overline{T}(\overline{\psi}\psi) = T^1(0)$. Therefore, in fact, the introduction of new matrices for sites with additional fermionic variables is obsolete and the non-normalised fermionic two-point function can be written in terms of the matrices $T^1(0)$ and $T^0(0)$ as

$$g^F(t) = \mathrm{Tr}\left[\left(T^1(0)\right)^{t+1}\left(T^0(0)\right)^{L_t - t - 1}\right]. \tag{4.11}$$

Yet, the formation of the fermionic correlation function is a little more subtle than the one of the bosonic correlation function. The translation invariance of the two-point function together with the invariance of a trace under cyclic permutations amounts to the fact that $g^F(t)$ is a superposition of *all possible* configurations with an open fermionic string where the fermionic source and the sink are separated by the distance Δt. For a given bosonic bond configuration, there are thus L_t different configurations with an open fermionic string. For Δt of them, the fermionic string crosses the boundary. Therefore, for antiperiodic boundary conditions, we have to account for those configurations which contain a fermionic string crossing the boundary as they pick up a negative sign. Keeping track of all the signs correctly, the fermionic correlation functions for periodic and antiperiodic boundary conditions read

$$C^F(t)_{PBC} = \frac{g^F(t)}{Z_0 - Z_1}, \qquad C^F(t)_{aPBC} = \frac{L_t - 2t}{L_t}\frac{g^F(t)}{Z_0 + Z_1}. \tag{4.12}$$

The exact correlation functions can now serve for the purpose of fitting exponentials such that the mass gaps[4] for the model can be extracted. Since we work with transfer matrices, there is, however, an even more elegant way to determine the mass gaps, i.e. they can be calculated directly via ratios of the eigenvalues of the transfer matrices. Before we discuss this technique in the following subsection, we observe that because of the fact that the configuration space decomposes in the bond language into the bosonic and the fermionic

---

[4]As we employ the same techniques to measure the energy gaps which are used in higher dimensional quantum field theories to extract the mass gaps, we will refer to the differences as mass gaps rather than energy gaps in the following. Yet, strictly speaking, this terminology does not apply in the case of quantum mechanics as a quantum field theory in one dimension.

sector, we are not only able to calculate the correlation functions for PBC and aPBC, but also for each sector individually. The correlation functions for each sector are then given by[5]

$$C_{0,1}^B(t) = \frac{g_{0,1}^B(t)}{Z_{0,1}} - \left(\frac{\langle\!\langle\phi\rangle\!\rangle_{0,1}}{Z_{0,1}} \right)^2, \qquad C_0^F = \frac{g^F(t)}{Z_0}. \tag{4.13}$$

4.1.3 The Mass Gaps Via Eigenvalues of T^F

As a last quantity, we will calculate the mass gaps in the transfer matrix formalism directly and without having to perform a fitting procedure. In appendix I, we show in detail how it is possible to project out the mass gaps via ratios of the eigenvalues of the transfer matrices. If for an $N \times N$ transfer matrix T^F the eigenvalues are ordered such that

$$\lambda_0^F > \lambda_1^F > \cdots > \lambda_{N-1}^F, \tag{4.14}$$

the calculation for the i-th fermionic mass gap yields

$$m_i^F = -\ln(\lambda_i^1/\lambda_0^0). \tag{4.15}$$

By interpreting the expectation value $\langle\overline{\psi}_t\psi_0\rangle = C^{\overline{F}}(t)$ as the correlator of the antifermion $\overline{F}$, we can similarly calculate its mass via

$$m_i^{\overline{F}} = -\ln(\lambda_i^0/\lambda_0^1). \tag{4.16}$$

The bosonic mass gaps are defined in each sector $F = 0, 1$ individually. They are calculated as

$$m_{F,i}^B = -\ln(\lambda_i^F/\lambda_0^F). \tag{4.17}$$

In figure 4.4, we illustrate schematically which mass gap is measured with respect to which vacuum via the ratios of the eigenvalues.

Here, we conclude the discussion of the transfer matrix technique. We will present in the following the exact lattice results for supersymmetric quantum mechanics employing this technique.

---

[5]Remember that the fermionic correlation function is only defined in the bosonic sector $F = 0$.
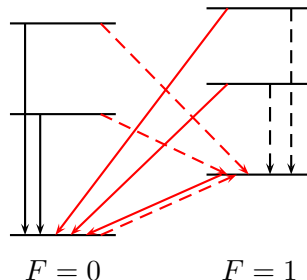
Figure 4.4: The mass gaps measured via ratios of the eigenvalues of T^0 and T^1. Bosonic masses (black) and fermionic masses (red) measured with respect to the bosonic (solid lines) and fermionic (dashed lines) vacuum. Note, that unless the vacua are degenerate, there is *always* one negative fermionic mass, i.e. the one measured from the energetically lower to the higher vacuum.

4.2 Results for the Action with Counterterm

In this section, we present exact lattice results for the action with counterterm by employing the transfer matrix technique. For the superpotentials P_u and P_b, the actions are given explicitly in appendix G. The lattice formulation provides a regularisation for this discretisation, such that we are able to study thoroughly both unbroken and broken supersymmetry. We will perform our calculations for couplings which lie outside of the perturbative regime, as this is the regime of most interest for a lattice calculation.

We will calculate different quantities for the formulation with the superpotential P_u and unbroken supersymmetry as well as for the formulation with the superpotential P_b and broken supersymmetry. For the interpretation of the results, we will benefit from our thorough discussion of supersymmetric quantum mechanics in chapter 2.

4.2.1 The Technical Aspects

We start with a brief discussion of some technical aspects for the numerical calculations in this formulation. First of all, we need to specify the transfer matrices for the actions with counterterm. Because, analogously to the standard discretised action S_L, for these actions the bosonic states are completely

characterised by the number of bonds of the type $b^B_{1\to1}$ and because the weight of a bosonic bond is also the same as for the action S_L, $w_{1\to1} = 1$, the transfer matrices for this discretisation are given by eq.(4.1) for both P_u and P_b. The entry $T_{m,n}$ thus represents also for S^c_L a state with $m^B_{1\to1}$ incoming and $n^B_{1\to1}$ outgoing bosonic bonds of the type $b^B_{1\to1}$ and only the site weights Q_F are different for each action.

It is also worth saying a few words about the extrapolation process we used to derive the continuum results. For all calculations, we set the cutoff for the bosonic occupation number to $N^{cut}_{1\to1} = 800$, such that we had to deal with transfer matrices of the size 801×801. We then calculated the observable of interest for lattices of different extents, ranging from $L_t = 20$ to $L_t = 700$. These lattice sizes were still manageable with a reasonable computational effort.

In a graph where an observable is plotted for different lattice spacings, possible effects of the bosonic cutoff manifest themselves as a sudden bend in an otherwise linear curve close to the continuum. In this region, the results are no longer reliable. In figure 4.5 we show an example of this effect by means of the expectation value $\langle \phi^2 \rangle_{aPBC} \cdot \mu$ versus $a\mu$ for different μL for unbroken supersymmetry and a coupling $f = 1$. The effect of the cutoff of the bosonic occupation numbers is illustrated by comparing the expectation value for two different cutoffs, $N^{cut}_{1\to1} = 800$ and $N^{cut}_{1\to1} = 500$.

The curves for the expectation value are indistinguishable for $a\mu \gtrsim 0.0075$. In this region, the values are reliable for both cutoffs. Closer to the continuum, the curve for the cutoff $N^{cut}_{1\to1} = 500$ diverges from the curve for the cutoff $N^{cut}_{1\to1} = 800$. This is the region where the values obtained are no longer reliable for the lower cutoff. Even closer to the continuum, for $a\mu \lesssim 0.005$, the curve calculated with the bosonic cutoff of $N^{cut}_{1\to1} = 800$ no longer shows linear behaviour either but bends suddenly towards minus infinity. In this region very close to the continuum, also the calculations with the higher cutoff cease to yield reliable results.

For our calculated lattice sizes and moderate values of $\mu L > 5$, a cutoff of $N^{cut}_{1\to1} = 800$ is therefore sufficient to guarantee that the results are not affected. For calculations closer to the continuum, data points in the region where the observable becomes divergent were omitted in the continuum extrapolation.
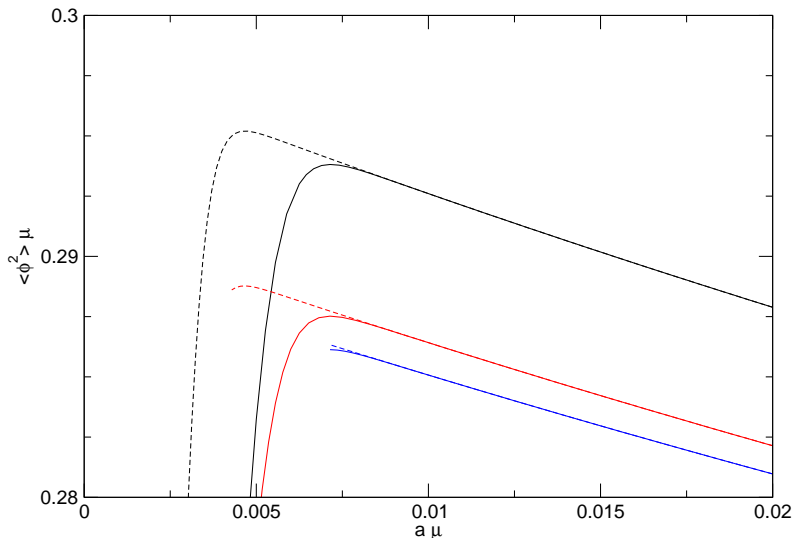
Figure 4.5: Cutoff effects of the bosonic states near the continuum. $\langle\phi^2\rangle_{aPBC}\cdot\mu$ versus $a\mu$ for different $\mu L = 2.0$ (black), $\mu L = 3.0$ (red), and $\mu L = 5.0$ (blue) for $N_{1\to1}^{cut} = 800$ (dashed line) and $N_{1\to1}^{cut} = 500$ (solid line) at $f = 1$.

For the extrapolation, where it is not indicated otherwise, we have fitted the data to the quadratic fitting function

$$f(x) = c_0 + c_1 x + c_2 x^2. \tag{4.18}$$

For almost all observables, these fits could be performed without any difficulties. Yet, there are some observables for which the continuum behaviour is not well approximated by a quadratic function. In the discussion, we mention explicitly how we performed the extrapolation for these observables.

4.2.2 The Ratio Z_{PBC}/Z_{aPBC} and the Witten Index

We start by calculating the ratio Z_{PBC}/Z_{aPBC}. This ratio is equal to the Witten index and represents therefore the most important indicator for the decision whether supersymmetry is broken or not. Hence, we already know what to expect for the case of unbroken supersymmetry as well as for the case of broken supersymmetry. For unbroken supersymmetry, the bosonic vacuum lies well below the fermionic vacuum. Thus, in the zero temperature limit $Z_1 \to 0$, and only the bosonic sector contributes to the partition function,
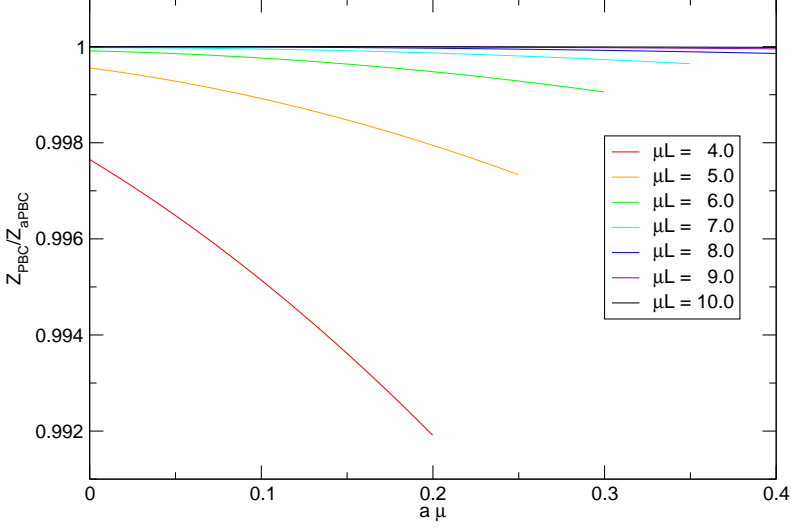
Figure 4.6: Unbroken supersymmetric quantum mechanics. Continuum extrapolation of the ratio Z_{PBC}/Z_{aPBC} versus $a\mu$ for different μL and $f = 1$.

such that

$$\Delta = \frac{Z_{PBC}}{Z_{aPBC}} = \frac{Z_0 - Z_1}{Z_0 + Z_1} \xrightarrow{\beta \to \infty} 1. \tag{4.19}$$

For broken supersymmetry, both vacua are equally preferable. Therefore, in the zero temperature limit $Z_0 = Z_1$, and the Witten index goes to zero,

$$\Delta = \frac{Z_{PBC}}{Z_{aPBC}} = \frac{Z_0 - Z_1}{Z_0 + Z_1} \xrightarrow{\beta \to \infty} 0. \tag{4.20}$$

We now need to confirm these results with our numerical calculations.

Unbroken Supersymmetry

First, we consider unbroken supersymmetry. In figure 4.6, we plot the ratio Z_{PBC}/Z_{aPBC} versus $a\mu$ for different values of fixed μL. The coupling is set to $f = 1$. For the continuum limit, we observe a small dependence on the parameter μL. Because a small value of μL corresponds to a high temperature, this behaviour is expected. Namely, for non-zero temperature, there are non-vanishing contributions from the fermionic vacuum to the partition function Z_1 due to quantum fluctuations, resulting in a ratio $Z_{PBC}/Z_{aPBC} < 1$. Note, that the ratio being $Z_{PBC}/Z_{aPBC} \neq 1$ is no contradiction with the Witten
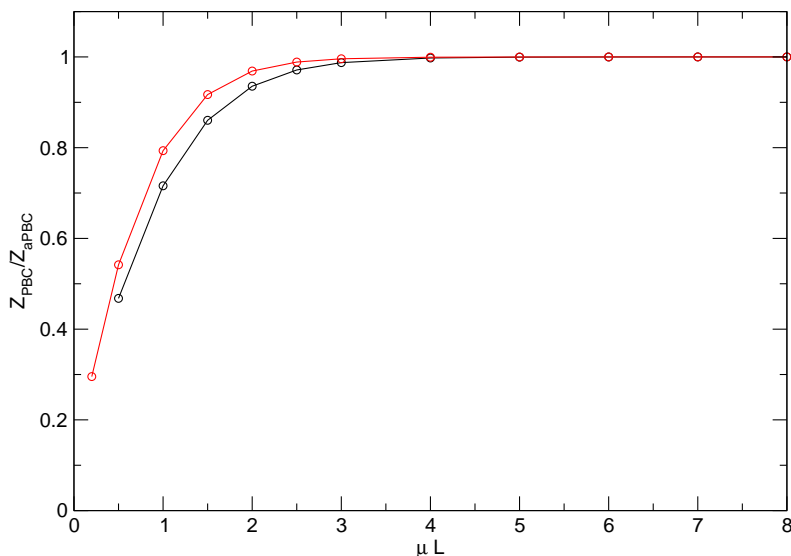
Figure 4.7: Unbroken supersymmetric quantum mechanics. The continuum values of the ratio Z_{PBC}/Z_{aPBC} versus μL for different couplings $f = 1$ (black circles) and $f = 2$ (red circles). The lines are only there to guide the eye.

index, since the index is defined at zero temperature where the ratio indeed goes to one, $Z_{PBC}/Z_{aPBC} \to 1$. In figure 4.7, we show the continuum value of the ratio Z_{PBC}/Z_{aPBC} in dependence of the parameter μL for two different couplings $f = 1$ and $f = 2$.

It can be seen that the system reaches the zero temperature behaviour already for moderate values of μL. This is to be expected, as the fermionic vacuum has the same energy as the first excited state in the bosonic sector. It is therefore very unlikely for the system to undergo a transition into this state for low temperatures, and contributions to the partition function from the fermionic vacuum are therefore negligible for $\mu L \gtrsim 5$.

Broken Supersymmetry

We now repeat the same considerations for broken supersymmetry. Analogously to unbroken supersymmetry we plot the continuum limit of the ratio Z_{PBC}/Z_{aPBC} versus $a\mu$ for different values of fixed μL in figure 4.8. Here too, the coupling is set to $f = 1$. The technical procedure is the same as above,

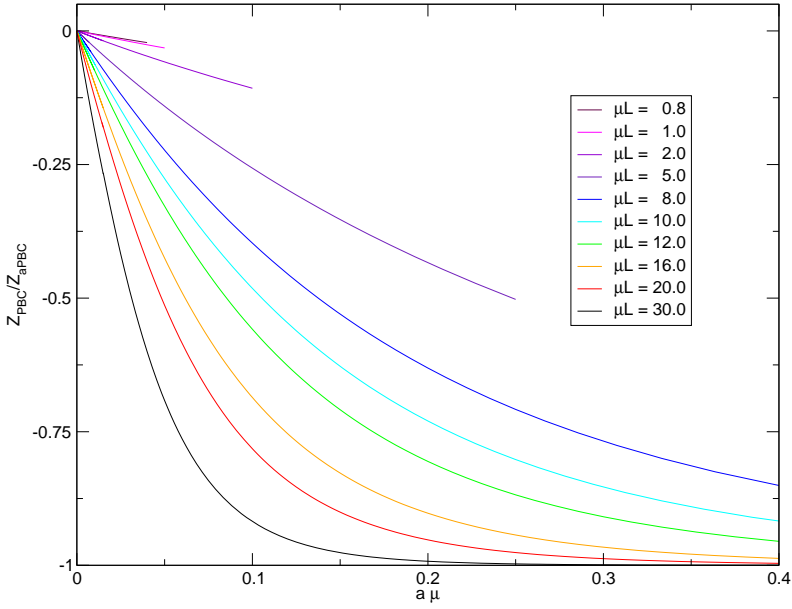**Figure 4.8:** Broken supersymmetric quantum mechanics. Continuum extrapolation of the ratio Z_{PBC}/Z_{aPBC} versus $a\mu$ for different μL and $f = 1$.

with the difference that for large μL, we did not use a quadratic fit, but rather an exponential fit to extrapolate the curves to the continuum.

The behaviour of the the ratio Z_{PBC}/Z_{aPBC} for unbroken supersymmetry is slightly different from the behaviour for unbroken supersymmetry. For unbroken supersymmetry, the continuum result has a dependence on the temperature, whereas for broken supersymmetry all curves extrapolate to zero. This can be understood as follows. In the continuum, all energy levels are degenerate, even for finite temperature. Therefore, in the continuum both vacua are equally favourable, such that $Z_0 = Z_1$ for all μL. However, the lattice discretisation breaks this degeneracy explicitly. From the plot we see that the fermionic vacuum is the preferred one because the continuum limit is approached from below and it is indeed the partition function in the fermionic sector which contributes to the partition function for aPBC with a negative sign. The rather strange exponential behaviour of the curves for small temperatures can be explained as follows. On the one hand, tunnelling rates from the energetically lower to the higher vacuum are very small for large μL. Yet, on the other hand, exactly these tunnellings would be needed for the bosonic vacuum, which is the one requiring more energy, to have a significant contribution to the partition function. Thus, for large μL the bosonic vacuum only has contributions when the effect of the lattice breaking the degeneracy of the vacua becomes very small, which is only the case close to the continuum.

4.2.3 Correlation Functions

In this section, we show some examples of exact correlation functions. As we do not extract the mass gaps via a fit, the discussion of the correlation functions themselves is merely meant to be an illustration. Yet, we will need them in the following section where we discuss Ward identities which relate fermionic and bosonic correlation functions.

Unbroken Supersymmetry

First, we show the bosonic and the fermionic correlation function for unbroken supersymmetry. In figure 4.9(a) we display the correlation functions for PBC and aPBC for a lattice of a temporal extension of $L_t = 60$ and a coupling strength of $f = 1$ for $\mu L = 2.0$, whereas in figure 4.9(b) the same correlation functions are displayed for $\mu L = 10.0$.
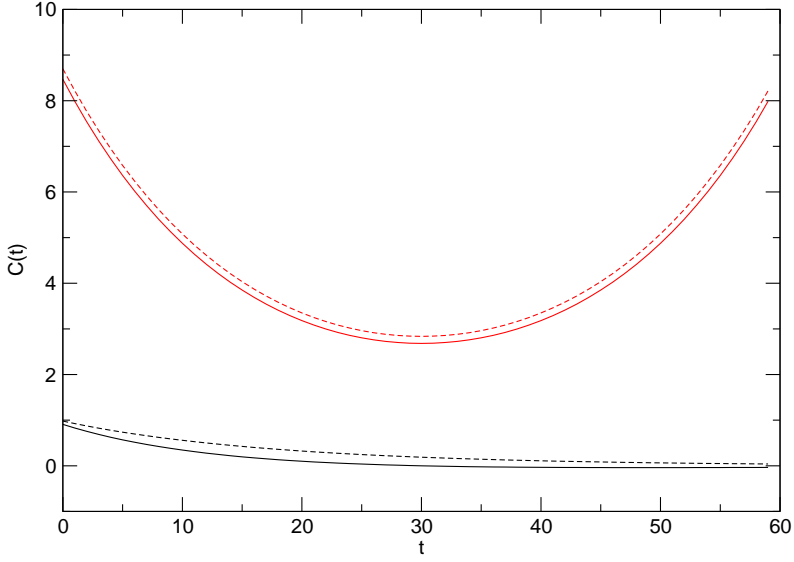
(a) $\mu L = 2.0$
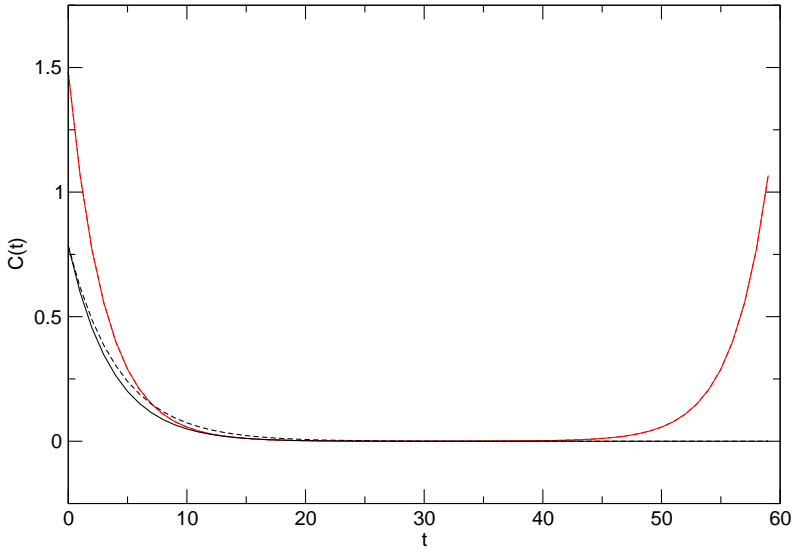
(b) $\mu L = 10.0$

Figure 4.9: Unbroken supersymmetric quantum mechanics. The bosonic (red) and fermionic (black) correlation functions for PBC (dashed line) and aPBC (solid line). $L_t = 60$ and $f = 1$.
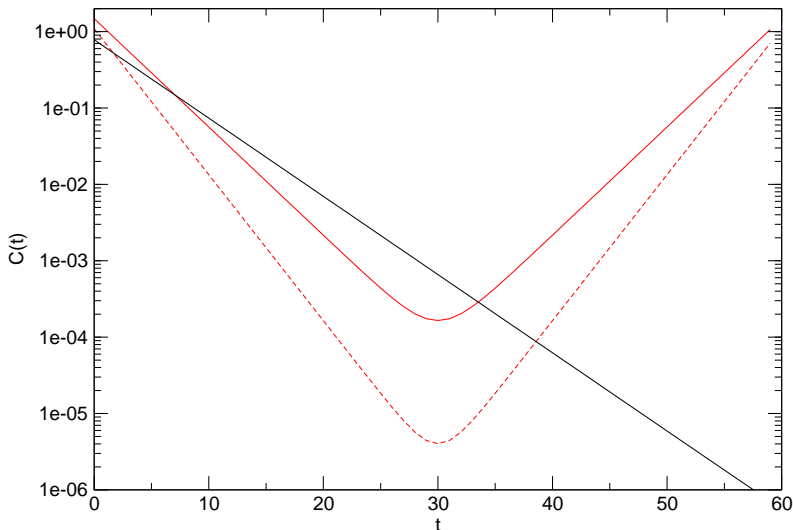
Figure 4.10: Unbroken supersymmetric quantum mechanics. The bosonic (red) and fermionic (black) correlation functions in the sector $F = 0$ (solid line) and $F = 1$ (dashed line). $L_t = 60$, $\mu L = 10.0$, and $f = 1$.

For $\mu L = 2.0$, we know from section 4.2.2 that finite temperature effects are not negligible. In figure 4.9(a) these effects are reflected in the fact that the bosonic correlation functions for PBC and aPBC are clearly distinguishable for $\mu L = 2.0$. For $\mu L = 10.0$, we are in the regime where the system has zero-temperature behaviour. Thus, in figure 4.9(b), the bosonic correlation functions are no longer distinguishable for PBC and aPBC and lie on top of each other. Yet, the fermionic correlation functions are different for PBC and aPBC for this choice of parameters, too. This difference originates in the translational invariance of the fermionic correlation function and the thus resulting incorporation of the boundary conditions via eq.(4.12).

To complete our discussion of the correlation functions for unbroken supersymmetry, in figure 4.10 we display the bosonic and the fermionic correlation functions for the same calculation as above in figure 4.9(b) for each sector F according to eq.(4.13) individually. Note, that the fermionic correlation function only exists in the bosonic sector $F = 0$ whereas the bosonic correlation function exists in both sectors. However, in this temperature regime $Z_0 \gg Z_1$ and therefore, the bosonic correlation function in the fermionic sector $C_1^B(t)$ is
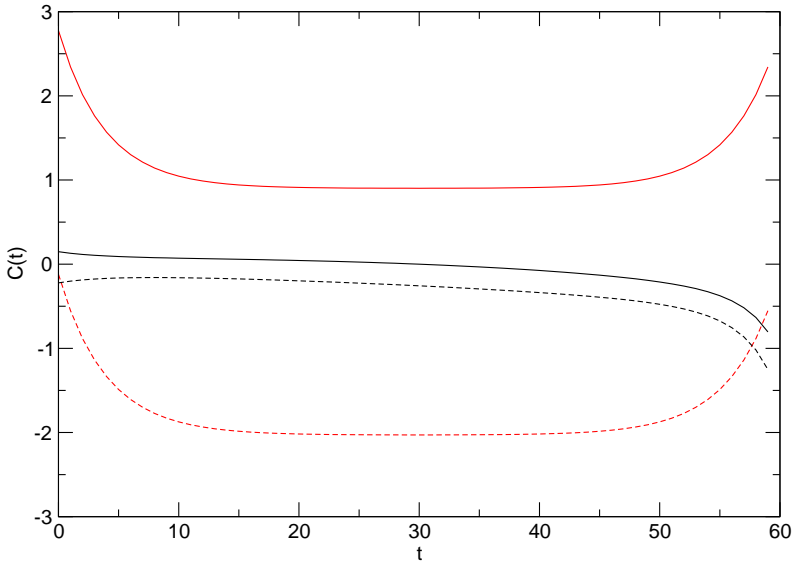
Figure 4.11: Broken supersymmetric quantum mechanics. The bosonic (red) and fermionic (black) correlation functions for PBC (dashed line) and aPBC (solid line). $L_t = 60$, $\mu L = 10.0$, and $f = 1$.

heavily suppressed with respect to the one in the bosonic sector $C_0^B(t)$. This is ignored in figure 4.10 as the relative weight of the different sectors is not taken into account in this graph.

Broken Supersymmetry

In this subsection we show the analogous correlation functions for broken supersymmetry. In figure 4.11, the bosonic and the fermionic correlation functions are displayed for PBC and aPBC for a lattice with $L_t = 60$ and a coupling of $f = 1$ for $\mu L = 10.0$.

Unlike in the case of unbroken supersymmetry, figure 4.11 shows a rather unexpected behaviour for the bosonic correlation functions for PBC and aPBC as they do not approach zero for $t \sim L_t/2$. To get an understanding for this, we first need to consider figure 4.12 where we show the continuum extrapolation for $\langle \phi \rangle$ for the same physical situation, e.g. for $\mu L = 10.0$ and $f = 1$.

The expectation value $\langle \phi \rangle_F$ extrapolates in the continuum for each sector to
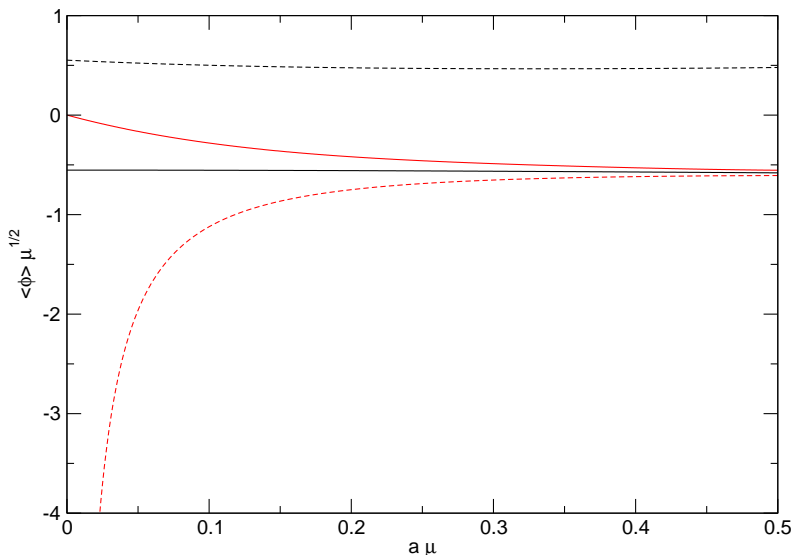
Figure 4.12: Broken supersymmetric quantum mechanics. Continuum extrapolation for $\langle\phi\rangle$ in the sectors Z_0 (black dashed line) and Z_1 (black solid line), for aPBC (solid red line) and for PBC (dashed red line). $\mu L = 10.0$ and $f = 1$.

the same value, however with an opposite sign. This is expected because of the accidental symmetry eq.(3.9) for this action. Furthermore, figure 4.8 suggests that both sectors F are weighted equally in the continuum. Therefore, on the one hand, $\langle\phi\rangle_{aPBC} \to 0$. On the other hand, for PBC, the numerator takes a fixed value while the denominator goes to zero. Thus, the expectation value for $\langle\phi\rangle_{PBC}$ is ill-defined in the continuum.

After these considerations concerning the expectation value of ϕ, we are now able to explain the rather strange fact that the bosonic correlation function has a negative offset. Instead of removing a possible constant offset of the bosonic two-point function, the term $\langle\phi\rangle^2_{PBC}$ shifts the correlation function to negative values. This problem of the shift into the negative worsens closer to the continuum because the term $-\langle\phi\rangle^2_{PBC}$ takes larger negative values for smaller lattice spacings. The bosonic correlation function is therefore an ill-defined observable in the continuum for PBC. It is therefore necessary to look at the correlation function in each sector individually.

In figure 4.13 we show the correlation functions for the same calculation as

above for each sector individually.

We observe that the bosonic correlation functions are very similar in each sector. Note, that the term $\langle\phi\rangle_F^2$ for the correlation functions measured in the bosonic and fermionic sector independently indeed removes the additional constant shift such that the bosonic correlator is close to zero for $t \sim L_t/2$. It is also worth to discuss the rather oddly shaped fermionic correlation function. The figure reveals that there are contributions of four dominant exponentials instead of only one. For $t \sim 0$ and for $t \sim L_t$, there are two separate exponentials with large slopes, one in forward direction and one in backward direction. We can interpret these parts as coming from the second mass gap for the fermion (e.g. the exponential decreasing) and for the antifermion (e.g. the exponential increasing for large t). In addition, we have two rather flat exponentials both increasing around $t \sim L_t/2$. These can be interpreted as the first mass gap for the fermion and the antifermion. The effective masses which are extracted in this region are very small. In fact, these are the masses of the Goldstino which appears in the spectrum for broken supersymmetry. We will elaborate further on this when we discuss the results for the mass gaps in section 4.2.7. As said before, in this interpretation due to lattice artefacts, the lowest mass gap for the fermion is *negative*.

4.2.4 Ward Identities

In this section, we investigate several Ward identities for unbroken and for broken supersymmetry. A very intuitive way to derive these identities is given in [37]. Consider the path integral formulation for the expectation value of an observable $\mathcal{O}(\phi)$. Now rewrite the path integral for a transformed variable, $\phi \rightarrow \phi' = \phi + \delta\phi$, assuming that the measure of the path integral is invariant under this variation, $\mathcal{D}\phi' = \mathcal{D}\phi$. Since physics cannot depend on the shift of the integration variable, we find

$$
\begin{aligned}
\langle\mathcal{O}\rangle &= \frac{1}{Z}\int \mathcal{D}\phi' \ \mathcal{O}(\phi') \ \mathrm{e}^{-S(\phi')} \\
&= \frac{1}{Z}\int \mathcal{D}\phi \ (\mathcal{O}(\phi) + \delta\mathcal{O}(\phi)) \ \mathrm{e}^{-S(\phi)}(1 - \delta S(\phi)) \\
&= \langle\mathcal{O}\rangle + \langle\delta\mathcal{O}\rangle - \langle\mathcal{O}\delta S\rangle.
\end{aligned}
$$

Therefore, for any observable the relation

$$
\langle\delta\mathcal{O}\rangle = \langle\mathcal{O}\delta S\rangle \tag{4.21}
$$
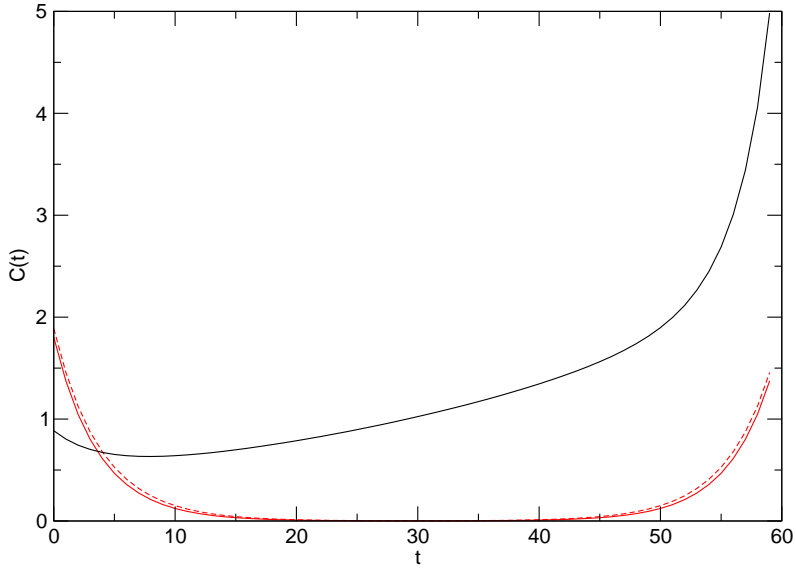
(a) Linear representation
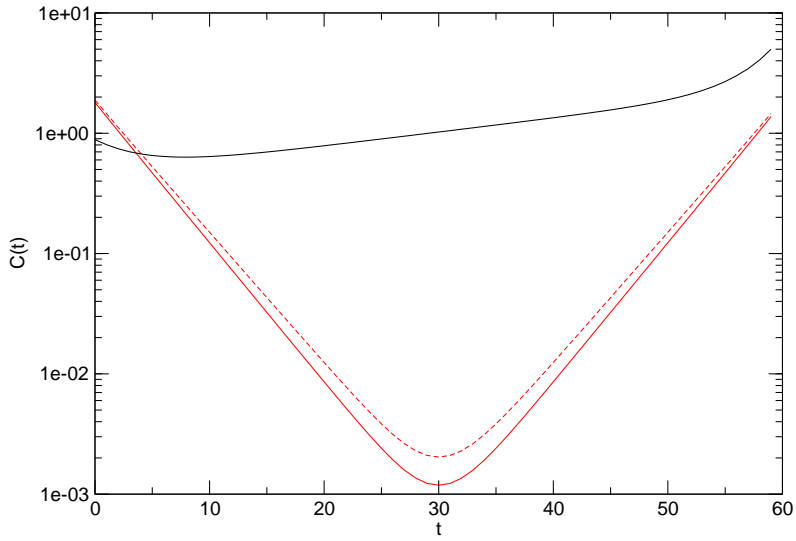
(b) Logarithmic plot

Figure 4.13: Broken supersymmetric quantum mechanics. The bosonic (red) and fermionic (black) correlation functions in the sector $F = 0$ (solid line) and $F = 1$ (dashed line). $\mu L = 10.0$, $L_t = 60$, and $f = 1$.

holds. Now, if the action as well as the ground state are invariant under the transformation δ, the rhs of the equation vanishes, leaving

$$\langle \delta \mathcal{O} \rangle = 0. \tag{4.22}$$

The Ward identities therefore serve us to test whether supersymmetry in the continuum is restored. All the actions we use are invariant under both supersymmetry transformations in the continuum limit. Yet, for broken supersymmetry, the ground state is not. Therefore, if the continuum extrapolation of a Ward identity indeed satisfies eq.(4.22), we can immediately conclude that for the system in question supersymmetry is restored in the continuum. In the following subsections, we will construct different Ward identities and use them to confirm supersymmetry breaking or restoration.

4.2.5 The Ward Identity W

As a first example, we consider the operator $\mathcal{O} = \overline{\psi}$. The variation of this operator under the lattice supersymmetry transformation δ_1 results in a very simple Ward identity,

$$\langle \delta_1 \mathcal{O} \rangle = \langle \delta_1 \overline{\psi} \rangle = \langle -\overline{\epsilon}(\Delta^- \phi + P') \rangle = -\overline{\epsilon}\langle P' \rangle \equiv W. \tag{4.23}$$

Thus, the vanishing of the expectation value of the first derivative of the superpotential $\langle P' \rangle$ in the continuum indicates restoration of supersymmetry[6]. Of course, it is also possible to vary the operator $\mathcal{O}$ under the supersymmetry transformation δ_2. However, for this transformation, the condition eq.(4.22) is satisfied trivially, since $\delta_2 \overline{\psi} = 0$ by definition.

Similarly, one can use the operator $\mathcal{O}' = \psi$ which yields the same Ward identity under the supersymmetry transformation δ_2.

Unbroken Supersymmetry

For unbroken supersymmetry, we need to check if the continuum extrapolation of the following expectation value vanishes,

$$\langle P'_u \rangle = \mu \langle \phi \rangle + g \langle \phi^3 \rangle. \tag{4.24}$$

---

[6]Note, that also in the two-dimensional $\mathcal{N} = 1$ Wess-Zumino model the analogous Ward identity is a suitable choice for the detection of spontaneous supersymmetry breaking.
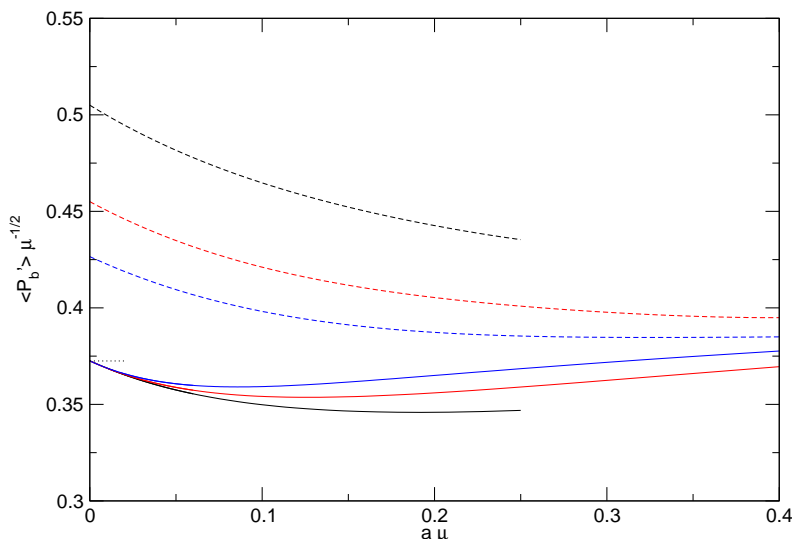
Figure 4.14: Broken supersymmetric quantum mechanics. Continuum extrapolation for $\langle P_b' \rangle / \sqrt{\mu}$ for $\mu L = 5.0$ (black), $\mu L = 8.0$ (red), and $\mu L = 12.0$ (blue) for PBC (dashed lines) and aPBC (solid lines) at $f = 1$.

Unfortunately, the above expectation value is trivially zero. This follows from the definition of the site weights, which for this action is zero for an odd argument, $Q_0(2n+1) = Q_1(2n+1) = 0$, $n \in \mathbb{N}_0$. Therefore, the site occupation number for a bond configuration with non-zero weight must be even, implying that the expectation value for an odd power of ϕ trivially vanishes. To be able to confirm the restoration of supersymmetry in the continuum for the unbroken case, we will find a suitable Ward identity in subsection 4.2.6.

Broken Supersymmetry

For broken supersymmetry, we need to check whether or not the following expectation value vanishes,

$$\langle P_b' \rangle = -\frac{\mu^2}{4\lambda} + \lambda \langle \phi^2 \rangle. \tag{4.25}$$

In figure 4.14, we plot the continuum extrapolation for $\langle P_b' \rangle$ for different μL and a coupling of $f = 1$. For aPBC, the Ward identity extrapolates to the value
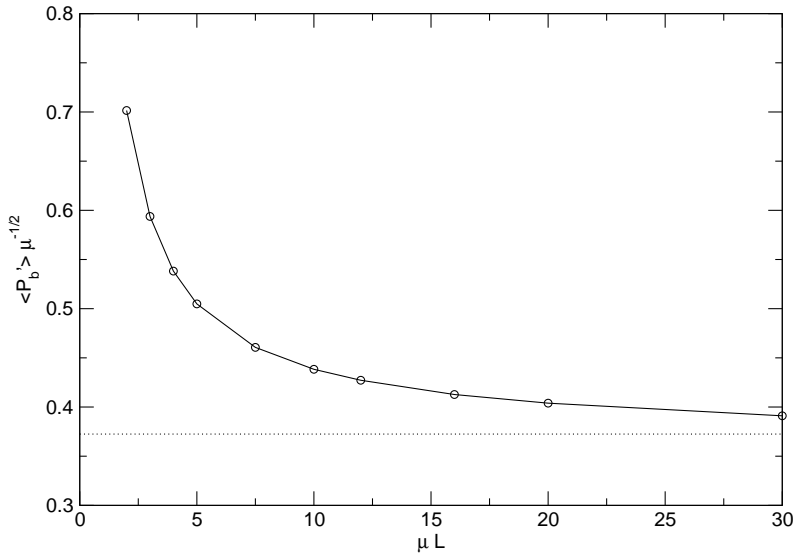
Figure 4.15: Broken supersymmetric quantum mechanics. The continuum values for $\langle P'_b \rangle / \sqrt{\mu}$ versus μL for PBC for $f = 1$. The continuum value for aPBC is indicated with the black dotted line. The solid black line is only there to guide the eye.

$\langle P' \rangle / \sqrt{\mu} = 0.3725 \dots$ [7] independently of the chosen μL. The continuum limit for PBC, however, depends on the chosen μL and approaches the continuum value for aPBC for large μL where the effects of the boundary conditions become smaller. In figure 4.15, we show the continuum values for PBC for different μL.

The figure reveals that for large μL, the continuum value of the Ward identity W for PBC indeed approaches the continuum value for aPBC. However, a value of $\mu L = 30.0$ is still not sufficient to yield the same continuum value for both PBC and aPBC.

Yet, the Ward identity W serves us indeed to verify that supersymmetry is broken for the superpotential P_b in the continuum.

---

[7]This value can be obtained in the operator formalism, [37].

4.2.6 The Ward Identities W_1 and W_2

The variation of the operator $\mathcal{O}_1 = \overline{\psi}_x \phi_y$ under the supersymmetry transformations $\delta_{1,2}$ yields Ward identities which connect bosonic and fermionic correlation functions. In particular, we deduct

$$\langle \delta_1 \mathcal{O}_1 \rangle = \langle \overline{\psi}_x \psi_y \rangle + \langle (\Delta^- \phi + P')_x \phi_y \rangle \equiv W_1(x - y). \qquad (4.26)$$

The variation of the operator $\mathcal{O}_1$ under the supersymmetry transformation δ_2 vanishes trivially. We will now use the Ward identity W_1 to verify supersymmetry restoration and breaking for the respective superpotentials. Note, that this Ward identity will be of special interest for the Q_1-exact action. Since for this action $\delta_1 S_L^{Q_1} = 0$ for finite lattice spacing, we should be able to confirm that $\langle \delta_1 \mathcal{O}_1 \rangle = 0$ exactly at finite lattice spacing for unbroken supersymmetry and periodic boundary conditions.

Analogously, one can use the operator $\mathcal{O}_2 = \psi_x \phi_y$ which under the supersymmetry transformations δ_2 yields a similar set of Ward identities,

$$\langle \delta_2 \mathcal{O}_2 \rangle = \langle \psi_x \overline{\psi}_y \rangle + \langle (\Delta^- \phi - P')_x \phi_y \rangle \equiv W_2(x - y).$$

The variation of the operator $\mathcal{O}_2$ under the other supersymmetry transformations δ_1 vanishes trivially, $\delta_1 \mathcal{O}_2 = 0$.

As both Ward identities W_1 and W_2 have a very similar behaviour for the action with counterterm, we consider only the Ward identity W_1 in this discussion. Results for the other Ward identity W_2 are obtained analogously and do not give any new physical insight.

Unbroken Supersymmetry

Using the translational invariance of the lattice, for the superpotential P_u we find the Ward identity $W_1(t)$

$$W_1(t) = -\langle \psi_t \overline{\psi}_0 \rangle + (1 + \mu)\langle \phi_t \phi_0 \rangle - \langle \phi_{t+1} \phi_0 \rangle + g\langle \phi_t \phi_0^3 \rangle. \qquad (4.27)$$

Note the last term which is a new kind of two-point function. The non-normalised two-point functions of the type $\langle\!\langle \phi_t \phi_0^n \rangle\!\rangle_F$ are easily calculated in the transfer matrix formalism via a generalised version of eq.(4.6),

$$\langle\!\langle \phi_t \phi_0^n \rangle\!\rangle_F = \begin{cases} \mathrm{Tr}\left[T^F(n) \left(T^F(0) \right)^{t-1} T^F(1) \left(T^F(0) \right)^{L_t - t - 1} \right] & \text{if } t \neq 0, \\ \mathrm{Tr}\left[T^F(n+1) \left(T^F(0) \right)^{L_t - 1} \right] & \text{if } t = 0. \end{cases} \qquad (4.28)$$

(a) $\mu L = 4.0, Z_{aPBC}$

(b) $\mu L = 4.0, Z_{PBC}$

(c) $\mu L = 10.0, Z_{aPBC}$

(d) $\mu L = 10.0, Z_{PBC}$

Figure 4.16: Unbroken supersymmetric quantum mechanics. The Ward identity W_1 for $L_t = 50$ (black), $L_t = 100$ (red), $L_t = 200$ (orange), $L_t = 300$ (green), and $L_t = 600$ (blue) for $f = 1$.

In figure 4.16, we show the Ward identity $W_1(t)$ for $\mu L = 4.0$ and for $\mu L = 10.0$ and different L_t at a coupling $f = 1$ for both PBC and aPBC. The figure illustrates how the Ward identity $W_1(t)$ is violated for finite lattice spacing. It can be seen that the violation for PBC becomes less severe as $a \to 0$, whereas in the case of aPBC, the violation does not become smaller in the continuum. The violation for either very small or very large t is much more severe than in the region where $t \backsim L_t/2$. As supersymmetry is only restored if $W_1(t) = 0 \; \forall t$, we are free to choose any t and trace the value for $W_1(t)$ into the continuum. We decide to go to the middle of the lattice and trace $W_1(L_t/2)$.

In figure 4.17, we plot the continuum extrapolation for $W_1(L_t/2)$ at a coupling

Figure 4.17: Unbroken supersymmetric quantum mechanics. Continuum extrapolation for W_1 for $\mu L = 3.0$ (black), $\mu L = 4.0$ (red), $\mu L = 5.0$ (orange), $\mu L = 7.0$ (green), and $\mu L = 10.0$ (blue) for PBC (sold lines) and aPBC (dashed lines) for $f = 1$.

of $f = 1$ for different μL. The Ward identity $W_1(L_t/2)$ extrapolates to zero for PBC, independent of the value for μL. Supersymmetry is therefore restored in the continuum for periodic boundary conditions, even at finite temperature. For aPBC, the Ward identity $W_1(L_t/2)$ does not extrapolate to zero for small μL. However, as the temperature is decreased, the violation weakens and for $\mu L > 10.0$, the extrapolation for W_1 also goes to zero, implying that for zero temperature supersymmetry is also restored for aPBC. On the level of the Ward identities W_1, this analysis hence confirms all the expected features of finite- as well as zero-temperature unbroken supersymmetry.

Broken Supersymmetry

For the superpotential P_b, we derive the Ward identity W_1 similarly to the unbroken case

$$W_1 = -\langle \psi_t \overline{\psi}_0 \rangle + \langle \phi_t \phi_0 \rangle - \langle \phi_{t+1} \phi_0 \rangle - \frac{\mu^2}{4\lambda} \langle \phi \rangle + \lambda \langle \phi_t \phi_0^2 \rangle. \qquad (4.29)$$

In figure 4.18, we show the Ward identity W_1 for $\mu L = 5.0$ and for $\mu L = 10.0$ and different L_t at a coupling $f = 1$ for both PBC and aPBC. This figure

(a) $\mu L = 5.0, Z_{aPBC}$

(b) $\mu L = 5.0, Z_{PBC}$

(c) $\mu L = 10.0, Z_{aPBC}$
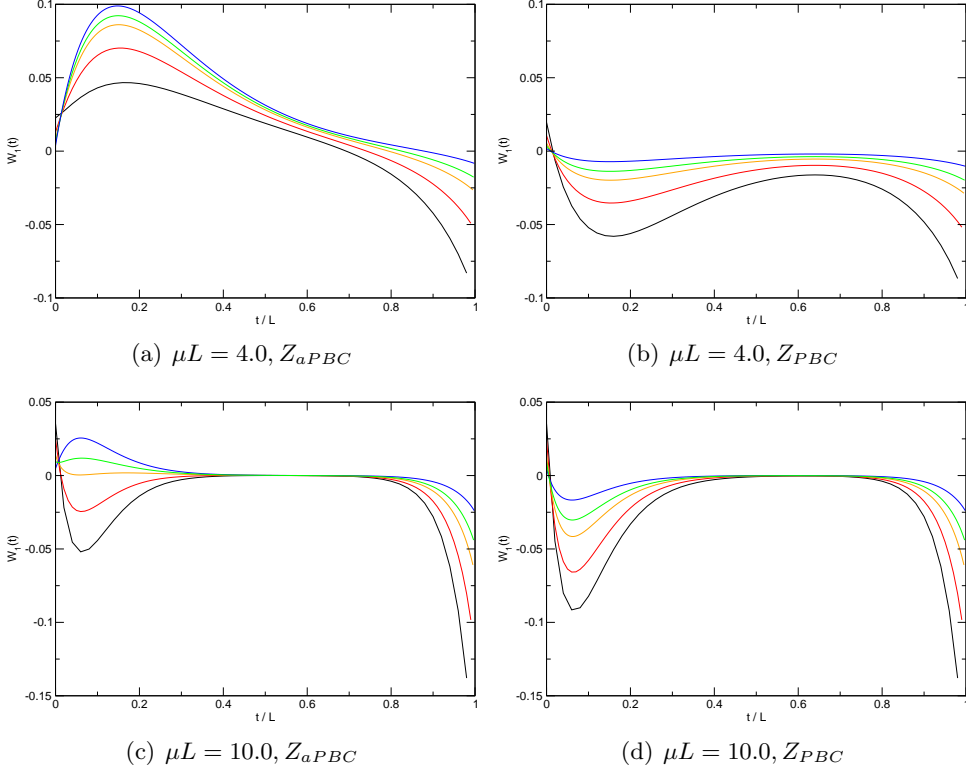
(d) $\mu L = 10.0, Z_{PBC}$
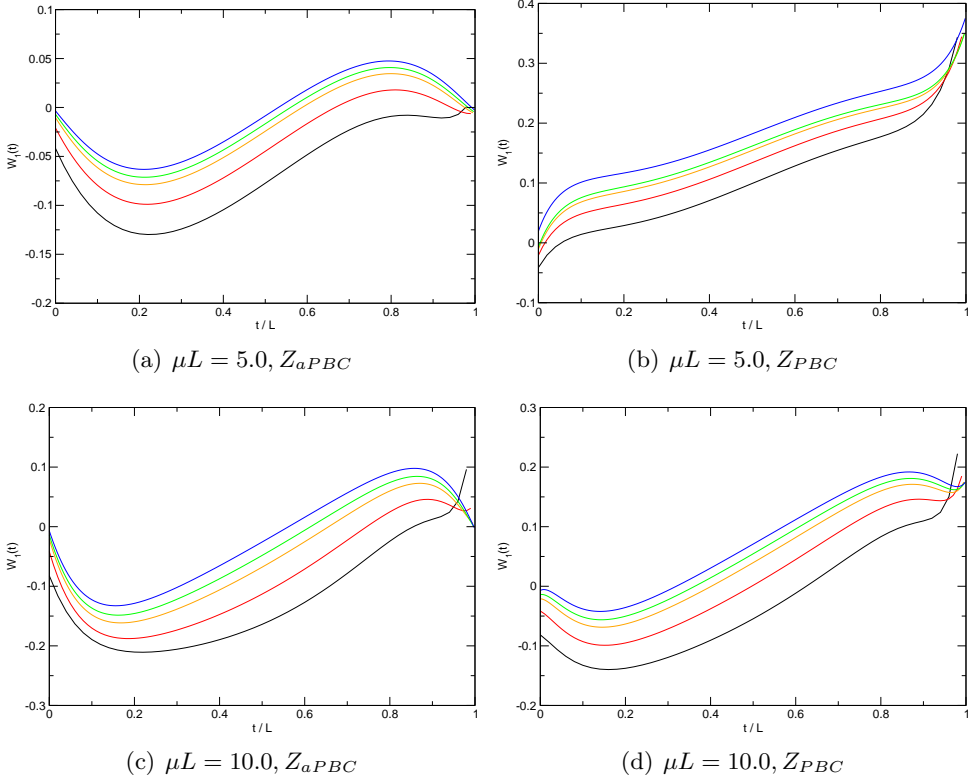
Figure 4.18: Broken supersymmetric quantum mechanics. The Ward identity W_1 for $L_t = 50$ (black), $L_t = 100$ (red), $L_t = 200$ (orange), $L_t = 300$ (green), and $L_t = 600$ (blue) for $f = 1$.
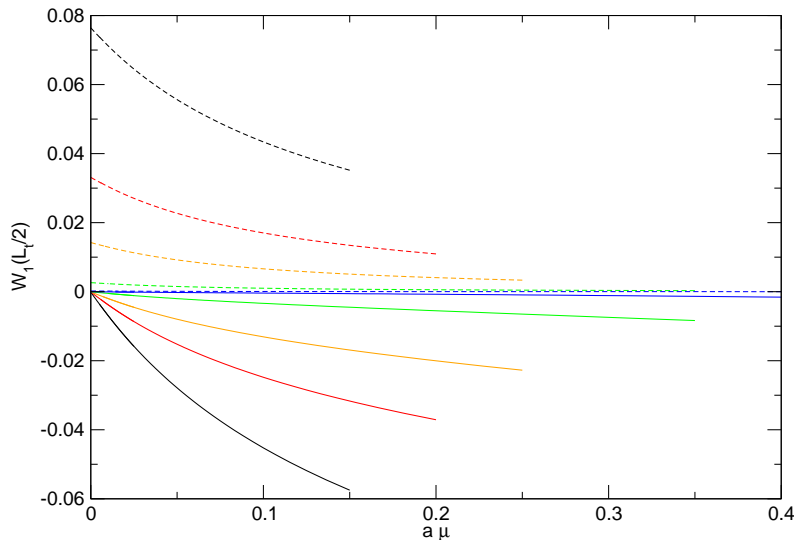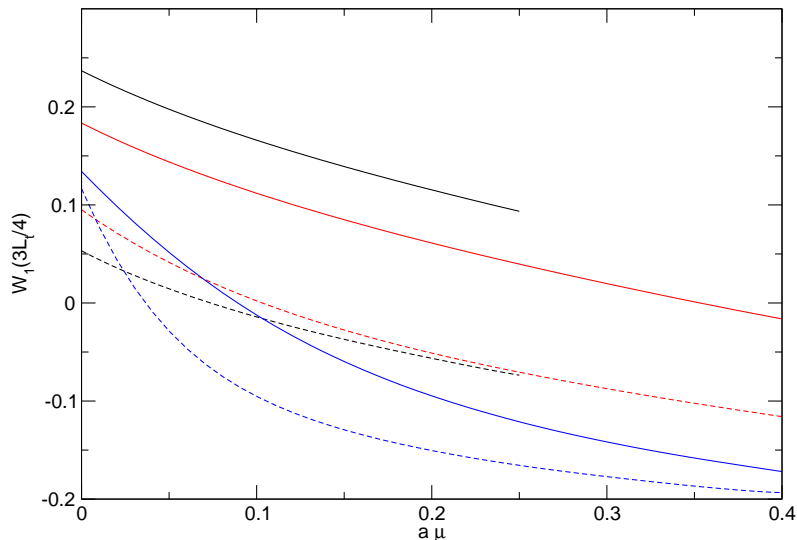
Figure 4.19: Broken supersymmetric quantum mechanics. Continuum extrapolation for W_1 for $\mu L = 5.0$ (black), $\mu L = 10.0$ (red), and $\mu L = 20.0$ (blue) for PBC (solid lines) and aPBC (dashed lines) for $f = 1$.

illustrates how the Ward identity W_1 is violated for broken supersymmetry at finite lattice spacing. However, unlike in the previous case of unbroken supersymmetry, neither with the lattice spacing going to zero, nor with the temperature going to zero, the violation of the Ward identity W_1 vanishes. To illustrate this further, we trace the Ward identity $W_1(3L_t/4)$ into the continuum for different μL. In figure 4.19 we show the continuum extrapolation of the results.

Clearly, the violation remains in the continuum. In this case too, all features of broken supersymmetry are numerically confirmed on the level of the Ward identities W_1.

4.2.7 Mass Gaps

Finally, we calculate the mass gaps by using ratios of eigenvalues of the transfer matrices as described in section 4.1.3.

From our discussion in chapter 2, we know what the mass spectrum looks like in the continuum and we even have the zero-temperature values in the

Figure 4.20: Unbroken supersymmetric quantum mechanics. Continuum extrapolation of the bosonic (black) and fermionic (red) masses with respect to the bosonic (solid lines) and the fermionic (dashed lines) vacuum for $f = 1$.

continuum to compare our results with. By the definition of the mass gaps in section 4.1.3 it is clear that we calculate the mass gaps for the boson in each sector separately. Alternatively, we could fit a cosh function to the bosonic correlation function in each sector and get the same results. The fermionic mass gaps, however, are measured via ratios of eigenvalues of the bosonic and the fermionic transfer matrix. This is a reflection of the fermionic correlation function which is only defined in the bosonic sector[8].

Unbroken Supersymmetry

As we have done in the previous sections, we start with unbroken supersymmetry. In figure 4.20, we plot the bosonic and the fermionic masses with respect to the vacua in $F = 0, 1$ for a coupling of $f = 1$.

We would like to point out that the results for this plot do not depend on μL.

---

[8]Remember that by reinterpreting the fermionic correlation function as an open string of the antifermionic correlator in the fermionic sector, one can define the mass of an antifermion.

(a) Finite lattice spacing   (b) Continuum

Figure 4.21: Unbroken supersymmetric quantum mechanics. The energy levels and the respective mass gaps for finite lattice spacing (figure 4.21(a)) and in the continuum (figure 4.21(b)). The representation of the arrows corresponds to the representation of the respective mass gaps in figure 4.20.

First, we note that the bosonic and the fermionic mass gaps measured with respect to the bosonic vacuum indeed extrapolate to the expected continuum values. Those mass gaps which are measured with respect to the fermionic vacuum also confirm the complete picture of the mass spectrum of unbroken supersymmetric quantum mechanics. The zero mode stems from the fact that the first excited bosonic state corresponds to the fermionic vacuum. Also, there is a negative fermionic mass. As we measure both the gap between the bosonic vacuum and the fermionic vacuum and vice versa, unless the vacua are exactly degenerate, there will always be a negative fermionic mass. For the unbroken case, contributions from the fermionic sector $F = 1$ vanish totally in the continuum, yielding exactly the desired degenerate spectrum with the correct continuum values. In figure 4.21 the energy levels for both sectors are depicted schematically for finite lattice spacing and in the continuum.

Broken Supersymmetry

The calculation of the mass gaps for broken supersymmetry works analogously. In figure 4.22, we display the plot for the bosonic and the fermionic masses.

Also for broken supersymmetry, the bosonic and the fermionic mass gaps ex-
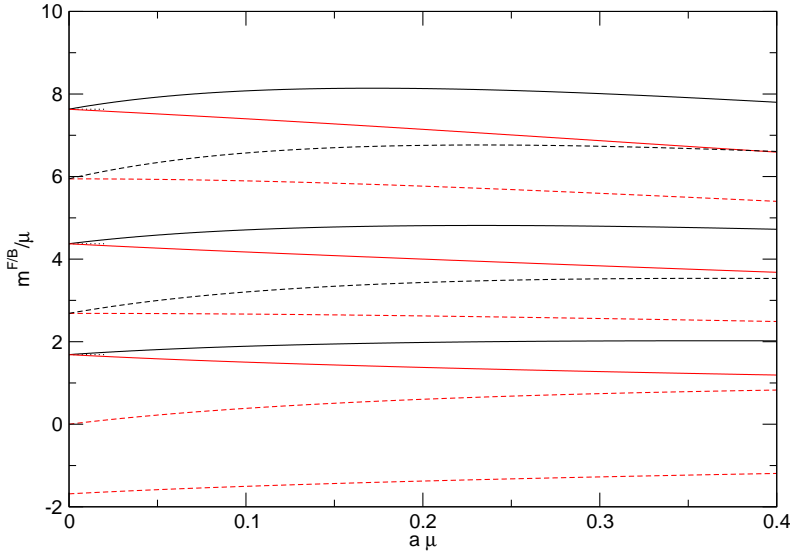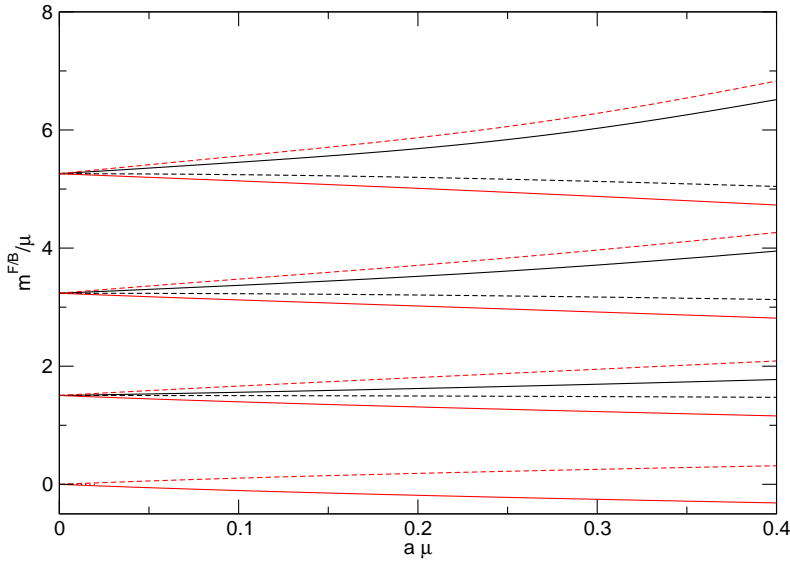
Figure 4.22: Broken supersymmetric quantum mechanics. Continuum extrapolation of the bosonic (black) and fermionic (red) masses with respect to the bosonic (solid lines) and the fermionic (dashed lines) vacuum for $f = 1$.

trapolate to the expected continuum values. The bosonic and fermionic vacua are exactly degenerate in the continuum, such that the mass gaps measured with respect to the respective vacua too become degenerate in the continuum. The lowest fermionic mass gap measured with respect to the bosonic vacuum is negative. This is a manifestation of the fact that for finite lattice spacing, the fermionic vacuum has less energy than the bosonic one. Note, that this is another reflection of the rather odd fermionic correlation function in the bosonic sector, where we interpreted one of the slopes as a very small negative mass for the fermion. The associated fermionic mass is the mass of the *Goldstino* [78] and it can be seen clearly that it indeed extrapolates to zero in the continuum. In figure 4.23 the energy levels for both sectors are depicted schematically for finite lattice spacing and in the continuum.

With these considerations, we conclude the discussion of supersymmetric quantum mechanics in the discretisation scheme of the action with counterterm.
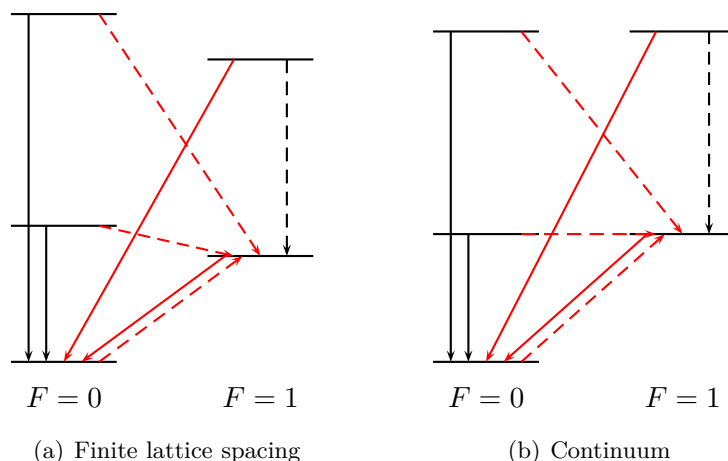
(a) Finite lattice spacing
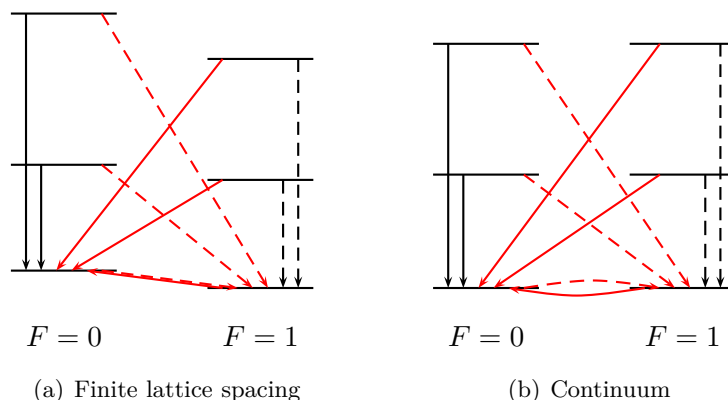
(b) Continuum

Figure 4.23: Broken supersymmetric quantum mechanics. The energy levels and the respective mass gaps for finite lattice spacing (figure 4.23(a)) and in the continuum (figure 4.23(b)). The representation of the arrows corresponds to the representation of the respective mass gaps in figure 4.22.

4.3 Results for the Q_1-Exact Action

We will now turn to the numerical investigation of the system with the Q_1-exact action $S_L^{Q_1}$. Again, the explicit form of $S_L^{Q_1}$ for both superpotentials P_u and P_b can be found in appendix G.

We will start by discussing some technical aspects for this action too. Since this action generates an additional type of bond, the construction of the transfer matrix needs to be modified, which we will show in detail. Furthermore, we will also discuss the bosonic cutoff and the effect it has on the continuum extrapolation of the observables and we will address the problem of the treatment of broken supersymmetry.

4.3.1 Technical Aspects

The Construction of the Transfer Matrix

For the Q_1-exact action, the construction of the transfer matrix needs to be modified since a bosonic state $|n\rangle$ is characterised by the number of bonds of the types $b_{1\to1}^B$ and $b_{1\to\nu}^B$, where $\nu = 3$ for the superpotential P_u and $\nu = 2$ for the superpotential P_b. We have to set a cutoff for both types of bonds

$N_{1\to 1}^{cut}$ and $N_{1\to \nu}^{cut}$ individually, such that the matrices have the size $N \times N$, with $N = (1 + N_{1\to 1}^{cut}) \cdot (1 + N_{1\to \nu}^{cut})$. We now label the bosonic states[9]

$$n = (1 + N_{1\to \nu}^{cut})n_{1\to 1}^B + n_{1\to \nu}^B, \quad m = (1 + N_{1\to \nu}^{cut})m_{1\to 1}^B + m_{1\to \nu}^B \qquad (4.30)$$

and calculate the transfer matrices as

$$T_{n,m}^F(i) = \sqrt{\frac{(w_{1\to 1})^{n_{1\to 1}^B + m_{1\to 1}^B}}{(n_{1\to 1}^B!)(m_{1\to 1}^B!)}} \sqrt{\frac{(w_{1\to \nu})^{n_{1\to \nu}^B + m_{1\to \nu}^B}}{(n_{1\to \nu}^B!)(m_{1\to \nu}^B!)}} \; Q_F(k+i). \qquad (4.31)$$

As usual, k is the site occupation number

$$k = n_{1\to 1}^B + n_{1\to \nu}^B + m_{1\to 1}^B + \nu \cdot m_{1\to \nu}^B. \qquad (4.32)$$

The Bosonic Cutoff and Calculated Lattices Sizes

For the Q_1-exact case, we set the bosonic cutoffs for our calculations to $N_{1\to 1}^{cut} = 64$ and $N_{1\to \nu}^{cut} = 16$, which yields transfer matrices of the size 1105×1105. We calculated the observables of interest on lattices of an extent ranging from $L_t = 20$ to $L_t = 500$.

For the extrapolations, we proceeded similarly to the case with the action with counterterm. Also for the Q_1-exact action, the region where the cutoff effects start to influence the observable is clearly indicated by a sudden bend with a divergent continuum limit in an otherwise linear curve close to the continuum. Excluding the data points which lie in the region with the cutoff effects allows for reliable continuum results for this action, too.

Also for this action, we could extrapolate the results with quadratic fits without difficulties.

The Superpotential P_b and Broken Supersymmetry

The treatment of broken supersymmetry for the Q_1-exact action turns out to be very difficult. On the one hand, the transfer matrices T^0 and T^1 using the superpotential P_b necessarily need to be *similar*. This can be seen from the fact that for this action the energy levels are degenerate for any lattice spacing. Numerical investigations for matrices of the size we are able to handle show

---

[9]Of course, there are many other possible ways to label the bosonic states.
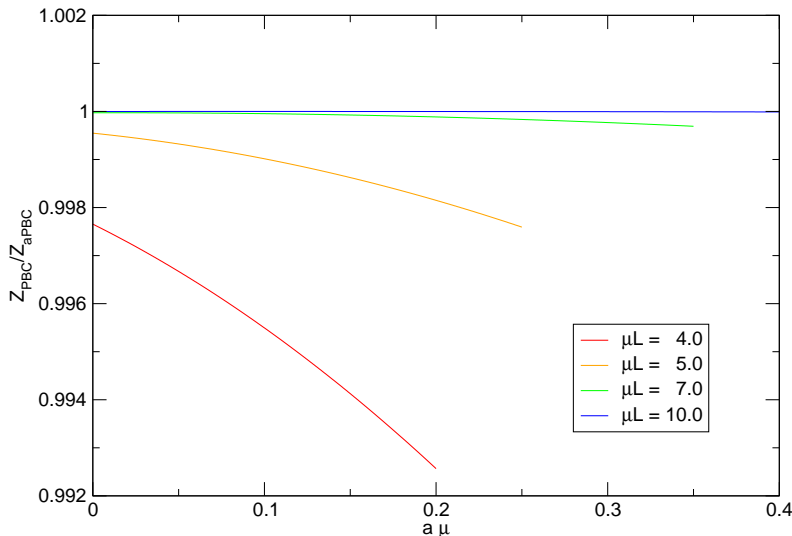
Figure 4.24: Unbroken supersymmetric quantum mechanics. Continuum extrapolation of the ratio Z_{PBC}/Z_{aPBC} versus $a\mu$ for different μL and $f = 1$.

that this indeed is the case. Furthermore, $Z_{PBC}/Z_{aPBC} = 0$, independently of both the chosen cutoff and the lattice spacing a. However, the bosonic occupation numbers explode even on very small lattices such that we do not have reliable data for any other observable in the context of broken supersymmetry. Therefore, we restrict the following investigation of the system with the Q_1-exact action to the case where we use the superpotential P_u and supersymmetry is unbroken.

4.3.2 The Ratio Z_{PBC}/Z_{aPBC}

We also start for this action by calculating the ratio Z_{PBC}/Z_{aPBC} and thus the Witten index. In figure 4.24 we plot the ratio Z_{PBC}/Z_{aPBC} versus $a\mu$ for different $\mu L = $ fix. The coupling is set to $f = 1$.

We observe the same small dependence on μL in the continuum limit for this ratio as in the calculation with the action with counterterm in figure 4.6. Also the lattice artefacts are almost identical for both actions. Yet, as expected the ratio $Z_{PBC}/Z_{aPBC} = \Delta \rightarrow 1$ in the continuum for large μL. Therefore, the Witten index $\Delta = 1$ is indeed reproduced for unbroken supersymmetry using

Figure 4.25: Unbroken supersymmetric quantum mechanics. The Ward identity W_1 for $L_t = 30$ (black), $L_t = 60$ (red), $L_t = 90$ (green), and $L_t = 120$ (blue) for aPBC (solid lines) and PBC (dashed lines) for $\mu L = 10.0$ and $f = 1$.

the Q_1-exact action.

4.3.3 The Ward Identities W_1 and W_2

Next, we show the results for the calculation of the Ward identities W_1 and W_2. As mentioned before, the Ward identity W_1 is of special interest for the Q_1-exact action, since this action is invariant under the variation of δ_1, such that for periodic boundary conditions the Ward identity $W_1(t)$ is expected to vanish exactly, $W_1 = 0 \ \forall t$. We will compare the behaviour of this Ward identity with the behaviour of the Ward identity $W_2{}^{10}$.

In figure 4.25 we show the Ward identity W_1 for different L_t at a coupling $f = 1$ for both periodic and antiperiodic boundary conditions.

The plot shows that the Ward identity W_1 is indeed satisfied for periodic boundary conditions. Note, that the dashed lines representing $W_1(t) = 0 \ \forall t$

---

[10]The analysis of the Ward identity W is not of interest in this case, since it vanishes trivially for unbroken supersymmetry also for the Q_1-exact action.

Figure 4.26: Unbroken supersymmetric quantum mechanics at finite lattice spacing. Continuum extrapolation of $W_1(L_t/2)$ for $\mu L = 3.0$ (black), $\mu L = 4.0$ (red), $\mu L = 5.0$ (green), and $\mu L = 10.0$ (blue) for aPBC (solid lines) and PBC (dashed lines). $f = 1$.

for periodic boundary conditions are composed of the bosonic and fermionic correlators as given in eq.(4.27) and are in fact non-trivially zero. For aPBC, the violation of the Ward identity at finite temperature is evident. To observe the behaviour for the Ward identity W_1 in the zero-temperature limit, we again trace $W_1(L_t/2)$ for different μL. In figure 4.26, the continuum extrapolation for this Ward identity is shown. Of course, $W_1(L_t/2)$ is zero for any $a\mu$ and any μL for PBC. However, for aPBC, the extrapolation of the violation of $W_1(L_t/2)$ shows a dependence of μL. For $\mu L > 10.0$, this violation also vanishes, as expected.

We now perform the same analysis for the Ward identity W_2 given in eq.(4.2.6). Explicitly, for the superpotential P_u, W_2 reads

$$W_2(t) = \langle \psi_t \overline{\psi}_0 \rangle + (1 - \mu)\langle \phi_t \phi_0 \rangle - \langle \phi_{t+1} \phi_0 \rangle - g\langle \phi_t \phi_0^3 \rangle. \qquad (4.33)$$

This Ward identity is not expected to vanish for finite lattice spacing, since the action $S_L^{Q_1}$ is not invariant under the supersymmetry transformation δ_2. In figure 4.27 we show $W_2(t)$ for different L_t for $\mu L = 10.0$ and a coupling $f = 1$.
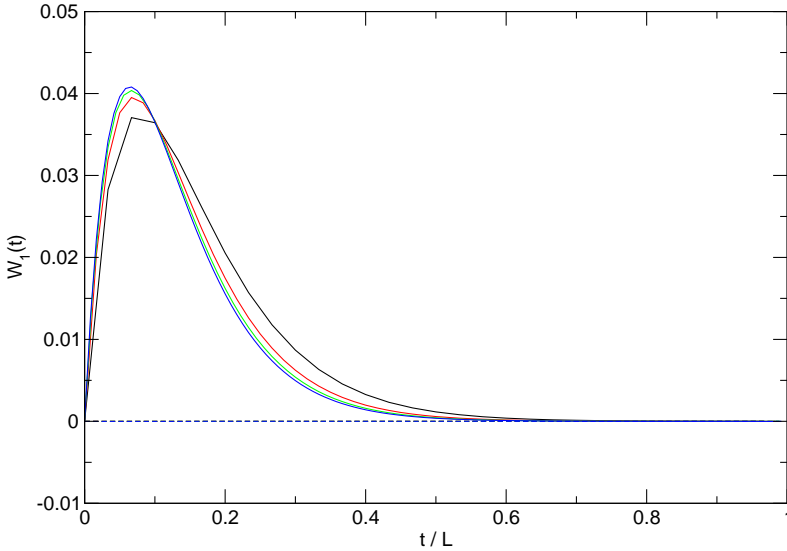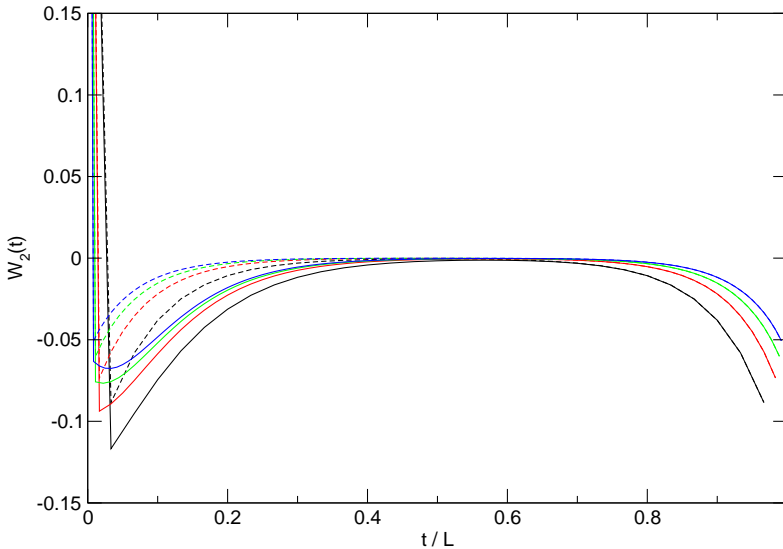
Figure 4.27: Unbroken supersymmetric quantum mechanics. The Ward identity W_2 for $L_t = 30$ (black), $L_t = 60$ (red), $L_t = 90$ (green), and $L_t = 120$ (blue) for aPBC (solid lines) and PBC (dashed lines) for $\mu L = 10.0$ and $f = 1$.

As expected, this Ward identity is violated for both PBC and aPBC at finite lattice spacing and for finite temperature. To observe the continuum behaviour, we trace $W_2(L_t/2)$ in this case too. The continuum extrapolation for different μL is shown in figure 4.28. For PBC, the violation for the Ward identity $W_2(L_t/2)$ vanishes in the continuum independent of the chosen μL. The restoration of supersymmetry in the continuum is thus also confirmed via the Ward identity $W_2(L_t/2)$. For aPBC however, the violation does not vanish for small μL. Rather, only where $\mu L > 10.0$, the Ward identity $W_2(L_t/2)$ goes to zero. Hence, on the level of the Ward identities W_1 and W_2, all the features of the unbroken supersymmetry formulated with the Q_1-exact action are numerically confirmed.

4.3.4 The Mass Gaps

We calculate for this case too the mass gaps via eigenvalues of the transfer matrices. In figure 4.29, we plot the fermionic and bosonic mass gaps with respect to the bosonic and the fermionic vacuum for $\mu L = 10.0$ and $f = 1$.

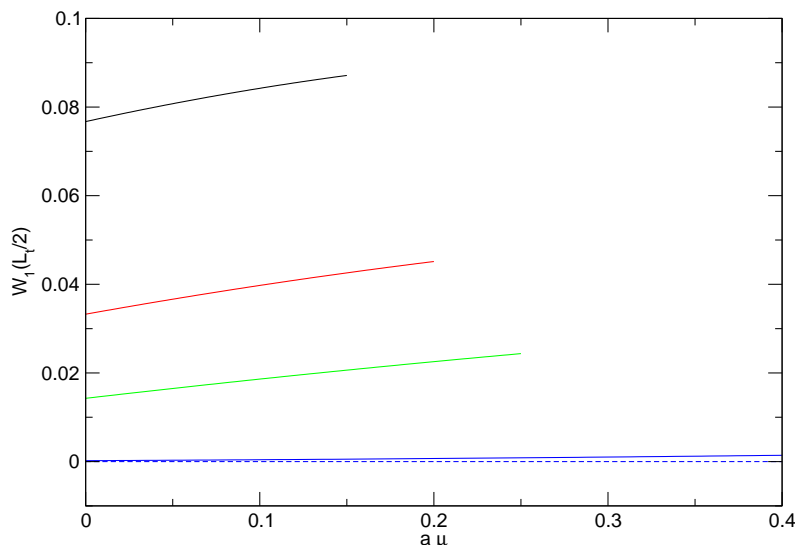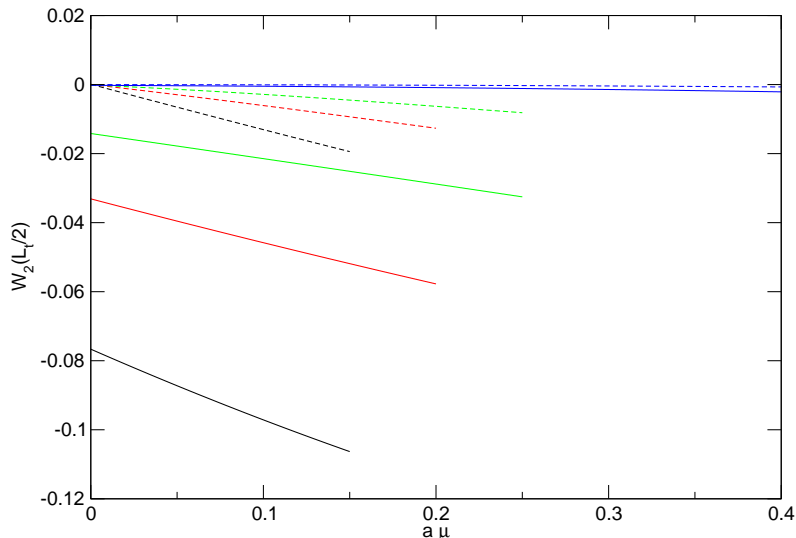**Figure 4.28:** Unbroken supersymmetric quantum mechanics. Continuum extrapolation of $W_2(L_t/2)$ for $\mu L = 3.0$ (black), $\mu L = 4.0$ (red), $\mu L = 5.0$ (green), and $\mu L = 10.0$ (blue) for aPBC (solid lines) and PBC (dashed lines). $f = 1$.

Similarly to the plots for the action with counterterm, this plot does not depend on μL either. The masses measured with respect to the bosonic vacuum are exactly degenerate even at finite lattice spacing. The plot therefore confirms numerically that it is indeed sufficient to preserve one supersymmetry exactly on the lattice to render the spectrum degenerate since the mass gaps measured with respect to the bosonic vacuum do extrapolate to the correct continuum values. Those mass gaps which are measured with respect to the fermionic vacuum are not relevant for the spectrum in the continuum since $Z_1 \rightarrow 0$ in the thermodynamic limit. Yet, these masses are also degenerate for finite lattice spacing. Note the fermionic zero mass mode which measures the gap between the first excited bosonic state and the fermionic vacuum. This is *not* a Goldstino mode since it does not mediate between two vacua. As usual, there is a negative fermionic mass which measures the gap between the bosonic and the fermionic vacuum. In figure 4.30, we show schematically the distribution of the energy levels in the bosonic and the fermionic sector both for finite lattice spacing and in the continuum.

The investigation of the masses therefore confirms all expected features for
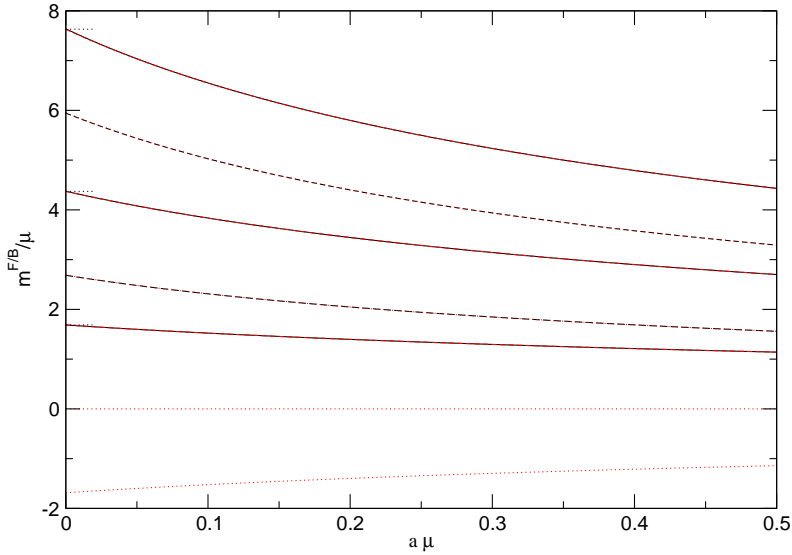
Figure 4.29: Unbroken supersymmetry. Continuum extrapolation of the bosonic masses measured with respect to the bosonic (black solid) and the fermionic (black dashed) vacuum and the fermionic masses measured with respect to the bosonic (red dashed) and the fermionic (red dotted) vacuum. $f = 1$.

(a) Finite lattice spacing
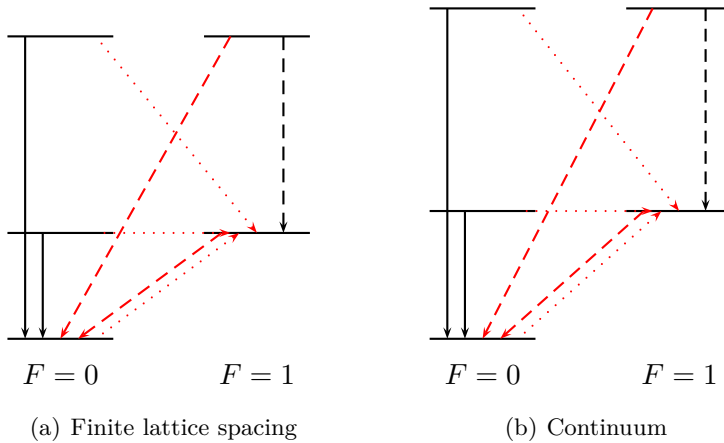
(b) Continuum

Figure 4.30: Unbroken supersymmetric quantum mechanics. The energy levels and the respective mass gaps for finite lattice spacing (figure 4.30(a)) and in the continuum (figure 4.30(b)). The representation of the arrows corresponds to the representation of the respective mass gaps in figure 4.29.

unbroken supersymmetric quantum mechanics using the Q_1-exact action.

4.3.5 The Ground State Energy E_0

As a last observable for the Q_1-exact action, we follow [35] and measure the ground state energy E_0 via the expectation value of the Hamilton operator H.

A priori, there are several possible candidates for an adequate Hamilton operator for the measurement of the ground state energy. The authors of [35] give reasons for the use of the Q_1-exact action in the off-shell formulation for the construction of the Hamilton operator which indeed measures the correct ground state energy. They argue that a Hamilton operator whose expectation value for unbroken supersymmetry vanishes identically for PBC at finite lattice spacing and for aPBC gives zero in the limit where $\mu L \to \infty$ is the one of choice. The Hamilton operator one finds thus is in fact the familiar one for supersymmetric quantum mechanics. In the lattice formulation, it reads

$$H = -\frac{1}{2}(\Delta^-\phi)^2 + \frac{1}{2}\left(P'\right)^2 - \frac{1}{2}\overline{\psi}(\Delta^- - P'')\psi. \qquad (4.34)$$

Using the superpotential P_u, the expectation value of this Hamilton operator is then explicitly given by

$$
\begin{aligned}
\langle H \rangle \;=\;& \frac{1}{2}(\mu^2 - 2)\langle\phi^2\rangle + \mu g\langle\phi^4\rangle + \frac{1}{2}g^2\langle\phi^6\rangle + \langle\phi_1\phi_0\rangle \\
&+\frac{1}{2}(\mu - 1)\langle\overline{\psi}\psi\rangle + \frac{1}{2}\langle\overline{\psi}_1\psi_0\rangle + \frac{3}{2}g^2\langle\overline{\psi}\psi\phi^2\rangle.
\end{aligned}
\qquad (4.35)
$$

In figure 4.31 we show the continuum extrapolation for $\langle H\rangle/\mu$ for different μL for both PBC and aPBC at a coupling $f = 1$.

The operator H measures zero per construction for PBC independently of the lattice spacing a and μL. Therefore, the zero line for $\langle H\rangle_{PBC}/\mu$ in the graph is expected. Yet, note that this zero is non-trivial. Rather, it comes about because of an exact cancellation of the expectation values in eq.(4.35). In our calculations, we thus find indeed that for PBC, $E_0/\mu = 0$ at finite lattice spacing. For aPBC, the continuum extrapolation shows an exponentially decreasing behaviour and the expectation value $\langle H\rangle/\mu$ goes to zero for large μL as well, such that we have $E_0/\mu = 0$ for $\mu L \to \infty$. We are thus able to confirm the results presented in [35] in our formulation.

At this point, we conclude our discussion of the exact lattice formulation and
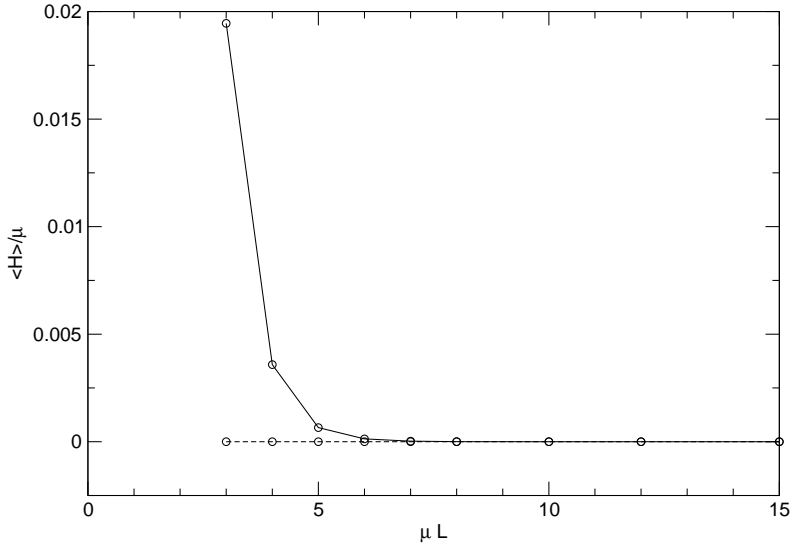
Figure 4.31: Unbroken supersymmetric quantum mechanics. Continuum extrapolation of $\langle H \rangle / \mu = E_0/\mu$ for PBC (dashed line) and aPBC (solid line) for $f = 1$. The lines are only there to guide the eye.

the transfer matrix technique for supersymmetric quantum mechanics. In the next chapter, we will start from the formulation of supersymmetric quantum mechanics in terms of bonds and derive a modified worm algorithm for the update of the bosonic and the fermionic bond configuration. We will then show and discuss the results for standard Monte Carlo simulations using the worm algorithm.

Chapter 5

Supersymmetric QM on the Lattice: Results Part II

In chapter 3 we have reformulated supersymmetric quantum mechanics in terms of bond configurations. We have used the hopping expansion in order to use it for Monte Carlo simulations with the worm algorithm. Nonetheless, in chapter 4 we have solved the model on the lattice in an exact way with the transfer matrix technique. In the present chapter, we now go back to the original purpose of the hopping expansion and develop a modified worm algorithm which will serve us to perform numerical simulations for supersymmetric quantum mechanics on the lattice. Even though the system has already been solved in an exact way, the effort for the development of an algorithm which allows for simulations of supersymmetric quantum mechanics is still worthwhile, because the insight gained will be applicable for the two-dimensional $\mathcal{N} = 1$ Wess-Zumino model in chapter 6.

The present chapter is organised in two parts. In the first part, we will construct in detail an algorithm based on the Prokof'ev and Svistunov worm algorithm, which is designed for updates of the bond configuration for the bosonic bonds as well as for the fermionic bonds and thus allows for a simulation of supersymmetric quantum mechanics. This discussion will include the explicit derivation of the acceptance ratios for all possible update steps. In the second part, we will then present the results we obtained using this algorithm. We will simulate supersymmetric quantum mechanics for the same discretisation schemes we have used in chapter 4. In particular, we will present results for the action with counterterm for broken supersymmetry. Yet, this section is merely meant as a validation of the algorithm and the discussion of the physics behind the results will be kept short. The exact lattice results from chapter 4 will serve as reference data.

5.1 The Worm Algorithm for Supersymmetric Quantum Mechanics

We will now adapt the worm algorithm to supersymmetric quantum mechanics. In the spirit of the previous chapters, we will do so by using the action S_L. First, we note that for supersymmetric quantum mechanics we have to update different fields, e.g. the fermionic and the bosonic one. After the hopping expansion, this amounts to an update of the bosonic and the fermionic bond configuration. This is in contrast to the worm algorithm for the Ising model, where we had to update the configuration for only one kind of bond. We will thus design an algorithm which updates alternately the bosonic and the fermionic bond configuration. This requires the algorithm to switch between the different configuration spaces we introduced in section 3.6.4.

We choose to do so by starting in the configuration space $\mathcal{Z}$, for example with a totally empty lattice. We then propose alternately to put bosonic and fermionic variables on the lattice, which, when accepted, allows us to enter the respective configuration space. The bond configuration associated with the additional variables is then updated with the worm algorithm. Once the sources are again removed from the lattice, we are back in the configuration space $\mathcal{Z}$ and the cycle restarts.

In the following, we need to work out the worm algorithm for both, the update of the bosonic and the fermionic bond configuration. In particular, we will derive the acceptance ratios $P_X(\varphi \to \varphi')$ for all Monte Carlo update steps X. These acceptance ratios combine to the total acceptance probability $P_{A,X}$ for the update step in question as given in eq.(A.13),

$$P_{A,X}(\varphi \to \varphi') = \min\{1, P_X(\varphi \to \varphi')\}. \tag{5.1}$$

5.1.1 Updating the Bosonic Bond Configuration

We first work out in detail the algorithm for the update of the bosonic bond configuration. We would like to point out that we derive the algorithm for an arbitrary superpotential, such that no restrictions on the bosonic bond configurations apply. For the update of the bosonic bond configuration, we can adapt the algorithm as it was introduced for the Ising model. In the following, we will refer to the source at the site x_1 as the head and the source at the site x_2 as the tail.

We probe the configuration space $\mathcal{G}_F^B$ to sample the Monte Carlo estimator for $g_F^B(x)$ via

$$g_F^B(x|\mathcal{G}_F^B) = g_F^B(x) + \delta_{x_1-x_2,x} \qquad (5.2)$$

The two elementary update steps we have encountered in the Ising demonstration, the remove step and the shift step, are adopted for the update of the bosonic bond configuration. As there are in general no restrictions on the bond configuration, we are free to decide for each Monte Carlo step whether to proceed by a remove update or a shift update. With probability p_{rm}, we propose to remove the sources from the lattice. The proposition to continue the worm update and to shift the head to either one of the next neighbouring sites is chosen with probability $p_1 = 1 - p_{\mathrm{rm}}$. Each configuration generated by a shift update step automatically contributes to $g_F^B(x)$. Using detailed balance, we calculate the acceptance ratios for each update step.

The Remove Update Step

The remove update step $x_1, x_2 \to \varnothing$ is needed to switch from the configuration space $\mathcal{G}_F^B$ to the configuration space $\mathcal{Z}_F$. This update step involves the removal of the bosonic sources from the lattice and it is suggested with probability p_{rm}. It is balanced with the step $\varnothing \to x_1, x_2$, where the additional bosonic sources are put back on the lattice at two randomly chosen sites x_1 and x_2. In the graphical representation, this update step corresponds to the erasing or drawing of the circles which represent the bosonic sources. This step allows the transition from the configuration space $\mathcal{G}_F^B$ to the configuration space $\mathcal{Z}_F$ and back. The removal step does not alter the bond configuration. Thus, only the ratios of the site weights Q_F are involved in the acceptance probability,

$$P_{\mathrm{rm}}(x_1, x_2 \to \varnothing) = \begin{cases} \dfrac{1}{p_{\mathrm{rm}}V^2} \dfrac{1}{R_F(k(y) - 2)} & \text{if } x_1 = x_2 \equiv y, \\[4mm] \dfrac{1}{p_{\mathrm{rm}}V^2} \dfrac{1}{R_F'(k(x_1) - 1)} \dfrac{1}{R_F'(k(x_2) - 1)} & \text{if } x_1 \neq x_2. \end{cases} \qquad (5.3)$$

Here, we have introduced the site weight ratios R_F and R_F'[1],

$$R_F(n) = \frac{Q_F(n+2)}{Q_F(n)}, \tag{5.4}$$

$$R_F'(n) = \frac{Q_F(n+1)}{Q_F(n)}. \tag{5.5}$$

The prefactor $1/(p_{\mathrm{rm}}V^2)$ is motivated as follows. The factor $1/V^2$ balances the probability for the proposition of putting the bosonic sources at the sites x_1 and x_2 when re-entering the configuration space $\mathcal{G}_F^B$, while the factor $1/p_{\mathrm{rm}}$ balances the proposition probability for the choice of proceeding by the shift update instead of the remove update. The acceptance ratios for the re-entering from the configuration space $\mathcal{Z}_F$ into the configuration space $\mathcal{G}_F^B$ is then given by

$$P_{\mathrm{rm}}(\varnothing \to x_1, x_2) = \begin{cases} p_{\mathrm{rm}}V^2 R_F(k(y)) & \text{if } x_1 = x_2 \equiv y, \\[2ex] p_{\mathrm{rm}}V^2 R_F'(k(x_1))R_F'(k(x_2)) & \text{if } x_1 \neq x_2. \end{cases} \tag{5.6}$$

The Shift Update Step

The shift update does change the bosonic bond configuration. This is in total analogy to the shift update for the Ising model. Shifting the head to a next neighbour site is always associated with an increase or a decrease of the bosonic bond number between the sites x and y by one. In the graphical representation, this corresponds to drawing or erasing one bosonic bond $b_{1\to1}^B$ between the sites x and y. In the following, we will use the shorthand notation

$$n_{xy}^B = \begin{cases} n_{1\to1}^B(x) & \text{if } y = x+1, \\ n_{1\to1}^B(y) & \text{if } y = x-1, \end{cases} \tag{5.7}$$

for the number of bosonic bonds between the sites x and y. The probability to propose the shift update is p_1. The proposition whether to add or to subtract a bond is, analogously to the Ising model, suggested with probability $1/2$. Since we have a one-dimensional lattice, the head can only move forward or

---

[1]The calculation of the ratios R_F and R_F' is not straightforward since the weights $Q(n)$ quickly become very large as n increases and a reliable numerical integration is no longer possible. Yet, the ratios themselves are of $\mathcal{O}(10^2)$. In appendix H we explain how a numerically stable evaluation of the ratios can be achieved.

backward. Both directions are proposed with equal probability $1/2$. Thus, the proposition probability is totally symmetric for each update step and all the factors cancel in the acceptance ratios. The shifts $x \to y$ and $n_{xy}^B \to n_{xy}^B + 1$ are balanced with shifts $y \to x$ and $n_{xy}^B \to n_{xy}^B - 1$, which gives the acceptance ratios

$$P_{\text{sh}}(x \to y, n_{xy}^B \to n_{xy}^B + 1) = \frac{R_F(k(y))}{n_{xy}^B + 1}, \tag{5.8}$$

$$P_{\text{sh}}(x \to y, n_{xy}^B \to n_{xy}^B - 1) = \frac{n_{xy}^B}{R_F(k(x) - 2)}. \tag{5.9}$$

With these update steps, we are so far able to alternate between the configuration space $\mathcal{Z}_F$ and the configuration space $\mathcal{G}_F^B$ in the same sector. Furthermore, we are able to update the bosonic bond configuration by moving one bosonic source around the lattice. What is still needed is the update algorithm for the fermionic bond configuration, and, consequently, the possibility to alternate between the configuration spaces $\mathcal{Z}_1$ and $\mathcal{Z}_0$. This part of the algorithm is discussed next.

5.1.2 Updating the Fermionic Bond Configuration

Because the fermionic bond number $n^F \in \{0, 1\}$, a fermionic bond configuration for one-dimensional supersymmetric quantum mechanics looks like a bond configuration for the one-dimensional Ising model in the dimer formulation. However, the algorithm has to undergo major modifications for the update of a fermionic bond configuration because of the Grassmann character of the fermionic field variables. Still, the algorithm probes the configuration space $\mathcal{G}^F$ to sample the Monte Carlo estimator g^F via

$$g^F(x|\mathcal{G}^F) = g^F(x) + \delta_{(x_1 - x_2) \bmod L_t, x}. \tag{5.10}$$

The update algorithm for the fermionic bond variables can no longer be divided into the two elementary update steps 'shift' and 'remove' as the Grassmann algebra forbids the closure of a fermionic loop with the additional fermionic sources still being on the lattice. Rather, one needs to close the loop and to remove the variables in one step. Therefore, for the closure of a loop, we will introduce a third update step combining both the shift and the remove update step in one.
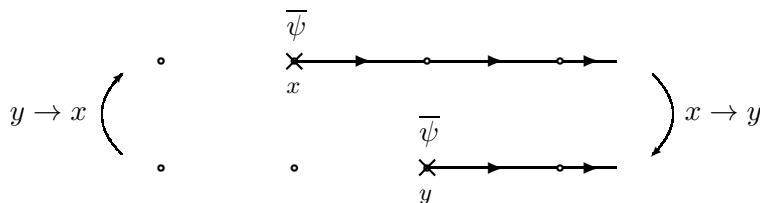
Figure 5.1: Fermionic bond configuration update algorithm. Graphical representation of the 'shift' update step $x \to y$ in forward direction, $y = x_2 + 1$ for an open string configuration. It is balanced with the shift update step in backward direction, $y \to x$. The bosonic bond configuration is not drawn.

The Shift Update Step

Let us first consider the shift update $x \to y$, where $y \neq x_1$, that is, the head $\overline{\psi}$ will not shift to the site where the tail ψ is. Eq.(3.78) implies, that for each configuration with an open fermionic string[2], the source $\overline{\psi}$ at site x_2 is necessarily saturated with a fermionic bond in forward direction, $n^F(x_2) = 1$. By the definition of an open string, there is no fermionic bond in the backward direction of the source, e.g. $n^F(x_2 - 1) = 0$. Consequently, a shift in forward direction, $x \to y$, where $y = x_2 + 1$, automatically involves the removal of the already existing bond $b^F(x_2)$, whereas a shift in backward direction, $x \to y$, where $y = x_2 - 1$, requires the addition of a new bond $b^F(x_2 - 1)$. Therefore, for the shift update, the proposition of the direction includes the decision whether to add or to subtract a fermionic bond. Both directions are proposed with equal probability $1/2$. In figure 5.1, the shift update step is depicted.

To simplify the notation as well as for keeping the numerics under control, we introduce the ratios

$$R_m(n) = \frac{Q_1(n)}{Q_0(n)} \tag{5.11}$$

similarly to eqs.(5.4,5.5)[3]. Shifts $x \to y$ and the condition that $y \neq x_1$ are balanced with shifts $y \to x$, $x \neq x_1$, and standard rules provide us with the

---

[2]Configurations where $x_1 = x_2$ and thus head and tail being at the same site are not considered as open string configurations because for these configurations, we also have to balance the remove step in the acceptance ratios.

[3]The numerical treatment of the ratios R_m can also be found in appendix H.

acceptance ratios

$$P_{\text{sh}}(x \to y | x_1 \neq x_2) = \begin{cases} R_m(k(x)) & \text{if } y = x_2 + 1, \\ \dfrac{1}{R_m(k(y))} & \text{if } y = x_2 - 1. \end{cases} \qquad (5.12)$$

Now let us consider the case where $x \to y$ and $y = x_2$, that is, we propose to shift the head $\overline{\psi}$ to the site where the tail ψ is. To calculate the acceptance ratios for this case, we have to distinguish between the proposition of a shift of the head in the forward direction and a shift in the backward direction. First, let us consider the forward shift, which generates a valid configuration, contributing to $\langle \psi_y \overline{\psi}_y \rangle$. These are the only configurations for which we propose the removal update step with probability $p_{\text{rm}} = 1/2$. The forward shift update step $x \to y$ with $y = x_2 + 1 = x_1$ is balanced with the backward shift update step $y \to x$, where $y = x_2 - 1$. This backward shift, however, is proposed with the probability 1 instead of probability $1/2$ since the shift $y \to x$ for $x = x_2 + 1$ would involve the creation of an open fermion string around the entire lattice. The asymmetry in the proposition probabilities is cured by the choice of the removal probability $p_{\text{rm}} = 1/2$, such that we find the acceptance ratio for a shift in forward direction where $y = x_2$ to be the same as in eq.(5.12), namely

$$P_{\text{sh}}(x \to y | x_1 \neq x_2 \cap y = x_2 + 1 = x_1) = R_m(k(x)). \qquad (5.13)$$

The shift step is balanced with

$$P_{\text{sh}}(x \to y | x_1 = x_2) = \begin{cases} \dfrac{1}{R_m(k(y))} & \text{if } y = x_2 - 1, \\ 0 & \text{if } y = x_2 + 1. \end{cases} \qquad (5.14)$$

The Hybrid Shift/Remove Update Step

The shift update in the backward direction is more subtle. As the backward update step always involves the addition of a fermionic bond, this update step would create a closed fermion loop. However, at the site $y = x_1 = x_2$, there would also be the additional pair of fermionic variables. Such a configuration has zero weight. There are several approaches to deal with this problem, for instance by introducing an artificial weight for these forbidden configurations. In our algorithm, we proceed differently. If a backward shift $x \to y$ is proposed
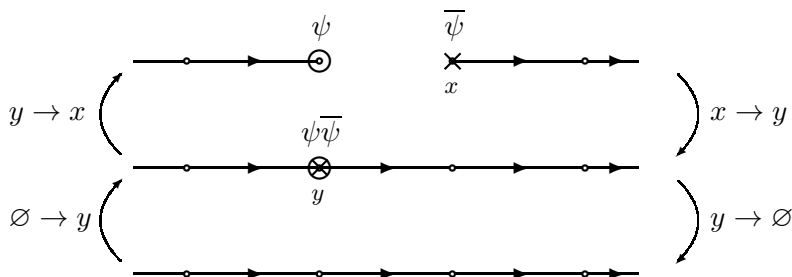
Figure 5.2: Fermionic bond configuration update algorithm. Graphical representation of the hybrid 'shift/remove' update step $x \to y \to \varnothing$ in backward direction, $y = x_2 - 1 = x_1$. It is balanced with the 'shift/remove' update step, $\varnothing \to y \to x$. We have omitted the drawing of the bosonic bonds.

such that $y = x_2 - 1 = x_1$, we close the loop and remove the additional fermionic variables in one step, thus forming a hybrid 'shift/remove' update step. This step is balanced with the step when we propose to put the additional fermionic variables on a closed loop configuration at a site $x_1 = x_2 \equiv y$. As this would also create a forbidden configuration, we modify the proposition to put only the tail on the site $x_2 = y$ and to put the head at the site $x_2 = x_1 + 1$ instead, while removing the fermionic bond $b^F(x_2)$. The acceptance ratio for the hybrid update shift/remove is given by

$$P_{\text{sh/rm}}(x \to y \to \varnothing | y = x_2 - 1 = x_1) \;\; = \;\; \frac{2}{V}, \qquad (5.15)$$

$$P_{\text{sh/rm}}(\varnothing \to x \to y | y = x_1 = x_2 - 1) \;\; = \;\; \frac{V}{2}. \qquad (5.16)$$

The factor V compensates for the proposition probability to choose the same lattice site y when putting back the additional variables on the lattice, whereas the factor 2 compensates for the proposition probability to shift in forward or backward direction. Note that there are no ratios of Q-weights involved, since neither the bosonic bond configuration is changed nor the monomer weight of a site is affected by the hybrid shift/remove update step. In figure 5.2, the hybrid shift/remove update step is depicted graphically. To complete the algorithm, we finally need to find the acceptance ratios for the regular 'remove' step.

The Remove Update Step

The remove update step $\varnothing \to x$ remains as usual. If $x_1 = x_2$, the algorithm proposes with probability $p_{\mathrm{rm}} = 1/2$ to remove head and tail from the lattice. This proposal probability is balanced with the probability to put head and tail at the site x of an empty configuration. The acceptance ratios for the remove update step are then given by

$$P_{\mathrm{rm}}(x \to \varnothing | x_1 = x_2) \quad = \quad \frac{2}{V} R_m(x), \tag{5.17}$$

$$P_{\mathrm{rm}}(\varnothing \to x | m(x) = 1) \quad = \quad \frac{V}{2} \frac{1}{R_m(x)}. \tag{5.18}$$

Analogously to the hybrid shift/remove step, the factors V and 2 balance the proposition probability for the re-entrance in the configuration space $\mathcal{G}^F$ as well as the asymmetric proposition probability for the move update if $x_1 = x_2$.

5.1.3 Updating the Monte Carlo Estimator for Z_F

As our algorithm is designed to sample the configuration spaces $\mathcal{G}^F$, $\mathcal{G}_F^B$, and $\mathcal{Z}_F$, the update for the Monte Carlo estimators for Z_F is particularly simple. Each configuration in the configuration space $\mathcal{Z}_F$, that is each configuration with no additional sources, contributes to the estimator of the partition function as

$$Z_F(\mathcal{Z}_F) = Z_F + 1. \tag{5.19}$$

The Monte Carlo estimator for the partition function completes our considerations for the set-up of a simulation. Equipped with the acceptance probabilities and estimators we have derived in this section, supersymmetric quantum mechanics can be simulated with worm algorithm updates for both the bosonic and the fermionic bond configurations. All our Monte Carlo data for supersymmetric quantum mechanics has been acquired using this algorithm. In the next section, we will present some simulation results for different discretisations.

5.2 Results for the Monte Carlo Simulations

For the following Monte Carlo simulations, we will consider the same superpotentials and actions as we have done in the previous chapter 4 for the transfer

matrix approach. In particular, we will simulate the system using the action with counterterm for both unbroken and broken supersymmetry as well as the Q_1-exact action for unbroken supersymmetry. We remind the reader that the actions can be found in appendix G. Because we have already solved the system exactly, the results in this section are merely thought of as a proof of feasibility for the algorithm. If needed, we will derive in detail necessary modifications of the algorithm before presenting the results for each action.

There are two main issues we will encounter for the actions we use. One is the adaption of the algorithm to bonds of the type $b^B_{1\rightarrow 3}$ for the Q_1-exact action, which amounts to a fairly straightforward extension of the basic algorithm derived in the previous section. The other concern will be the weight ratios R_F, R'_F and R_m. As they are now interpreted as probabilities, they are required to be positive. However, this will not always be the case for the action with counterterm for broken supersymmetry and we will have to deal with this problem by incorporating the sign of the configuration into the observables. Furthermore, similar to the Ising model, constraints on the site occupation number will arise[4] for unbroken supersymmetry. We will reveal the origin of these constraints and discuss how they affect the algorithm.

In analogy to the number of sweeps for a standard Monte Carlo simulation, we count the number of times the algorithm is in either one of the configuration spaces $\mathcal{Z}_F$. The statistics for a simulation are therefore given by $Z_0 + Z_1 = Z_{aPBC}$.

5.2.1 The Action with Counterterm, P_u

First, we consider the action with counterterm and the superpotential P_u such that supersymmetry is unbroken. We start by discussing how this choice for the action affects the algorithm and then show some examples of results obtained employing the algorithm to demonstrate its feasibility.

---

[4]Note, that these constraints are also inherently present in the transfer matrix. Entries for those states violating the constraints on the bond occupation numbers are zero, such that configurations containing sites where the constraints are violated do not contribute to any observable.

The Algorithm

As we have pointed out in section 4.2, the bosonic bond configurations for the system discretised with the action with counterterm as well as with the standard discretised action S_L are completely characterised by bonds of the type $b^B_{1\to 1}$. Furthermore, the weight of a bosonic bond is the same for either of these actions too, $w_{1\to 1} = 1$. Thus, the algorithm as derived in the previous section is directly applicable for the action with counterterm and the super-potential P_u and all the acceptance ratios can be adopted[5].

The potential $V(\phi)$ is even for the action with counterterm and the super-potential P_u, $V(\phi) = \frac{1}{2}(2 + \mu^2 + 3g)\phi^2 + \mu g\phi^4 + \frac{1}{2}g\phi^6$. Also the monomer weight is even, $M(\phi) = 1 + \mu + 3g\phi^2$. Therefore, for $\mu \geq 0$ and $g \geq 0$, we have site weights $Q_F(n) \geq 0$, such that this action is suitable for Monte Carlo simulations and there is no sign problem involved in this simulation. Furthermore, it is easy to see that all site weights vanish for odd arguments, $Q_0(2n + 1) = Q_1(2n + 1) = 0$, $n \in \mathbb{N}_0$. In other words, the site occupation number $k(x)$ for configurations with non-zero weight must be even for each site. This has consequences for the remove step for the bosonic variables. The bond configurations in the configuration spaces $\mathcal{G}^B_F$ and $\mathcal{Z}_F$ are no longer equal, but the bond configurations in the configuration space $\mathcal{Z}_F$ are a subset of the bond configurations in the configuration space $\mathcal{G}^B_F$. Therefore, the remove update step $x_1, x_2 \to \varnothing$, eq.(5.3), is only accepted if both additional variables are at the same site, $x_1 = x_2$. Likewise, entering the configuration space $\mathcal{G}^B_F$ from $\mathcal{Z}_F$, $\varnothing \to x_1, x_2$, also has only non-zero acceptance probability if both bosonic variables are put on the same site, $x_1 = x_2$. Taking into account these constraints, the obvious modification to render the algorithm more efficient for this action is to propose the removal step for the bosonic sources only if both sources are at the same site.

We now illustrate the feasibility of the algorithm for the action with counterterm and unbroken supersymmetry under consideration of the modification discussed above.

---

[5]Of course, the site weights Q_F and therefore the weight ratios R_F, R'_F, and R_m are affected by the choice of the action.
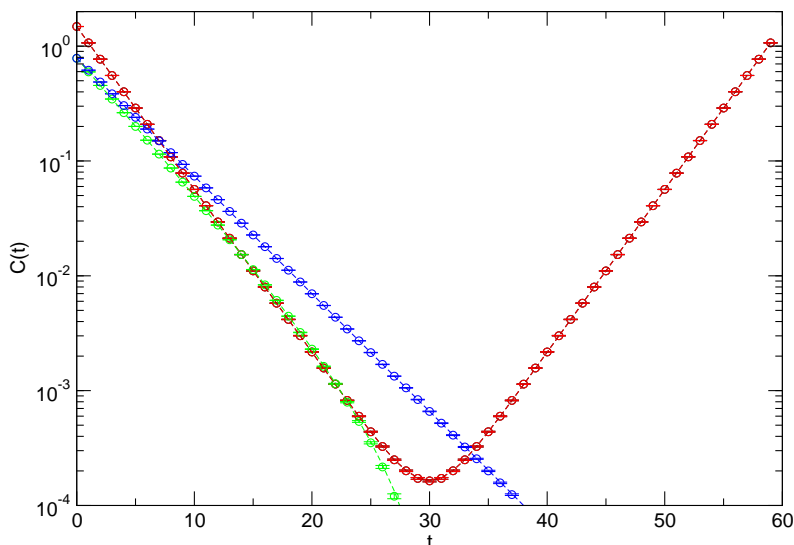
Figure 5.3: Unbroken supersymmetric quantum mechanics. Bosonic correlation function for aPBC (black) and PBC (red) (lying on top of each other) and fermionic correlation function for aPBC (green) and PBC (blue) and $f = 1$.

Simulation Results

As a first observable, we show the results for the bosonic and fermionic correlation functions for $\mu L = 10.0$, $L_t = 60$, and $f = 1$ for $Z_{aPBC} = 10^7$ in figure 5.3.

This is essentially the same plot as figure 4.9(b) with the additional data from the Monte Carlo simulation. The simulation indeed reproduces the exact result within very small statistical errors. These small errors indicate the efficiency of the algorithm.

As a second example, we show the mass gaps for different μL at a coupling $f = 1$ and statistics of $Z_{aPBC} = 10^6$ in figure 5.4.

The μL considered are in the region where thermal effects are negligible and essentially only Z_0 contributes to the total partition function, such that $Z_{aPBC} \simeq Z_0$. Therefore, the extracted masses, when expressed in units of μ, indeed extrapolate to the correct zero-temperature continuum limit. Note, that those masses very close to the continuum should not be taken into ac-
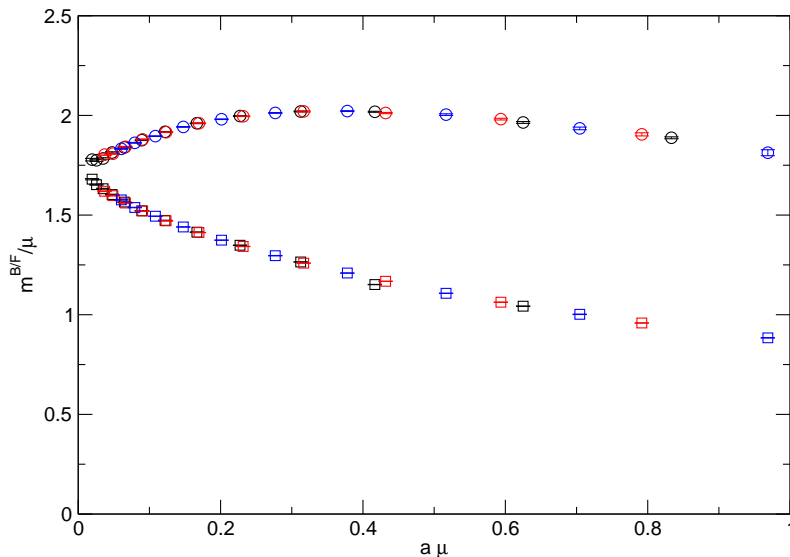
Figure 5.4: Unbroken supersymmetric quantum mechanics. Bosonic (circles) and fermionic (squares) mass gaps for $\mu L = 10.0$ (black), $\mu L = 19.0$ (red), $\mu L = 31.0$ (blue), and $f = 1$.

count since the performance of the fits for the extraction of the masses on large lattices turns out to be quite difficult, yielding a systematic error. The boson mass reaches the continuum limit from above, whereas the fermion mass reaches the limit from below. This is the same behaviour as we have seen in figure 4.20 for the lowest mass gaps in the relevant bosonic sector.

These results illustrate that it is indeed possible to simulate efficiently supersymmetric quantum mechanics with the action with counterterm for unbroken supersymmetry with the proposed algorithm.

5.2.2 The Action with Counterterm, P_b

Next, we consider the action with counterterm and the superpotential P_b such that supersymmetry is broken. Using this action, it will be possible to confirm numerically that the Witten index goes to zero in the continuum limit. This is due to the fact that the algorithm not only samples the bosonic and the fermionic sector individually but also relative weights thereof. Before we show the results, we also need to discuss how this choice of the superpotential affects
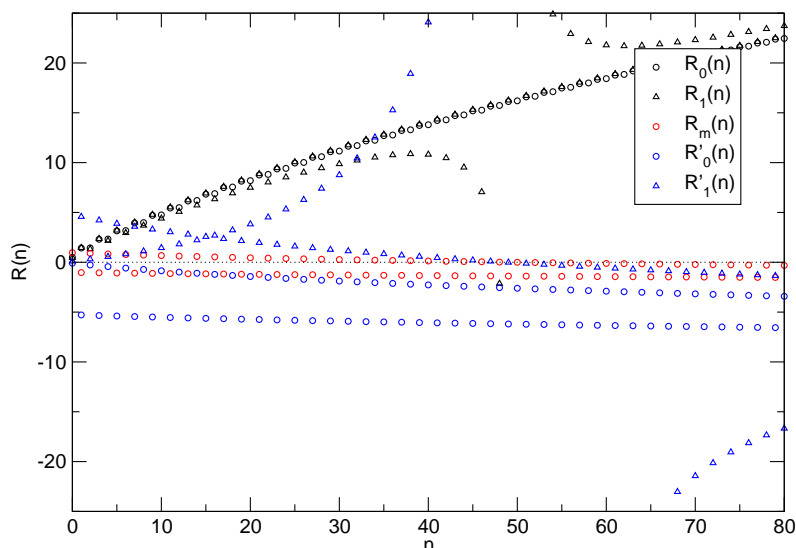
Figure 5.5: Broken supersymmetric quantum mechanics. The ratios R_F, R'_F, and R_m for $\mu L = 10.0$ and $L_t = 30$.

the algorithm.

The Algorithm

Using the superpotential P_b instead of P_u does neither affect the types of the bosonic bonds, nor the weight of the bosonic bonds. Therefore, the acceptance ratios from the previous section can also be adopted for the simulation of broken supersymmetry with the action with counterterm under the premise that the ratios $R_F(n), R'_F(n)$ and $R_m(n)$ are positive.

However, we face the difficulty that by using the superpotential P_b, the site weights are in fact no longer necessarily positive for this action. This can be seen by considering the potential $V(\phi) = \lambda\phi + \frac{1}{2}(2 + \mu^2)\phi^2 + \mu\lambda\phi^3 + \frac{1}{2}\lambda^2\phi^4$ and the monomer weight $M(\phi) = 1 + \mu + 2\lambda\phi$. For this potential and monomer weight, the site weights $Q_0(n)$ and $Q_1(n)$ are indefinite, even if $\mu \geq 0$ and $\lambda \geq 0$. So are the ratios R_F, R'_F, and R_m which we use for the algorithm. In figure 5.5, we show the ratios for $\mu L = 10.0$ and $L_t = 30$.

As Monte Carlo simulations require a positive weight, we take the sign of the configuration into the observable, such that we use the absolute values

of the ratios, $R_F \to |R_F|, R'_F \to |R'_F|$, and $R_m \to |R_m|$. Still, this could be problematic for the simulations, since all contributions to an observable might cancel to zero and we might run into a severe sign problem. Fortunately, it turns out that by using the superpotential P_b, this sign problem, which is only a lattice artefact, is basically absent such that the algorithm is suitable for simulations. This absence of the sign problem can be explained by the fact that the bond occupation numbers are always below the region where the sign of the ratios plays a role. In the example in figure 5.5, the system is only in the fermionic sector, such that only $R_1(n)$ and $R'_1(n)$ occur in the simulation. In addition, the bond occupation numbers are very small on a lattice of this extent. As can be seen in the figure, the ratios involved are therefore all positive, such that each generated configuration contributes with a positive sign. This observation holds for any lattice size.

Before we proceed by showing the results for the simulations, we have a remark on the constraints of the bond configurations. Since the site weights $Q_F(n)$ are non-zero for any n, there are no constraints on the site occupation number. Thus, in this formulation, the bond configurations in the configuration spaces $\mathcal{Z}_F$ and $\mathcal{G}_F^B$ are equal and for the bosonic update steps, the algorithm proposes to remove the additional sources after each step.

Simulation Results

As a first observable, we show the bosonic and fermionic two-point functions, $\langle \phi_t \phi_0 \rangle$ and $\langle \psi_t \overline{\psi}_0 \rangle$, for PBC and aPBC for $\mu L = 10.0$ and at a coupling $f = 1$ in figure 5.6. The statistics were $Z_{aPBC} = 10^8$.

In the figure, we plot the exact results from a calculation with the transfer matrix as well. Also for broken supersymmetry, the simulation yields results which agree with the exact results within statistical errors. Note, that the errors are very small. That is, because of the efficiency of the algorithm, we are able to simulate the system to an arbitrary precision for broken supersymmetry.

As a second observable, we show the ratio Z_{PBC}/Z_{aPBC} for different μL and $f = 1$ in figure 5.7.

As discussed in the previous section, for zero temperature, this ratio corresponds to the Witten index. To compare the results, we have drawn the exact
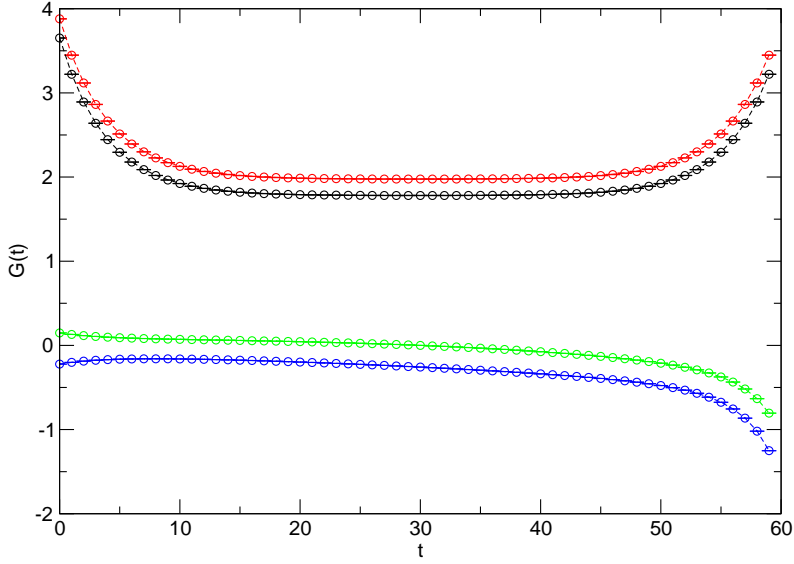
Figure 5.6: Broken supersymmetric quantum mechanics. The bosonic two-point function for aPBC (black) and PBC (red) and the fermionic one for aPBC (green) and PBC (blue) for $L_t = 60$ and $f = 1$.
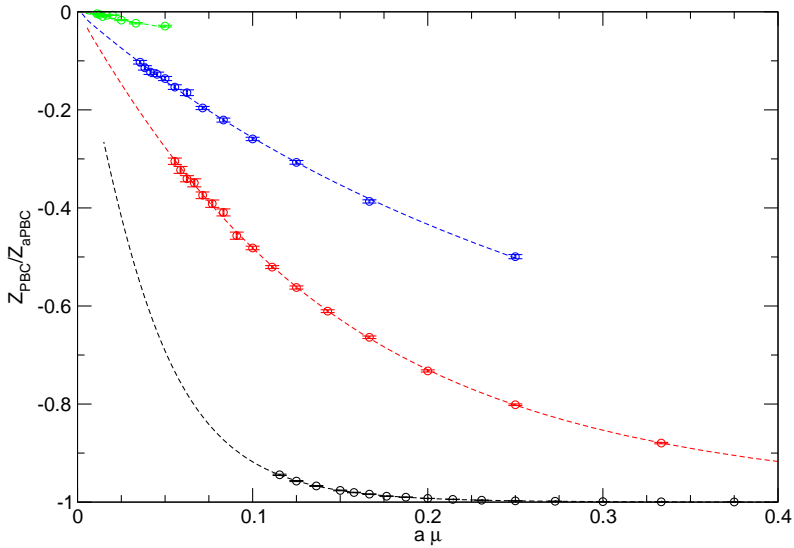
Figure 5.7: Broken supersymmetric quantum mechanics. Z_{PBC}/Z_{aPBC} for $\mu L = 1.0$ (green), $\mu L = 5.0$ (blue), $\mu L = 10.0$ (red), $\mu L = 30.0$ (black) for $f = 1$.

lattice results from figure 4.8. Also for this quantity, the simulation yields results which agree with the exact results within statistical errors. This figure demonstrates that the hopping expansion and the worm algorithm are indeed means to regularise the Witten index thus that reliable simulation results are possible even in the context of broken supersymmetry.

5.2.3 The Q_1-Exact Action, P_u

The last system we consider for the simulation with the worm algorithm is unbroken supersymmetry formulated with the Q_1-exact action[6]. For this action, we now need to modify the algorithm, as there are the bonds of the type $b^B_{1\to3}$ we need to incorporate. Furthermore, the bond weights are different from one for this action, such that we need to adapt some of the acceptance ratios.

The Algorithm

To be able to simulate supersymmetric quantum mechanics with the Q_1-exact discretisation, we need to adjust the algorithm. As we have seen in chapter 4, for the Q_1-exact action, the bosonic states are not only characterised by the bonds $b^B_{1\to1}$ but also by additional bonds of the type $b^B_{1\to3}$. Therefore, we need to modify the algorithm such that the bond configurations for both types are updated. Furthermore, we have to alter the probabilities for the shift update of the bond $b^B_{1\to1}$ since for the Q_1-exact action, the weight for both types of bonds is different from one, $w_{1\to1} = 1 + \mu$ and $w_{1\to3} = g$.

In order to be able to incorporate the update for the bond configuration of the bonds $b^B_{1\to3}$, we introduce the probability $p_{1\to3}$. We then modify the shift update step such that instead of proposing to alter the bond configuration for the bonds of the type $b^B_{1\to1}$ for each shift update, we propose with probability $p_{1\to3}$ to alter the bond configuration for the bonds of the type $b^B_{1\to3}$.

Consider first the acceptance ratios for the shift update of the configurations for the bonds of the type $b^B_{1\to1}$. As the proposition probability of this intermediate step is completely symmetric, the newly introduced probability $p_{1\to3}$ does not affect the ratios. Remembering that the bond weight for the

---

[6] Monte Carlo simulations for broken supersymmetry using the Q_1-exact action, we encounter the very same problems we ran into in the transfer matrix approach. The bond occupation number blows up even for small lattices such that the generation of reliable results turned out to be impossible.

bonds of the type $b_{1\to1}^{B}$ is no longer equal to one, we find the modifications for eqs.(5.8,5.9) as

$$P_{\mathrm{sh}}(x \to y, n_{xy}^{B} \to n_{xy}^{B} + 1) \quad = \quad \frac{w_{1\to1}}{n_{xy}^{B} + 1} R_{F}(k(y)), \tag{5.20}$$

$$P_{\mathrm{sh}}(x \to y, n_{xy}^{B} \to n_{xy}^{B} - 1) \quad = \quad \frac{n_{xy}^{B}}{w_{1\to1}} \frac{1}{R_{F}(k(x) - 2)}. \tag{5.21}$$

Let us now turn to the acceptance ratios for the shift update of the configurations for the bonds of the type $b_{1\to3}^{B}$. In order to simplify the notation, we introduce similarly to eq.(5.7) the abbreviation for the number of bosonic bonds of the type $n_{1\to3}^{B}$ between the sites x and y as

$$\overline{n}_{xy}^{B} \quad = \quad \begin{cases} n_{1\to3}^{B}(x) & \text{if } y = x + 1, \\ n_{1\to3}^{B}(y) & \text{if } y = x - 1. \end{cases} \tag{5.22}$$

It is easy to see that the proposition probabilities for the bonds of the type $b_{1\to3}^{B}$ are totally symmetric too, such that all factors which balance the proposition cancel. However, since the bond itself is asymmetric, the weight of a configuration is affected by the direction where the head moves to. Balancing shifts $x \to y$ and $\overline{n}_{xy}^{B} \to \overline{n}_{xy}^{B} + 1$ as usual with shifts $y \to x$ and $\overline{n}_{xy}^{B} \to \overline{n}_{xy}^{B} - 1$, we find the acceptance ratios for each case separately,

$$P_{\mathrm{sh}}(x \to y, \overline{n}_{xy}^{B} \to \overline{n}_{xy}^{B} + 1) = \begin{cases} \dfrac{w_{1\to3}}{\overline{n}_{xy}^{B} + 1} R_{F}(k(y)) R_{F}(k(y) + 2) & \text{if } y = x + 1, \\[4mm] \dfrac{w_{1\to3}}{\overline{n}_{xy}^{B} + 1} R_{F}(k(x)) R_{F}(k(y)) & \text{if } y = x - 1, \end{cases} \tag{5.23}$$

$$P_{\mathrm{sh}}(x \to y, \overline{n}_{xy}^{B} \to \overline{n}_{xy}^{B} - 1) = \begin{cases} \dfrac{\overline{n}_{xy}^{B}}{w_{1\to3}} \dfrac{1}{R_{F}(k(x) - 2)} \dfrac{1}{R_{F}(k(y) - 2)} & \text{if } y = x + 1, \\[4mm] \dfrac{\overline{n}_{xy}^{B}}{w_{1\to3}} \dfrac{1}{R_{F}(k(x) - 2)} \dfrac{1}{R_{F}(k(x) - 4)} & \text{if } y = x - 1. \end{cases} \tag{5.24}$$

Modifying the algorithm thus allows for the update of all needed bond configurations in the appropriate way.
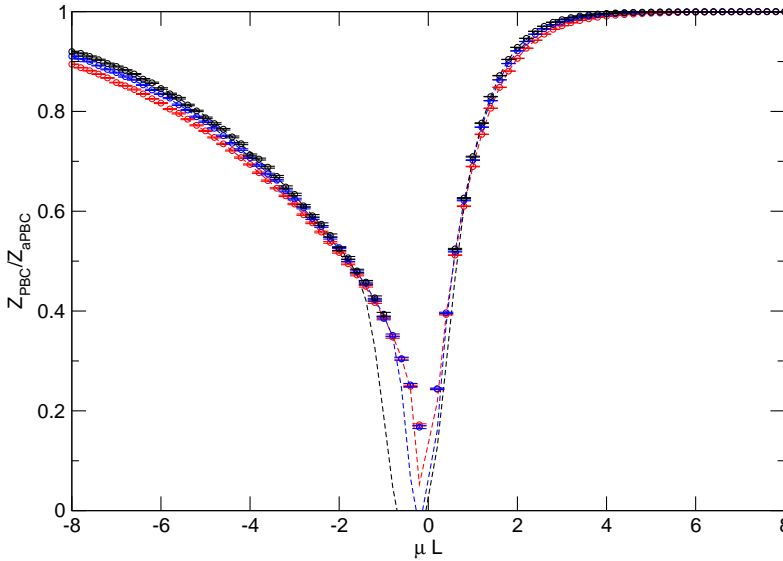
Figure 5.8: Unbroken supersymmetric quantum mechanics. Z_{PBC}/Z_{aPBC} for $L_t = 16$ (red), $L_t = 32$ (blue), $L_t = 64$ (black), for $f = 1$ and $Z_{aPBC} = 10^8$.

Finally, we would like to point out that also for the Q_1-exact action and unbroken supersymmetry the site weights $Q_F(n) \geq 0$ because of similar reasons we gave for the case with the action with counterterm and unbroken supersymmetry. Analogously, the constraint that the site occupation number $k(x)$ must be even applies. Therefore, the bond configurations in the configuration space $\mathcal{Z}_F$ are a subset of the bond configurations in the configuration space $\mathcal{G}_F^B$ and the removal step has only non-zero acceptance probability if both additional bosonic variables are at the same position, $x_1 = x_2$.

We now illustrate by means of the following two examples that the proposed algorithm works.

Simulation Results

In figure 5.8, we show first the phase diagram of the ratio Z_{PBC}/Z_{aPBC} in dependence on μL for different fixed L_t from data for statistics of $Z_{aPBC} = 10^8$.

In this plot, we have included exact lattice results from transfer matrix calcu-
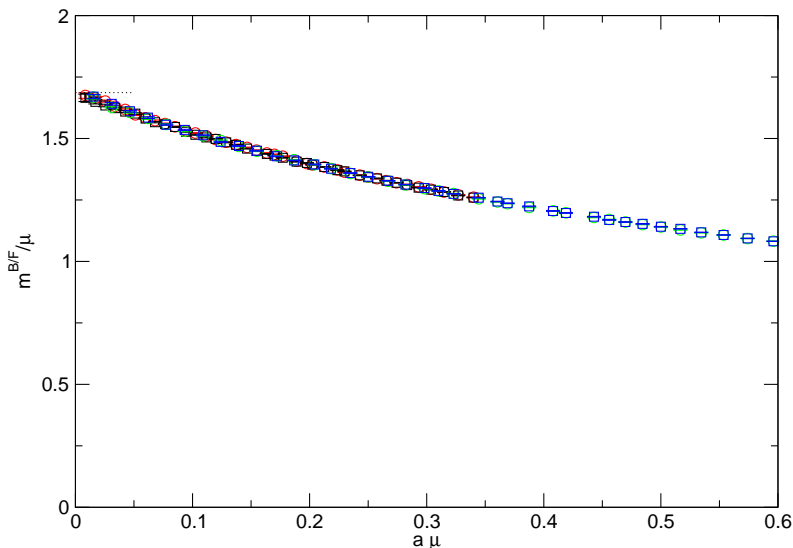
Figure 5.9: Unbroken supersymmetric quantum mechanics. Bosonic (black squares) and fermionic (red circles) mass gaps for $\mu L = 17.0$; bosonic (blue squares) and fermionic (green circles) mass gaps for $\mu L = 31.0$. The coupling is $f = 1$.

lations as well. Also for this quantity, the simulated observable agrees within reasonably small statistical errors with the exact result. Note, that we have simulated negative bare masses, too. This is in contrast to the calculations for broken supersymmetry with counterterm in figure 5.7, where we show only positive μL in the plot. The reason for this is that the latter action is invariant under a change of the sign of the bare mass. For negative μL, the cutoff effects near the continuum for the transfer matrix are much more severe than for positive μL which explains the difference between the results for the transfer matrix and the ones obtained from the simulation. Therefore, for small negative μL, reliable results can only be achieved by means of the Monte Carlo simulations.

The last quantity we calculate are the bosonic and the fermionic mass gaps for different μL and a coupling of $f = 1$ for the statistics of $Z_{aPBC} = 10^6$. In figure 5.9, we show the masses we have obtained by fitting exponentials to the respective correlation functions.

The results displayed in this figure show that the masses for the boson and

the fermion are indeed indistinguishable within statistical errors. The degeneracy of the masses for finite lattice spacing due to the Q_1-exactness of the action emerges also for the results via Monte Carlo simulations. Note that the chosen μL lie well within the region where thermal effects are negligible and the masses extrapolate nicely to the correct zero-temperature continuum limit which is indicated by the black dotted line.

All results in this section therefore confirm the expected features of unbroken supersymmetry discretised with the Q_1-exact action. Furthermore, the Monte Carlo results agree within the statistical errors with the exact lattice results. After having undergone the modifications derived at the beginning of the section, the algorithm is thus also applicable for this discretisation.

Chapter 6

The $\mathcal{N}=1$ Wess-Zumino Model in Two Dimensions

In this chapter, we will adopt our previous considerations for the reformulation of the degrees of freedom in terms of bonds to the two-dimensional $\mathcal{N}=1$ Wess-Zumino model [79]. This is a minimal model allowing for dynamical supersymmetry breaking, which is in contrast to supersymmetric quantum mechanics in one dimension where the breaking of supersymmetry is pre-determined by the choice of the superpotential. Yet, the regime of this phase transition may not be accessible perturbatively. Therefore, the $\mathcal{N}=1$ Wess-Zumino model provides an ideal testing ground for the non-perturbative studying of spontaneous supersymmetry breaking.

Furthermore, we note that restraining the $\mathcal{N}=2$ Wess-Zumino model [32, 33, 42–44, 80] to real valued fields, e.g. replacing the complex valued bosonic field with a real one and to changing the Dirac fermions to Majorana fermions, yields the $\mathcal{N}=1$ Wess-Zumino model. Now, because the $\mathcal{N}=2$ Wess-Zumino model provides a dimensionally reduced model of the matter sector of the minimal supersymmetric standard model (MSSM) [81], a physical motivation for the investigation of the $\mathcal{N}=1$ Wess-Zumino model is given, too.

The chapter itself is organised as follows. We will start by reviewing briefly the main features of the two-dimensional $\mathcal{N}=1$ Wess-Zumino model. Following Golterman and Petcher [45], we will then construct a lattice action of the model with a Wilson-type discretisation. We will then apply the hopping expansion to the discretised model in two dimensions and work out in detail the lattice representation of the model in terms of bosonic and fermionic bonds. On the one hand, we will thus recover the fermion 8-vertex model for the fermionic bond configurations. Yet, on the other hand, we will find that the bond representation for the bosonic degrees of freedom leads to a severe

sign problem. We will address this problem by proposing a hybrid form of the worm algorithm for the fermionic degrees of freedom and of the standard Metropolis update for the bosonic degrees of freedom. Finally, we will conclude the chapter by presenting first results obtained using this technique.

We would like to stress at this point that in this chapter the focus lies on the application of the hopping expansion to the two-dimensional $\mathcal{N} = 1$ Wess-Zumino model and on the reformulation of its degrees of freedom in terms of bond variables. The technical aspects of the simulation, such as the explicit presentation of the worm algorithm for a two-dimensional Majorana fermion and the standard Metropolis update for the bosonic degrees of freedom will be discussed elsewhere [82]. Furthermore, we will also set aside a detailed interpretation of the presented simulation results and not address subtleties such as how to take the continuum limit of the model and the renormalisation of the theory either.

6.1 The Model in the Continuum

6.1.1 The Action and the Supersymmetry Transformations

The on-shell continuum action of the two-dimensional $\mathcal{N} = 1$ Wess-Zumino model in Euclidean space with imaginary time x_0 reads

$$S = \int_0^\beta dx_0 \int dx_1 \; \frac{1}{2} \left[(\partial_\mu \phi(x))^2 + P'(\phi(x))^2 + \overline{\psi}(x) \left(\slashed{\partial} + P''(\phi(x)) \right) \psi(x) \right],$$

(6.1)

where in the Feynman slash notation $\slashed{\partial} = \gamma_\mu \partial_\mu$ the summation over $\mu = 0, 1$ is left implicit, $\phi(x)$ is a real scalar field, and $\psi(x)$ is a real two-component Majorana spinor

$$\psi(x) = \left(\begin{array}{c} \psi_0(x) \\ \psi_1(x) \end{array} \right).$$

(6.2)

Note that in the following, we will suppress the space-time index x for notational convenience. The superpotential $P(\phi)$ is an arbitrary polynomial in ϕ and $P' = \frac{\partial P}{\partial \phi}$ its derivative with respect to ϕ. In Euclidean space, the definition for $\overline{\psi}$ is given by

$$\overline{\psi} = \psi^T \mathcal{C},$$

(6.3)

where the matrix $\mathcal{C}$ is the charge conjugation operator, obeying the relations

$$\mathcal{C}\gamma_\mu\mathcal{C}^{-1} = -\gamma_\mu^T = -\gamma_\mu^*, \qquad \mathcal{C} = -\mathcal{C}^T, \qquad \mathcal{C}^\dagger = \mathcal{C}^{-1}. \tag{6.4}$$

The Dirac matrices γ_μ obey the anticommutation rules

$$\{\gamma_\mu, \gamma_\nu\} = \gamma_\mu\gamma_\nu + \gamma_\nu\gamma_\mu = 2\delta_{\mu\nu} \cdot 1_{2\times2}. \tag{6.5}$$

As usual, the bosonic degrees of freedom obey PBC. Imposing aPBC in the time direction and PBC in the spatial direction[1] upon the fermionic degrees of freedom, β can be interpreted as the inverse temperature.

At zero temperature, the continuum action eq.(6.1) is invariant under the single supersymmetry transformation δ,

$$\delta\phi = \bar{\epsilon}\psi, \qquad \delta\psi = (\slashed{\partial}\phi - P')\epsilon, \qquad \delta\bar{\psi} = 0, \tag{6.6}$$

where ϵ is a constant Majorana spinor. For finite temporal extent however, analogously to the one-dimensional case, the action is only invariant under the supersymmetry transformation δ if PBC are imposed upon the fermionic degrees of freedom in the time direction as well,

$$\psi(x_0 = \beta) = \psi(x_0 = 0). \tag{6.7}$$

Thus, and this is in analogy to the one-dimensional case too, the natural choice of aPBC in time direction for the fermionic degrees of freedom breaks supersymmetry explicitly.

6.1.2 The Discrete $\mathbb{Z}_2$ Chiral Symmetry

Similarly to supersymmetric quantum mechanics, we can choose the superpotential such that an additional symmetry of the action emerges. We consider it worthwhile to discuss briefly our choice for the superpotential and the resulting additional symmetry.

In particular, we will use the minimal interacting superpotential

$$P(\phi) = -\frac{\mu^2}{4\lambda}\phi + \frac{1}{3}\lambda\phi^3 \tag{6.8}$$

---

[1]This choice of boundary conditions is usually referred to as *thermal boundary conditions.*

throughout the rest of this chapter. The derivatives of the superpotential appearing in the action are then given by

$$P'(\phi) = -\frac{\mu^2}{4\lambda} + \lambda\phi^2 \quad \text{and} \quad P''(\phi) = 2\lambda\phi. \tag{6.9}$$

Note, that the superpotential eq.(6.8) is exactly the same one as the superpotential P_b for broken supersymmetry in the one-dimensional case. With this choice of the superpotential, we follow [62] rather than [45][2].

Introducing the matrix $\gamma_5 \equiv i\gamma_0\gamma_1$ which anticommutes with all Dirac matrices,

$$\{\gamma_5, \gamma_\mu\} = 0, \tag{6.10}$$

we now find for the action eq.(6.1) in addition to the supersymmetry δ the discrete $\mathbb{Z}_2$ chiral symmetry

$$\phi \quad \rightarrow \quad -\phi, \tag{6.11}$$
$$\psi \quad \rightarrow \quad \gamma_5\psi, \tag{6.12}$$
$$\overline{\psi} \quad \rightarrow \quad -\overline{\psi}\gamma_5. \tag{6.13}$$

On the one hand, the superpotential eq.(6.8) amounts in the action eq.(6.1) for the bosonic self-interaction to a ϕ^4-theory,

$$\frac{1}{2}\left(P'(\phi)\right)^2 = \frac{1}{2}\left(-\frac{1}{2}\mu^2\phi^2 + \lambda^2\phi^4\right), \tag{6.14}$$

preserving the $\mathbb{Z}_2$-symmetry $\phi \rightarrow \tilde{\phi} = -\phi$. The interacting theory thus has two classical vacua at

$$\phi = \pm\frac{\mu}{2\lambda} \tag{6.15}$$

for the bosonic field. On the other hand, the fermionic fields acquire a Yukawa interaction.

The careful analysis of the Witten index reveals one fermionic and one bosonic ground state [70]. Therefore, $\text{Tr}[(-1)^F] = 0$, which implies that this superpotential allows for spontaneous supersymmetry breaking.

---

[2]That the superpotential eq.(6.8) can be transformed into the one used in [45] simply by applying a shift in the bosonic variable. Therefore, the physics is the same for both choices.

6.2 The Lattice Action

We now formulate the two-dimensional Wess-Zumino model on a discrete lattice which extends over $L_0 = L_t$ lattice spacings in the temporal direction x_0 and $L_1 = L$ lattice spacings in the spatial direction x_1. For a given lattice spacing a, the lattice Λ is then defined as

$$\Lambda = \{x \equiv (x_0, x_1) \in a\mathbb{Z}^2 \mid 0 \leq x_\mu \leq a(L_\mu - 1)\}, \tag{6.16}$$

with $\mu = 0, 1$. For the discretisation, the integration over the variables x_0 and x_1 is replaced by a sum over all lattice points,

$$\int_0^\beta dx_0 \int dx_1 \rightarrow a^2 \sum_x, \tag{6.17}$$

where the factor a in front of the sum accounts for the integration measures dx_μ. In analogy to eqs.(3.14), we define the lattice forward derivative operator Δ_μ^+ and the backward derivative operator Δ_μ^- in direction μ,

$$\Delta_\mu^- f_x = \frac{1}{a}(f_x - f_{x-a\hat{\mu}}), \tag{6.18}$$

$$\Delta_\mu^+ f_x = \frac{1}{a}(f_{x+a\hat{\mu}} - f_x). \tag{6.19}$$

These finite difference operators combine to the symmetric difference operator Δ_μ^S in direction μ and to the operator Δ^2 as

$$\Delta_\mu^S = \frac{1}{2}(\Delta_\mu^+ + \Delta_\mu^-), \tag{6.20}$$

$$\Delta^2 = \sum_{\mu=0}^1 \Delta_\mu^+ \Delta_\mu^-. \tag{6.21}$$

As we have done for supersymmetric quantum mechanics, we use Wilson fermions to remove the doublers from the system. Representing the finite difference operators in matrix form, the Wilson term reads in two dimensions

$$-\frac{ra}{2}\Delta^2 = -\frac{r}{2a}\sum_{\mu=0}^1 (\delta_{x,y+a\hat{\mu}} + \delta_{x,y-a\hat{\mu}} - 2\delta_{x,y}), \tag{6.22}$$

where the Wilson parameter $r \in [-1, 1]\backslash\{0\}$. Yet, in contrast to the one-dimensional case where the Wilson term was added directly to the lattice

derivative, we write it for the two-dimensional theory into the derivative of the superpotential,

$$P'(\phi_x) \equiv P'_x = -\frac{\mu^2}{4\lambda} + \lambda\phi_x^2 - \frac{r}{2a} \sum_y \sum_{\mu=0}^{1} (\delta_{x,y+a\hat{\mu}} + \delta_{x,y-a\hat{\mu}} - 2\delta_{x,y})\phi_y, \quad (6.23)$$

where the sum over y runs over all lattice points. We now define the second derivative of the superpotential as the matrix

$$P''_{x,y} \equiv \frac{\partial P'_x}{\partial \phi_y} = 2\lambda\phi_x\delta_{x,y} - \frac{r}{2a} \sum_{\mu=0}^{1} (\delta_{x,y+a\hat{\mu}} + \delta_{x,y-a\hat{\mu}} - 2\delta_{x,y}), \quad (6.24)$$

where the multiplication with the unit matrix in spin space is left implicit. Furthermore, for notational convenience, we introduce the slashed symmetric lattice derivative in matrix representation,

$$\sum_{\mu=0}^{1} \gamma_\mu \Delta_\mu^S = \sum_{\mu=0}^{1} \gamma_\mu \frac{1}{2a} (\delta_{y,x+a\hat{\mu}} - \delta_{y,x-a\hat{\mu}}) \equiv \displaystyle{\not{D}}_{x,y}. \quad (6.25)$$

In the following, we set the Wilson parameter $r = 1$ and work in lattice units, such that the lattice spacing is set $a = 1$. For the kinetic term of the bosonic field, we replace the continuum derivative by the symmetric difference operator. This yields the discretised action of the $\mathcal{N} = 1$ Wess-Zumino model written out in lattice units,

$$S_L = \frac{1}{2} \sum_x \left\{ \sum_\mu (\Delta_\mu^S \phi_x)^2 + P_x'^2 + \sum_y \psi_x^T \mathcal{C} (\displaystyle{\not{D}}_{x,y} + P''_{x,y})\psi_y \right\}. \quad (6.26)$$

An explicit representation for the Dirac matrices γ_μ and the charge conjugation matrix $\mathcal{C}$ is given by

$$\gamma_0 = \begin{pmatrix} 1 & 0 \\ 0 & -1 \end{pmatrix}, \quad \gamma_1 = \begin{pmatrix} 0 & -1 \\ -1 & 0 \end{pmatrix}, \quad \mathcal{C} = \begin{pmatrix} 0 & 1 \\ -1 & 0 \end{pmatrix}. \quad (6.27)$$

The matrix γ_5 is then easily seen to be

$$\gamma_5 = \begin{pmatrix} 0 & -i \\ i & 0 \end{pmatrix}. \quad (6.28)$$

We define the measure for the path integral as

$$\int \mathcal{D}\phi\mathcal{D}\psi \equiv \prod_{x,\alpha} \int_{-\infty}^{\infty} d\phi_x \int d\psi_{\alpha,x}, \tag{6.29}$$

where the Dirac index $\alpha = 0,1$ labels the two components of the spinor. For notational convenience, we suppress the Dirac index in the following, such that we can write the partition function as

$$Z = \int \mathcal{D}\phi\mathcal{D}\psi \ e^{-S_L(\phi,\psi)}. \tag{6.30}$$

Having thus established a lattice formulation of the $\mathcal{N} = 1$ Wess-Zumino model, we can now benefit from our previous considerations and apply the hopping expansion to the path integral, such that the degrees of freedom are expressed in terms of bonds. However, before we actually reformulate the system in section 6.4, we will motivate the necessity for this technique.

6.3 The Pfaffian and the Sign Problem

Analogously to the one-dimensional case, the usual way to proceed is to integrate out the fermionic degrees of freedom, such that only the integration over the bosonic degrees of freedom has to be performed explicitly. Employing Majorana fermions, the integration of the degrees of freedom yields a Pfaffian [83]

$$\int \mathcal{D}\psi \ \exp\left(-\psi^T M \psi\right) = \mathrm{Pf}(M), \tag{6.31}$$

where the Paffian follows from Grassmann integration and corresponds, up to a sign, to the square root of the determinant, $(\mathrm{Pf}(M))^2 = \det(M)$. For an arbitrary antisymmetric $2N \times 2N$ matrix M it is defined as

$$\mathrm{Pf}(M) = \frac{1}{N! \, 2^N} \epsilon_{\alpha_1,\beta_1,\dots,\alpha_N,\beta_N} M_{\alpha_1,\beta_1} \cdots M_{\alpha_N,\beta_N}. \tag{6.32}$$

Therefore, integrating out the fermionic degrees of freedom in eq.(6.30) yields

$$Z = \int \mathcal{D}\phi \ e^{-S^B(\phi)} \ \mathrm{Pf}(M(\phi)), \tag{6.33}$$

where $M(\phi) = \mathcal{C}(\slashed{\partial} + P''(\phi))$ is the fermion matrix and the bosonic part of the superpotential $S^B(\phi)$ is given by

$$S^B(\phi) = \int d^2x \ \frac{1}{2} \left[(\partial_\mu\phi)^2 - \frac{1}{2}\mu^2\phi^2 + \lambda^2\phi^4 \right]. \tag{6.34}$$

The partition function with the boundary conditions PBC, PBC is proportional to the Witten index Δ,

$$Z_{PBC,PBC} = \int \mathcal{D}\phi \; e^{-S^B(\phi)} \; \mathrm{Pf}(M(\phi)) \propto \Delta. \qquad (6.35)$$

The bosonic action is invariant under the $\mathbb{Z}_2$-symmetry $\phi \to \tilde{\phi} = -\phi$. However, the Pfaffian $\mathrm{Pf}(M(\phi))$ is not necessarily invariant under this parity transformation. In particular, for periodic boundary conditions in both directions PBC, PBC we have

$$S^B(\tilde{\phi}) = S^B(\phi), \qquad \mathrm{Pf}(M(\tilde{\phi})) = -\mathrm{Pf}(M(\phi)). \qquad (6.36)$$

Therefore, similar to the one-dimensional case, for each configuration there is an other one, e.g. the parity transformed one, with the same weight and the opposite sign. For thermal boundary conditions $aPBC, PBC$ however, one finds

$$S^B(\tilde{\phi}) = S^B(\phi), \qquad \mathrm{Pf}(M(\tilde{\phi})) = \mathrm{Pf}(M(\phi)). \qquad (6.37)$$

The lattice action with a Wilson type discretisation explicitly breaks the $\mathbb{Z}_2$ chiral symmetry, such that the above relations only apply in the continuum limit.

The standard way to simulate the model is by using the effective action

$$S^B_{\mathrm{eff}}(\phi) = S^B(\phi) - \ln\left(|\mathrm{Pf}(M(\phi))|\right) = S^B(\phi) - \frac{1}{2}\ln\left(|\det(M(\phi))|\right), \quad (6.38)$$

such that

$$Z = \int \mathcal{D}\phi \; e^{-S^B_{\mathrm{eff}}(\phi)}. \qquad (6.39)$$

Yet, in this approach, the sign of the contribution of a particular configuration to the partition function still has to be taken into account by reweighing. In general, this leads to a severe sign problem [37, 62]. We therefore propose to employ the reformulation of the fermionic degrees of freedom in terms of bonds. This will be reviewed in detail next.

6.4 The Hopping Expansion of the Partition Function

In this section, we will work out the hopping expansion for the two-dimensional $\mathcal{N} = 1$ Wess-Zumino model. As we have done for supersymmetric quantum

mechanics, we will apply the expansion to both the fermionic and the bosonic degrees of freedom in order to use it for the worm algorithm. However, to start with, we point out here that the bond formulation for the bosonic degrees of freedom leads to a severe sign problem. We will discuss in detail the origin of this newly arising sign problem and conclude the section with the presentation of a modification of the algorithm which provides a solution for the problem.

6.4.1 Separating the Bosonic from the Fermionic Action

We apply the hopping expansion technique to the partition function eq.(6.30), such that we are able to represent it in terms of constrained paths,

$$Z = \sum_{CP} W_{CP}. \tag{6.40}$$

For the derivation of the constrained path representation, analogously to the one-dimensional case, we split the action into a purely bosonic part and a part containing the fermionic variables in combination with the bosonic variables,

$$S_L = S_L^B(\phi) + S_L^F(\phi, \psi), \tag{6.41}$$

where the individual parts of the action are given by

$$S_L^B(\phi) = \frac{1}{2} \sum_x \left\{ \sum_\mu (\Delta_\mu^S \phi)_x^2 + P_x'^2 \right\}, \tag{6.42}$$

$$S_L^F(\phi, \psi) = \frac{1}{2} \sum_{x,y} \psi_x^T \mathcal{C}(\displaystyle{\not{D}}_{x,y} + P_{x,y}'') \psi_y. \tag{6.43}$$

Decomposing the action thus allows us to factorise the path integral as

$$Z = \int \mathcal{D}\phi \; e^{-S_L^B(\phi)} \int \mathcal{D}\psi \; e^{-S_L^F(\phi,\psi)}. \tag{6.44}$$

This is the representation of the partition function which we will use for the expansion of the action.

6.4.2 Expanding the Fermionic Part

We start by expanding the fermionic part of the action. This is a much more subtle task in two dimensions than it was in one dimension. To be able to expand this part, we first need to transform the fermionic action into a more suitable form.

The Wilson Projector Representation

By using the representations eqs.(6.24,6.25), we write the fermion matrix as

$$\slashed{D}_{x,y} + P''_{x,y} = M(\phi_x)\delta_{x,y} \cdot 1_{2\times 2} - \frac{1}{2}\sum_{\mu=0}^{1}\left\{(1_{2\times 2} - \gamma_\mu)\delta_{y,x+\hat{\mu}} + (1_{2\times 2} + \gamma_\mu)\delta_{y,x-\hat{\mu}}\right\},$$

(6.45)

where the monomer weight $M(\phi)$ is given by $M(\phi) = 2 + 2\lambda\phi$. Furthermore, it is convenient to define the Wilson projection operators $\mathcal{P}(n)$ for arbitrary lattice unit vectors $n = \pm\hat{\mu}$ as

$$\mathcal{P}(n) = \frac{1}{2}\left(1_{2\times 2} - \slashed{n}\right).$$

(6.46)

These projectors have the properties

$$\mathcal{P}(n)^2 = \mathcal{P}(n), \qquad \mathcal{P}(n)\mathcal{P}(-n) = 0, \qquad \text{Tr}[\mathcal{P}(n)] = 1.$$

(6.47)

Rewriting the fermionic part of the action with the help of the Wilson projection operators yields

$$S_L^F(\phi,\psi) = \frac{1}{2}\sum_x M(\phi_x)\psi_x^T \mathcal{C}\psi_x - \frac{1}{2}\sum_{x,\mu}\left\{\psi_x^T \mathcal{C}\mathcal{P}(\hat{\mu})\psi_{x+\hat{\mu}} + \psi_x^T \mathcal{C}\mathcal{P}(-\hat{\mu})\psi_{x-\hat{\mu}}\right\}.$$

(6.48)

It is easy to see that the identity

$$(\mathcal{C}\mathcal{P}(n))^T = -\mathcal{C}\mathcal{P}(-n)$$

(6.49)

holds. Consequently, the fermionic hopping terms appearing in eq.(6.48) are in fact identified to be identical,

$$\psi_x^T \mathcal{C}\mathcal{P}(n)\psi_{x+n} = \psi_{x+n}^T \mathcal{C}\mathcal{P}(-n)\psi_x,$$

(6.50)

and the hopping term for a fermion in Majorana representation is therefore an *unoriented* bond. This is in contrast to the one-dimensional case, where a direction is assigned to each fermionic bond. Combining both hopping terms according to eq.(6.50) in eq.(6.48), we write the fermionic part of the action as

$$S_L^F(\phi,\psi) = \frac{1}{2}\sum_x M(\phi_x)\psi_x^T \mathcal{C}\psi_x - \sum_{x,\mu}\psi_x^T \mathcal{C}\mathcal{P}(\hat{\mu})\psi_{x+\hat{\mu}}.$$

(6.51)

Using this representation, we are now able to apply the hopping expansion technique to the fermionic Boltzmann factor.

The Loop Representation

Employing the fermionic action eq.(6.51) and exploiting the nilpotency of the Grassman numbers yields for the expansion of the fermionic Boltzmann factor

$$
\mathrm{e}^{-S_L^F} = \prod_x \left(1 - \frac{1}{2} M(\phi_x) \psi_x^T \mathcal{C} \psi_x \right) \prod_{x,\mu} \left(1 + \psi_x^T \mathcal{C} \mathcal{P}(\hat{\mu}) \psi_{x+\hat{\mu}} \right). \tag{6.52}
$$

By introducing the occupation number for the fermionic monomers $m(x) \in \{0,1\}$ and the fermionic bond number $n^F(x,\mu) \in \{0,1\}$ in the direction μ, we rewrite the Boltzmann factor as

$$
\begin{aligned}
\mathrm{e}^{-S_L^F} = \prod_x \Bigg(\sum_{m(x)=0}^{1} & \left(-\frac{1}{2} M(\phi_x) \psi_x^T \mathcal{C} \psi_x \right)^{m(x)} \Bigg) \times \\
& \prod_{x,\mu} \left(\sum_{n^F(x,\mu)=0}^{1} \left(\psi_x^T \mathcal{C} \mathcal{P}(\hat{\mu}) \psi_{x+\hat{\mu}} \right)^{n^F(x,\mu)} \right).
\end{aligned} \tag{6.53}
$$

As usual, to give a non-zero contribution to the path integral, each site x must be saturated with exactly one pair of fermionic variables $\psi_{1,x}$ and $\psi_{2,x}$. In two dimensions, this yields the constraint

$$
m(x) + \frac{1}{2} \sum_\mu \left(n^F(x,\mu) + n^F(x-\hat{\mu},\mu) \right) = 1 \qquad \forall x, \tag{6.54}
$$

on the monomer number and the fermionic bond number. Thus, after the Grassmann integration, only self-avoiding non-backtracking closed fermionic loops survive. Having established the geometry of the fermionic loops in this fashion, we now need to proceed by computing the fermionic contribution to the weight of a configuration.

For this calculation, we follow [84] and evaluate first the weight of one single arbitrary closed fermion loop ℓ. We assume that the loop ℓ does not cross the boundary because such loops may alter the overall sign of the configuration according to the boundary conditions which are imposed upon the fermionic fields. The overall sign will be addressed in detail along with the discussion of the boundary conditions in section 6.5.

Assuming the loop ℓ visits l sites on the lattice, we start by defining the set of those lattice sites $\mathscr{L} = \{x_1, x_2, \ldots, x_l\}$ along which the loop proceeds.

Condition eq.(6.54) tells us, that to each one of these sites in the loop two fermionic bonds are attached. Note, that the site x_1 (so to speak the 'starting point' of the loop) can be chosen arbitrarily. Next-neighbouring sites are separated by lattice unit vectors n, thus forming a chain of sites $x_{i+1} = x_i + n_i$. The last step closes the loop via $x_l + n_l = x_1$. To perform the fermionic integration of the l sites involved in the path integral along the closed loop, the product of bilinears

$$\prod_{x \in \mathcal{L}} \int d\psi_{1,x} d\psi_{2,x} (\psi_{x_1}^T \mathcal{C} \mathcal{P}(n_1) \psi_{x_2})(\psi_{x_2}^T \mathcal{C} \mathcal{P}(n_2) \psi_{x_3}) \cdots (\psi_{x_l}^T \mathcal{C} \mathcal{P}(n_l) \psi_{x_1}) \quad (6.55)$$

has to be evaluated. For the following calculation, the integration rules

$$\int d\psi_1 d\psi_2 \ \psi \psi^T \mathcal{C} = 1_{2 \times 2}, \quad (6.56)$$

$$\int d\psi_1 d\psi_2 \ \psi^T \mathcal{C} \psi = -2, \quad (6.57)$$

will be useful. Applying repeatedly the identity eq.(6.56), eq.(6.55) reduces to the integral

$$\int d\psi_{1,x_1} d\psi_{2,x_1} \ \psi_{x_1}^T \mathcal{C} \mathcal{X} \psi_{x_1}, \quad (6.58)$$

where the product of the projection operators has been defined as

$$\mathcal{X} = \mathcal{P}(n_1) \mathcal{P}(n_2) \cdots \mathcal{P}(n_l). \quad (6.59)$$

Evaluating the integral finally yields a fermionic contribution to the weight of the path integral of

$$\int d\psi_{1,x_1} d\psi_{2,x_1} \ \psi_{x_1}^T \mathcal{C} \mathcal{X} \psi_{x_1} = -\text{Tr}[\mathcal{X}], \quad (6.60)$$

that is, the weight of a loop is dictated by the geometry of the loop via the projection operators $\mathcal{P}(n)$. Note the minus sign in front of the trace which is the usual minus sign associated with a closed fermionic loop. Furthermore, the cyclicity of the trace confirms that it is indeed irrelevant which point x_1 along the loop has been chosen as the starting point. The evaluation of the trace is worked out in appendix J and yields

$$\text{Tr}[\mathcal{X}] = (-1)^\nu 2^{n_c/2}, \quad (6.61)$$

where n_c represents the total number of corners in the loop and $\nu \in \{0,1\}$ counts the number of rotations of the loop. Since a closed loop which must not wind around the lattice necessarily completes one rotation, $\nu = 1$ and the minus signs in eqs.(6.60,6.61) compensate each other. The total weight for the loop therefore yields

$$\prod_{x \in \mathscr{L}} \int d\psi_{1,x} d\psi_{2,x} (\psi_{x_1}^T \mathcal{C} \mathcal{P}(n_1) \psi_{x_2}) \cdots (\psi_{x_l}^T \mathcal{C} \mathcal{P}(n_l) \psi_{x_1}) = 2^{n_c/2}. \qquad (6.62)$$

The same calculation goes through for any closed fermionic loop which does not cross the boundaries. To complete the fermionic contribution to the weight of a configuration, we still have to take into account those sites which are not part of a fermionic loop. Their contribution is rather easily calculated as follows.

For any site x where $m(x) = 1$, that is, for any site which is not part of a fermionic loop, the site is saturated via the monomer term. For these sites the Grassman integration via eq.(6.57) simply yields the monomer weight,

$$\int d\psi_{1,x} d\psi_{2,x} \left(-\frac{1}{2} M(\phi_x) \right) \psi_x^T \mathcal{C} \psi_x = M(\phi_x). \qquad (6.63)$$

This concludes our considerations concerning the fermionic contribution to the weight of a configuration where none of the fermionic loops crosses the boundary. The generalisation of the above calculation for configurations with any kind of fermionic loops will be discussed in section 6.5 along with the various choices for the boundary conditions.

The Fermionic 8-Vertex Representation

Before we proceed with the hopping expansion for the bosonic degrees of freedom, we would like to point out that similarly to the Ising model in the dimer formulation, the fermionic configurations can be represented by the 8-vertex model [65]. Because the fermionic bonds are undirected, the plaquettes look the same for both models, yet they differ in their weights.

Eq.(6.62) tells us that each corner in a loop contributes with a factor $1/\sqrt{2}$ to the total weight whereas a straight line contributes with a factor 1. Furthermore, the weight of an empty site is given by eq.(6.63) and intersecting loops are forbidden. Collecting these weights, we show in figure 6.1 the plaquettes
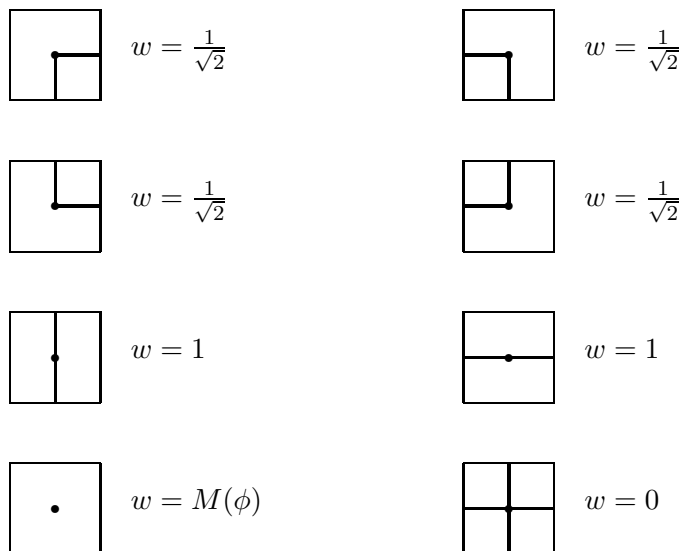
Figure 6.1: The eight different plaquettes for the fermion 8-vertex model and their respective weights w. This is analogous to the 8-vertex model for the dimer formulation for the Ising model in figure 1.4. Note, that corners are suppressed by a factor of $1/\sqrt{2}$ with respect to straight lines and that intersecting loops are excluded.

for a Majorana fermion in two dimensions and their respective weights. Of course, the overall sign of the configuration needs to be fixed at the end for the 8-vertex representation as well.

With this remark on the fermionic 8-vertex model, we conclude our considerations concerning the bond formulation of the fermionic degrees of freedom in two dimensions. Next, we will turn to the bosonic degrees of freedom and work out their bond formulation in detail.

6.4.3 Expanding the Bosonic Part

The Bosonic Bond Representation

Employing the derivative of the superpotential including the Wilson term eq.(6.23), the bosonic part of the action eq.(6.42) written out explicitly reads

$$
S_L^B(\phi) = \sum_x \left\{ V(\phi_x) + \frac{1}{4} \sum_{\nu=\pm 0} \sum_{\mu=\pm 1} \phi_{x+\hat\nu}\phi_{x+\hat\mu} \right.
$$
$$
\left. - \frac{1}{2}\lambda \sum_\mu (\phi_x^2 \phi_{x+\hat\mu} + \phi_x^2 \phi_{x-\hat\mu}) - \sum_\mu (\phi_x \phi_{x+\hat\mu} + \phi_x \phi_{x-\hat\mu}) \right\},
$$

(6.64)

where the potential $V(\phi)$ for the bosonic self-interaction is given by

$$
V(\phi_x) = \frac{1}{4}\left(12 - \mu^2\right)\phi_x^2 + 2\lambda\phi_x^3 + \frac{1}{2}\lambda^2 \phi_x^4.
$$

(6.65)

Note, that in this completely symmetric representation, there are a total of 12 different bosonic hopping terms. For a more compact representation, we find it convenient to define the *diagonal* next-neighbouring unity vectors $\hat d_{ij}$ as

$$
\hat d_{ij} = (-1)^i \hat 0 + (-1)^j \hat 1, \qquad i, j = 0, 1.
$$

(6.66)

Using this definition we can rewrite the action such, that the number of different hopping terms and therefore the number of different bonds is reduced,

$$
S_L^B(\phi) = \sum_x \left\{ V(\phi_x) + \frac{1}{2}\sum_{i=0}^{1} \phi_x\phi_{x+\hat d_{0i}} - \frac{\lambda}{2}\sum_{\mu=0}^{1}(\phi_x^2\phi_{x+\hat\mu}+\phi_x^2\phi_{x-\hat\mu}) - 2\sum_{\mu=0}^{1}\phi_x\phi_{x+\hat\mu} \right\}.
$$

(6.67)

Apparently, expanding this action amounts to the introduction of three different kinds of bosonic bonds. The first kind is the familiar bond connecting two next-neighbouring sites x and $x + \hat\mu$, carrying one variable ϕ at each ending. This bond is represented in figure 6.2 and will be denoted by $b_{1\to 1}^B$. Its weight of $w_{1\to 1}^B = 2$ can be read off directly from the action. The second kind of bond connects two next-neighbouring sites x and $x \pm \hat\mu$, carrying a variable ϕ^2 at the ending attached to the site x and one single variable ϕ at the ending attached to the site $x \pm \hat\mu$. This bond, represented in figure 6.3, will be denoted by $b_{2\to 1}^B$ and has a weight of $w_{2\to 1}^B = \lambda/2$. In addition to the two already familiar bonds, there is a third kind of bosonic bond, connecting two *diagonally* next-neighbouring sites x and $x + \hat d_{0i}$. This bond carries one variable ϕ at each
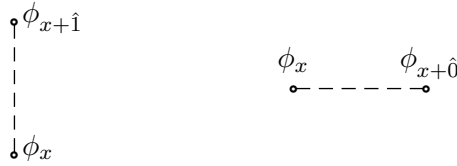
Figure 6.2: The graphical representation of the bosonic bonds $b^B_{1\to1}$. They have a weight of $w_{1\to1} = 2$.
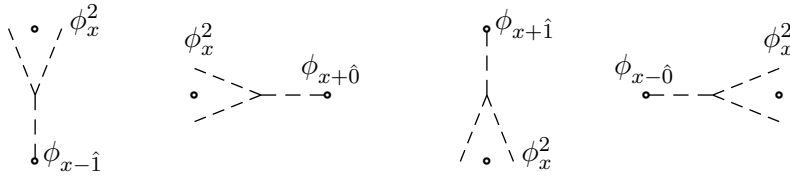
Figure 6.3: The graphical representation of the bosonic bonds $b^B_{2\to1}$. They have a weight of $w_{2\to1} = 1/2\lambda$.
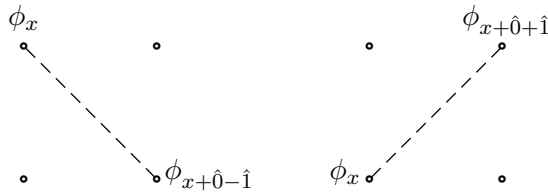
Figure 6.4: The graphical representation of the diagonal bosonic bonds $b^B_{1\to1,d}$. They have a *negative* weight of $w_{1\to1,d} = -1/2$.

ending and will be denoted by $b^B_{1\to1,d}$. It is represented in figure 6.4 and it comes with a *negative* weight of $w^B_{1\to1,d} = -1/2$.

For the discretisation above, the bosonic site occupation number $k(x)$ is given by

$$k(x) = \sum_{\mu=0}^{1} \left\{ n^B_{1\to1}(x,\mu) + n^B_{1\to1}(x-\hat\mu,\mu) + 2n^B_{2\to1}(x,\pm\mu) \right.$$
$$\left. + n^B_{2\to1}(x\pm\hat\mu,\mp\mu) + n^B_{1\to1,d}(x,d_{0\mu}) + n^B_{1\to1,d}(x-\hat d_{0\mu},d_{0\mu}) \right\},$$
(6.68)

where $n^B_{1\to1}(x,\mu)$ represents the bond number for bonds of the type $b^B_{1\to1}$ in the direction μ, $n^B_{2\to1}(x,\mu)$ represents the bond number for bonds of the type $b^B_{2\to1}$ in the direction μ, and $n^B_{1\to1,d}(x,d_{0\mu})$ represents the bond number for bonds of the type $b^B_{1\to1,d}$ in the direction $d_{0\mu}$. In this notation, we identify the total weight of a configuration as

$$W = 2^{N_c/2} \left(\prod_x \prod_\mu \frac{2^{n^B_{1\to1}(x,\mu)}}{n^B_{1\to1}(x,\mu)!} \frac{(\frac{\lambda}{2})^{n^B_{2\to1}(x,\pm\mu)}}{n^B_{2\to1}(x,\pm\mu)!} \frac{(-\frac{1}{2})^{n^B_{1\to1,d}(x,d_{0\mu})}}{n^B_{1\to1,d}(x,d_{0\mu})!} \right) \times$$
$$\left[\prod_x Q(k(x),m(x)) \right],$$
(6.69)

where N_c counts the total number of corners in the fermionic loops. The site weight $Q(k,m)$ is defined as usual,

$$Q(k,m) = \int_{-\infty}^{\infty} d\phi \; \phi^k e^{-V(\phi)} M(\phi)^m. \tag{6.70}$$

We stress again that the overall sign of eq.(6.69) depends on the geometry of the fermionic loops as well as on boundary conditions and has to be determined yet.

The Sign Problem

In principle, it is possible to simulate the model from here by adjusting the algorithm we used for the one-dimensional case to two dimensions. However, it turns out that the sign problem due to the negative weight of the diagonal bond $b^B_{1\to1,d}$ is severe. Absorbing the sign in the observable, all contributions

to the observable in question in fact cancel and therefore make measurements impossible. Because, in addition, the weight $w^B_{1 \to 1,d} = -1/2$ is independent of the bare parameters, the problem does not relax when one approaches the continuum limit. Hence, surprisingly enough, the bond formulation causes a *bosonic* sign problem. It is therefore futile to simulate the system in the reformulation of bonds for both the fermionic and the bosonic degrees of freedom.

The Standard Metropolis Update for the Bosonic Degrees of Freedom

We note, however, that the bosonic action itself as given in eq.(6.64) does not cause any issues in a standard Metropolis update algorithm. The solution to the bosonic sign problem is therefore to design an algorithm which combines the bond formulation for the fermionic degrees of freedom and the standard formulation for the bosonic degrees of freedom. This is perfectly well possible and this hybrid algorithm combining a worm-type algorithm for the fermion and a standard Metropolis update for the bosonic field configuration provides indeed a means for the simulation of the two-dimensional $\mathcal{N} = 1$ Wess-Zumino model. With this algorithm, the original fermionic sign problem stemming from the indefinite sign of the Pfaffian is still under control.

Therefore, instead of expressing the bosonic degrees of freedom in terms of bonds, the bosonic action eq.(6.64) is kept as it stands and the bosonic field is updated at each site x individually via the update step $\phi \to \phi' = \phi + \delta\phi$. The acceptance ratio for this update step is then given by

$$P(\phi_x \to \phi'_x) = \frac{\mathrm{e}^{-S^B_L(\phi'_x)}}{\mathrm{e}^{-S^B_L(\phi_x)}} \left(\frac{M(\phi'_x)}{M(\phi_x)} \right)^{m(x)} . \tag{6.71}$$

To render the bosonic update algorithm efficient, the variation of the field $\delta\phi$ is changed dynamically in the course of a simulation.

Further technical details of the algorithm, in particular the extension of the worm algorithm for two-dimensional fermionic loops, will be presented elsewhere. Nonetheless, we will conclude this chapter by presenting first results obtained by applying the above sketched hybrid algorithm in section 6.6.

6.5 Boundary Conditions

Up to this point, we have neither addressed the determination of the overall sign of a configuration nor discussed the boundary conditions of interest. This

section is devoted to clarify these open points.

6.5.1 The Topological Classes $\mathcal{L}_{ij}$

The bosonic fields obey periodic boundary conditions in both directions $\mu = 0, 1$,

$$\phi_{x+L_\mu \cdot \hat{\mu}} = \phi_x. \tag{6.72}$$

For the fermionic fields, we encode the boundary conditions into a binary vector ε. If we assign $\varepsilon_\mu = 0$ to the choice of periodic boundary conditions in direction μ and $\varepsilon_\mu = 1$ to antiperiodic boundary conditions in direction μ, the condition

$$\psi_{x+L_\mu \cdot \hat{\mu}} = (-1)^{\varepsilon_\mu} \psi_x \tag{6.73}$$

describes the periodicity of the fields correctly. To determine the overall sign of a configuration, we again assign each configuration to a topological class $\mathcal{L}_{ij}$ [84, 85]. For the two-dimensional $\mathcal{N} = 1$ Wess-Zumino model, there are four possible classes, which we denote by $\mathcal{L}_{00}$, $\mathcal{L}_{01}$, $\mathcal{L}_{10}$, and $\mathcal{L}_{11}$. The subscripts i and j count the total number of windings around the torus (modulo 2) in the directions $\mu = 0$ and $\mu = 1$ for a fermionic bond configuration, respectively. In figure 6.5, a representative fermionic bond configuration of each class is shown.

For aPBC in direction μ, the overall weight picks up a factor (-1) each time a fermionic bond crosses the boundary in this particular direction. For the determination of the overall sign of a configuration, we start by considering those loops with $\nu = 1$ (and thus completing a total rotation). Such loops cross each boundary 0 (mod 2) times and, independent of the choice for the boundary conditions, the positive sign obtained in eq.(6.62) is not affected. Thus, loops with $\nu = 1$ *always* yield a positive contribution to the sign of the weight of the configuration. Next, we note that pairs of loops winding around the lattice in the same direction yield a positive sign for any choice of boundary conditions as well. Such loops acquire a factor (-1) for a closed fermionic loop each. Yet, these factors cancel and so do the factors $(-1)^{\varepsilon_\mu}$ which are picked up when crossing the boundary. Consequently, all bond configurations in the topological class $\mathcal{L}_{00}$ come with a *positive* sign. Configurations in the classes $\mathcal{L}_{10}$ and $\mathcal{L}_{01}$ contain an odd number of fermionic loops winding around the boundary. For these loops $\nu = 0$, such that they acquire only the factor (-1) for a closed fermionic loop. In addition, each loop crossing the boundary picks
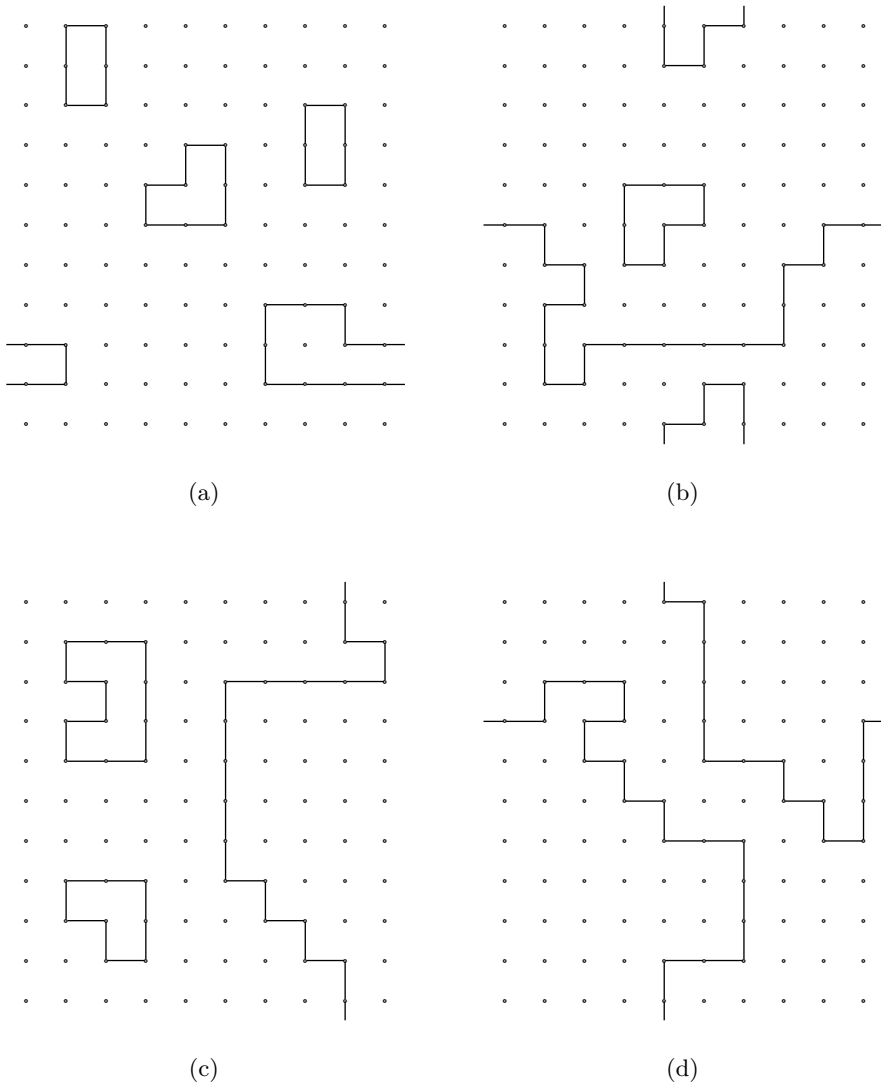
Figure 6.5: Graphical representation of possible fermionic configurations in the topological classes $\mathcal{L}_{00}$ (a), $\mathcal{L}_{10}$ (b), $\mathcal{L}_{01}$ (c), and $\mathcal{L}_{11}$ (d) on a 10×10 lattice.

up the factor $(-1)^{\varepsilon_0}$ and $(-1)^{\varepsilon_1}$, respectively. Therefore, the overall sign is determined to be $(-1)^{\varepsilon_0+1}$ and $(-1)^{\varepsilon_1+1}$ for configurations in the classes $\mathcal{L}_{10}$ and $\mathcal{L}_{01}$. Finally, configurations in the class $\mathcal{L}_{11}$ contain an odd number of fermionic loops winding around the lattice in both directions $\mu = 0, 1$. For these loops $\nu = 0$ as well, yielding one factor of (-1) for a closed fermionic loop. Using similar arguments as above, it is now easy to see that the overall sign for the bond configurations in this topological class is given by $(-1)^{\varepsilon_0+\varepsilon_1+1}$.

6.5.2 The Partition Function

Having determined the overall sign of each configuration, we are now able to incorporate the signs into the partition functions accordingly. For this purpose, we define the *positive* partition functions $Z_{\mathcal{L}_{ij}}$ for each topological sector $\mathcal{L}_{ij}$. The positive partition function Z is given by

$$Z = Z_{\mathcal{L}_{00}} + Z_{\mathcal{L}_{10}} + Z_{\mathcal{L}_{01}} + Z_{\mathcal{L}_{11}}. \tag{6.74}$$

With the above definition, we are then able to compose the partition function Z_ε for specific boundary conditions ε as

$$Z_\varepsilon = Z_{\mathcal{L}_{00}} + (-1)^{\varepsilon_0+1} Z_{\mathcal{L}_{10}} + (-1)^{\varepsilon_1+1} Z_{\mathcal{L}_{01}} + (-1)^{\varepsilon_0+\varepsilon_1+1} Z_{\mathcal{L}_{11}}. \tag{6.75}$$

The boundary conditions of interest are the thermal boundary conditions $\varepsilon = (1,0)$ with $aPBC$ in time direction and with PBC in the spatial direction and the boundary conditions $\varepsilon = (0,0)$ which are periodic in both the time and the spatial direction PBC, PBC. The partition function is explicitly given by

$$Z_{aPBC,PBC} = Z_{(1,0)} = Z_{\mathcal{L}_{00}} + Z_{\mathcal{L}_{10}} - Z_{\mathcal{L}_{01}} + Z_{\mathcal{L}_{11}} \tag{6.76}$$

for thermal boundary conditions and by

$$Z_{PBC,PBC} = Z_{(0,0)} = Z_{\mathcal{L}_{00}} - Z_{\mathcal{L}_{10}} - Z_{\mathcal{L}_{01}} - Z_{\mathcal{L}_{11}} \tag{6.77}$$

for PBC in both directions. Similarly to the one-dimensional case, we now see how the bosonic and the fermionic sector are composed. In two dimensions, the bosonic sector $F = 0$ corresponds to the topological class $\mathcal{L}_{00}$, such that $Z_{F=0} = Z_{\mathcal{L}_{00}}$. The fermionic sector $F = 1$ consists of the combination of the other topological sectors, such that $Z_{F=1} = Z_{\mathcal{L}_{01}} + Z_{\mathcal{L}_{10}} + Z_{\mathcal{L}_{11}}$.

6.5.3 Observables

We need to find the explicit expressions for the expectation values of observables for any choice of boundary conditions as well. Recall the definition of the expectation value of any observable $\mathcal{O}$,

$$\langle \mathcal{O} \rangle = \frac{1}{Z} \int \mathcal{D}\phi \mathcal{D}\psi \ \mathcal{O} \ \mathrm{e}^{-S}. \tag{6.78}$$

Labelling the expectation value of the observable $\mathcal{O}$ for the boundary conditions ε with $\langle \mathcal{O} \rangle_\varepsilon$, we derive analogously to the construction of the partition functions that

$$\langle \mathcal{O} \rangle_\varepsilon = \frac{\langle\!\langle \mathcal{O} \rangle\!\rangle_{\mathcal{L}_{00}} + (-1)^{\varepsilon_0+1}\langle\!\langle \mathcal{O} \rangle\!\rangle_{\mathcal{L}_{10}} + (-1)^{\varepsilon_1+1}\langle\!\langle \mathcal{O} \rangle\!\rangle_{\mathcal{L}_{01}} + (-1)^{\varepsilon_0+\varepsilon_1+1}\langle\!\langle \mathcal{O} \rangle\!\rangle_{\mathcal{L}_{11}}}{Z_{\mathcal{L}_{00}} + (-1)^{\varepsilon_0+1}Z_{\mathcal{L}_{10}} + (-1)^{\varepsilon_1+1}Z_{\mathcal{L}_{01}} + (-1)^{\varepsilon_0+\varepsilon_1+1}Z_{\mathcal{L}_{11}}}, \tag{6.79}$$

where we denote the *positive*, non-normalised expectation value of the observable in the topological class $\mathcal{L}_{ij}$ with

$$\langle\!\langle \mathcal{O} \rangle\!\rangle_{\mathcal{L}_{ij}} = \sum_{\ell \in \mathcal{L}_{ij}} \int \mathcal{D}\phi \ \mathcal{O} \ W_\ell(\phi) \ \mathrm{e}^{-S^B(\phi)}, \tag{6.80}$$

where $W_\ell(\phi)$ is the weight of a fermionic loop configuration ℓ. The expressions for the boundary conditions of interest are explicitly given by

$$\langle \mathcal{O} \rangle_{aPBC,PBC} = \frac{\langle\!\langle \mathcal{O} \rangle\!\rangle_{\mathcal{L}_{00}} + \langle\!\langle \mathcal{O} \rangle\!\rangle_{\mathcal{L}_{10}} - \langle\!\langle \mathcal{O} \rangle\!\rangle_{\mathcal{L}_{01}} + \langle\!\langle \mathcal{O} \rangle\!\rangle_{\mathcal{L}_{11}}}{Z_{\mathcal{L}_{00}} + Z_{\mathcal{L}_{10}} - Z_{\mathcal{L}_{01}} + Z_{\mathcal{L}_{11}}}. \tag{6.81}$$

for thermal boundary conditions and by

$$\langle \mathcal{O} \rangle_{PBC,PBC} = \frac{\langle\!\langle \mathcal{O} \rangle\!\rangle_{\mathcal{L}_{00}} - \langle\!\langle \mathcal{O} \rangle\!\rangle_{\mathcal{L}_{10}} - \langle\!\langle \mathcal{O} \rangle\!\rangle_{\mathcal{L}_{01}} - \langle\!\langle \mathcal{O} \rangle\!\rangle_{\mathcal{L}_{11}}}{Z_{\mathcal{L}_{00}} - Z_{\mathcal{L}_{10}} - Z_{\mathcal{L}_{01}} - Z_{\mathcal{L}_{11}}}, \tag{6.82}$$

for PBC in both directions.

Here, we conclude our technical considerations for the two-dimensional $\mathcal{N} = 1$ Wess-Zumino model and terminate this chapter by presenting first simulation results.

6.6 Simulation Results

The following numerical results have been developed in collaboration with K. Steinhauer and U. Wenger.

The physics of the $\mathcal{N} = 1$ Wess-Zumino model is governed by the dimensionless coupling parameter $f = \lambda/\mu$. As the parameter λ is not renormalised, we will express all quantities in units of λ.

6.6.1 Theoretical Background

Before we present the simulation results, we need to establish some physical background.

The model has a Witten index which is zero, $\Delta = 0$ [70]. For the superpotential eq.(6.8), this is due to two zero-energy states in perturbation theory, the one of these vacua being bosonic and the other being fermionic. In infinite volume, supersymmetry is unbroken as there is no tunnelling possible between these two states. In finite volume, however, supersymmetry is spontaneously broken. For the superpotential eq.(6.8), the two vacuum states are located at $\phi = \pm\frac{\mu}{2\lambda}$. Now, in a finite volume, tunnelling between these two vacua is always possible, triggering spontaneous supersymmetry breaking.

Recall that for our choice of the superpotential, the bosonic action eq.(6.14) represents a ϕ^4-theory. It is well known that the ϕ^4-theory has a phase where the $\mathbb{Z}_2$-symmetry is unbroken and a phase where the $\mathbb{Z}_2$-symmetry is broken [86], depending on the bare parameters μ and λ. The $\mathcal{N} = 1$ Wess-Zumino model inherits this feature of the spontaneous breaking of the $\mathbb{Z}_2$-symmetry. A broken $\mathbb{Z}_2$-symmetry implies that either one of the bosonic or fermionic ground states is selected, which will be the physical one in infinite volume and supersymmetry is thus unbroken. It has been argued further that the phases of the $\mathbb{Z}_2$-symmetry and the supersymmetry are in fact opposite such that the breaking of the $\mathbb{Z}_2$-symmetry coincides with the restoration of supersymmetry and vice versa [37, 56]. However, numerical results indicate that this claim seems to bear some ambiguity [37].

Because the question of if and how the phases of the $\mathbb{Z}_2$-symmetry and the supersymmetry are related has not yet been cleared conclusively, the investigation of this feature is one of the goals for future analysis. In the following, we present first results of an analysis of the $\mathbb{Z}_2$-symmetry phases for the $\mathcal{N} = 1$ Wess-Zumino model. These results do not only confirm that the hybrid algorithm we propose works for the problem at hand, but they also clear the way for a thorough analysis for the above posed question.

6.6.2 The Phases of the $\mathbb{Z}_2$-Symmetry

As a starting point, we aim at a confirmation of the two distinct $\mathbb{Z}_2$-symmetry phases for this model. To do so, we choose two different settings, once adjusting the coupling f and the lattice spacing $a\lambda$, such that the system is in the phase where the $\mathbb{Z}_2$-symmetry is broken, and once forcing the system to be in the phase where the $\mathbb{Z}_2$-symmetry is unbroken through the choice of these parameters. We find it convenient to define the volume averaged value for the bosonic field,

$$\overline{\phi} = \frac{1}{V} \sum_x \phi_x, \tag{6.83}$$

even though this is not a true order parameter of the $\mathbb{Z}_2$-symmetry due to the explicit breaking of the symmetry by the Wilson term in the discretisation.

The Monte Carlo Histories of $\overline{\phi}$

First, we outline the Monte Carlo histories for $\overline{\phi}$ for two different physical situations. In figure 6.6, the histories are plotted for a coupling $f = 0.16$ at a lattice spacing $a\lambda = 0.03125$ and for a coupling $f = 4$ at a lattice spacing $a\lambda = 0.125$, simulated on a $L^2 = 8^2$ square lattice each.

In figure (a) for a weak coupling $f = 0.16$ and at a lattice spacing $a\lambda = 0.03125$, the volume averaged value for the bosonic field $\overline{\phi}$ fluctuates around zero, $\overline{\phi} \simeq 0$. Hence, the $\mathbb{Z}_2$-symmetry is unbroken for this physical situation. In figure (b) at a strong coupling $f = 4$ and at a lattice spacing $a\lambda = 0.125$, the value of $\overline{\phi}$ fluctuates around two different values, $\overline{\phi} \simeq \pm\frac{\mu}{2\lambda}$. In this physical situation, the $\mathbb{Z}_2$-symmetry is broken. Note that the tunnelling between the vacua is still possible due to the finite size of the lattice.

For the set-ups of choice, the Monte Carlo history for $\overline{\phi}$ hence reveals the expected characteristics for two distinguishable phases of the $\mathbb{Z}_2$-symmetry.

The Probability Distributions for the Partition Functions $Z_{\mathcal{L}_{ij}}$

It is interesting to observe how the partition functions for the various topological classes are affected by the fact that there are the two different phases of the $\mathbb{Z}_2$-symmetry. In figure 6.7, the histograms of the probability distributions of the partition functions $Z_{\mathcal{L}_{ij}}$ and Z versus the volume averaged value of the bosonic field $\overline{\phi}$ are plotted. The simulations are again run on a $L^2 = 8^2$ lattice
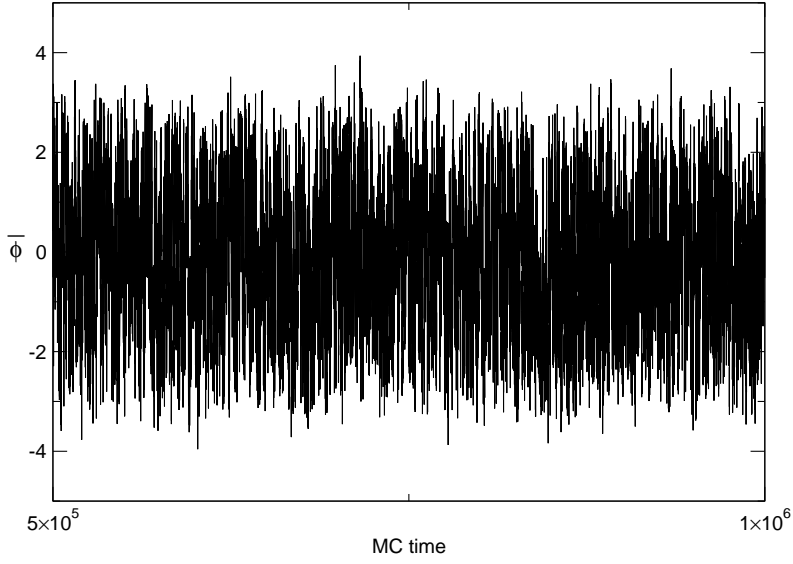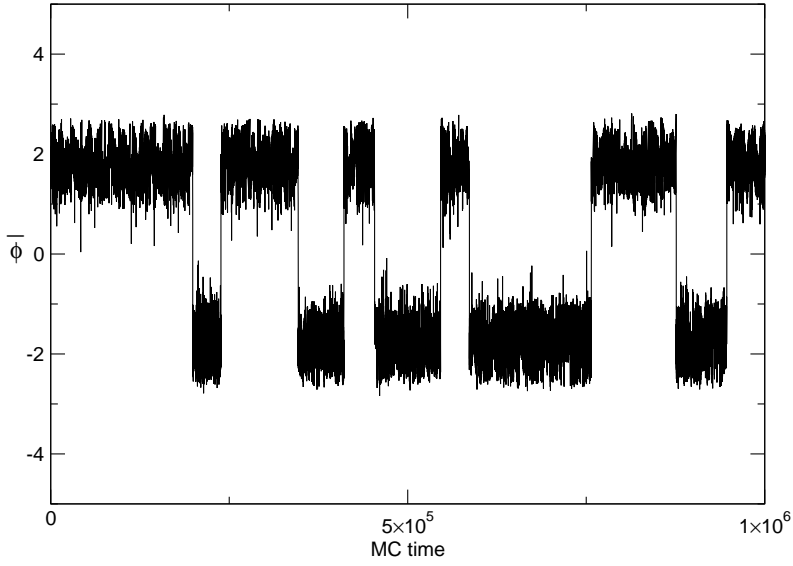
(a) $f = 0.16$, $a\lambda = 0.03125$

(b) $f = 4$, $a\lambda = 0.125$

Figure 6.6: The volume averaged bosonic field $\overline{\phi}$ versus the Monte Carlo time of the bosonic field for the parameters $f = 0.16$ and $a\lambda = 0.03125$ in figure (a) and for the parameters $f = 4$, $a\lambda = 0.125$ in figure (b) on a $L^2 = 8^2$ lattice.

for a coupling $f = 0.16$ at a lattice spacing of $a\lambda = 0.03125$ with a statistics of $Z = 10^5$ and for a coupling $f = 4$ at a lattice spacing $a\lambda = 0.125$ with a statistics of $Z = 4 \cdot 10^5$.

In figure (a), the system is again in the phase where the $\mathbb{Z}_2$-symmetry is unbroken. The expectation value of $\overline{\phi}$ fluctuates around zero, $\overline{\phi} \simeq 0$ for all partition functions $Z_{\mathcal{L}_{ij}}$. Because of lattice artefacts, the expectation value of the boson field is slightly asymmetric with respect to zero in each sector.

Figure (b) shows the probability distributions for the partition functions in the phase where the $\mathbb{Z}_2$-symmetry is broken. The expectation value for the bosonic field is located around the values $\overline{\phi} \simeq \pm 2 = \pm\frac{\mu}{2\lambda}$, which is in accordance with the Monte Carlo history plotted in figure 6.6 (b). The physical interpretation of this distribution is given as follows:

- If $\langle\overline{\phi}\rangle \simeq 2$, the system resides almost exclusively in the topological sector $\mathcal{L}_{00}$ such that the partition functions are $Z_{\mathcal{L}_{00}} \simeq Z$ and $Z_{\mathcal{L}_{01}} \simeq Z_{\mathcal{L}_{10}} \simeq Z_{\mathcal{L}_{11}} \simeq 0$. This corresponds to the bosonic ground state.

- If $\langle\overline{\phi}\rangle \simeq -2$, all topological sectors are equally favourable and the partition functions are equal $Z_{\mathcal{L}_{00}} \simeq Z_{\mathcal{L}_{01}} \simeq Z_{\mathcal{L}_{10}} \simeq Z_{\mathcal{L}_{11}} \simeq Z/4$. In contrast to the above case, this combination represents the fermionic ground state.

Therefore we have a consistent picture of the broken and unbroken phase for the $\mathbb{Z}_2$-symmetry and we are able to confirm the existence of either a fermionic or a bosonic ground state in the phase where this symmetry is broken. As a next step, we will elaborate on the phase transition of the $\mathbb{Z}_2$-symmetry for fixed lattice spacing.

The $\mathbb{Z}_2$-Symmetry Phase Transition

Yet another way to observe the breaking of the $\mathbb{Z}_2$-symmetry is given via the measurement of the quantity s_ϕ, which we define as

$$s_\phi = \left| \frac{1}{V} \sum_x \mathrm{sgn}(\phi_x) \right|. \tag{6.84}$$

This quantity projects out the sign of the bosonic field values at each site, such that it actually corresponds to the measurement of the magnetisation in the Ising model. In the phase where the $\mathbb{Z}_2$-symmetry is broken, the fields ϕ fluctuate around either of the values $\overline{\phi} \simeq \pm 2$ and projecting out the sign
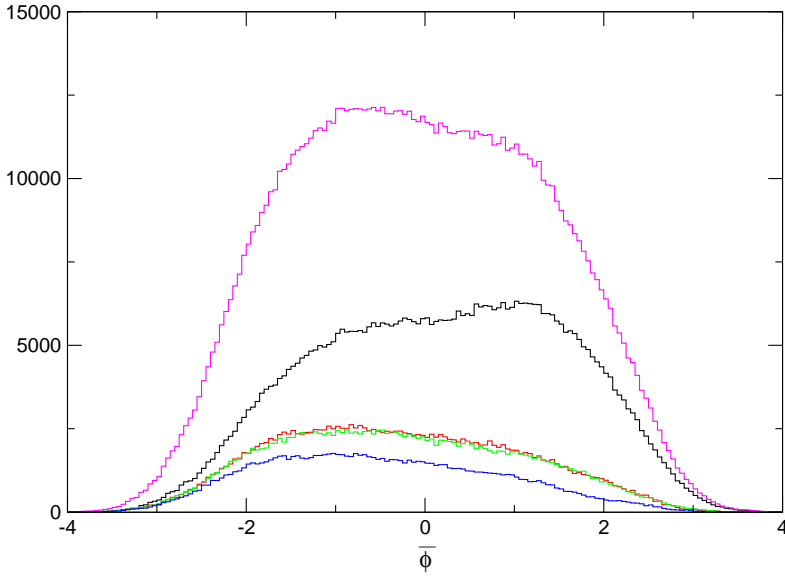
(a) $f = 0.16$, $a\lambda = 0.03125$
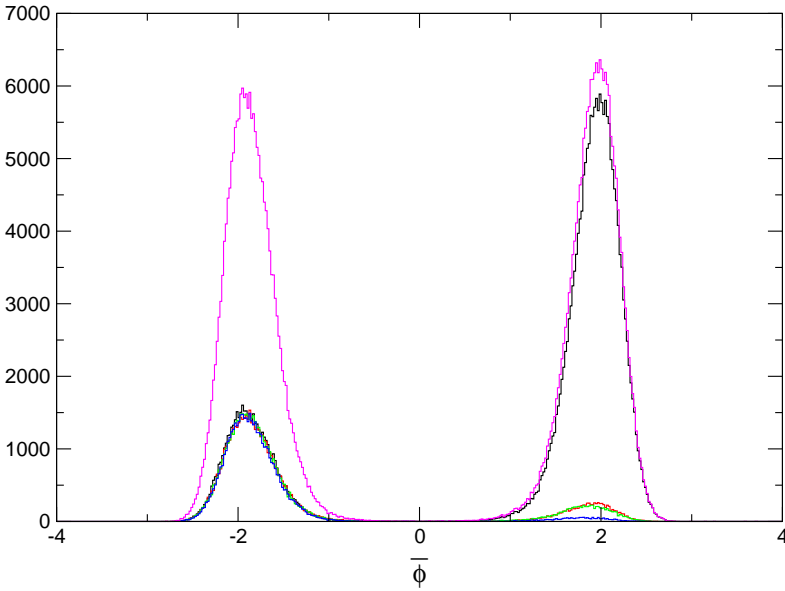
(b) $f = 4$, $a\lambda = 0.125$

Figure 6.7: The probability distributions of the partition functions $Z_{\mathcal{L}_{00}}$ (black), $Z_{\mathcal{L}_{01}}$ (green), $Z_{\mathcal{L}_{10}}$ (red), $Z_{\mathcal{L}_{11}}$ (blue), and of the total partition function Z (purple) in the phase where the $\mathbb{Z}_2$-symmetry is unbroken (figure (a)) and in the phase where the $\mathbb{Z}_2$-symmetry is broken (figure (b)) as a function of $\overline{\phi}$.

183
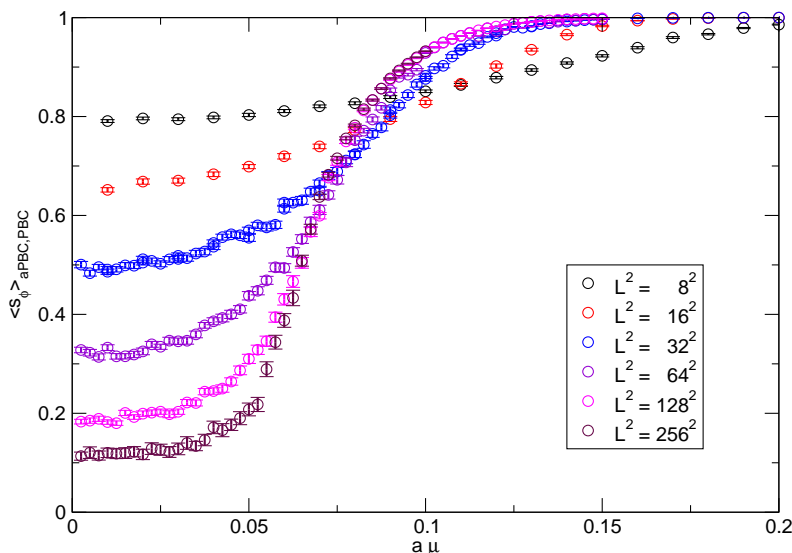
Figure 6.8: The expectation value $\langle s_\phi \rangle_{aPBC,PBC}$ as a function of $a\mu$ at fixed lattice spacing of $a\lambda = 0.03125$ for square lattices of different extents.

of the field values yields the same sign for most of the sites, hence $s_\phi \simeq 1$. This corresponds to the magnetised phase in the Ising model. In contrast, in the phase where the $\mathbb{Z}_2$-symmetry is unbroken, the values of the fields ϕ fluctuate around zero, $\overline{\phi} \simeq 0$, and there is no preferred sign for the bosonic fields, yielding $s_\phi \simeq 0$. This corresponds to the unmagnetised phase in the Ising model. The transition from the unordered phase to the ordered phase of the expectation value s_ϕ therefore indicates the breaking of the $\mathbb{Z}_2$-symmetry.

In figure 6.8, the expectation value $\langle s_\phi \rangle_{aPBC,PBC}$ versus the bare mass $a\mu$ at a lattice spacing $a\lambda = 0.03125$ is shown for various lattice extents. Note that the expectation value is calculated for thermal boundary conditions, such that the division by zero in the phase where the $\mathbb{Z}_2$-symmetry is unbroken can be avoided. The statistics for the simulation with $Z = 10^6$ and a total of 10^7 sweeps for the update of the bosonic field are given as above.

The plot reveals that, independently of the lattice size, the system is in the ordered phase for large $a\mu$. The phase transition, however, can only be observed on fairly large lattices. On these lattices, the choice of thermal boundary conditions rather than the choice of periodic boundary conditions in both directions,

becomes less relevant. Note that in the unordered phase for small masses on large lattices, the expectation value $\langle s_\phi \rangle$ does not go to zero exactly. This is not only because the Wilson discretisation breaks the $\mathbb{Z}_2$-symmetry explicitly, but also because of the choice of the thermal boundary conditions. Nonetheless, the plot confirms qualitatively the transition from the phase where the $\mathbb{Z}_2$-symmetry is unbroken to the phase where the symmetry is broken for a critical mass $a\mu_c \simeq 0.06$.

The presentation of this plot concludes the considerations about the two-dimensional $\mathcal{N} = 1$ Wess-Zumino model. The feasibility of the proposed hybrid algorithm has been demonstrated with these first results, and the breaking of the $\mathbb{Z}_2$-symmetry was observed. Of course, a more extensive study is needed for a quantitative determination of the critical coupling f_c for the breaking of the $\mathbb{Z}_2$-symmetry as well as for the comparison with the supersymmetry phase transition. Moreover, the entire subject of renormalisation has not been touched yet. These tasks will be left for future studies [82].

Summary and Outlook

The main part of this work is dedicated to the investigation of numerical aspects of $\mathcal{N} = 2$ supersymmetric quantum mechanics on the lattice in the non-perturbative regime. Moreover, we demonstrate the applicability of our approach to the two dimensional $\mathcal{N} = 1$ Wess-Zumino model.

We present two different approaches to solve the problem, namely the transfer matrix technique and Monte Carlo simulations with a modified Prokof'ev-Svistunov worm algorithm, both of which are based on the constrained path formulation. With these techniques we are able to study in detail how the supersymmetric spectrum is recovered in the continuum limit and how the Witten index is regularised on the lattice.

We discuss the fermion sign problem in the context of broken supersymmetry on the lattice and its close relation to the vanishing of the Witten index. We argue that in the constrained path formulation the partition function naturally separates into bosonic and fermionic contributions, which is crucial for containing this very fermion sign problem for broken supersymmetry. The transitions between the bosonic and fermionic sectors are controlled by the Goldstino mode which becomes massless in the continuum limit. Since massless fermion modes can be efficiently simulated with the fermion loop algorithm proposed in [38, 65] our approach provides a way to circumvent the sign problem.

We describe in detail the exact reformulation of the lattice path integral for the partition function in terms of fermionic and bosonic bonds for $\mathcal{N} = 2$ supersymmetric quantum mechanics. We then present results from lattice simulations as well as exact lattice results obtained via the transfer matrix technique. For the formulation on the lattice, for both the fermion field as well as for the boson field a Wilson-type discretisation is employed. For a superpotential with unbroken supersymmetry, we calculate the mass spectrum, the Witten index, and several Ward identities, using an action with a fine-tuned counterterm as well as a Q-exact action which preserves one supersymmetry

exactly on the lattice. For the Q-exact action, the bosonic and the fermionic spectrum are degenerate even for finite lattice spacing, whereas for the action with counterterm they become only degenerate in the continuum. We then present results for broken supersymmetry using the action with the counterterm for which we reproduce the degenerate mass spectrum in the continuum. In this spectrum, the massless Goldstino emerges. We also calculate the Witten index, which for broken supersymmetry approaches the continuum limit exponentially slowly in the lattice spacing. In practice, due to the efficiency of our tools, this is not a problem.

For all calculations, the exact results via the transfer matrix approach and the Monte Carlo simulations agree within statistical errors. Furthermore, we confirm all continuum results for the mass spectrum by comparing them with results obtained by solving the Schroedinger equation numerically.

It is also interesting to apply our approach to higher dimensions where it allows to investigate the spontaneous breaking of supersymmetry non-perturbatively and from first principles [87]. In particular, we demonstrate the reformulation of the two-dimensional $\mathcal{N} = 1$ Wess-Zumino model - a model including one Majorana fermion and one scalar field - in terms of fermionic and bosonic bonds. Yet, the hopping expansion for both the fermion and boson field induces a severe bosonic sign problem due to a negative bosonic bond weight. To cure this problem, we suggest a hybrid algorithm combining the worm algorithm for the update of the fermionic degrees of freedom and the standard Metropolis update for the bosonic degrees of freedom. We are able to confirm qualitatively the phase transition of the model by using this algorithm [88].

A thorough analysis of the two-dimensional $\mathcal{N} = 1$ Wess-Zumino model including a qualitative determination of the renormalised critical coupling leading to a complete phase diagram for the supersymmetric phase transition as well as the measurement of the mass spectrum is still left open. In addition, the issue of the connection between the phases of the $\mathbb{Z}_2$-symmetry and the supersymmetry has not yet been settled satisfactorily. Work in this direction is in progress [82].

Furthermore, the constrained path formulation has a wide range of other applications, such as supersymmetric matrix models, higher dimensional theories, gauge theories, staggered fermions, or multi-fermion models [89], some of which have a sign problem.

Acknowledgements

First and foremost, my thanks go to Urs Wenger for offering me the opportunity to work on this very interesting subject, for his support, and for his ability to arouse scientific curiosity in others. Secondly, I would like to thank Jacek Wosiek for accepting the responsibility of being the co-referee for this thesis.

I benefited a great deal from our regular lattice discussion group and I would like to express my gratefulness to Uwe-Jens Wiese, Matthias Nyfeler, and Urs Gerber for these interesting sessions. Many thanks go to the other members of our research group, especially Vidushi Maillart and Kyle Steinhauer, for countless and invaluable discussions about lattice physics. Furthermore, I would like to thank my office mates Michael Bögli and Vidushi Maillart for many on and off topic debates. Special thanks go to Stefan Lanz and Lorenzo Mercolli for their friendship and for their essential help with all the thinkable and unthinkable problems one encounters on a journey of writing a PhD thesis. Concerning the concept of supersymmetry, I am obliged to Daniel Arnold for giving me enlightening insights in the course of numerous discussions.

I would also like to express my gratitude to the secretaries of our institute, Ruth Bestgen, Esther Fiechter, and Ottilia Hänni, for without their help with administrative issues a successful graduation would have been an impossible task. Regarding the support of our computing equipment, I would like to thank Markus Moser for taking care of the computer system, as well as Kyle Steinhauer and Peter Stoffer for their efforts in maintaining the institute's cluster Neumann.

Many thanks go to Barbara Bürki for dedicating an immense amount of work to the linguistic enhancement of this thesis.

Last but not least, I am deeply indebted to my friends and my family, especially to my mother and brother, for their endless support and encouragement during the past years.

Appendix A

Statistics and Monte Carlo

In this appendix, we will follow [90] and review briefly some of the statistical concepts used in this work. As an example, we will use a thermal system where the states occur according to their Boltzmann weight. Only in the last section, we will give the acceptance probabilities for an arbitrary probability distribution of the states.

A.1 The Estimator

Performing Monte Carlo simulations, one is usually interested in calculating the expectation value $\langle A \rangle$ of a quantity A in a thermal system. This is done by measuring A when the system is found in a the state φ, taking the value A_φ,

$$\langle A \rangle = \sum_\varphi A_\varphi p_\varphi. \tag{A.1}$$

Gibbs (1902) [91] showed that the probability p_φ with which a state φ of the system in thermal equilibrium at temperature T is occupied is given by

$$p_\varphi = \frac{1}{Z} e^{-E_\varphi/kT}, \tag{A.2}$$

where E_φ is the energy of the state and k is the Boltzmann constant. It is conventional to introduce the symbol β to replace the combination $1/kT$ as $\beta = 1/kT$. The normalisation factor Z is called the *partition function* and it is calculated as

$$Z = \sum_\varphi W(\varphi) = \sum_\varphi e^{-\beta E_\varphi}, \tag{A.3}$$

where $W(\varphi) = e^{-\beta E_\varphi}$ is the *weight* of the state φ. Besides being the normalisation factor, the partition function can also be used for the calculation of

expectation values. (See for example section 1.5 and the calculation of $\langle E \rangle$ and C.)

The explicit evaluation of eq.(A.1) turns out to be impossible in almost all cases. Even for reasonably large systems, there are simply too many states φ to sum over. Therefore, one picks a subset $\mathcal{N} = \{\varphi_1, \varphi_2, \ldots, \varphi_n\}$ of all states, where the states are distributed with some probability $\tilde{p}_{\varphi_i}$. For this subset $\mathcal{N}$, the quantity A is estimated via the *estimator* $A_{\mathcal{N}}$,

$$A_{\mathcal{N}} = \frac{\sum_{i=1}^{n} A_{\varphi_i} (\tilde{p}_{\varphi_i})^{-1} \mathrm{e}^{-\beta E_{\varphi_i}}}{\sum_{i=1}^{n} (\tilde{p}_{\varphi_i})^{-1} \mathrm{e}^{-\beta E_{\varphi_i}}}, \tag{A.4}$$

where the probability distribution $\tilde{p}_{\varphi_i}$ has to be specified yet. Since we calculate the estimator via the states in the subset $\mathcal{N}$ and all other states are ignored, the probability distribution of $\tilde{p}_{\varphi_i}$ should ensure that the sample $\mathcal{N}$ consists of states which contribute significantly to the expectation value. This technique of picking only the the important states from a very large ensemble is called *importance sampling*.

A.2 Importance Sampling

A.2.1 Markov Processes

We now need to find a suitable probability distribution $\tilde{p}_{\varphi}$ for the sampling of the states. In analogy to nature where the states are distributed according to their energy via the Boltzmann weight given in eq.(A.2), it is common to most importance sampling algorithms to choose a particular state φ with the probability $\tilde{p}_{\varphi} = 1/Z \; \mathrm{e}^{-\beta E_{\varphi}}$. With this probability distribution, the Boltzmann factors cancel out in eq.(A.4) and the estimator simplifies to the *mean value*,

$$A_{\mathcal{N}} \equiv \frac{1}{n} \sum_{i=1}^{n} A_{\varphi_i} = \overline{A}. \tag{A.5}$$

To generate new states in the sample, almost all Monte Carlo schemes use the concept of *Markov processes*. Given a state φ, the Markov mechanism generates randomly a new state φ'. The probability with which the system accepts the transition from state φ to state φ' is called the *transition probability* $P(\varphi \to \varphi')$. The transition probabilities should neither vary over time nor

depend on any other state than the initial state φ and the final state φ'. Furthermore, the transition probabilities are normalised,

$$\sum_{\varphi'} P(\varphi \to \varphi') = 1. \tag{A.6}$$

Note, that the probability for the system to remain in the same state need not be zero, $P(\varphi \to \varphi') \neq 0$. In a Monte Carlo simulation, the system repeatedly undergoes Markov steps, forming a *Markov chain*. When the states thus generated are Boltzmann distributed, the system is said to be in equilibrium. Yet, to reach the equilibrium, there are further constraints on the Markov process, *ergodicity* and *detailed balance*.

A.2.2 Ergodicity and Detailed Balance

According to the Boltzmann distribution, each state appears with a non-zero probability. Now, ergodicity is the requirement that starting from a given state φ, it must be possible to reach *any* other state φ' with a non-zero probability via a Markov chain. This guarantees that the algorithm is able to sample the entire space of states.

To ensure that it is indeed the Boltzmann probability distribution which is generated in the equilibrium, the other additional constraint required is the one of detailed balance. The defining condition is that the transition rate into and out of a state φ must be the same,

$$\sum_{\varphi'} p_\varphi P(\varphi \to \varphi') = \sum_{\varphi'} p_{\varphi'} P(\varphi' \to \varphi). \tag{A.7}$$

With the normalisation condition eq.(A.6) this equation simplifies to

$$p_\varphi = \sum_{\varphi'} p_{\varphi'} P(\varphi' \to \varphi). \tag{A.8}$$

If the transition probabilities are chosen according to this equation, the probability distribution p_φ will be an equilibrium of the dynamics. However, this condition is not rigorous enough since it is possible that the probability distribution does not converge but rather rotates around a number of values. This is called a limit cycle. We therefore have to put yet another constraint upon the probability distribution, which is the *detailed balance* condition

$$p_\varphi P(\varphi \to \varphi') = p_{\varphi'} P(\varphi' \to \varphi). \tag{A.9}$$

Detailed balance is a sufficient but not necessary condition providing a means which ensures that the system changes from the state φ to the state φ' as many times as it changes from the state φ' to the state φ and thus eliminates cycle limits. Since we still want to have a probability distribution according to the Boltzmann weights, the transition probabilities must satisfy

$$\frac{P(\varphi \to \varphi')}{P(\varphi' \to \varphi)} = \frac{p_{\varphi'}}{p_\varphi} = \mathrm{e}^{-\beta(E_{\varphi'} - E_\varphi)} \tag{A.10}$$

To be able to design a specific algorithm, it is useful to factorise the transition probability as

$$P(\varphi \to \varphi') = P_C(\varphi \to \varphi') P_A(\varphi \to \varphi'). \tag{A.11}$$

$P_C(\varphi \to \varphi')$ is called the *selection probability*, the probability with which the algorithm, given an initial state φ, proposes to generate a new state φ'. $P_A(\varphi \to \varphi')$ is called the *acceptance probability*, the probability with which the algorithm accepts the proposed state φ'. The selection probability may be chosen freely, since eq.(A.10) only fixes the ratio

$$\frac{P(\varphi \to \varphi')}{P(\varphi' \to \varphi)} = \frac{P_C(\varphi \to \varphi') P_A(\varphi \to \varphi')}{P_C(\varphi' \to \varphi) P_A(\varphi' \to \varphi)}. \tag{A.12}$$

Thus, if an algorithm proposes transitions from states φ to states φ' with probability $P_C(\varphi \to \varphi')$, the new states need to be accepted with the acceptance probabilities $P_A(\varphi \to \varphi')$. For an algorithm designed such, the generated states in the equilibrium will indeed appear according to the Boltzmann weight.

A.3 The Metropolis Algorithm

To generate as many different states as possible, it is desirable that the transition probability is close to 1. Otherwise, most of the proposed state transitions will be rejected, causing the system to remain in the same configuration most of the time. To avoid this problem, Nicolas Metropolis and collaborators (1953) [92] introduced an algorithm which is used in most Monte Carlo simulations. The key idea is to design the acceptance step such, that the proposed change of state is always accepted if the weight of the new state $W(\varphi')$ is higher than the weight of the present state $W(\varphi)$. Note that the states here need not be distributed necessarily according to the Boltzmann distribution.

Balancing this condition correctly and including the selection probabilities, the acceptance probability is given by

$$P_A(\varphi \to \varphi') = \min\left\{1, \frac{P_C(\varphi \to \varphi')W(\varphi')}{P_C(\varphi' \to \varphi)W(\varphi)}\right\}. \tag{A.13}$$

This is the formula for the acceptance probability we will be referring to for all our algorithms.

Appendix B

Error Calculation

If in an experiment expectation values of certain quantities are measured, it is also important to know how accurate they are. Therefore, one needs to calculate the errors of the measured quantities as well. As Monte Carlo simulations are in many ways similar to laboratory experiments, we analyse the results in the same way we would do for the latter case. The sources of the experimental errors can be divided into two different classes. On the one hand, there are systematic errors. These are errors which originate from the procedure chosen to do the measurements. In a Monte Carlo simulation for example, the error due to the finite amount of time we allow the system to thermalise falls into this class. Ideally, we would have to wait for an infinite amount of time for the system to equilibrate. On the other hand, there are the statistical errors. They arise for example from thermal fluctuations around the equilibrium state in a thermodynamic system. These errors can be reduced by increasing the statistics.

In the following, we discuss some tools with which we are able to calculate a reliable error estimate for measured quantities of Monte Carlo simulations.

In a run with n measurements taken, our best estimation for the expectation value $\langle A \rangle$ of a quantity A is the mean value $\overline{A}$ of all measurements, eq.(A.5),

$$\overline{A} = \frac{1}{n} \sum_{i=1}^{n} A_i. \tag{B.1}$$

Our best estimation for the standard deviation of the mean is given by

$$\sigma_A^2 = \frac{1}{n-1} \left(\overline{A^2} - \overline{A}^2 \right). \tag{B.2}$$

This expression holds only if all samples A_i are statistically independent. In a Monte Carlo experiment, however, the generated configurations are correlated

and so are the data points A_i. In general, for a run of the length $t_{\max}$, the number of independent measurements n is of the order

$$n = \frac{t_{\max}}{2\tau}, \tag{B.3}$$

where τ is the correlation time. It can be shown that the correlation of the data can be accounted for by modifying eq.(B.2) as

$$\sigma_A^2 = \frac{2\tau}{t_{\max}} \left(\overline{A^2} - \overline{A}^2 \right). \tag{B.4}$$

Unfortunately, for results that are derived in a more complex way than by just averaging measurement data, it is not possible to estimate the error in a straightforward way using this method.

A simple way to estimate the error is the blocking method, where one blocks the data repeatedly and calculates the error for each blocking step with eq.(B.2) until the error stabilises. We will make use of more sophisticated methods, the *bootstrap method* and the *jackknife method*, which we explain below.

B.1 The Bootstrap Method

The bootstrap method is a resampling method, proposed by Bradley Efron (1979). Consider a sample Z with n data points, $Z = (Z_1, \ldots, Z_n)$, with an unknown distribution P. The variables Z can be real-valued, where they are usually denoted by $Z_i = X_i$, or vector-valued, such that for example $Z_i = (X_i, Y_i)$. These measurements should be independent from each other. However, it turns out that it is sufficient if the measurements are independent in a sense that they are taken at least two correlation times apart. Now define the estimator of a statistical procedure by

$$\hat{A}_n = \varphi(Z_1, \ldots, Z_n), \tag{B.5}$$

where φ is a known function of the data points $Z_1, \ldots, Z_n$. Because we do not know the true distribution P of the data points Z, we use the empirical distribution $\hat{P}$ which provides each Z_i with probability $1/n$. We then draw randomly n of the data points $Z_1, \ldots, Z_n$ to form a bootstrap sample $Z^* = (Z_1^*, \ldots, Z_n^*)$. As we explicitly allow ourselves to pick the same data point Z_i of the original data set Z several times, the bootstrap sample may contain more

than one duplicate of a data point Z_i. We then calculate the bootstrapped estimator

$$\hat{A}_n^* = \varphi(Z_1^*, \ldots, Z_n^*). \tag{B.6}$$

By repeating this procedure N times, we form a set of bootstrapped estimators $\hat{A}_n^{*1}, \ldots, \hat{A}_n^{*N}$. These estimators can be used as approximations for the bootstrapped estimate $\tilde{A}_n$ and the bootstrap variance $\sigma_{\tilde{A}_n}^2$ as

$$\tilde{A}_n = \frac{1}{N} \sum_{i=1}^N \hat{A}_n^{*i}, \tag{B.7}$$

$$\sigma_{\tilde{A}_n}^2 = \frac{1}{N-1} \sum_{i=1}^N (\hat{A}_n^{*i} - \tilde{A}_n)^2. \tag{B.8}$$

B.2 The Jackknife Method

The jackknife method works similar to the bootstrap method. Again, consider a sample Z with n data points, $Z = (Z_1, \ldots, Z_n)$, with an unknown distribution P. Define the estimator of a statistical procedure as

$$\hat{A} = \varphi(Z_1, \ldots, Z_n), \tag{B.9}$$

where φ is a known function of the data points $Z_1, \ldots, Z_n$. However, this time, we form n jackknife samples $Z^{*i} = (Z_1, \ldots, Z_{i-1}, Z_{i+1}, \ldots, Z_n)$ by removing exactly one data point in all possible ways each time. The j-th partial estimate is then calculated as

$$\hat{A}^{*j} = \varphi(Z_1, \ldots, Z_{j-1}, Z_{j+1}, \ldots, Z_n). \tag{B.10}$$

These estimators can be used as approximations for the jackknife estimate $\tilde{A}$ and the jackknife variance $\sigma_{\tilde{A}}^2$ as

$$\tilde{A} = \frac{1}{n} \sum_{i=1}^n \hat{A}^{*i}, \tag{B.11}$$

$$\sigma_{\tilde{A}}^2 = \frac{n-1}{n} \sum_{i=1}^n (\hat{A}^{*i} - \tilde{A})^2. \tag{B.12}$$

Both, the bootstrap method as well as the jackknife method give good estimates of errors for large data sets. The question of which one to use depends

on how much work is involved in applying them. For the bootstrap procedure, one usually needs to take about $N = 100$ or more resampled data sets. The jackknife, however, requires that we calculate the desired quantity exactly as many times as we have data points. So, if our data exceeds $n = 100$, the bootstrap is usually more efficient.

Appendix C

The Grassmann Algebra

For the path integral formulation of fermion fields *Grassmann numbers* are introduced. Each fermionic state requires one pair (η^*, η) of Grassmann variables. The Grassmann variables are totally anticommuting, such that they fulfil the relations

$$\{\eta_i^*, \eta_j\} = \{\eta_i, \eta_j\} = \{\eta_i^*, \eta_j^*\} = 0. \tag{C.1}$$

The definition eq.(C.1) implies that the square of every Grassmann variable is zero. Thus, functions of these variables are finite polynomials and in the case of a single Grassmann pair (η^*, η), the most general function is

$$F(\eta^*, \eta) = F^{(0,0)} + F^{(0,1)}\eta + F^{(1,0)}\eta^* + F^{(1,1)}\eta^*\eta, \tag{C.2}$$

where $F^{(\alpha,\beta)} \in \mathbb{C}$. Requiring linearity and invariance under a shift, the integral over the function $F(\eta^*, \eta)$ is defined as

$$\int d\eta d\eta^* \ F(\eta^*, \eta) = -\int d\eta^* d\eta \ F(\eta^*, \eta) = F^{(1,1)}. \tag{C.3}$$

Note that the integration measure inherits the anticommutativity. The derivatives with respect to Grassmann variables are defined as

$$\frac{\partial}{\partial \eta^*}F(\eta^*, \eta) = F^{(1,0)} + F^{(1,1)}\eta, \qquad \frac{\partial}{\partial \eta}F(\eta^*, \eta) = F^{(0,1)} - F^{(1,1)}\eta^*, \quad \text{(C.4)}$$

from which immediately follows that

$$\frac{\partial}{\partial \eta}\frac{\partial}{\partial \eta^*}F(\eta^*, \eta) = -\frac{\partial}{\partial \eta^*}\frac{\partial}{\partial \eta}F(\eta^*, \eta) = F^{(1,1)}. \tag{C.5}$$

Thus, the integration and the derivative of a function of Grassmann variables yields the same result. Similarly, for the most general function of N pairs of

Grassmann variables we have

$$
\begin{aligned}
F[\eta^*, \eta] \;=\;& F(\eta_1^*, \ldots, \eta_N^*, \eta_1, \ldots, \eta_N) \\
=\;& F^{(0,0)} + \sum_{i_1} F_{i_1}^{(0,1)} \eta_{i_1} + \sum_{j_1} F_{j_1}^{(1,0)} \eta_{j_1}^* + \sum_{i_1,j_1} F_{(j_1 i_1)}^{(1,1)} \eta_{j_1}^* \eta_{i_1} \\
& + \sum_{i_2 > i_1} F_{i_2, i_1}^{(0,2)} \eta_{i_2} \eta_{i_1} + \sum_{j_2 > j_1} F_{j_2, j_1}^{(2,0)} \eta_{j_2}^* \eta_{j_1}^* \\
& + \sum_{j_1} \sum_{i_2 > i_1} F_{i_2, (j_1 i_1)}^{(1,2)} \eta_{i_2} \eta_{j_1}^* \eta_{i_1} + \sum_{j_2 > j_1} \sum_{i_1} F_{j_2, (j_1 i_1)}^{(2,1)} \eta_{j_2}^* \eta_{j_1}^* \eta_{i_1} \\
& + \sum_{j_2 > j_1} \sum_{i_2 > i_1} F_{(j_2 i_2), (j_1 i_1)}^{(2,2)} \eta_{j_2}^* \eta_{i_2} \eta_{j_1}^* \eta_{i_1} + \ldots \\
& + \sum_{j_N > \cdots > j_1} \sum_{i_N > \cdots > i_1} F_{(j_N i_N), \ldots, (j_1 i_1)}^{(N,N)} \eta_{j_N}^* \eta_{i_N} \cdots \eta_{j_1}^* \eta_{i_1}. \qquad \text{(C.6)}
\end{aligned}
$$

The last sum consists of only one single combination which we abbreviate as $F_{(NN),\ldots,(11)}^{(N,N)} = F^{(N,N)}$. Using this notation, we can evaluate the integral over a function with N pairs of Grassmann variables,

$$
\int d\eta_1 d\eta_1^* \ldots d\eta_N d\eta_N^* \; F[\eta^*, \eta] = F^{(N,N)}. \qquad \text{(C.7)}
$$

It is very useful to calculate also the Gaussian integral with a complex valued matrix A,

$$
\int d\eta_1 d\eta_1^* \ldots d\eta_N d\eta_N^* \; \mathrm{e}^{-\eta_i^* A_{ij} \eta_j} = \det A, \qquad \text{(C.8)}
$$

where the sum over repeated indices is implied.

Appendix D

Lattice Fermions

For our construction of lattice field theories in one as well as two dimensions, we use a Wilson type discretisation for the fermions and the bosons. In this appendix, we discuss the reason why a naive discretisation for the fermions fails and how the fermion propagator we have used for the loop integral in the lattice perturbation theory calculation arises.

D.1 The Fermion Doubling Problem

The naive lattice formulation of fermions causes serious issues. In particular, the Nielsen-Ninomiya theorem states that a local, translational invariant, real, and chirally invariant action for free fermions necessarily has fermion doubling.

To illustrate this fact, we consider the continuum Euclidean action for a free Dirac fermion in d dimensions,

$$S = \int d^d x \, \overline{\psi}(x)(\gamma_\mu \partial_\mu + m)\psi(x). \tag{D.1}$$

For the formulation of this action on a lattice, one needs to replace the continuum fermion fields $\overline{\psi}(x)$ and $\psi(x)$ by Grassmann variables $\overline{\psi}_x$ and ψ_x on each site and the integral by a sum over all lattice sites. Furthermore, the continuum derivative ∂_μ is replaced by the finite difference operator Δ_μ^S,

$$(\Delta_\mu^S f)_x = \frac{1}{2a}(f_{x+\hat{\mu}} - f_{x-\hat{\mu}}). \tag{D.2}$$

As usual, $\hat{\mu}$ represents a lattice unit vector of length a in direction μ. The lattice version of the action eq.(D.1) then reads

$$S = a^d \sum_{x,\mu} \frac{1}{2a}(\overline{\psi}_x \gamma_\mu \psi_{x+\hat{\mu}} - \overline{\psi}_x \gamma_\mu \psi_{x-\hat{\mu}}) + a^d \sum_x m\overline{\psi}_x \psi_x. \tag{D.3}$$

This discretisation results in a lattice fermion propagator of the form

$$\tilde{\Delta}^F(k) = \frac{1}{i \sum_\mu \gamma_\mu \frac{1}{a} \sin(k_\mu a) + m}, \tag{D.4}$$

where the momenta k_μ are inside the d-dimensional Brillouin zone, $k_\mu \in [-\pi/a, \pi/a]^d$. In the limit where the lattice spacing a goes to zero, $a \to 0$, the discrete momenta go over into their continuum values, $\frac{1}{a}\sin(k_\mu a) \to k_\mu$, and one recovers the correct continuum propagator,

$$\tilde{\Delta}^F_{\text{cont}}(k) = \frac{1}{i\gamma_\mu k_\mu + m}. \tag{D.5}$$

However, besides the pole at $\vec{k} = \vec{0}$, the discretised propagator eq.(D.4) features additional poles. If at least one of the spatial momenta k_i is around the corner of the Brillouin zone, $k_i = \pi/a$, and therefore $\sin(k_i a) = 0$, the lattice dispersion relation gives rise to a fermionic state. The total number of fermionic states is then 2^d, out of which all except the one at $\vec{k} = \vec{0}$ are non-physical. These extra states are called fermion doublers and they cause severe problems in the case of any interacting theory.

One way of avoiding them is the introduction of the Wilson term, which we discuss in the following.

D.2 Wilsons Fermions

Wilson (1975) proposed to remove the doublers by breaking explicitly chiral symmetry. This is done by replacing the finite difference operator with the Wilson derivative Δ_μ^W in the discretisation process. The Wilson derivative is defined as

$$\Delta_\mu^W(r) = \Delta_\mu^S - \frac{ra}{2}\Delta^2, \tag{D.6}$$

where Δ^2 is the d-dimensional lattice Laplacian

$$\Delta^2 = \sum_{\nu=0}^{d-1} \Delta_\nu^+ \Delta_\nu^- \tag{D.7}$$

which is composed of the forward and backward derivative

$$(\Delta_\nu^+ f)_x = \frac{1}{a}(f_{x+\hat{\nu}} - f_x), \qquad (\Delta_\nu^- f)_x = \frac{1}{a}(f_x - f_{x-\hat{\nu}}). \tag{D.8}$$

The parameter $r \in [-1, 1] \backslash \{0\}$ is called the Wilson parameter. By including the Wilson term, the discretised action reads

$$
\begin{aligned}
S \;=\;& a^d \sum_{x,\mu} \frac{1}{2a} (\overline{\psi}_x \gamma_\mu \psi_{x+\hat{\mu}} - \overline{\psi}_x \gamma_\mu \psi_{x-\hat{\mu}}) + a^d \sum_x m \overline{\psi}_x \psi_x \\
& + a^d \sum_{x,\mu} \frac{r}{2a} (2\overline{\psi}_x \psi_x - \overline{\psi}_x \psi_{x+\hat{\mu}} - \overline{\psi}_x \psi_{x-\hat{\mu}}).
\end{aligned} \tag{D.9}
$$

Using the above action, the modified lattice propagator takes the form

$$
\tilde{\Delta}^F(k) = \frac{1}{i \sum_\mu \gamma_\mu \frac{1}{a} \sin(k_\mu a) + m + \sum_\mu \frac{2r}{a} \sin^2\left(\frac{k_\mu a}{2}\right)}. \tag{D.10}
$$

For small momenta, the part stemming from the Wilson term vanishes quadratically. Therefore, in the continuum limit, the physical fermions are not affected. However, for the doubler fermions, the term in question is non-zero. Rather, it adds a mass of the order of $1/a$ to the mass of the doubler fermions, thus eliminating the doublers from the spectrum in the continuum.

The propagator eq.(D.10) in one dimension is the one we use for the calculation of the counterterm via lattice perturbation theory in chapter 3.

Appendix E

Numerov-Algorithm and Shooting Method

To get a complete picture of the behaviour of supersymmetric quantum mechanics, it is very useful to be able to calculate numerically the energy spectrum of the Schroedinger equation for arbitrary potentials. One possibility to do so is by employing the shooting method. The shooting method is based on the efficiency of Numerov's algorithm for solving ordinary second order differential equations without any first order term. In this appendix, we review in detail the Numerov algorithm and how it is used for the shooting method.

E.1 The Numerov Algorithm

The algorithm in question was developed by Boris Numerov (1927). It is designed to solve numerically differential equations of the form

$$y''(x) + k(x)y(x) = 0. \tag{E.1}$$

This differential equation corresponds to the one-dimensional time independent Schroedinger equation for a particle of mass m in the potential $V(x)$,

$$\left(-\frac{\hbar^2}{2m} \frac{\partial^2}{\partial x^2} + V(x) \right) \psi(x) = E\psi(x), \tag{E.2}$$

if we identify

$$k(x) = \frac{2m}{\hbar^2} \left(E - V(x) \right). \tag{E.3}$$

Now, the Numerov algorithm works by tracing the solution iteratively for the discretised differential equation eq.(E.1) for two given starting points. The exact discretisation procedure is explained in the following.

To begin with, we discretise the x-axis in intervals of h[1], such that $x_i + h = x_{i+1}$. We now Taylor expand $y(x_n)$ in $\pm h$ to order $\mathcal{O}(h^4)$ and get

$$
y(x_n + h) = y(x_n) + hy'(x_n) + \frac{h^2}{2}y''(x_n) + \frac{h^3}{3!}y'''(x_n) + \frac{h^4}{4!}y^{\text{iv}}(x_n), \quad \text{(E.4)}
$$

$$
y(x_n - h) = y(x_n) - hy'(x_n) + \frac{h^2}{2}y''(x_n) - \frac{h^3}{3!}y'''(x_n) + \frac{h^4}{4!}y^{\text{iv}}(x_n). \quad \text{(E.5)}
$$

Identifying $y(x_n + h) = y_{n+1}$ and $y(x_n - h) = y_{n-1}$, it follows from this expansion immediately that

$$
y_{n+1} + y_{n-1} = 2y_n + h^2 y''(x_n) + \frac{h^4}{12}y^{\text{iv}}(x_n) + \mathcal{O}(h^6). \quad \text{(E.6)}
$$

By rearranging the terms, we get for the second derivative y'' the expression

$$
y''(x_n) = \frac{1}{h^2}\left(y_{n+1} + y_{n-1} - 2y_n - \frac{h^4}{12}y^{\text{iv}}(x_n)\right) + \mathcal{O}(h^4). \quad \text{(E.7)}
$$

We now use the differential equation eq.(E.1) to rewrite the fourth derivative y^{iv} in terms of a second derivative

$$
y^{\text{iv}}(x) = -\frac{d^2}{dx^2}\left(k(x)y(x)\right). \quad \text{(E.8)}
$$

For the discretised version of the second derivative, we combine the forward and backward derivative, which gives

$$
y''(x_n) = \frac{y_{n+1} - 2y_n + y_{n-1}}{h^2} + \mathcal{O}(h^4). \quad \text{(E.9)}
$$

Employing this discretised second derivative, the discretised version of eq.(E.8) reads

$$
y^{\text{iv}}(x_n) = -\frac{k_{n+1}y_{n+1} - 2k_n y_n + k_{n-1}y_{n-1}}{h^2}. \quad \text{(E.10)}
$$

By plugging eq.(E.10) into eq.(E.7), we get a discretised expression for the second derivative $y''(x_n)$. Using the second derivative thus discretised, the discretised version of the original differential equation eq.(E.1) reads

$$
\frac{1}{h^2}\left(y_{n+1} + y_{n-1} - 2y_n + \frac{h^2}{12}\left(k_{n+1}y_{n+1} - 2k_n y_n + k_{n-1}y_{n-1}\right)\right) + k_n y_n = 0. \quad \text{(E.11)}
$$

---

[1]Of course, this parameter has nothing to do with Planck's constant.

Rearranging the coefficients leads to the recursion condition

$$y_{n+1} = \frac{(2 - \frac{5h^2}{6}k_n)y_n - (1 + \frac{h^2}{12}k_{n-1})y_{n-1}}{1 + \frac{h^2}{12}k_{n+1}} + \mathcal{O}(h^6). \qquad \text{(E.12)}$$

This is the Numerov formula. For two given starting points

$$y(x_0) = y_0, \qquad y(x_1) = y_1, \qquad \text{(E.13)}$$

it solves recursively any second order differential equation of the form eq.(E.1).

As we will use it to trace the wave function of a particle in an arbitrary potential, we need to make sure that the x-axis is larger than the typical scale of the system we describe. As starting points eq.(E.13) we choose

$$y(x_0) = 0, \qquad y(x_1) = \varepsilon, \qquad \text{(E.14)}$$

where ε is an arbitrary small number. In order to get a properly normalised wave function, we still need to rescale the calculated function by the discrete normalisation condition

$$\sum_{i=0}^{N-1} h y_i^2 = 1, \qquad \text{(E.15)}$$

where i runs over all points of the discretised abscissa.

E.2 The Shooting Method

For a given energy E, the Numerov algorithm allows us to calculate a corresponding wave function of the stationary Schroedinger equation. Yet, we are only interested in wave functions which are truly eigenfunctions of the Hamilton operator. Therfore, we are still left with the task of finding the eigenvalues of the Hamilton operator. Keeping in mind that we have at hand a very efficient algorithm for solving second order differential equations of the form eq.(E.1), such as the Schroedinger equation, we approximate the true eigenvalues of the Hamilton operator iteratively. This technique is called *shooting method*.

To distinguish the starting energies which are good approximations to the true eigenvalues of the Hamilton operator from all the others, we make use of the fact that eigenfunctions of the Hamilton operator are normalisable. In other
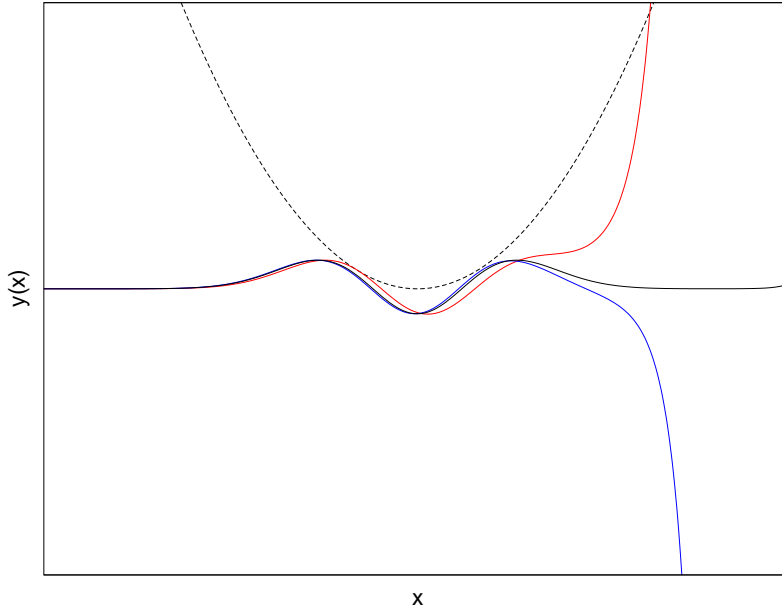
Figure E.1: Illustration of the shooting algorithm. Approximation of the second excited state E_2 of the harmonic oscillator (dashed black line). Drawn are the Numerov solutions for a starting energy that is too small (solid red line, divergence $y(x) \to +\infty$ for $x \backsim \lambda$) and a starting energy that is too large (solid blue line, divergence $y(x) \to -\infty$ for $x \backsim \lambda$). The solution for a starting value E close to the true eigenvalue E_2 remains stable for $x \gg \lambda$ (black line).

words, each eigenfunction decays quickly towards zero outside of some typical length of the system λ. However, if we calculate a wave function starting with an energy E that is too small or too large, the Numerov solution for the wave function will not decay towards zero. Rather, it will diverge within the the typical length of the system, $x \backsim \lambda$. In particular, if the starting energy E is too small, $y(x) \to \infty$, whereas if E is too large, $y(x) \to -\infty$. Only if the true eigenvalue E is approximated closely, the Numerov solution remains stable such that $y(x) \approx 0$ even for $x \gg \lambda$. Thus, we find the energy eigenvalues and functions by scanning the energy range and repeatedly tracing wave functions with Numerov's algorithm. Those energies for which the calculated wave functions remain stable for $x \gg \lambda$, e.g. these eigenfunctions which are normalisable, are the only ones that are accepted as good approximations for the true energy eigenvalues. In figure E.1, the behaviour of the Numerov so-

lution is illustrated for different starting energies E.

To make sure that the energy scan does not miss any energy levels, we can make use of the node theorem. The node theorem states that each excited state successively generates one additional node in the corresponding wave function, starting from no node for the ground state with energy E_0. Therefore, by counting the number of nodes of a wave function calculated with the Numerov method, we automatically know to which energy state the wave function is an eigenfunction and thus we can guarantee that we approximate every energy eigenvalue within the scanned energy range.

Appendix F

Analytical Calculation of the Fermion Determinant

In this appendix, we work out in detail the analytical expression for the fermion determinant for supersymmetric quantum mechanics, following Gozzi [74]. The determinant stems from the fermionic path integral in the continuum for a temporal extent of β,

$$\int \mathcal{D}\overline{\psi}\mathcal{D}\psi \, \exp\left(-\int_0^\beta dt \, \overline{\psi} \left(\partial_t + P''(\phi)\right)\psi\right) = \det\left(\partial_t + P''(\phi)\right). \quad \text{(F.1)}$$

We evaluate the determinant by writing it as a product,

$$\det\left(\partial_t + P''(\phi)\right) = \prod_{n=-\infty}^{\infty} \lambda_n, \quad \text{(F.2)}$$

where λ_n are the eigenvalues of the equations

$$\left(\partial_t + P''(\phi)\right)\psi_n = \lambda_n \psi_n. \quad \text{(F.3)}$$

The solutions to these differential equations are

$$\psi_n(t) = C_n \exp\left(\int_0^t dt' \, \left(\lambda_n - P''(\phi)\right)\right). \quad \text{(F.4)}$$

We now evaluate these expressions for antiperiodic and for periodic boundary conditions for the fermionic degrees of freedom.

F.1 Antiperiodic Boundary Conditions

We start with the case of antiperiodic boundary conditions. Imposing $\psi_n(t = \beta) = -\psi_n(t = 0)$ on eqs.(F.4) yields the eigenvalues

$$\lambda_n = \frac{i\pi(2n + 1)}{\beta} + \frac{1}{\beta}\int_0^\beta dt' \, P''(\phi). \quad \text{(F.5)}$$

Thus, for each eigenvalue λ_n, $n \geq 0$, there is a complex conjugate counterpart $\lambda_n^* = \lambda_{-(n+1)}$. Pairing the complex conjugate eigenvalues

$$\lambda_n \lambda_{-(n+1)} = |\lambda_n|^2 = \frac{1}{\beta^2} \left(\pi^2 (2n+1)^2 + \int_0^\beta dt' \ P''(\phi) \right), \qquad \text{(F.6)}$$

allows us to rewrite eq.(F.2) as

$$\det \left(\partial_t + P''(\phi) \right) = \prod_{n=0}^\infty |\lambda_n|^2. \qquad \text{(F.7)}$$

The product in eq.(F.7) is divergent. Therefore, the fermion determinant needs to be regularised. As suitable regularisation is provided by dividing the fermion determinant of the interacting theory by the fermion determinant of the free theory, $\det(\partial_t + \mu)$. The factors $1/\beta^2$ cancel in the thus regularised fermion determinant, yielding the ratio

$$\det \left(\frac{\partial_t + P''(\phi)}{\partial_t + \mu} \right) = \frac{\prod_{n=0}^\infty \left(\pi^2 (2n+1)^2 + \left(\int_0^\beta dt' \ P''(\phi) \right)^2 \right)}{\prod_{n=0}^\infty \left(\pi^2 (2n+1)^2 + \beta^2 \mu^2 \right)}. \qquad \text{(F.8)}$$

Furthermore, we factor out $\pi^2 (2n+1)^2$ in each term in both the nominator and the denominator such that we end up with

$$\det \left(\frac{\partial_t + P''(\phi)}{\partial_t + \mu} \right) = \frac{\prod_{n=0}^\infty \left(1 + \left(\int_0^\beta dt' \ P''(\phi) \right)^2 / \left(\pi^2 (2n+1)^2 \right) \right)}{\prod_{n=0}^\infty \left(1 + \beta^2 \mu^2 / \left(\pi^2 (2n+1)^2 \right) \right)}. \qquad \text{(F.9)}$$

Recalling that the cosine function can be represented as the infinite product

$$\cos(x) = \prod_{n=0}^\infty \left(1 - \frac{4x^2}{\pi^2 (2n+1)^2} \right), \qquad \text{(F.10)}$$

we get an infinite product representation of the cosh function by replacing the argument $x \to ix$ as well. Both the nominator and the denominator of eq.(F.9) can easily be identified to be of that form, such that the regularised fermion determinant can be written as

$$\det \left(\frac{\partial_t + P''(\phi)}{\partial_t + \mu} \right) = \frac{\cosh \left(\frac{1}{2} \int_0^\beta dt' \ P''(\phi) \right)}{\cosh \left(\frac{1}{2} \beta \mu \right)}. \qquad \text{(F.11)}$$

F.2 Periodic Boundary Conditions

Next, we repeat the calculation for periodic boundary conditions. Imposing $\psi_n(t = \beta) = \psi_n(t = 0)$ on eqs.(F.4) yields the eigenvalues

$$\lambda_n = \frac{2n\pi i}{\beta} + \frac{1}{\beta} \int_0^\beta dt' \ P''(\phi). \tag{F.12}$$

Thus, for each eigenvalue λ_n, $n > 0$, there is again a complex conjugate counterpart, $\lambda_n^* = \lambda_{-n}$. However, for periodic boundary conditions, the eigenvalue λ_0 remains unpaired. Pairing the complex conjugate eigenvalues for $n > 0$,

$$\lambda_n \lambda_{-n} = |\lambda_n|^2 = \frac{1}{\beta^2} \left(4\pi^2 n^2 + \int_0^\beta dt' \ P''(\phi) \right), \tag{F.13}$$

allows us to rewrite eq.(F.2) as

$$\det \left(\partial_t + P''(\phi) \right) = \lambda_0 \prod_{n=1}^\infty |\lambda_n|^2. \tag{F.14}$$

As we have done for antiperiodic boundary conditions, we regularise the fermion determinant for periodic boundary conditions by dividing it by the determinant of the free theory, yielding

$$\det \left(\frac{\partial_t + P''(\phi)}{\partial_t + \mu} \right) = \frac{\left(\int_0^\beta dt' \ P''(\phi) \right) \prod_{n=1}^\infty \left(4\pi^2 n^2 + \left(\int_0^\beta dt' \ P''(\phi) \right)^2 \right)}{(\beta\mu) \prod_{n=1}^\infty \left(4\pi^2 n^2 + \beta^2 \mu^2 \right)}. \tag{F.15}$$

In this case, we factor out $4\pi^2 n^2$ in each term in both the nominator and the denominator such that we end up with

$$\det \left(\frac{\partial_t + P''(\phi)}{\partial_t + \mu} \right) = \frac{\left(\int_0^\beta dt' \ P''(\phi) \right) \prod_{n=1}^\infty \left(1 + \left(\int_0^\beta dt' \ P''(\phi) \right)^2 / (4\pi^2 n^2) \right)}{(\beta\mu) \prod_{n=1}^\infty \left(1 + \beta^2 \mu^2 / (4\pi^2 n^2) \right)}. \tag{F.16}$$

Recalling that the sine function can be represented as the infinite product

$$\sin(x) = x \prod_{n=1}^\infty \left(1 - \frac{x^2}{\pi^2 n^2} \right), \tag{F.17}$$

we get an infinite product representation of the sinh function by replacing the argument $x \to ix$. Multiplying both the nominator and the denominator with $i/2$, eq.(F.16) can then easily be brought into the form

$$\det \left(\frac{\partial_t + P''(\phi)}{\partial_t + \mu} \right) = \frac{\sinh \left(\frac{1}{2} \int_0^\beta dt' \; P''(\phi) \right)}{\sinh \left(\frac{1}{2}\beta\mu \right)}. \tag{F.18}$$

Appendix G

Summary of the Discretisations

In this appendix, we write out explicitly the actions we used in our simulations for the superpotentials P_u and P_b. We also table the coefficients which go into the calculations of the weights for the simulation. First, we recall the definitions for the potential for bosonic self-interaction and the monomer term,

$$V(\phi) = \sum_{n=1}^{6} k_n \phi^n, \qquad M(\phi) = \sum_{n=0}^{2} m_n \phi^n. \tag{G.1}$$

The weight of the bosonic bonds is given by $w_{1 \to n}$, where n indicates the number of bosonic sources that the particular bond carries at the right ending. The lattice actions we use in lattice units are given by eqs.(3.18,3.95,3.100),

$$S_L = \sum_x \frac{1}{2}(\Delta^- \phi_x)^2 + \frac{1}{2}P'(\phi_x)^2 + \overline{\psi}_x(\Delta^- + P''(\phi_x))\psi_x, \tag{G.2}$$

$$S_L^c = S_L + \frac{1}{2}\sum_x P''(\phi_x), \tag{G.3}$$

$$S_L^{Q_1} = S_L + \sum_x P'(\phi_x)(\Delta^- \phi_x). \tag{G.4}$$

As throughout our work, the superpotentials are given by

$$P_u(\phi) = \frac{1}{2}\mu\phi^2 + \frac{1}{4}g\phi^4, \tag{G.5}$$

$$P_b(\phi) = -\frac{\mu^2}{4\lambda}\phi + \frac{1}{3}\lambda\phi^3. \tag{G.6}$$

G.1 The Actions for the Superpotential P_u

Writing out explicitly the actions for this superpotential, we have

$$
S_L = \sum_x \left\{ \frac{1}{2} \left(2 + \mu^2 \right) \phi_x^2 + \mu g \phi_x^4 + \frac{1}{2} g^2 \phi_x^6 - \phi_x \phi_{x-1} \right.
$$
$$
\left. + \left(1 + \mu + 3g\phi_x^2 \right) \overline{\psi}_x \psi_x - \overline{\psi}_x \psi_{x-1} \right\}, \tag{G.7}
$$

$$
S_L^c = \sum_x \left\{ \frac{1}{2} \left(2 + \mu^2 + 3g \right) \phi_x^2 + \mu g \phi_x^4 + \frac{1}{2} g^2 \phi_x^6 - \phi_x \phi_{x-1} \right.
$$
$$
\left. + \left(1 + \mu + 3g\phi_x^2 \right) \overline{\psi}_x \psi_x - \overline{\psi}_x \psi_{x-1} \right\}, \tag{G.8}
$$

$$
S_L^{Q_1} = \sum_x \left\{ \frac{1}{2} \left(2 + 2\mu + \mu^2 \right) \phi_x^2 + g(\mu+1)\phi_x^4 + \frac{1}{2} g^2 \phi_x^6 - g\phi_x^3 \phi_{x-1} \right.
$$
$$
\left. - (1 + \mu) \phi_x \phi_{x-1} + \left(1 + \mu + 3g\phi_x^2 \right) \overline{\psi}_x \psi_x - \overline{\psi}_x \psi_{x-1} \right\}. \tag{G.9}
$$

The coefficients which go into the simulations can be read off directly from the above actions. They are tabled below.

	S_L	S_L^c	$S_L^{Q_1}$
k_1	0	0	0
k_2	$1 + \frac{1}{2}\mu^2$	$1 + \frac{1}{2}\mu^2 + \frac{3}{2}g$	$1 + \mu + \frac{1}{2}\mu^2$
k_3	0	0	0
k_4	μg	μg	$g(1 + \mu)$
k_5	0	0	0
k_6	$\frac{1}{2}g^2$	$\frac{1}{2}g^2$	$\frac{1}{2}g^2$
$w_{1\to1}$	1	1	$1 + \mu$
$w_{1\to3}$	0	0	g
m_0	$1 + \mu$	$1 + \mu$	$1 + \mu$
m_1	0	0	0
m_2	$3g$	$3g$	$3g$

Table G.1: Unbroken supersymmetric quantum mechanics: Coefficients for the superpotential $P_u(\phi) = \frac{1}{2}\phi^2 + \frac{1}{4}g\phi^4$.

G.2 The Actions for the Superpotential P_b

Writing out explicitly the actions for this superpotential, we have

$$
S_L = \sum_x \left\{ \frac{1}{2} \left(2 + \mu^2 \right) \phi_x^2 + \mu\lambda\phi_x^3 + \frac{1}{2}\lambda^2\phi_x^4 - \phi_x\phi_{x-1} \right.
$$
$$
\left. + \left(1 + \mu + 2\lambda\phi_x^2 \right) \overline{\psi}_x\psi_x - \overline{\psi}_x\psi_{x-1} \right\}, \tag{G.10}
$$

$$
S_L^c = \sum_x \left\{ \lambda\phi_x + \frac{1}{2} \left(2 + \mu^2 \right) \phi_x^2 + \mu\lambda\phi_x^3 + \frac{1}{2}\lambda^2\phi_x^4 - \phi_x\phi_{x-1} \right.
$$
$$
\left. + \left(1 + \mu + 2\lambda\phi_x^2 \right) \overline{\psi}_x\psi_x - \overline{\psi}_x\psi_{x-1} \right\}, \tag{G.11}
$$

$$
S_L^{Q_1} = \sum_x \left\{ \frac{1}{2} \left(2 + 2\mu + \mu^2 \right) \phi_x^2 + \lambda(\mu + 1)\phi_x^3 + \frac{1}{2}\lambda^2\phi_x^4 - \lambda\phi_x^2\phi_{x-1} \right.
$$
$$
\left. - (1 + \mu) \phi_x\phi_{x-1} + \left(1 + \mu + 2\lambda\phi_x^2 \right) \overline{\psi}_x\psi_x - \overline{\psi}_x\psi_{x-1} \right\}. \tag{G.12}
$$

For the superpotential P_b too, we read off the coefficients from the actions directly. They are tabled below.

	S_L	S_L^c	$S_L^{Q_1}$
k_1	0	λ	0
k_2	$\frac{1}{4}(4 - \mu^2)$	$\frac{1}{4}(4 - \mu^2)$	$\frac{1}{4}(4 - \mu^2)$
k_3	0	0	λ
k_4	$\frac{1}{2}\lambda^2$	$\frac{1}{2}\lambda^2$	$\frac{1}{2}\lambda^2$
k_5	0	0	0
k_6	0	0	0
$w_{1\to1}$	1	1	1
$w_{1\to2}$	0	0	λ
m_0	1	1	1
m_1	2λ	2λ	2λ
m_2	0	0	0

Table G.2: Broken supersymmetric quantum mechanics: Coefficients for the superpotential $P_b(\phi) = -\frac{\mu^2}{4\lambda}\phi + \frac{1}{3}\lambda\phi^3$.

Appendix H

Calculation of the Site Weight Ratios

In order to calculate the weight of a configuration for supersymmetric quantum mechanics as well as for the Wess-Zumino model, it is necessary to know the site weight Q for each lattice site. However, the numerical calculation of the site weights is not straightforward. In this appendix, we show how it is possible to master the occurring numerical issues.

We start by recalling the definition for the superpotential

$$P(\phi) = \sum_{i=1}^{4} p_i \phi^i, \tag{H.1}$$

and the subsequent definitions for the bosonic self-interaction potential $V(\phi)$ as well as the monomer weight $M(\phi)$ in d dimensions,

$$V(\phi) = \frac{1}{2}P'(\phi)^2 + 2d\phi^2 + f(\phi), \tag{H.2}$$

$$M(\phi) = P''(\phi) + d. \tag{H.3}$$

The summands $2d\phi^2$ for the potential $V(\phi)$ and d for the monomer weight $M(\phi)$ stem from the Wilson discretisation. The polynomial function $f(\phi)$ depends on the chosen lattice action and its degree is less than or equal to the degree of the superpotential, $\deg(f) \leq \deg(P)$. Therefore, we can write (by omitting the constant summand k_0 for $V(\phi)$)

$$V(\phi) = \sum_{i=1}^{6} k_i \phi^i, \tag{H.4}$$

$$M(\phi) = \sum_{i=0}^{2} m_i \phi^i. \tag{H.5}$$

Appendix H · Calculation of the Site Weight Ratios

Recall now the definition of the weight $Q_F(n)$ from eq.(3.50) as the integral over the bosonic degrees of freedom as

$$Q_F(n) = \int_{-\infty}^{\infty} d\phi \, \phi^n e^{-V(\phi)} M(\phi)^{1-F}, \tag{H.6}$$

where $F = 0, 1$ is the fermion number. Explicitly, the site weights in each sector are given by

$$Q_0(n) = \int_{-\infty}^{\infty} d\phi \, \phi^n e^{-V(\phi)} \tag{H.7}$$

and

$$Q_1(n) = \sum_{i=0}^{2} m_i Q_0(n+i). \tag{H.8}$$

In principle, it is possible to calculate the desired integrals for an arbitrary potential $V(\phi)$ via numerical integration from here. Yet, in practice, it turns out that even for modest values of n the numerical integration is no longer reliable.

We observe that the site weights $Q_F(n)$ are not needed explicitly for a Monte Carlo simulation. Rather, the acceptance ratios require only ratios of the site weights $Q_F(n)$, which we denote by

$$R_F(n) = \frac{Q_F(n+2)}{Q_F(n)}, \tag{H.9}$$

$$R'_F(n) = \frac{Q_F(n+1)}{Q_F(n)}, \tag{H.10}$$

$$R_m(n) = \frac{Q_1(n)}{Q_0(n)}. \tag{H.11}$$

For later use, we note that the ratios $R_0(n)$ can be expressed in terms of $R'_0(n)$ as

$$R_0(n) = R'_0(n+1)R'_0(n). \tag{H.12}$$

Similarly, $R_m(n)$ can be expressed via the ratios $R_0(n)$ and $R'_0(n)$ as

$$R_m(n) = m_0 + m_1 R'_0(n) + m_2 R_0(n), \tag{H.13}$$

and the ratios $R'_1(n)$ and $R_1(n)$ via the ratios $R_m(n)$, $R_0(n)$ and $R'_0(n)$ as

$$R_1(n) = \frac{R_m(n+2)}{R_m(n)} R_0(n), \tag{H.14}$$

$$R'_1(n) = \frac{R_m(n+1)}{R_m(n)} R'_0(n). \tag{H.15}$$

222

First, we will discuss how to gain numerical stability for the special case of an even superpotential $P(\phi)$. Only in a second step we will adapt the idea to treat the somewhat more subtle case of an arbitrary superpotential.

H.1 Even Superpotential

Unbroken supersymmetric quantum mechanics require a superpotential $P(\phi)$ with $\deg(P(\phi)) = 0 \mod 2$. In particular, it allows for an even superpotential $P(\phi) = p_2\phi^2 + p_4\phi^4$. Because $f(\phi)$ then is an even function and the ratios $R'_F(n)$ are automatically excluded from any Monte Carlo simulation by construction of the algorithm, these ratios are not considered in the following.

Independent of the chosen action, the potential $V(\phi)$ can be written as

$$V(\phi) = k_2\phi^2 + k_4\phi^4 + k_6\phi^6. \tag{H.16}$$

For moments of the form eq.(H.7), we observe that by using an even superpotential $Q_0(n) = 0$ for $n = 1 \mod 2$. Thus, we only need to take into account moments $Q_0(2n)$ with $n \in \mathbb{N}_0$, such that

$$Q_0(2n) = \int_{-\infty}^{\infty} d\phi \ \phi^{2n} \mathrm{e}^{-V(\phi)}. \tag{H.17}$$

To keep the integrals numerically under control, we apply a variable transformation $\phi \to \widetilde{\phi} = \phi/\phi_0$, such that we have rescaled weights $\widetilde{Q}_0(2n)$ as

$$Q_0(2n) = \phi_0^{2n+1}\widetilde{Q}_0(2n). \tag{H.18}$$

Eq.(H.17) implies that $Q_0(2n) \geq 0$, and we choose the rescaling factor to be $\phi_0 = Q_0(2n)^{1/(2n+1)}$. Then, the integral $\widetilde{Q}_0(2n) = 1$ per definition. Furthermore, $R_0(2n) = \phi_0^2\widetilde{R}_0(2n)$ if we define the rescaled ratios $\widetilde{R}_0(2n)$ as

$$\widetilde{R}_0(2n) = \frac{\widetilde{Q}_0(2n+2)}{\widetilde{Q}_0(2n)} = \widetilde{Q}_0(2n+2), \tag{H.19}$$

where both integrals $\widetilde{Q}_0(2n+2)$ and $\widetilde{Q}_0(2n)$ are rescaled with the same rescaling factor $\phi_0 = Q_0(2n)^{1/(2n+1)}$. The integral $\widetilde{Q}_0(2n+2)$ is now of $\mathcal{O}(1)$ and can be evaluated reliably via numerical integration. If we thus start by integrating directly the numerically stable site weight $Q_0(0)$, we can recursively generate ratios $R_0(2n)$ up to any n. Note that after each calculation of a ratio

$R_0(2n)$, one needs to update the rescaling factor $\phi_0 \to \phi_0'$. This is done most easily via

$$\phi_0' = (\phi_0)^{\frac{2n+1}{2n+3}} R_0(2n)^{\frac{1}{2n+3}}. \tag{H.20}$$

This algorithm guarantees that all involved quantities are of $\mathcal{O}(1)$. Once all ratios $R_0(2n)$ are known, one can calculate the ratios $R_m(n)$, noting at the same time that for an even superpotential eq.(H.13) simplifies to

$$R_m(2n) = m_0 + m_2 R_0(2n). \tag{H.21}$$

The calculation of the ratios $R_1(2n)$ as given in eq.(H.14) is then straightforward.

H.2 Arbitrary Superpotential

In the context of broken supersymmetric quantum mechanics and the $\mathcal{N} = 1$ Wess-Zumino model, we encounter a superpotential with $\deg(P(\phi)) = 1$ mod 2. We now adapt the algorithm from above for superpotentials of this form. For simplicity, we restrict ourselves to superpotentials with $\deg(P(\phi)) = 3$,

$$P(\phi) = \sum_{i=1}^{3} p_i \phi^i. \tag{H.22}$$

If at least one of the coefficients p_1 and p_2 is non-zero, which is always the case for the superpotentials we use, $V(\phi)$ reads

$$V(\phi) = k_1 \phi + k_2 \phi^2 + k_3 \phi^3 + k_4 \phi^4, \tag{H.23}$$

and at least one of the coefficients k_1 and k_3 is non-zero either. This has a two-fold relevance for the following considerations: Firstly, the moments defined in eq.(H.7) are non-zero for $n = 1$ mod 2, from which follows that the ratios $R_F'(n)$ defined in eq.(H.10) have to be calculated as well. Secondly, the weights $Q_0(n)$ are no longer necessarily positive.

For the evaluation of the integrals, we apply the same variable transformation as in the case of an even superpotential $\phi \to \widetilde{\phi} = \phi/\phi_0$, such that we have rescaled weights $\widetilde{Q}_0(n)$ as

$$Q_0(n) = \phi_0^{n+1} \widetilde{Q}_0(n). \tag{H.24}$$

We now choose $\phi_0 = |Q_0(n)|^{1/(n+1)} \cdot \text{sgn}(Q_0(n))$. Then, the integral $\widetilde{Q}_0(n) = 1$ again per definition. Furthermore, $R'_0(n) = \phi_0 \widetilde{R}'_0(n)$ if we define the rescaled ratios $\widetilde{R}'_0(n)$ to be

$$\widetilde{R}'_0(n) = \frac{\widetilde{Q}_0(n+1)}{\widetilde{Q}_0(n)} = \widetilde{Q}_0(n+1), \tag{H.25}$$

where both integrals $\widetilde{Q}_0(n+1)$ and $\widetilde{Q}_0(n)$ are rescaled with the rescaling factor $\phi_0 = |Q_0(n)|^{1/(n+1)} \cdot \text{sgn}(Q_0(n))$. By doing so, we proceed analogously to the case of an even superpotential, with the only exception that we generate the ratios $R'_0(n)$ instead of the ratios $R_0(n)$. The update for the rescaling factor $\phi_0 \to \phi'_0$ is done via

$$\phi'_0 = |\phi_0|^{\frac{n+1}{n+2}} |R'_0(n)|^{\frac{1}{n+2}} \cdot \text{sgn}(R'_0(n)). \tag{H.26}$$

Once all ratios $R'_0(n)$ are known, one can calculate the ratios $R_0(n)$ via eq.(H.12), the ratios $R_m(n)$ via eq.(H.13), and the ratios $R_1(n)$ via eq.(H.14).

Appendix I

Calculating the Masses Via Eigenvalues of the Transfer Matrix

I.1 The Fermionic Masses

First, we derive the calculation of the fermionic masses via the eigenvalues of the transfer matrices. Setting the cutoff for the bosonic states to $N^{cut} = N$, the transfer matrices are of the dimension $N \times N$. The eigenvalues λ_i^F of the transfer matrix T^F are assumed to be ordered according to their values,

$$\lambda_0^F > \lambda_1^F > \cdots > \lambda_{N-1}^F. \tag{I.1}$$

The fermionic correlation function is only defined in the bosonic sector. Recall the structure of the correlation function for $t > 0$,

$$C^F(t) = \frac{1}{Z_0} \mathrm{Tr} \left[\overline{T}(\overline{\psi})(T^1(0))^{t-1} \overline{T}(\psi)(T^0(0))^{L_t - t - 1} \right]. \tag{I.2}$$

As discussed in chapter 4, the transfer matrices $\overline{T}(\overline{\psi})$ and $\overline{T}(\psi)$ including additional fermionic variables are equal to the transfer matrix $T^1(0)$. For pedagogical reasons, we keep the notation with the bars in this appendix. Consider now the trace in the numerator, where unit matrices $\mathbb{1} = P^F(P^F)^{-1}$ are inserted such that the matrices $T^F(0)$ are diagonalised as $D^F = P^F T^F(0)(P^F)^{-1}$,

$$\mathrm{Tr}[\overline{T}(\overline{\psi})(P^1)^{-1}P^1 T^1(0)(P^1)^{-1} \cdots (P^1)T^1(0)(P^1)^{-1}$$
$$\times P^1 \overline{T}(\psi)(P^0)^{-1}P^0 T^0(0)(P^0)^{-1} \cdots P^0 T^0(0)(P^0)^{-1}P^0]. \tag{I.3}$$

By executing all possible diagonalisations and using the cyclicity of the trace, we get

$$\mathrm{Tr} \left[P^0 \overline{T}(\overline{\psi})(P^1)^{-1}(D^1)^{t-1} P^1 \overline{T}(\psi)(P^0)^{-1}(D^0)^{L_t - t - 1} \right]. \tag{I.4}$$

Introducing the matrices

$$\overline{A} = P^0 \overline{T}(\overline{\psi})(P^1)^{-1}, \qquad \overline{B} = P^1 \overline{T}(\psi)(P^0)^{-1}, \tag{I.5}$$

we write the trace

$$\mathrm{Tr}[\dots] = \sum_{ij} \overline{A}_{ij} (\lambda_j^1)^{t-1} \overline{B}_{ji} (\lambda_i^0)^{L_t - t - 1}. \tag{I.6}$$

The correlation function can then be manipulated as

$$C^F(t) = \frac{\sum_{ij} \overline{A}_{ij} (\lambda_j^1)^{t-1} \overline{B}_{ji} (\lambda_i^0)^{L_t - t - 1}}{\sum_i (\lambda_i^0)^{L_t}}, \tag{I.7}$$

$$= \frac{(\lambda_0^0)^{L_t} \sum_{ij} \overline{A}_{ij} \overline{B}_{ji} (\lambda_j^1/\lambda_0^0)^{t-1} (\lambda_i^0/\lambda_0^0)^{L_t} (\lambda_i^0)^{-2}}{(\lambda_0^0)^{L_t} \left(1 + \sum_{i=1}^{N-1} (\lambda_i^0/\lambda_0^0)^{L_t}\right)}. \tag{I.8}$$

If not indicated explicitly, sums run over the indices $i = 0, \dots, N-1$. We now introduce the coefficients

$$\overline{c}_{ij} = \overline{A}_{ij} \overline{B}_{ji} (\lambda_i^0)^{-2} (\lambda_i^0/\lambda_j^1), \tag{I.9}$$

(no summation over i and j) and observe that in the limit $L_t \to \infty$ only terms with $i = 0$ survive. Therefore, we write the correlation function as

$$\begin{aligned} C^F(t) &= \sum_j \overline{c}_{0j} \left(\lambda_j^1/\lambda_0^0\right)^t, \\ &= \sum_j \overline{c}_{0j} \exp\left[-\left(-\ln\left(\lambda_j^1/\lambda_0^0\right)\right) t\right]. \end{aligned} \tag{I.10}$$

By the definition of the mass of a particle, we immediately obtain in this limit the j-th mass as

$$m_j^F = -\ln(\lambda_j^1/\lambda_0^0). \tag{I.11}$$

Note that the fermionic masses are *always* measured with respect to the lowest eigenvalue of the transfer matrix T^0 which is associated with the bosonic sector. This reflects the fact that the fermionic correlation function only exists in the bosonic sector. Interpreting the two-point function $\langle \overline{\psi}_t \psi_0 \rangle = -C^F(L_t - t) \equiv C^{\overline{F}}(t)$ as the correlation function of the antifermion $\overline{F}$, the above derivation goes through and

$$m_j^{\overline{F}} = -\ln(\lambda_j^0/\lambda_0^1). \tag{I.12}$$

In accordance with what we would expect, the masses of the antifermion are measured in the fermionic sector.

Now, let us adapt this calculation for the bosonic masses.

I.2 The Bosonic Masses

The bosonic correlator is defined in each sector $F = 0, 1$ independently and for $t > 0$, it is given by

$$C_F^B(t) = \frac{1}{Z_F} \text{Tr} \left[T^F(1) \left(T^F(0) \right)^{t-1} T^F(1) \left(T^F(0) \right)^{L_t - t - 1} \right]. \qquad (I.13)$$

Similarly to the fermionic correlation function, we insert in the trace unit matrices $\mathbb{1} = P^F (P^F)^{-1}$ such that we can diagonalise the matrices $T^F(0)$ as $D^F = (P^F)^{-1} T^F(0) P^F$. This yields

$$\text{Tr} \left[P^F T^F(1)(P^F)^{-1}(D^F)^{t-1} P^F T(1)(P^F)^{-1}(D^F)^{L_t - t - 1} \right]. \qquad (I.14)$$

Introducing the matrix

$$A^F = P^F T^F(1)(P^F)^{-1}, \qquad (I.15)$$

we write the trace

$$\text{Tr}[\dots] = \sum_{ij} A_{ij}^F (\lambda_j^F)^{t-1} A_{ji}^F (\lambda_i^F)^{L_t - t - 1}. \qquad (I.16)$$

The correlation function can then be manipulated as

$$
\begin{aligned}
C_F^B(t) &= \frac{\sum_{ij} A_{ij}^F (\lambda_j^F)^{t-1} A_{ji}^F (\lambda_i^F)^{L_t - t - 1}}{\sum_i (\lambda_i^F)^{L_t}}, & (I.17) \\
&= \frac{(\lambda_0^F)^{L_t} \sum_{ij} A_{ij}^F A_{ji}^F (\lambda_j^F / \lambda_i^F)^{t-1} (\lambda_i^F / \lambda_0^F)^{L_t} (\lambda_i^F)^{-2}}{(\lambda_0^F)^{L_t} \left(1 + \sum_{i=1}^{N-1} (\lambda_i^F / \lambda_0^F)^{L_t} \right)}. & (I.18)
\end{aligned}
$$

By introducing the coefficients

$$c_{ij} = A_{ij} A_{ji} (\lambda_i^F)^{-2} (\lambda_i^F / \lambda_j^F), \qquad (I.19)$$

we find in the limit $L_t \to \infty$, where again only terms with $i = 0$ survive,

$$
\begin{aligned}
C_F^B(t) &= \sum_j c_{0j} \left(\lambda_j^F / \lambda_0^F \right)^t \\
&= \sum_j c_{0j} \exp \left[- \left(- \ln \left(\lambda_j^F / \lambda_0^F \right) \right) t \right].
\end{aligned}
\tag{I.20}
$$

Analogously to the fermionic masses, we obtain in this limit for the j-th bosonic mass in the sector F

$$
m_{F,j}^B = - \ln(\lambda_j^F / \lambda_0^F).
\tag{I.21}
$$

The bosonic masses are calculated via the ratio $\lambda_j^F / \lambda_0^F$. Therefore, in contrast to the fermionic masses, each mass is calculated with respect to the largest eigenvalue in the respective sector.

Appendix J

Evaluation of the Spin Phase in Two Dimensions

In this appendix we evaluate the trace over the product of the projection operators which appears when integrating out the fermionic variables of the two-dimensional path integral along a closed fermionic loop for the Wess-Zumino model. Different techniques for this calculation can be found in [84, 93–95] out of which we follow closely [84].

Explicitly, we need to evaluate the trace given in eq.(6.60),

$$\mathrm{Tr}[\mathcal{X}] = \mathrm{Tr}[\mathcal{P}(n_1)\mathcal{P}(n_2)\cdots\mathcal{P}(n_l)]. \tag{J.1}$$

For convenience, we start by recalling some definitions which will be used later. The Dirac matrices γ_μ, with $\mu = 0, 1$, obey the Dirac algebra,

$$\{\gamma_\mu, \gamma_\nu\} = \gamma_\mu\gamma_\nu + \gamma_\nu\gamma_\mu = 2\delta_{\mu\nu}\mathbb{1}, \qquad \mathrm{Tr}[\gamma_\mu] = 0. \tag{J.2}$$

Note that in contrast to chapter 6, we will in the following denote the 2×2 unity matrix explicitly by $1_{2\times 2} = \mathbb{1}$. We will also use the matrix $\gamma_5 = i\gamma_0\gamma_1$ with the properties

$$\{\gamma_5, \gamma_\mu\} = 0, \qquad (\gamma_5)^2 = \mathbb{1}. \tag{J.3}$$

The projection operators $\mathcal{P}(n)$ are chiral projectors and are defined for lattice unit vectors $n = \pm\hat{\mu}$ as

$$\mathcal{P}(n) = \frac{1}{2}(\mathbb{1} - \slashed{n}), \tag{J.4}$$

where $\slashed{n} = n_\mu\gamma_\mu$ is the Feynman slash notation and the summation over μ is left implicit. The projection operators obey the conditions

$$\mathcal{P}(n)^2 = \mathcal{P}(n), \qquad \mathcal{P}(n)\mathcal{P}(-n) = 0, \qquad \mathrm{Tr}[\mathcal{P}(n)] = 1. \tag{J.5}$$

Note, that the second one of these conditions forbids backtracking loops and that the case $n_{i+1} = -n_i$ is therefore automatically excluded. After these preliminaries, we now proceed by executing the calculation over the trace.

First, we observe that for the projection operators for any two consecutive bonds in the same direction $n_{i+1} = n_i$, that is, for any straight section in the loop, only one of the projection operators remains because of the property

$$\mathcal{P}(n_{i+1})\mathcal{P}(n_i) = \mathcal{P}(n_i)^2 = \mathcal{P}(n_i). \tag{J.6}$$

Applying this rule to all straight sections, we end up with a subset n'_i, $i = 1, \ldots, l'$, $l' \leq l$, of the original set of unit vectors n_i, $i = 1, \ldots, l$. For this new subset $n'_{i+1} \neq n'_i$, $\forall i$ and the product of the projection operators may be written as

$$\prod_{i=1}^{l} \mathcal{P}(n_i) = \prod_{i=1}^{l'} \mathcal{P}(n'_i). \tag{J.7}$$

With the exception of straight loops winding once around the lattice, implying

$$\prod_{i=1}^{l} \mathcal{P}(n_i) = \mathcal{P}(n_1), \tag{J.8}$$

all loops can be reduced to this form where $n'_{i+1} \neq n'_i$, $\forall i$.

The special case of the fermion loop being a straight line and all unit vectors in the argument of the projectors being the same ones $n_{i+1} = n_i$, $\forall i$, can easily be seen to yield

$$\text{Tr}[\mathcal{P}(n_1)\mathcal{P}(n_2)\cdots\mathcal{P}(n_l)] = \text{Tr}[\mathcal{P}(n_1)^l] = \text{Tr}[\mathcal{P}(n_1)] = 1. \tag{J.9}$$

For any other kind of loop, the computation of the trace requires some more work. Without loss of generality, we now assume that the loop in question consists only of corners, such that $n_i \neq n_{i+1}$ $\forall i$, $i = 1, \ldots, l$.

To evaluate the trace for such a loop, we start by introducing the $\pi/2$ spinor rotation matrix

$$R(n, m) = e^{\frac{\pi}{8}[\not{n}, \not{m}]}, \tag{J.10}$$

with $n, m = \pm\hat{\mu}$ and $n \cdot m = 0$. Evaluating the commutator in the exponent gives

$$[\not{n}, \not{m}] = \not{n}\not{m} - \not{m}\not{n} = -2i\alpha\gamma_5, \tag{J.11}$$

where we have defined

$$\alpha \equiv (n_0 m_1 - m_0 n_1) \in \{-1, +1\}. \tag{J.12}$$

Plugging eq.(J.11) in eq.(J.10) and using the trigonometric identities for the sine and cosine function, the rotation matrix may be written as

$$R(n, m) = e^{\frac{\pi}{8}[\not{n}, \not{m}]} = e^{-i\frac{\pi}{4}\alpha\gamma_5} = \cos\left(\frac{\pi}{4}\right) \mathbb{1} - i\alpha\gamma_5 \sin\left(\frac{\pi}{4}\right) = \frac{1}{\sqrt{2}}\left(\mathbb{1} - i\alpha\gamma_5\right). \tag{J.13}$$

The inverse $R^{-1}(n, m) = R(m, n)$ of the rotation matrix $R(n, m)$ is easily seen to be

$$R(n, m)^{-1} = \frac{1}{\sqrt{2}}\left(\mathbb{1} + i\alpha\gamma_5\right). \tag{J.14}$$

Next, we observe that with the help of the rotation matrices R, we can rotate any projection operator into another one,

$$
\begin{aligned}
R(n, m)\mathcal{P}(m)R(n, m)^{-1} &= \frac{1}{\sqrt{2}}\left(\mathbb{1} - i\alpha\gamma_5\right)\frac{1}{2}(\mathbb{1} - \not{m})\frac{1}{\sqrt{2}}\left(\mathbb{1} + i\alpha\gamma_5\right) \\
&= \frac{1}{2}\left(\mathbb{1} + i\alpha\not{m}\gamma_5\right) \\
&= \frac{1}{2}\left(\mathbb{1} + \alpha(m_0\gamma_1 + m_1\gamma_0)\right) \\
&= \frac{1}{2}\left(\mathbb{1} - \left(n_0(m_1)^2\gamma_0 + n_1(m_0)^2\gamma_1\right)\right) \\
&= \frac{1}{2}\left(\mathbb{1} - \not{n}\right) = \mathcal{P}(n), \tag{J.15}
\end{aligned}
$$

where we have used eqs.(J.2,J.3) and, in addition, made use of the fact that $n, m = \pm\hat{\mu}$ and that $n \cdot m = 0$. Using eq.(J.15), we are now able to write any combination of two successive projection operators $\mathcal{P}(n)\mathcal{P}(m)$ as

$$
\begin{aligned}
\mathcal{P}(n)\mathcal{P}(m) &= R(n, m)\mathcal{P}(m)R(n, m)^{-1}\mathcal{P}(m) \\
&= \frac{1}{\sqrt{2}}(\mathbb{1} - i\alpha\gamma_5)\frac{1}{2}(\mathbb{1} - \not{m})\frac{1}{\sqrt{2}}(\mathbb{1} + i\alpha\gamma_5)\frac{1}{2}(\mathbb{1} - \not{m}) \\
&= \frac{1}{8}(\mathbb{1} - \not{m} - i\alpha\gamma_5 + i\alpha\gamma_5\not{m})(\mathbb{1} - \not{m} + i\alpha\gamma_5 - i\alpha\gamma_5\not{m}) \\
&= \frac{1}{4}(\mathbb{1} - \not{m} - i\alpha\gamma_5 + i\alpha\gamma_5\not{m}) \\
&= \frac{1}{\sqrt{2}}\frac{1}{\sqrt{2}}(\mathbb{1} - i\alpha\gamma_5)\frac{1}{2}(\mathbb{1} - \not{m}) \\
&= \frac{1}{\sqrt{2}}R(n, m)\mathcal{P}(m). \tag{J.16}
\end{aligned}
$$

Here, we have again used eqs.(J.2,J.3) and exploited the fact that $m^2 = n^2 = 1$, such that $\not{n}^2 = \mathbb{1}$ and $\alpha^2 = 1$. Applying the substitution eq.(J.16) $l-1$ times yields

$$\text{Tr}\left[\mathcal{P}(n_1) \cdots \mathcal{P}(n_l)\right] = 2^{-(l-1)/2}\text{Tr}[R(n_1, n_2) \cdots R(n_{l-1}, n_l)\mathcal{P}(n_l)]. \quad \text{(J.17)}$$

Inserting a unit matrix in the form

$$\mathbb{1} = R(n_l, n_1)R(n_l, n_1)^{-1} = R(n_l, n_1)R(n_1, n_l) \quad \text{(J.18)}$$

in front of the remaining projection operator, we write the trace as

$$\text{Tr}\left[\mathcal{P}(n_1) \cdots \mathcal{P}(n_l)\right] = 2^{-(l-1)/2}\text{Tr}[\mathcal{R}(\Theta)R(n_1, n_l)\mathcal{P}(n_l)], \quad \text{(J.19)}$$

where we have defined

$$\mathcal{R}(\Theta) = R(n_1, n_2)R(n_2, n_3) \cdots R(n_l, n_1), \quad \text{(J.20)}$$

the total rotation of the closed fermion loop, accumulating a total angle of Θ. To evaluate eq.(J.20), we divide the set of all rotation matrices in the subsets R_{CCW} and R_{CW}, which consist of the rotation matrices for counter-clockwise and clockwise rotations, respectively. Explicitly, these subsets are given by

$$\begin{aligned} R_{CCW} &= \{R(0, 1), R(1, -0), R(-0, -1), R(-1, 0)\}, & \text{(J.21)} \\ R_{CW} &= \{R(-0, 1), R(1, 0), R(0, -1), R(-1, -0)\}. & \text{(J.22)} \end{aligned}$$

Inspection shows that the parameter α is the same one for rotation matrices in the same subset, e.g. if $R \in R_{CCW}$, $\alpha = 1$, whereas if $R \in R_{CW}$, $\alpha = -1$. Now, we define n_{CCW} and n_{CW} to count the number of counter-clockwise rotation matrices and clockwise rotation matrices appearing in the total rotation $\mathcal{R}$, respectively. For any non-intersecting closed loop, the totally accumulated angle Θ is either $\Theta = \pm 2\pi$ and $|n_{CCW} - n_{CW}| = 4$, or, for loops winding around the lattice, $\Theta = 0$, such that $|n_{CCW} - n_{CW}| = 0$. It is now straightforward to evaluate the total rotation matrix for a loop with a complete rotation,

$$\mathcal{R}(\pm 2\pi) = \left(e^{-i\frac{\pi}{4}(\mp 1)\gamma_5}\right)^4 = \cos(\pi)\mathbb{1} \pm i\gamma_5 \sin(\pi) = -\mathbb{1}. \quad \text{(J.23)}$$

For $\Theta = 0$ and all angles adding up to zero, the total rotation trivially gives

$$\mathcal{R}(0) = \mathbb{1}. \quad \text{(J.24)}$$

Therefore, $\mathcal{R}(\Theta)$ only contributes with a sign to the value of the trace. Finally, we need to calculate

$$
\begin{aligned}
\mathrm{Tr}[R(n_1, n_l)\mathcal{P}(n_l)] &= \mathrm{Tr}\left[\frac{1}{\sqrt{2}}(\mathbb{1} - i\alpha\gamma_5)\frac{1}{2}(\mathbb{1} - \slashed{n}_l)\right] \\
&= \frac{1}{2}\frac{1}{\sqrt{2}}\mathrm{Tr}\left[\mathbb{1} - \slashed{n}_l - i\alpha\gamma_5 + i\alpha\gamma_5\slashed{n}_l\right] \\
&= \frac{1}{\sqrt{2}}.
\end{aligned}
\tag{J.25}
$$

This calculation is trivial too because, except for the unit matrix, all appearing matrices are traceless. Collecting the sign from eqs.(J.23,J.24), for the final result for the trace of a loop of the length l consisting only of corners we thus get the value

$$
\mathrm{Tr}[\mathcal{P}(n_1)\mathcal{P}(n_2)\cdots\mathcal{P}(n_l)] = (-1)^\nu 2^{-l/2},
\tag{J.26}
$$

where $\nu \in \{0, 1\}$ denotes the number of complete rotations of the loop. It is easy to see that for the generalisation of this result to any arbitrary geometry of the loop, one has to take into account the property of the projection operator, eq.(J.8). This amounts to the replacement of the total length of the loop l by n_c, the total number of corners along the loop, yielding the result for any arbitrary loop,

$$
\mathrm{Tr}[\mathcal{P}(n_1)\mathcal{P}(n_2)\cdots\mathcal{P}(n_l)] = (-1)^\nu 2^{-n_c/2}.
\tag{J.27}
$$

This is the formula we use in section 6.4.2 in the derivation of the fermionic contribution to the weight of a configuration.

Bibliography

[1] S. L. Glashow, *Partial Symmetries of Weak Interactions*, *Nucl.Phys.* **22** (1961) 579.

[2] A. Salam and J. C. Ward, *Electromagnetic and weak interactions*, *Phys.Lett.* **13** (1964) 168.

[3] S. Weinberg, *A Model of Leptons*, *Phys.Rev.Lett.* **19** (1967) 1264.

[4] H. Fritzsch, M. Gell-Mann, and H. Leutwyler, *Advantages of the Color Octet Gluon Picture*, *Phys.Lett.* **B47** (1973) 365.

[5] S. R. Coleman and J. Mandula, *All possible symmetries of the S matrix*, *Phys.Rev.* **159** (1967) 1251.

[6] R. Haag, J. T. Lopuszanski, and M. Sohnius, *All Possible Generators of Supersymmetries of the S Matrix*, *Nucl.Phys.* **B88** (1974) 257.

[7] J. Wess and B. Zumino, *A Lagrangian model invariant under supergauge transformations*, *Phys.Lett.* **B49** (1967) 52.

[8] M. F. Sohnius, *Introducing supersymmetry*, *Physics Reports* **128** (1985), no. 2–3 39 – 204.

[9] S. P. Martin, *A Supersymmetry primer*, `hep-ph/9709356`.

[10] J. Wess and J. Bagger, *Supersymmetry and supergravity*. Princeton University Press, 1992.

[11] L. O'Raifeartaigh, *Spontaneous symmetry breaking for chirals scalar superfields*, *Nuclear Physics* **B96** (1975), no. 2 331 – 352.

[12] I. Montvay, *Supersymmetric gauge theories on the lattice*, *Nucl.Phys.Proc.Suppl.* **53** (1997) 853–855, [`hep-lat/9607035`].

[13] A. Feo, *Predictions and recent results in SUSY on the lattice*, *Mod.Phys.Lett.* **A19** (2004) 2387–2402, [`hep-lat/0410012`].

[14] J. Giedt, *Deconstruction and other approaches to supersymmetric lattice field theories*, *Int.J.Mod.Phys.* **A21** (2006) 3039–3094, [`hep-lat/0602007`].

[15] T. Takimi, *Relationship between various supersymmetric lattice models*, *Journal of High Energy Physics* **2007** (2007), no. 07 010.

[16] P. H. Damgaard and S. Matsuura, *Lattice supersymmetry: equivalence between the link approach and orbifolding*, *Journal of High Energy Physics* **2007** (2007), no. 09 097.

[17] S. Catterall, *From twisted supersymmetry to orbifold lattices*, *Journal of High Energy Physics* **2008** (2008), no. 01 048.

[18] J. Bartels and G. Kramer, *A lattice version of the Wess-Zumino model*, *Zeitschrift für Physik C Particles and Fields* **20** (1983) 159–170. 10.1007/BF01573219.

[19] P. H. Dondi and H. Nicolai, *Lattice supersymmetry*, *Nuovo Cim* **A41** (1977) 1.

[20] K. Fujikawa, *Supersymmetry on the lattice and the Leibniz rule*, *Nucl.Phys.* **B636** (2002) 80–98, [`hep-th/0205095`].

[21] F. Bruckmann and M. de Kok, *Noncommutativity approach to supersymmetry on the lattice: SUSY quantum mechanics and an inconsistency*, *Phys.Rev.* **D73** (2006) 074511, [`hep-lat/0603003`].

[22] J. Giedt and E. Poppitz, *Lattice supersymmetry, superfields and renormalization*, *JHEP* **0409** (2004) 029, [`hep-th/0407135`].

[23] J. Giedt, R. Koniuk, E. Poppitz, and T. Yavin, *Less naive about supersymmetric lattice quantum mechanics*, *JHEP* **0412** (2004) 033, [`hep-lat/0410041`].

[24] M. Creutz and B. Freedman, *A statistical approach to quantum mechanics*, *Annals of Physics* **132** (1981), no. 2 427 – 462.

[25] J. Wosiek, *Spectra of supersymmetric Yang-Mills quantum mechanics*, *Nucl.Phys.* **B644** (2002) 85–112, [`hep-th/0203116`].

[26] J. Wosiek, *Supersymmetric Yang-Mills quantum mechanics in various dimensions*, *Int.J.Mod.Phys.* **A20** (2005) 4484–4491, [`hep-th/0410066`].

[27] M. Campostrini and J. Wosiek, *Exact Witten index in D = 2 supersymmetric Yang-Mills quantum mechanics*, *Phys.Lett.* **B550** (2002) 121–127, [`hep-th/0209140`].

[28] S. Catterall and E. Gregory, *A Lattice path integral for supersymmetric quantum mechanics*, *Phys.Lett.* **B487** (2000) 349–356, [`hep-lat/0006013`].

[29] S. Catterall, D. B. Kaplan, and M. Unsal, *Exact lattice supersymmetry*, *Phys.Rept.* **484** (2009) 71–130, [`arXiv:0903.4881`]. Invited review for Physics Reports. 126 pages.

[30] S. Catterall, *Twisted lattice supersymmetry and applications to AdS/CFT*, *PoS* **LATTICE2010** (2010) 002, [`arXiv:1010.6224`].

[31] M. Beccaria, G. Curci, and E. D'Ambrosio, *Simulation of supersymmetric models with a local Nicolai map*, *Phys.Rev.* **D58** (1998) 065009, [`hep-lat/9804010`].

[32] G. Bergner, T. Kaestner, S. Uhlmann, and A. Wipf, *Low-dimensional Supersymmetric Lattice Models*, *Annals Phys.* **323** (2008) 946–988, [`arXiv:0705.2212`].

[33] T. Kastner, G. Bergner, S. Uhlmann, A. Wipf, and C. Wozar, *Supersymmetric lattice models in one and two dimensions*, *PoS* **LAT2007** (2007) 265, [`arXiv:0709.0822`].

[34] G. Bergner, *Complete supersymmetry on the lattice and a No-Go theorem*, *JHEP* **1001** (2010) 024, [`arXiv:0909.4791`].

[35] I. Kanamori, F. Sugino, and H. Suzuki, *Observing dynamical supersymmetry breaking with euclidean lattice simulations*, *Prog.Theor.Phys.* **119** (2008) 797–827, [`arXiv:0711.2132`].

[36] I. Kanamori, H. Suzuki, and F. Sugino, *Euclidean lattice simulation for dynamical supersymmetry breaking*, *Phys.Rev.* **D77** (2008) 091502, [`arXiv:0711.2099`].

[37] C. Wozar and A. Wipf, *Supersymmetry breaking in low dimensional models*, *Annals Phys.* **327** (2012) 774–807, [`arXiv:1107.3324`].

Bibliography

[38] U. Wenger, *Simulating Wilson fermions without critical slowing down*, *PoS* **LAT2009** (2009) 022, [`arXiv:0911.4099`].

[39] N. V. Prokof'ev and B. V. Svistunov, *Worm algorithms for classical statistical models*, *Phys.Rev.Lett.* **87** (2001) 004, [`160601`].

[40] K. Fujikawa, *N = 2 Wess-Zumino model on the d = 2 Euclidean lattice*, *Phys.Rev.* **D66** (2002) 074510, [`hep-lat/0208015`].

[41] S. Elitzur and A. Schwimmer, *N = 2 two-dimensional Wess-Zumino model on the lattice*, *Nucl.Phys.* **B226** (1983), no. 1 109 – 120.

[42] S. Catterall and S. Karamov, *Exact lattice supersymmetry: The Two-dimensional N=2 Wess-Zumino model*, *Phys.Rev.* **D65** (2002) 094501, [`hep-lat/0108024`].

[43] T. Kastner, G. Bergner, S. Uhlmann, A. Wipf, and C. Wozar, *Two-Dimensional Wess-Zumino Models at Intermediate Couplings*, *Phys.Rev.* **D78** (2008) 095001, [`arXiv:0807.1905`].

[44] C. Wozar, G. Bergner, T. Kaestner, S. Uhlmann, and A. Wipf, *Numerical Investigation of the 2D N=2 Wess-Zumino Model*, *PoS* **LATTICE2008** (2008) 234, [`arXiv:0809.2176`].

[45] M. F. L. Golterman and D. N. Petcher, *A local interactive lattice model with supersymmetry*, *Nucl.Phys.* **B319** (1989) 307.

[46] J. Ranft and A. Schiller, *Hamiltonian Monte Carlo study of (1+1)-dimensional models with restricted supersymmetry on the lattice*, *Physics Letters* **B138** (1984), no. 1–3 166 – 170.

[47] M. Beccaria, M. Campostrini, and A. Feo, *Hamiltonian Monte Carlo simulation of the two-dimensional Wess-Zumino model*, *Nucl.Phys.Proc.Suppl.* **106** (2002) 944–946, [`hep-lat/0110056`].

[48] M. Beccaria, M. Campostrini, and A. Feo, *A Hamiltonian lattice study of the two-dimensional Wess-Zumino model*, *Nucl.Phys.Proc.Suppl.* **119** (2003) 891–893, [`hep-lat/0209010`].

[49] M. Beccaria, M. Campostrini, and A. Feo, *The two-dimensional Wess-Zumino model in the Hamiltonian lattice formulation*, *Nucl.Phys.Proc.Suppl.* **129** (2004) 874–876, [`hep-lat/0309054`].

240

[50] M. Beccaria and C. Rampino, *World line path integral study of supersymmetry breaking in the Wess-Zumino model*, *Phys.Rev.* **D67** (2003) 127701, [`hep-lat/0303021`].

[51] M. Beccaria, M. Campostrini, and A. Feo, *Supersymmetry breaking in two-dimensions: The Lattice N = 1 Wess-Zumino model*, *Phys.Rev.* **D69** (2004) 095010, [`hep-lat/0402007`].

[52] M. Beccaria, G. F. De Angelis, M. Campostrini, and A. Feo, *Phase diagram of the lattice Wess-Zumino model from rigorous lower bounds on the energy*, *Phys.Rev.* **D70** (2004) 035011, [`hep-lat/0405016`].

[53] M. Beccaria, G. De Angelis, M. Campostrini, and A. Feo, *Study of dynamical supersymmetry breaking for the two dimensional lattice Wess-Zumino model*, *AIP Conf.Proc.* **756** (2005) 451–453, [`hep-lat/0412020`].

[54] M. Beccaria, G. F. De Angelis, M. Campostrini, and A. Feo, *Dynamical supersymmetry breaking and phase diagram of the lattice Wess-Zumino model*, *PoS* **LAT2005** (2006) 269, [`hep-lat/0509126`].

[55] F. Synatschke, H. Gies, and A. Wipf, *The Phase Diagram for Wess-Zumino Models*, *AIP Conf.Proc.* **1200** (2010) 1097–1100, [`arXiv:0909.4189`].

[56] F. Synatschke, H. Gies, and A. Wipf, *Phase Diagram and Fixed-Point Structure of two dimensional N=1 Wess-Zumino Models*, *Phys.Rev.* **D80** (2009) 085007, [`arXiv:0907.4229`].

[57] S. D. Drell, M. Weinstein, and S. Yankielowicz, *Strong-coupling field theories. II. Fermions and gauge fields on a lattice*, *Phys.Rev.* **D14** (Sep, 1976) 1627–1647.

[58] J. Bartels and J. B. Bronzan, *Supersymmetry on a lattice*, *Phys.Rev.* **D28** (Aug, 1983) 818–829.

[59] S. Nojiri, *Continuous 'translation' and supersymmetry on the lattice*, *Progress of Theoretical Physics* **74** (1985), no. 4 819–831.

[60] S. Nojiri, *The Spontaneous Breakdown of Supersymmetry on the Finite Lattice*, *Progress of Theoretical Physics* **74** (Nov., 1985) 1124–1138.

Bibliography

[61] A. Kirchberg, J. Lange, and A. Wipf, *From the Dirac operator to Wess-Zumino models on spatial lattices*, *Annals Phys.* **316** (2005) 357–392, [`hep-th/0407207`].

[62] S. Catterall and S. Karamov, *A Lattice study of the two-dimensional Wess-Zumino model*, *Phys.Rev.* **D68** (2003) 014503, [`hep-lat/0305002`].

[63] N. V. Prokof'ev, B. V. Svistunov, and I. S. Tupitsyn, *"Worm" algorithm in quantum Monte Carlo simulations*, *Phys.Lett.* **A238** (1998).

[64] U. Wolff, *Simulating the All-Order Strong Coupling Expansion I: Ising Model Demo*, *Nucl.Phys.* **B810** (2009) 491–502, [`arXiv:0808.3934`].

[65] U. Wenger, *Efficient simulation of relativistic fermions via vertex models*, *Phys.Rev.* **D80** (2009) 071503, [`arXiv:0812.3565`].

[66] R. Baxter, *Exactly solved models in statistical mechanics*. Academic Press Limited, 1982.

[67] B. Kaufman, *Crystal statistics. II. Partition function evaluated by spinor analysis*, *Phys.Rev.* **76** (Oct, 1949) 1232–1243.

[68] F. Cooper, A. Khare, and U. Sukhatme, *Supersymmetry in quantum mechanics*. World Scientific Publishing Co Pte. Ltd., 2001.

[69] A. Wipf, *Non-perturbative methods in supersymmetric theories*, `hep-th/0504180`.

[70] E. Witten, *Constraints on Supersymmetry Breaking*, *Nucl.Phys.* **B202** (1982) 253.

[71] M. Grisaru, W. Siegel, and M. Roček, *Improved methods for supergraphs*, *Nucl.Phys.* **B159** (1979), no. 3 429 – 450.

[72] P. Howe, K. Stelle, and P. Townsend, *Miraculous ultraviolet cancellations in supersymmetry made manifest*, *Nucl. Phys.* **B236** (1984), no. 1 125 – 166.

[73] I. Montvay and G. Münster, *Quantum fields on a lattice*. Cambridge University Press, 1994.

[74] E. Gozzi, *Functional-integral approach to Parisi-Wu stochastic quantization: Scalar theory*, *Phys.Rev.* **D28** (Oct, 1983) 1922–1930.

[75] T. Reisz, *A power counting theorem for Feynman integrals on the lattice*, *Commun.Math.Phys.* **116** (1988).

[76] S. Catterall, *Lattice supersymmetry and topological field theory*, *JHEP* **0305** (2003) 038, [`hep-lat/0301028`].

[77] H. Ezawa and J. R. Klauder, *Fermions without fermions*, *Progress of Theoretical Physics* **74** (1985), no. 4 904–915.

[78] A. Salam and J. Strathdee, *On goldstone fermions*, *Physics Letters* **B49** (1974), no. 5 465 – 467.

[79] S. Ferrara, *Supersymmetric gauge theories in two dimensions*, *Lettere Al Nuovo Cimento (1971 – 1985)* **13** (1975) 629–635. 10.1007/BF02742426.

[80] A. Schiller and J. Ranft, *The 1+1 dimensional N=2 Wess-Zumino model on the lattice in the local Hamiltonian method*, *Journal of Physics G: Nuclear Physics* **12** (1986), no. 10 935.

[81] S. Dimopoulos and H. Georgi, *Softly broken supersymmetry and SU(5)*, *Nuclear Physics* **B193** (1981), no. 1 150 – 162.

[82] D. Baumgartner, K. Steinhauer, and U. Wenger, *in progress.*

[83] I. Montvay, *Majorana fermions on the lattice*, `hep-lat/0108011`.

[84] U. Wolff, *Simulating the All-Order Hopping Expansion. II. Wilson Fermions*, *Nucl.Phys.* **B814** (2009) 549–572, [`arXiv:0812.0677`].

[85] U. Wolff, *Cluster simulation of two-dimensional relativistic fermions*, *PoS* **LAT2007** (2007) 284, [`arXiv:0710.2179`].

[86] S.-J. Chang, *Existence of a second-order phase transition in a two-dimensional ϕ^4 field theory*, *Phys.Rev.* **D13** (May, 1976) 2778–2788.

[87] D. Baumgartner and U. Wenger, *Simulation of supersymmetric models on the lattice without a sign problem*, *PoS* **LAT2010** (2011).

[88] D. Baumgartner, K. Steinhauer, and U. Wenger, *Supersymmetry breaking on the lattice: the N=1 Wess-Zumino model*, `arXiv:1111.6042`.

[89] V. Maillart and U. Wenger, *Worm algorithm for the O(2N) Gross-Neveu model*, *PoS* **LAT2010** (2010) 257, [`arXiv:1104.0569`].

[90] M. Newman and G. Barkema, *Monte Carlo methods in statistical physics*. Oxford University Press, 1999.

[91] J. W. Gibbs, *Elementary principles in statistical mechanics*. Cambridge University Press, 1902.
[`www.archive.org/details/elementaryprinci00gibbrich`].

[92] N. Metropolis, A. W. Rosenbluth, M. N. Rosenbluth, A. H. Teller, and E. Teller, *Equation of State Calculations by Fast Computing Machines*, *J.Chem.Phys.* **21** (June, 1953) 1087–1092.

[93] I. O. Stamatescu, *Note on the lattice fermionic determinant*, *Phys.Rev.* **D25** (Feb, 1982) 1130–1135.

[94] C. Gattringer, *Loop representation for 2-D Wilson lattice fermions in a scalar background field*, *Nucl.Phys.* **B543** (1999) 533–542, [`hep-lat/9811014`].

[95] C. Gattringer, *A Formula for the Hopping Expansion of Eight-Vertex Models Coupled to an External Field*, *International Journal of Modern Physics* **A14** (1999) 4853–4863, [`cond-mat/9811139`].

Erklärung

gemäss Art. 28 Abs. 2 RSL 05

Name, Vorname: Baumgartner, David

Matrikelnummer: 02-112-704

Studiengang: Physik

                     Bachelor ☐   Master ☐   Dissertation ☒

Titel der Arbeit: Supersymmetric Models in Low Dimensions on
                     the Lattice

Leiter der Arbeit: Prof. Dr. Urs Wenger

Ich erkläre hiermit, dass ich diese Arbeit selbständig verfasst und keine anderen als die angegebenen Quellen benutzt habe. Alle Stellen, die wörtlich oder sinngemäss aus Quellen entnommen wurden, habe ich als solche gekennzeichnet. Mir ist bekannt, dass andernfalls der Senat gemäss Artikel 36 Absatz 1 Buchstabe o des Gesetzes vom 5. September 1996 über die Universität zum Entzug des auf Grund dieser Arbeit verliehenen Titels berechtigt ist.

Bern, den 14. August 2012

David Baumgartner

Curriculum vitæ

Personal Data

Name	**Baumgartner, David**
Date of birth	January 8, 1978
Place of origin	Bangerten, BE
Nationality	Swiss
Marital status	Single

Education

2008 - 2012	University of Bern *Supersymmetric Models in Low Dimensions on the Lattice* PhD, supervised by Prof. Dr. Urs Wenger
February 2008	University of Bern *Spiral Phases in Doped Antiferromagnets* MSc in physics, supervised by Prof. Dr. Uwe-Jens Wiese
2005/06	Université Pierre et Marie Curie, Paris 6, F Erasmus exchange semester
2002 - 2008	University of Bern Studies in physics, mathematics, and philosophy
2001 - 2002	Scuola di Musica Moderna, Lugano, TI Corso pre-professionale, saxophone
1999 - 2001	Wirtschaftsgymnasium Bern-Kirchenfeld
1998	Green River Community College, Auburn, WA, USA
1994 - 1998	Lehrwerkstätten der Stadt Bern Apprenticeship as draftsman